CANADIAN THESES

THÈSES CANADIENNES

NOTICE

The quality of this microfiche is heavily dependent upon the quality of the original thesis submitted for microfilming. Every effort has been made to ensure the highest quality of reproduction possible.

If pages are missing, contact the university which granted the degree.

Some pages may have indistinct print especially if the original pages were typed with a poor typewriter ribbon or if the university sent us an inferior photocopy.

Previously copyrighted materials (journal articles, published tests, etc.) are not filmed.

Reproduction in full or in part of this film is governed by the Canadian Copyright Act, R.S.C. 1970, c. C-30.

AVIS

La qualité de cette microfiche dépend grandement de la qualité de la thèse soumise au microfilmage. Nous avons tout fait pour assurer une qualité supérieure de reproduction.

S'il manque des pages, veuillez communiquer avec l'université qui a conféré le grade.

La qualité d'impression de certaines pages peut laisser à désirer, surtout si les pages originales ont été dactylographiées à l'aide d'un ruban usé ou si l'université nous a fait parvenir une photocopie de qualité inférieure.

Les documents qui font déjà l'objet d'un droit d'auteur (articles de revue, examens publiés, etc.) ne sont pas microfilmés.

La reproduction, même partielle, de ce microfilm est soumise à la Loi canadienne sur le droit d'auteur, SRC 1970, c/C-30.

THIS DISSERTATION
HAS BEEN MICROFILMED
EXACTLY AS RECEIVED

LA THÈSE A ÉTÉ
MICROFILMÉE TELLE QUE
NOUS L'AVONS REÇUE

TWO INVESTIGATIONS ON THE BAND STRUCTURE OF EVEN-EVEN NUCLEI

by

Jean PARI

Thesis submitted
to the School of Graduate Studies
of the University of Ottawa
in partial fulfillment of the
requirements for the degree of
Master of Science
in
Physics

Ottawa, Ontario, 1986

ISBN 0-315-36543-9

UNIVERSITÉ D'OTTAWA
UNIVERSITY OF OTTAWA

ABSTRACT

Aspects of the band structures of even–even nuclei have been studied in detail. Negative–parity bands are considered for the following even–even nuclei: dysprosium, erbium, ytterbium, hafnium and tungstem. Phenomenological models have been applied to reproduce the energy level sequences. The results obtained from the Variable Moment of Inertia Model, the Bohr–Mottelson Model and the Varshni formula by a least–squares fitting procedure are presented and the relative merits of the models are analyzed. A graphical analysis is also carried out. From our results and observations emerges a classification scheme for negative–parity bands.

In the second part of the thesis, the backbending effect has been studied for even–even nuclei within a two–band crossing formalism. A recent model, the Variable Moment of Inertia and Bohr–Mottelson band crossing model, is studied by a least–squares fitting procedure and is compared to a model we propose: the Variable Moment of Inertia and Varshni formula band crossing model. The comparative merits of the models are analyzed by using the Gauss criterion. Typical backbending plots are also presented and we discuss some limitations of these models.

ACKNOWLEDGEMENTS

I would like to sincerely thank Professor Y. P. Varshni for his suggestion of the problems studied in this thesis, his constant assistance and his patience during the completion of this work. The many interesting discussions we had concerning topics in physics were most instructive and formative.

J'aimerais aussi remercier ma mère et mon père pour leurs encouragements et pour avoir su créer une atmosphère propice à la rédaction de ce travail de même que ma soeur Giovanna pour son aide durant l'apport des touches finales à la thèse.

Je remercie également le CNRSG pour son soutien financier.

CONTENTS

LIST OF TABLES

LIST OF FIGURES

Chapter I Introduction and Review of Work on Even–even Nuclei

1. Introduction

In this thesis, we study two aspects of the energy spectrum of even–even nuclei: negative-parity bands and the backbending effect in the yrast band (the levels of the yrast band are those which lie lowest in energy for a given value of the spin). In both cases, we will adopt a phenomenological approach to systematically study the many experimentally observed bands we consider.

Chapter II of this work consists of an analysis of negative–parity bands observed for the even–even nuclei dysprosium, erbium, ytterbium, hafnium and tungsten. We have applied three different models: the Variable Moment of Inertia Model, the Bohr-Mottelson Model and the Varshni formula obtained within the framework of boson Hamiltonian models. Our aim is to compare the relative merits of these three approaches and obtain as much information as possible about the properties of these bands. The method of analysis used was least–squares fitting of the energy level sequence of the bands (30 negative–parity bands were considered). Results concerning classification schemes, structural properties of the bands, and suitable parametrizations are obtained.

Chapter III of this work is a study of the backbending effect in the yrast band of even–even nuclei. We propose, within a two–band crossing model, a parametrization which provides satisfactory results for the energy levels of the yrast band: the Variable Moment of Inertia and Varshni formula band crossing model. This model is compared with another recent model: the Variable Moment of Inertia and Bohr–Mottelson band crossing model for 22 even–even nuclei. The performance of the two models for their prediction of the energy levels is investigated by using a least–squares fitting procedure. The theoretical results are compared and the relative merits of the models is studied by using the Gauss criterion. Difficulties arising within the framework of band crossing calculations are discussed.

We first proceed, however, to give a brief review of works concerning even–even nuclei. In Chapter I, we consider those models which we have found useful in the analyses presented in Chapter II and Chapter III. The initial model explaining nuclear collective properties, the Bohr–Mottelson Model, has been considered for negative–parity bands and its principal results, as well as its extension to octupole bands are reviewed. We have also found it useful to study the Variable Moment of Inertia Model. This model provides an accurate description of the ground state band and is applicable over a wide range of even–even nuclei (i.e. the model spans the vibrational as well as the rotational regions, Sec 3.2 of this chapter). The third theoretical framework we consider is that of the Interacting Boson Model. This recent model has generated a lot of interest and we review the principal results obtained.

2. The Bohr–Mottelson Model and Octupole Bands

2.1. Introduction

The nuclear Shell Model (Mayer, 1949, 1950; Haxel, Jensen and Suess, 1949, 1950) has been the most influential model in nuclear structure. This model is believed to provide the correct framework for the analysis of nuclear properties. Although it assumes independent nucleons moving in the average field they generate, collective behavior in light nuclei (A $\sim$ 25) has been reproduced with the model. The calculations, however, rapidly become intractable (according to Talmi (1982), the Shell Model predicts 3.46×10^{14} 2^+ states for the nucleus ^{154}Sm). It is therefore necessary, for heavy nuclei, to introduce assumptions allowing a reduction in the number of degrees of freedom involved.

The initial model which provided an interpretation of the collective properties of heavy nuclei (energy band levels linked by strong quadrupole transitions, large quadrupole moments indicating spheroidal nuclei, the mechanism of fission, etc.) was the liquid drop model proposed by Bohr (1952) and Bohr and Mottelson (1953). Of importance was the

idea of collective coordinates, which greatly limited the number of degrees of freedom, and the straightforward analytical results which were obtained. Certainly, the direct physical interpretation of the model (the nucleus is assumed to possess an ellipsoidal equilibrium shape, which can rotate or vibrate because of the collective movement of valence nucleons), due to its semi-classical origin, accounted for its large popularity. We will quote the model's results which we have found to be important to our work. Derivations and complete discussions are provided in different textbooks (Bohr and Mottelson, 1975; Eisenberg and Greiner, 1970).

2.2. The Model Hamiltonian

The Bohr–Mottelson Model considers rotations and vibrations of the nucleus' surface. Accordingly, the following Hamiltonian is assumed:

$$H = H_{rotational} + H_{vibrational} + H_{coupling} \tag{2.1}$$

where $H_{coupling}$ represents the coupling of the vibrational and rotational motions. The adiabatic assumption is also made: rotational motion is easier to excite and the level spectrum will therefore result in rotational bands built on vibrational levels (this is similar to the situation in molecular spectra).

The explicit form of the rotational part of the Hamiltonian is

$$H_{rotational} = \sum_k \frac{\hbar^2}{2\Im_k}(I_k - J_k)^2 \tag{2.2}$$

where I_k is the component of the total angular momentum along the intrinsic k–axis, J_k is k^{th} component of the intrinsic angular momentum and $\{\Im_1, \Im_2, \Im_3\}$ is the set of principal axis moments of inertia (in writing down such an expression, it is necessary to define an intrinsic set of nuclear coordinates, the k–axis system, which are related to the space–fixed coordinates by the conventional Euler angles).

For the previous rotational Hamiltonian, the moments of inertia are all different and we have the case of an asymmetric rotator (this was studied in detail by Davydov and

Filippov (1958)). We will, however, restrict the discussion to the case of the symmetric rotator, for which two of the moments of inertia are equal, say $\Im_1 = \Im_2 = \Im$. In nuclear physics, the symmetric rotator is applicable if one assumes that the nucleus possesses axial symmetry, say about the intrinsic 3-axis (the symmetric rotator is well known from the study of diatomic molecules (Herzberg, 1950)). The symmetry assumption imposes the condition $I_3 = J_3$, (this can be demonstrated by considering rotations of the rotational wavefunction and the intrinsic wavefunction and imposing the invariance of the total product wavefunction (Rowe, 1967)). A further symmetry condition is assumed: the nucleus is symmetrical with respect to π-rotations about an axis perpendicular to the symmetry axis. These symmetry conditions constructed the image that nuclei had ellipsoidal shapes.

Hence,

$$\begin{aligned} H_{\text{rotational}} &= \frac{\hbar^2}{2\Im}\{(I_1 - J_1)^2 + (I_2 - J_2)^2\} + \frac{\hbar^2}{2\Im_3}(I_3 - J_3)^2 \\ &= \frac{\hbar^2}{2\Im}(I^2 - I_3^2 - J_3^2) + \frac{\hbar^2}{2\Im_3}(I_3 - J_3)^2 - \frac{\hbar^2}{2\Im}(I_+J_- + I_-J_+) + \frac{\hbar^2}{2\Im}J^2 \qquad (2.3) \\ &\approx \frac{\hbar^2}{2\Im}(I^2 - I_3^2 - J_3^2) + \frac{\hbar^2}{2\Im}J^2 \end{aligned}$$

where $\frac{\hbar^2}{2\Im_3}(I_3 - J_3)^2 = 0$ because of symmetry considerations. The last term, $\frac{\hbar^2}{2\Im}J^2$, operates only on the intrinsic degrees of freedom and is not considered because it results in a constant shift of all rotational energies. $I_\pm$ and $J_\pm$ are the usual raising and lowering operators defined by $I_\pm = I_1 \pm iI_2$ and $J_\pm = J_1 \pm iJ_2$. The term

$$-\frac{\hbar^2}{2\Im}(I_+J_- + I_-J_+) \qquad (2.4)$$

represents the Coriolis and centrifugal interactions. The standard Bohr–Mottelson model assumes this term to be small and neglects it in first order (except for $K = 1/2$ bands). The importance of the Coriolis interaction was first investigated by Kerman (1956) in his study of ^{183}W, and gained much importance as the mechanism responsible for rotation–alignment in the model of Stephens and Simon (1972).

2.3. Energy Relations

It is beyond the scope of our work to discuss about the Bohr–Mottelson Model wave-functions Ψ_{IKM}. When the expectation value of the rotational Hamiltonian

$$\langle \Psi_{IKM} | H_{rotational} | \Psi_{IKM} \rangle \tag{2.5}$$

is evaluated, one obtains the characteristic energy relation

$$E_I = E_K + \frac{\hbar^2}{2\Im}\{I(I+1) - K^2\} \tag{2.6}$$

where K is the eigenvalue of the 3^{rd} component of the intrinsic angular momentum. This energy equation is applicable in the description of the ground state band ($K = 0$; $E_k = 0$) and of excited bands (K = positive integer for even–even nuclei).

Experiment dictated that for the ground state band, too many approximations had been made and that the effect of the rotation–vibration coupling had to be taken into account. The 1^{st} order correction due to the rotation–vibration interaction is a term proportional to $I^2(I+1)^2$ (Eisenberg and Greiner, 1970). Higher order corrections lead to an expansion of the energy in powers of $I(I+1)$:

$$E_I = A\{I(I+1)\} + B\{I(I+1)\}^2 + C\{I(I+1)\}^3 + \cdots \tag{2.7}$$

This general equation does not, however, explain well the experimentally observed energies of the ground state band of even–even nuclei (Sood, 1968; Singh and Sahota, 1985). The inclusion of the $2^{nd.}$ and 3^{rd} order terms is not useful: departures of importance are noted for ground state band energy levels with spin values as low as $10\hbar$ and the equation is incapable of explaining Mallmann's curves (1959) (see Sec. 3).

The case of excited bands is however different. The moment of inertia for these bands in rare–earth even–even nuclei is much larger and its variation with spin is different than for the ground state band. These two facts indicate that in such situations the nucleus might

approximate a rigid rotator and that the Bohr–Mottelson model would work reasonably well. It is however necessary for excited bands to introduce the omitted Coriolis terms

$$\langle \Psi_{IKM} | I_{\pm} | \Psi_{IKM} \rangle \tag{2.8}$$

(the terms $\langle \Psi_{IKM} | J_{\pm} | \Psi_{IKM} \rangle$ are left undefined and considered as independent parameters, called decoupling parameters). We then obtain another type of energy relation:

$$E_I = \sum_{i=0} (A_i + (-1)^{I+K} \frac{(I+K)!}{(I-K)!} B_i) \{ I(I+1) - K^2 \}^i \tag{2.9}$$

(Bohr and Mottelson, 1975). This energy equation is applicable to the study of negative–parity bands (the parity of the band being determined from the properties of the intrinsic state on which is built the rotational sequence).

2.4. Octupole Bands

The experimental discovery of negative–parity energy levels immediately led to theoretical efforts to explain them in the framework of the Bohr–Mottelson model. The initial suggestion, by Christy in 1956, was that the negative–parity levels were constructed on pear–shaped states (pear–shaped deformations correspond to the shape obtained by relinquishing the π–reflectional symmetry about an axis perpendicular to the symmetry axis). Strutinsky (1957) proposed the following mechanism that could generate pear–shaped deformations in nuclei: the deformation would arise from the coupling of a filled and unfilled level with opposite parities.

The possibility of the existence of stable pear–shaped deformations in the nuclear energy states attracted much interest because, as mentioned, it could account for the negative–parity of energy levels, but also, it could explain the asymmetry of fission fragments (Johansson, 1961). Lee and Inglis (1957) used perturbation theory to evaluate the deforming tendency of a spheroidal potential in their investigation of the stability of this type of deformation. Lee and Haertle (1968) extended the perturbation treatment to 4^{th}

order. Johansson (1961) included in the calculation the spin–orbit coupling term the previous workers had omitted and Vogel (1968) found that for heavy transuranic elements, all equilibrium shapes contained some degree of pear–shaped deformation. The general conclusion obtained was that the nucleus did not have stable pear–shaped deformations but rather, that it was soft to this type of deformation, i.e. in terms of quadrupole and octupole degrees of freedom, the nucleus possessed small octupole contributions superimposed to the stable quadrupole deformations. Recently, a lot of research has been devoted to the settling of this question for nuclei in the actinide region. References to these works can be found in a paper by Kvasil and Nazmitdinov (1985).

Although not yet made explicit, pear–shaped deformations are equivalent to considering spherical harmonics of the form $Y^3_\mu(\theta,\phi)$ in the usual Bohr–Mottelson expansion of the nuclear surface. It is argued that the parity of these octupole deformations is $(-1)^\lambda$ (Bohr, 1969), and here, $\lambda = 3$. This, however, should be considered with circumspectness since there is nothing in the collective Schrödinger equation to establish the parity–multipolarity link (Davidson, 1970). In any case, we will briefly review the theoretical attempts which assume that the octupole deformations are responsible for negative–parity levels.

A direct extension of the Bohr–Mottelson model was done by Lipas and Davidson (1961). They assumed that, superimposed to the quadrupole nuclear shape, there were contributions proportional to the $Y^3_0(\theta,\phi)$ and $Y^3_{\pm 2}(\theta,\phi)$, the harmonics $Y^3_{\pm 1}(\theta,\phi)$ being arbitrarily set to zero. The model yielded rotational negative–parity bands built on vibrational excitations similar in character to levels of the β– and γ– vibrational bands, i.e. a $K^\pi = 0^-$ band, with I = 1, 3, 5, $\cdots$, and a $K^\pi = 2^-$ band, with I = 2, 3, 4, $\cdots$. This model therefore produces octupole bands. We also note that the model retains nuclear axial symmetry.

The asymmetric rotor model, applied to nuclear physics by Davydov and Filippov (1958) and Davydov and Chaban (1960), was also extensively used to explain negative–parity levels. The initial attempts of Davidson (1962) and Davidson (1965) encountered

difficulties because of the assumption of pure octupole deformations (as discussed, it seems that octupole deformations are small and superimposed to stable quadrupole shapes). Davidson (1967) then assumed a nuclear surface of the form

$$R(\theta,\phi) = R_o\Big\{1 + \sum_{\mu=-2}^{2} \alpha_{2\mu} Y_\mu^2(\theta,\phi) + \sum_{\nu=-3}^{3} \alpha_{3\nu} Y_\nu^3(\theta,\phi)\Big\} \tag{2.10}$$

and evaluate the negative–parity level energies in the Davydov-Filippov–Chaban model framework. What is most interesting is that in a subsequent work, Davidson (1970) assumed that the pure quadrupole asymmetric model could predict the position of the negative–parity levels in ^{228}Th, ^{232}U and ^{234}U. His results, when compared to the pure octupole asymmetric model (Davidson, 1962) and the mixed quadrupole–octupole model (Davidson, 1967), showed that all three models were essentially equivalent: the inclusion of octupole degrees of freedom in the asymmetric model did not correspond to better theoretical agreement with experiment.

These initial phenomenological attempts to derive the properties of negative–parity bands in even–even nuclei were followed by microscopic calculations (Neergård and Vogel, 1969, 1970a, 1970b). Their method, however, retained the principal physical ideas of the octupole–type studies. For the intrinsic component, H_{intr}, of the general Hamiltonian

$$H = H_s + H_{intr} + H_{coupl} \tag{2.11}$$

Neergård and Vogel (1970a) assumed the following separable form:

$$H_{intr} = H_{average} + H_{short\ range} + H_{long\ range} \tag{2.12}$$

The individual potentials respectively represent an average Nilsson type potential (Nilsson, 1955), a short range potential simulating the pairing interaction (as in superconductivity), and a long range octupole potential. The matrix elements of the long range octupole potential are of the form

$$\langle \alpha\beta^{-1}|V|\gamma\delta^{-1}\rangle = -\sum_{\mu=-3}^{3} \kappa_\mu \langle \alpha|Y_\mu^3(\vec{r})|\beta\rangle \langle \gamma|Y_\mu^3(\vec{r})|\delta\rangle^* \tag{2.13}$$

where $Y^3_\mu(\vec{r})$ are the 3^{rd} order spherical harmonics, the arguments $\vec{r}$ being a set of transformed space coordinates linearly related to the intrinsic coordinates, $\alpha\beta\gamma\delta$ are single-particle quantum numbers and κ_μ are interaction constants (which may be used as independent parameters as in the case of the calculation of Neergård and Vogel (1969) for the dysprosium isotopes).

The calculation of the matrix elements of H_{intr} is done in the framework of the second quantization method; the random phase approximation, RPA, is used. The usual Bohr-Mottelson model results for the rotational and Coriolis contributions are included to obtain the final level energies.

We remark that the work of Neergård and Vogel (1969, 1970a) was able to account for the general ordering of the low-lying (levels up to 5^- were considered) negative-parity levels in rare-earths. Their calculations did not, however, produce the correct energy level values. Departures of the order of 250 keV to 500 keV are frequent between the theoretical predictions and the experimentally observed levels in their study of the dysprosium isotopes (Neergård and Vogel, 1969). The comparison of theoretical and experimental negative-parity spectra for other rare-earth elements also shows discrepancies of a similar order (Neergård and Vogel, 1970a). We note that the Neergård-Vogel calculations were also carried out for transuranic elements (Neergård and Vogel, 1970b).

3. The Variable Moment of Inertia Model

3.1. Introduction

The Variable Moment of Inertia Model (Mariscotti *et al*, 1969; Scharff-Goldhaber *et al*, 1976) remains to date the most accurate 2-parameter model describing the ground state band of well-deformed even-even nuclei. This model also satisfactorily describes the ground state band of nuclei exhibiting transitional, i.e. intermediate between rotational and vibrational characteristics (Das *et al*, 1970). We will review the empirical approach which led to the discovery of the model and discuss about its subsequent semi-empirical generalizations and extensions. Typically, the generalizations allowed better intermediate spin (here, we mean by intermediate spin the region of spins just preceeding the occurrence of backbending, $I \approx 10 - 18$) energy level results while the extensions allowed the the integration of near-magic nuclei in the Variable Moment of Inertia Model framework. Recently, a three parameter generalization of the Variable Moment of Inertia Model has incorporated the results obtained in the dynamical symmetry cases of the Interacting Boson Model.

3.2. The Model

The incentives to find a new formalism which could produce with reasonable accuracy the energy level values for the ground state band of even-even nuclei were twofold. On one hand, the Bohr-Mottelson eqs. (2.6) and (2.7) of this chapter gave poor results for the energies (Sood, 1967) and had no predictive power (Stephens *et al*, 1965), i.e. information on higher spin states could not be obtained by fitting the lower spin states. On the other hand, Mallmann (1959) had shown that the experimental data indicated the existence of simple "universal" relations between the ratios of the energy levels.

It was primarily the explanation of Mallmann's curves, which show that the points obtained by plotting the ratio $\frac{E_4}{E_2}$ versus the ratio $\frac{E_6}{E_2}$ for different nuclei fall on simple

curves, that motivated Mariscotti *et al* (1969) in their work. Their starting point was the β–stretching theory (Diamond *et al*, 1964) which proposes the energy equation

$$E_I(\beta_I) = \frac{1}{2\Im(\beta_I)} I(I+1) + \frac{1}{2} C(\beta_I - \beta_0)^2 \tag{3.1}$$

subject to the variational constraint

$$\frac{\partial E_I}{\partial \beta_I} = 0 \tag{3.2}$$

The quantity $\Im$ is the moment of inertia and it is assumed that the deformation parameter β is related to $\Im$ by $\Im \sim \beta^2$. This model gave good results for nuclei close to the rotational limit but was unable to explain Mallmann's curves for nuclei close to the vibrational limit (Although Da Providencia and Urbano (1972) later affirmed that the β–stretching Model performed better than the Variable Moment of Inertia Model Model in the vibrational limit, a close investigation of the experimental data by Gorfinkiel *et al* (1974) indicated that this was not the case).

It was the replacement of the hydrodynamical constraint $\Im \sim \beta^2$ by the relation $\Im \sim \beta$ (which was indicated by empirical evidence) which allowed for great improvement. The Variable Moment of Inertia Model ground state band energy equation was then obtained:

$$E_I = \frac{1}{2\Im} I(I+1) + \frac{1}{2} C(\Im - \Im_0)^2 \tag{3.3}$$

subject to the condition

$$\frac{\partial E_I}{\partial \Im} = 0 \tag{3.4}$$

The Variable Moment of Inertia Model was successful in explaining the Mallmann curves in the transitional and vibrational regions. Mariscotti *et al* (1969) showed that the Variable Moment of Inertia Model validity range was between $E_4/E_2 = 2.23$, which is close to the vibrational limit ($E_4/E_2 = 2$), and $E_4/E_2 = 10/3$, which corresponds to the rotational limit. Satisfactory results were obtained in the representation of vibrational spectra. Typically, the rms % deviation for such cases was between 0.5 and 1 (Varshni and

Bose, 1972). Excellent agreement was found for the well-deformed nuclei. Here, the rms % deviation is usually smaller than 0.5.

Because of the model's relevance to our work, we will discuss about some of its particular points. When the condition $\partial E_I/\partial \Im = 0$ is applied, a cubic equation in $\Im$

$$\Im^3 - \Im^2 \Im_0 - \frac{1}{2C} I(I+1) = 0 \tag{3.5}$$

is found. This equation can be solved for $\Im$. It has one real root for $\Im_0$, $C \geq 0$:

$$\begin{aligned} \Im = \frac{\Im_0}{3} &+ \sqrt[3]{\frac{\Im_0^3}{27} + \frac{1}{4C} I(I+1) + \sqrt{\frac{1}{4}\left(\frac{2\Im_0^3}{27} + \frac{1}{2C} I(I+1)\right)^2 - \frac{\Im_0^6}{27^2}}} \\ &+ \sqrt[3]{\frac{\Im_0^3}{27} + \frac{1}{4C} I(I+1) - \sqrt{\frac{1}{4}\left(\frac{2\Im_0^3}{27} + \frac{1}{2C} I(I+1)\right)^2 - \frac{\Im_0^6}{27^2}}} \end{aligned} \tag{3.6}$$

Having obtained $\Im$ as a function of I then allows direct programming of the energy equation. We note that the two independent parameters are $\Im_0$ and C. Sometimes, C is replaced by the softness parameter $\sigma = \{\frac{d\Im}{\Im dI}\}_{I=0} = \frac{1}{2C\Im_0^3}$. Scharff-Goldhaber (1980) and Scharff-Goldhaber and Dresden (1980) have studied the physical meaning of eq. (3.5) but any clear physical picture of its interpretation is not yet known.

The Variable Moment of Inertia Model is found to be equivalent to the two-parameter Harris Model (1964):

$$E_\omega = \frac{1}{2}\omega^2(\Im_0 + 3C\omega^2) \tag{3.7}$$

$$\sqrt{I(I+1)} = \omega(\Im_0 + 2C\omega^2) \tag{3.8}$$

where ω is the angular frequency of rotation of the nucleus. This model originates from a truncation to 4^{th} power in ω of a perturbation treatment of the Cranking Model (Inglis, 1954). The complete series expansions for the energy and the spin can be written as

$$E_\omega = \frac{1}{2}\omega^2\left(\Im_0 + 3C\omega^2 + 5D\omega^4 + 7F\omega^6 + \cdots\right) \tag{3.9}$$

$$\sqrt{I(I+1)} = \omega\left(\Im_0 + 2C\omega^2 + 3D\omega^4 + 4F\omega^6 + \cdots\right) \tag{3.10}$$

(Harris, 1965). We note that a detailed comparison of the results of this type of series with experiment has been done by Saethre *et al* (1973).

The physical foundations of the Variable Moment of Inertia Model Model have been studied in different contexts by Da Providencia and Urbano (1970, 1972). Work in this direction is reviewed by Scharff-Goldhaber *et al* (1976). We also note the classical analogy given by Thieberger (1970). In his work, he obtains equations for the energy and moment of inertia of the classical system consisting of two reservoirs, able to exchange mass, with one reservoir fixed and the other one rotating with angular frequency ω about the fixed one. The equations obtained are equivalent to those of the Variable Moment of Inertia, which would then possibly suggest that the low-energy properties of nuclei might arise from the variations in mass of a nuclear fluid rotating about a fixed core. It is, however, with the help of the Cranking Model, that important physical insights are gained. This model is essentially a reduction of the nuclear many-body problem to the problem of solving Schrödinger's equation for an assembly of non-interacting particles contained in an external rotating potential well. This observation somewhat explains the good results of the Variable Moment of Inertia Model ground state band equation for deformed nuclei. The fact that the Variable Moment of Inertia Model works well for vibrational nuclei is not completely understood (work in this direction (Marshalek, 1971) is ambiguous).

3.3. Extensions and Generalizations of the Variable Moment of Inertia Model

As mentioned, the range of validity of the Variable Moment of Inertia Model is found to be $2.23 \leq \frac{E_4}{E_2} \leq 3.33$. Two extensions of the model were simultaneously proposed by Mariscotti (1970) and Scharff-Goldhaber and Goldhaber (1970). Mariscotti used the Harris Model framework to calculate the effect of $\Im_0 < 0$. He found that one of the solutions obtained for eq. (3.5) allowed an extension of the range of validity of the model to $E_4/E_2 = 1.825$. Another solution extended the model to $E_4/E_2 = 1$, which therefore allows to span all nuclei. The results obtained were in good agreement with Mallmann's

curves. Scharff-Goldhaber and Goldhaber also tackled the problem of $\Im_0 < 0$, but this time, in the Variable Moment of Inertia Model framework. They extended the model to $E_4/E_2 = 1.825$ and found that at this value, a phase transition appeared. Indeed, Mallmann's curves show a discontinuity at this value of E_4/E_2.

It was soon realized that the Variable Moment of Inertia Model could be considered a special case of the general equation

$$E_I = \frac{1}{2\Im(t)} I(I+1) + \frac{1}{2} C t^2 \tag{3.11}$$

subject to

$$\frac{\partial E_I}{\partial t} = 0 \tag{3.12}$$

Many attempts to improve agreement with experimental results started from a modification of the potential energy term. These are reviewed by Scharff-Goldhaber *et al* (1976). It is found that the models are either equivalent in quality to the Variable Moment of Inertia Model (Stockmann and Zelevinsky (1972)) or provide worse results. In this context, we may also refer to the work by Draper (1972), who proposed the equation

$$E_I = S \ln^2 \rho + \frac{1}{\rho} I(I+1) \tag{3.13}$$

subject to

$$\left(\frac{\partial E}{\partial \rho}\right)_I = 0 \tag{3.14}$$

This equation is found to give better results than the Variable Moment of Inertia Model for energy levels with spin values approaching the critical backbending spin value (only selected applications were made).

Other workers proceeded differently to extend the Variable Moment of Inertia Model. Varshni and Bose (1972) have considered the inclusion of an anharmonic energy term in the Variable Moment of Inertia Model expression:

$$E_I = \frac{1}{2\Im} I(I+1) + \frac{1}{2} C_2 (\Im - \Im_0)^2 + \frac{1}{6} C_3 (\Im - \Im_0)^3 \tag{3.15}$$

and found that in many cases such a term was justified. Das and Banerjee (1973) postulated higher expansion terms in the potential energy and found that they were necessary if one wanted to reproduce qualitative backbending behavior within the Variable Moment of Inertia Model framework.

Recently, the Interacting Boson Model "dynamical symmetry" results have been added to the Variable Moment of Inertia Model framework. The equations obtained explicitly consider vibrational degrees of freedom and have the form (to a few modifications close)

$$E_I = \frac{AI + BI(I+1)}{\Im} + \frac{1}{2}C(\Im - \Im_0)^2 \tag{3.16}$$

(Begzhanov and Belen'kii, 1979; Klein, 1980),

$$E_I = AI + \frac{1}{\Im}I(I+1) + \frac{1}{2}C(\Im - \Im_0)^2 \tag{3.17}$$

(Bonatsos and Klein, 1984; Bhattacharya and Sen, 1984).

3.4. Applications of the Variable Moment of Inertia Model for Excited Bands

There have not been many studies of excited bands within the Variable Moment of Inertia Model framework. In their original work, Mariscotti *el al* (1969) briefly considered the applicability of the model for the K = 2 (γ–vibrational) bands of the even–even nuclei ^{166}Er and ^{186}Os. For ^{166}Er, the fit to the levels was good while oscillations in the first energy difference of the K = 2 band of ^{186}Os prevented good results. Gupta (1973) also considered γ–vibrational bands, but modified the Variable Moment of Inertia Model by introducing asymmetric degrees of freedom. For negative–parity bands, an application of the Variable Moment of Inertia Model was carried out for the nucleus ^{150}Sm by Thompson *et al* (1975).

The ad hoc extension of the Variable Moment of Inertia Model equation to excited bands is given by

$$E_I = E_K + \frac{1}{2\Im}\{I(I+1) - K^2\} + \frac{1}{2}C(\Im - \Im_0)^2 \tag{3.18}$$

subject to the usual variational condition

$$\frac{\partial E_I}{\partial \Im} = 0 \tag{3.19}$$

where K is the projection of the total angular momentum along the along the intrinsic symmetry axis (Sec. 2.3) and E_K the bandhead energy.

4. The Interacting Boson Model

4.1. Introduction

The Interacting Boson Model for even-even nuclei (Arima and Iachello, 1976, 1978, 1979), and the subsequent approaches giving it a microscopic basis (the IBM-2 of Arima *et al*, 1977; Otsuka *et al*, 1978) and extending it to odd-A nuclei (the IBFM of Iachello and Scholten, 1979; Iachello, 1980) are presently generating much theoretical work in low-energy nuclear physics. Many review articles (Arima and Iachello, 1981, 1984; Elliot, 1985; Lipas, 1984) and summer school proceedings (Iachello, 1979, 1981; Scholten, 1984) have provided detailed descriptions of the Interacting Boson Model and related subjects. We will limit our study to a brief discussion of the physical grounds on which is constructed the model, its energy equations for the ground state band (here, the IBM-2 and the IBFM will not be discussed since both are beyond the scope of our study) and its agreement with experiment. Closely related to our work are extensions of the model to high spin energy levels and negative-parity bands.

4.2. Physical Picture

The phenomenological Interacting Boson Model could represent the physics of a system of interacting quadrupole phonons described by L = 2 bosons (or d-bosons). The L = 0 boson (or s-boson) would then be a mathematical object producing, upon destruction, the creation of L = 2 bosons (Elliot, 1985). The physical interpretation of interest resides, however, in the microscopic identification of the s-boson and d-boson. The bosons would represent correlated pairs of identical nucleons coupled to angular momenta zero or two (Arima *et al*, 1977; Otsuka *et al*, 1978). The s-boson could then be a way of treating the pairing interaction on the same footing as the quadrupole (d-boson) degrees of freedom in nuclear systems (Arima and Iachello, 1981). This approach therefore includes 6 degrees

of freedom (1 s–boson and 5 d–bosons) in the model rather than the usual 5 degrees of freedom of, for example, the Bohr–Mottelson Model. We note that the question of a relation between the collective models and the Interacting Boson Model has generated a lot of interest (Dieperink *et al*, 1980; Chen and Van Isacker, 1981). This stems from the fact that the Interacting Boson Model could bridge the gap between independent–particle and collective models. The Interacting Boson Model originated (Feshback and Iachello, 1974) as an approximation method to carry out intractable Shell Model calculations.

Another point of interest is the fact that the model Hamiltonian and operators conserve the total boson number N, defined as the number of valence nucleon pairs (we note that in the microscopy, difference is made between proton–proton pairs and neutron–neutron pairs). This gives N a particular importance and allows the definition, through the theory, of a cut–off angular momentum at L = 2N. The observation of this cut–off, or related effects, has generated much experimental work (Cizewski, 1984). Due to quasiparticle alignments at high–spin, it is now believed that only subtle effects can be seen in low–spin levels of spectra depending in some way on N (Warner, 1984). Certainly, the conservation of bosons implies that the low–energy spectrum will be due only to valence particles.

4.3. Dynamical Symmetries

The Interacting Boson Model Hamiltonian for even–even nuclei is constructed according to the second quantization method by considering the most general rotationally invariant bilinear form of the s–boson and d–boson creation and annihilation operators (Janssen *et al*, 1974; Arima and Iachello, 1976). The inclusion of only s–bosons and d–bosons implies that only positive–parity states are described by the Hamiltonian. This Hamiltonian includes all boson–boson interactions up to 2^{nd} order:

$$H = \sum_{i=1}^{N} \epsilon_i + \sum_{i<j} V_{ij} \qquad (4.1)$$

where ϵ_i are the single–boson energies (N–boson system) and V_{ij} are the interaction potentials.

We will not present a discussion of the microscopy of the boson Hamiltonian since this is beyond the scope of our work. We note, however, that the Hamiltonian contains 9 independent parameters and that to describe the energy spectrum of excited levels, only 6 are required. The 6–parameter phenomenological form is

$$H = \epsilon'' n_d + a_0 P^\dagger P + a_1 L^2 + a_2 Q^2 + a_3 T_3^2 + a_4 T_4^2 \tag{4.2}$$

where we have followed the notation of Lipas (1984). Physically, n_d counts the number of d–bosons, L^2 is the square of the angular momentum, Q^2, T_3^2 and T_4^2 are respectively generalized quadrupole, octupole and hexadecupole interaction operators and $P^\dagger P$ represents the pairing interaction (Iachello, 1979). The set of independent parameters is $\{\epsilon'', a_0, a_1, a_2, a_3, a_4\}$.

Arima and Iachello (1974) used group theory rather than numerical calculations to obtain solutions to the 6–parameter Hamiltonian. Their important insight was to realize that under certain limiting conditions, the Hamiltonian could be written as a sum of Casimir operators corresponding to chains of subgroups of the general group structure of the model (the model group structure is $U(6)$, i.e. the unitary group in 6-dimensions, because general transformations are considered in the 6–dimensional space spanned by the s–boson and the 5 d–bosons). When such a situation arises, one has a dynamical symmetry, and analytical solutions for the Hamiltonian can be written in terms of the Casimir operators' eigenvalues. Before we discuss the three well–studied dynamical symmetries of the Interacting Boson Model, we give a brief reminder of definitions of some of the concepts we just mentioned.

A continuous group, such as $U(6)$, is defined by a set of operators called the generators of the group (for $U(6)$, there are 36 such operators). These operators are

$$s^\dagger s,\ s^\dagger d_\mu,\ d_\mu^\dagger s,\ d_\mu^\dagger d_\nu \tag{4.3}$$

or linear combinations of these; $\mu, \nu = 0, \pm 1, \pm 2$. If a particular generator happens to

commute with all the others, it is said to be a Casimir operator for the group. There are 7 Casimir operators for $U(6)$, six of which can be used to rewrite the phenomenological Hamiltonian as

$$\mathrm{H} = \epsilon'''C_1(U(5)) + \alpha C_2(U(5)) + \beta C_2(O(5)) + \gamma C_2(O(3)) + \delta C_2(SU(3)) + \eta C_2(O(6)) \quad (4.4)$$

The two parameter sets

$$\{\epsilon'',\ a_0,\ a_1,\ a_2,\ a_3,\ a_4\} \quad \{\epsilon''',\ \alpha,\ \beta,\ \gamma,\ \delta,\ \eta\} \quad (4.5)$$

are related by linear transformations (Lipas, 1984) and $U(5)$, $O(5)$, $O(3)$, $SU(3)$, $O(6)$ are subgroups of $U(6)$.

The previous Hamiltonian is not written in terms of Casimir operators associated with a chain of subgroups of $U(6)$. For such chains to emerge, i.e. dynamical symmetries to exist, some of the parameters must be set equal to zero. Then, the following chains correspond to dynamical symmetries (the group $O(3)$ must be included because L is a good quantum number):

$$\begin{aligned}
&\mathrm{I} \quad U(6) \subset U(5) \subset O(5) \subset O(3) \subset O(2) \qquad \eta = \delta = 0 \\
&\mathrm{II} \quad U(6) \subset SU(3) \subset O(3) \subset O(2) \qquad \epsilon''' = \alpha = \beta = \eta = 0 \\
&\mathrm{III} \quad U(6) \subset O(6) \subset O(5) \subset O(3) \subset O(2) \qquad \epsilon''' = \alpha = \delta = 0
\end{aligned} \quad (4.6)$$

Chain I (Arima and Iachello, 1976) is obtained by physically assuming that only the d-bosons contribute to the energy level spectrum and corresponds to the vibrational limit of the model. The energy bands, when written in terms of the eigenvalues of the Casimir operators are

$$\mathrm{E_I} = \epsilon''' n_d + \alpha n_d(n_d + 4) + 2\beta\nu(\nu + 3) + 2\gamma L(L + 1) \quad (4.7)$$

The relations between eigenvalues and operators are:

$$\begin{aligned} n_d &\longleftrightarrow C_1(U(5)) \\ n_d(n_d+4) &\longleftrightarrow C_2(U(5)) \\ 2\nu(\nu+3) &\longleftrightarrow C_2(O(5)) \\ 2L(L+1) &\longleftrightarrow C_2(O(3)) \end{aligned} \tag{4.8}$$

The ground state band for even–even nuclei satisfying the characteristics of this limit is expressed as:

$$|n_d\ \nu\ n_\Delta\ L\ M\rangle = |N\ N\ 0\ 2N\ M\rangle \tag{4.9}$$

where n_Δ is an additional quantum number required to specify the state uniquely and M is the 3^{rd} component of L (M does not appear in the energy equations). If we use the fact that the maximum angular momentum can be $L = 2N$ to replace the quantum numbers in E_I, we find

$$\begin{aligned} E_I &= \frac{\epsilon'''L}{2} + \alpha\frac{L}{2}(\frac{L}{2}+4) + 2\beta\frac{L}{2}(\frac{L}{2}+3) + 2\gamma L(L+1) \\ &= \left\{\frac{\epsilon'''}{2} + \frac{7\alpha}{2} + 5\beta\right\}L + \left\{\frac{\alpha}{2} + \beta + 2\gamma\right\}L(L+1) \end{aligned} \tag{4.10}$$

This type of ground state band equation was proposed empirically by Ejiri (1966).

Chain II (Arima and Iachello, 1978) corresponds to the rotational limit. Only two Casimir operators contribute to the spectrum: $C_2(SU(3))$ and $C_2(O(3))$. The general energy equation is

$$E_{II} = 2\gamma L(L+1) + \frac{2}{3}\delta(\lambda^2 + \mu^2 + \lambda\mu + 3\lambda + 3\mu) \tag{4.11}$$

where (λ, μ) specifies the irreducible representations of $SU(3)$ (these are well known from elementary particle physics: the famous octet and decuplet classifications respectively correspond to (1,1) and (3,0).

As in the previous case, we investigate the ground state band results for this chain: the quantum numbers specifying the band are

$$|(\lambda,\mu)\ K\ L\ M\rangle = |(2N,0)\ 0\ 2N\ M\rangle \tag{4.12}$$

and direct substitution yields again the Ejiri equation:

$$\begin{aligned} \mathrm{E_{II}} &= 2\gamma L(L+1) + \frac{2}{3}\delta(\frac{L^2}{4} + \frac{3}{2}L) \\ &= \frac{5}{6}\delta L + (2\gamma + \frac{\delta}{6})L(L+1) \end{aligned} \tag{4.13}$$

Chain III is the $O(6)$ limit which has generated much interest because such a symmetry structure was not known for even–even nuclei before its theoretical discovery. The general energy equation in this limit is

$$\mathrm{E_{III}} = 2\beta\nu(\nu+3) + 2\gamma L(L+1) + 2\eta\sigma(\sigma+4) \tag{4.14}$$

where the quantum number σ corresponds to the Casimir operator $C_2(O(6))$. The ground state band is given by

$$|\sigma\ \nu\ n_\Delta\ L\ M\rangle = |N\ N\ 0\ 2N\ M\rangle \tag{4.15}$$

which implies:

$$\begin{aligned} \mathrm{E_{III}} &= 2\beta\frac{L}{2}(\frac{L}{2}+3) + 2\gamma L(L+1) + 2\eta\frac{L}{2}(\frac{L}{2}+4) \\ &= \left\{\frac{5\beta}{2} + \frac{7\eta}{2}\right\}L + \left\{\frac{\beta}{2} + 2\gamma + \frac{\eta}{2}\right\}L(L+1) \end{aligned} \tag{4.16}$$

which is similar to the previous equations of the ground state band. We note that the fact that all three dynamical symmetries produce the Ejiri equation as the ground state band is a well-known result (Scharff–Goldhaber, 1984).

4.4. Comparison with Experiment

The Interacting Boson Model has been compared with experimental data for a few selected nuclei. Since comparisons have been made primarily for nuclei which we have not

directly studied in our work (Pt, Os, Sm, Gd), we will only briefly discuss the results. Complete reviews are given by Casten (1981) and Wood (1983).

The previous nuclei were studied because they presented vibrational characteristics (Os, Sm, Gd) or because they possessed near $O(6)$ symmetry structure. This type of symmetry presented a lot of interest because its discovery for ^{196}Pt (Cizewski *et al*, 1978) followed the theoretical prediction of its existence. A more recent comparison (Davidson *et al*, 1981) with experiment is the one concerning ^{168}Er, a nucleus presenting rotational characteristics. Such nuclei were not immediately studied because the large number of valence bosons involved usually implied computational difficulties.

Speaking in general terms, we may describe the agreement between theoretical predictions of the model and the experiment as being, on the average, somewhere between 50 keV and 100 keV for the energy levels (Castaños *et al*, 1981). Such quality of prediction is not very useful to the experimentalist. We mention, however, that fits to a large number of levels (40–60) are done with few parameters (2–4).

To summarize the symmetries used to study the different nuclei, we present in Figure 1.1 the "dynamical symmetry" triangle (Casten, 1981), and the positions of the nuclei on such a diagram.

Fig. 1.1

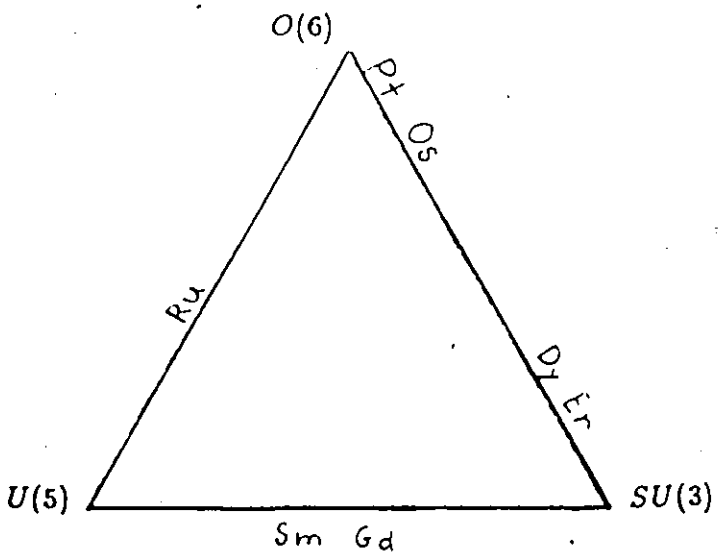

We note that for nuclei which are not close to the limiting symmetries, a full analysis must be carried out using the program PHINT of Scholten (1975).

4.5. High Spin States and Excited Bands

The Interacting Boson Model is valid for energy levels with associated spins $\leq 10\hbar$. In the model framework, the first few levels of excited positive–parity bands come out naturally by changing the quantum numbers associated with the dynamical symmetry. This gives rise to excited bands defined by the relation between the boson number N and the angular momentum.

Negative–parity levels and bands do not, however, come out naturally from the analysis in terms of s–boson and d–bosons. An f–boson, associated with $L_\pi = 3$, must be introduced (Arima and Iachello, 1976, 1978, 1979). These f–bosons are then allowed to couple with the d–bosons and negative–parity bands arise from the interaction.

The first application of the Interacting Boson Model to negative–parity bands was done in 1975 by Arima and Iachello. They found analytical expressions for the energy levels of even–spin and odd–spin sequences by considering the dynamical symmetries of the model Hamiltonian containing s, d and f bosons. The results they obtained are:

$$E_I(odd) = E_{gsb} + \epsilon_3 + \frac{c_5^{(23)}}{2}(I-3) \tag{4.17}$$

$$E_I(even) = E_I(odd) + \frac{3}{5}\Delta_4^{(23)} + \frac{\Delta_4^{(23)}}{5}(I-2) \tag{4.18}$$

where we have used the same nomenclature as in Arima and Iachello (1975) for the parameters but have replaced the boson number N by its corresponding expression in terms of the spin (for the odd sequence $I = 2N + 3$ and for the even sequence $I = 2N + 2$).

The first observation concerning these results is that the negative–parity bands are dependent upon the properties of the ground state band. Piercey *et al* (1976) applied this model and found that for the odd–spin negative–parity band of ^{74}Se the model predictions

and experimental values did not agree. This was attributed to the different moments of inertia of the ground state band and of the excited band. We may remark, in this context, that for all the regular negative–parity bands we studied, the moments of inertia are always substantially greater than those calculated for the ground state band.

A second point of interest is that the properties of negative–parity bands will be determined in the case of the odd–spin bands by a single parameter $c_5^{(23)}$ (the rest of the expression being a translation in energy of the ground state band). Even less freedom is allowed for the even–spin sequence.

This model has been used to investigate the properties of negative–parity bands of vibrational nuclei. De Voigt *et al* (1976) applied it to ^{100}Ru, Sujkowski *et al* (1977) to ^{150}Sm, Konijn *et al* (1981) to ^{156}Gd and Konijn *et al* (1982) to ^{152}Sm.

As for negative–parity bands, high–spin energy levels of the yrast band do not come out naturally from the Interacting Boson Model framework, in the sense that large departures between theory and experiment are observed when the spin reaches the backbending region. The initial idea to correct discrepancies was to introduce g–bosons. This additional L=4 boson was considered in the study of Ru (Stachel *et al*, 1982; Heyde *et al*, 1983), Gd (Van Isacker *et al*, 1982) and Ra (Dukelsky, 1983). The assumption of the g–boson was supplemented by that of band crossings in the Interacting Boson Model framework to explain the backbending effect. Development in this "Extended" Interacting Boson Model is just beginning. Work in this direction has been carried out for ^{126}Ba by Gelberg and Zemel (1980), for ^{126,128}Ba and $^{130-134}$Ce by Yoshida *et al* (1982), for Xe isotopes by Kusukari and Sugawara (1984) and for Dy isotopes by Heyde *et al* (1984). The performance of the "Extended" Interacting Boson Model is not very good. The microscopic approach of the last three references might explain some of the problems encountered.

4.6. Boson Hamiltonians and the Varshni Formula

The idea of bosons in nuclei is nowadays a well–established concept due to the im-

portant development of the Interacting Boson Model. Certainly, the nuclear bosons can be understood microscopically as pairs of correlated fermions or macroscopically in terms of the defining collective coordinates. Historically, nuclear boson Hamiltonians had been known for many years prior to the advent of the Interacting Boson Model. During the 60's, Kerman and Shakin (1962), Brink *et al* (1965) and Ferreira *et al* (1964) constructed the foundations of such a theoretical framework (detailed information about these developments is provided by Holzwarth (1982)). Even the Interacting Boson Model Hamiltonian is to be credited to Janssen *et al* (1974).

The result of interest to our work, which is derived within the framework of boson models, is the Varshni formula (1968). The angular momentum dependence form of the energy equation is:

$$E_I = aI(I+1) + pI + qI^2(I+1) \tag{4.19}$$

The first term of the equation is the rotational term, the second term is a vibrational term while the last term can be considered as a cross term arising from the interplay of vibrational and rotational motions. Das *et al* (1970) were the first to obtain this result from a consideration of boson Hamiltonians. More recently, Baktybaev and Strygin (1979) obtained a similar result from a perturbation treatment of selected terms of the Interacting Boson Model Hamiltonian. Das *et al* (1970) and Varshni (1974) compared the results obtained from this equation to the experimental data. Very good agreement is found for nuclei with characteristics ranging from vibrational to rotational. Indeed, the rms % deviations given are in most cases smaller than 0.25. The better performance of the Varshni formula over other phenomenological models has been estalished by Sood and Jain (1975) and Begzhanov *et al* (1976). Noteworthy of mention is the prediction by this formula of the upbending of the ground state bands of even–even nuclei.

References

Arima, A., and F. Iachello, 1974, Phys. Lett. **53B** 309

Arima, A., and F. Iachello, 1975, Phys. Lett. **57B** 39

Arima, A., and F. Iachello, 1976, Ann. Phys. **99** 253

Arima, A., and F. Iachello, 1978, Ann. Phys. **111** 201

Arima, A., and F. Iachello, 1979, Ann. Phys. **123** 468

Arima, A., and F. Iachello, 1981, Ann. Rev. Nucl. Part. Sci. **31** 75

Arima, A., and F. Iachello, 1984, in *Advances in Nuclear Physics*, eds. J. W. Negele and E. Vogt, Plenum Press, New York, p. 139

Arima, A., T. Otsuka, F. Iachello and I. Talmi, 1977, Phys. Lett. **66B** 205

Baktybaev, K. B., and D. P. Strygin, 1979, Bull. Acad. Sci. USSR Phys. Ser. **43** no. 1 p. 99

Begzhanov, R. B., and V. M. Belen'kii, 1979, Bull. Acad. Sci. USSR Phys. Ser. **43** no. 11 p. 72

Begzhanov, R. B., V. M. Belen'kii and S. R. Abdurakhamanov, 1976, Bull. Acad. Sci. USSR Phys. Ser. **40** no. 10 p. 101

Bhattacharya, S., and S. Sen, 1984, Phys. Rev. C **30** 1014

Bohr, A., 1952, Dan. Mat. Fys. Medd. **26**, no. 14

Bohr, A., 1969, Theory of Nuclear Structure in *Trieste Lectures*, International Atomic Agency, Vienna, p. 187

Bohr, A., and B. R. Mottelson, 1953, Dan. Mat. Fys. Medd. **27**, no. 16

Bohr, A., and B. R. Mottelson, 1963, At. Energ. (USSR), **14** 41

Bohr, A., and B. R. Mottelson, 1975, *Nuclear Structure*, Vol. II, W. A. Benjamin Inc., Reading, Mass.

Bonatsos, D., and A. Klein, 1984, Phys. Rev. C **29** 1879

Brink, D. M., A. F. R. de Toledo Piza and A. K. Kerman, 1965, Phys. Lett. **19** 413

Castaños, O., P. Federman and A. Frank, 1981, in *Interacting Bose-Fermi Systems*, ed. F. Iachello, Plenum, New York, p. 21

Casten, R. F., 1981, in *Interacting Bose-Fermi Systems*, ed. F. Iachello, Plenum, New York, p. 3

Chen, J. Q., and P. Van Isacker, 1981, in *Interacting Bose-Fermi Systems in Nuclei*, ed. F. Iachello, Plenum, New York

Christy, R. F., 1956, private communication quoted by Alaga *et al.*, Rev. Mod. Phys. **28** 432

Cizewski, J. A., 1984, in Bosons in Nuclei, eds. D. H. Feng, S. Pittel and M. Vallieres, World Scientific, Singapore, p. 175

Cizewski, J. A., *et al*, 1978, Phys. Rev. Lett. **40** 167

Da Providencia, J., and J. N. Urbano, 1970, Nucl. Phys. **A158** 161

Da Providencia, J., and J. N. Urbano, 1971, Nucl. Phys. **A182** 174

Das, T. K., and B. Banerjee, 1973, Phys. Rev. C **7** 2590

Das, T. K., R. M. Dreizler and A. Klein, 1970, Phys. Rev. C **2** 632

Davidson, J. P., 1962, Nucl. Phys. **33** 664

Davidson, M. G., 1965, Nucl. Phys. **69** 455

Davidson, M. G., 1967, Nucl. Phys. **A103** 153

Davidson, M. G., 1970, Phys. Rev. C **2** 1814

Davidson, W. F., *et al*, 1981, J. Phys. G **7** 455

Davydov, A. S., and A. A. Chaban, 1960, Nucl. Phys. **20** 499

Davydov, A. S., and G. F. Filippov, 1958, Nucl. Phys. **8** 237

De Voigt, M. J. A., J. F. W. Jansen, F. Bruining and Z. Sujkowski, 1976, Nucl. Phys. **A270** 141

Diamond, R. M., F. S. Stephens and W. J. Swiatecki, 1964, Phys. Rev. Lett. **11** 315

Dieperink, A. E. L., O. Scholten and F. Iachello, 1980, Phys. Rev. Lett. **44** 1747

Draper, J. E., 1972, Phys. Lett. **41B** 105

Dukelsky, J., J. Fernández Niello, H. M. Sofia and R. P. J. Perazzo, 1983, Phys. Rev. C **28** 2183

Eisenberg, J. M., and W. Greiner, 1970, *Nuclear Models*, North Holland Publishing Company, New York

Ejiri, 1966, Rep. No. INSJ 101

Elliot, J. P., 1985, Rep. Prog. Phys. **48** 171

Ferreira, P. L., J. A. C. Alcarás and V. C. A. Navarro, 1964, Phys. Rev. **136B** 1243

Feshbach, H., and F. Iachello, 1974, Ann. Phys. **84** 211

Gelberg, A., and A. Zemel, 1980, Phys. Rev. C **22** 937

Gorfinkiel, J. I., M. A. J. Mariscotti and C. Pomar, 1974, Phys. Rev. C **9** 1243

Gupta, R. K., 1973, Phys. Rev. C **7** 2476

Harris, S. M., 1964, Phys. Rev. Lett. **13** 663

Harris, S. M., 1965, Phys. Rev. **138** B509

Haxel, O., J. H. D. Jensen and H. E. Suess, 1949, Phys. Rev. **75** 1766

Haxel, O., J. H. D. Jensen and H. E. Suess, 1950, Z. Phys. **128** 295

Herzberg, G., 1950, *Molecular Spectra and Molecular Structure*, Vol. I, Van Nostrand Reinhold Company, New York

Heyde, K., J. Jolie, P. Van Isacker, J. Moreau and M. Waroquier, 1984, Phys. Rev. C **29** 1428

Heyde, K., P. Van Isacker, M. Waroquier, G. Wenes, Y. Gigase and J. Stachel, 1983, Nucl. Phys. **A398** 235

Holzwarth, G., 1982, Nucl. Phys., *Proceedings of the Nuclear Physics Workshop*, I.C.T.P., North–Holland, Amsterdam, p. 1–13

Iachello, F., 1979, in *Interacting Bosons in Nuclear Physics*, ed. F. Iachello, Plenum Press, New York, p. 1

Iachello, F., 1980, Nucl. Phys. **A347** 51

Iachello, F., 1981, *Interacting Bose–Fermi Systems in Nuclei*, Plenum, New York

Iachello, F. and O. Scholten, 1979, Phys. Rev. Lett. **43** 679

Inglis, D. R., 1954, Phys. Rev. **96** 1059

Janssen, D., R. V. Jolos and F. Dönau, 1974, Nucl. Phys. **A224** 93

Johansson, S. A. E., 1961, Nucl. Phys. **22** 529

Kerman, A. K., 1956, Dan. Mat. Fys. Medd. **30**, no. 15

Kerman, A. K., and C. M. Shakin, 1962, Phys. Lett. **1** 151

Klein, A., 1980, Phys. Lett. 93B 1

Konijn, J., F. W. N. de Boer, A. Van Poelgeest, W. H. A. Hesselink, M. J. A. de Voigt, and H. Verheul; 1981, Nucl. Phys. **A352** 191

Konijn, J., *et al*, 1982, Nucl. Phys. **A373** 397

Kusukari, H., and M. Sugawara, 1984, Z. Phys. A **317** 287

Kvasil, J., and R. G. Nazmitdinov, 1985, Nucl. Phys. **A439** 86

Larabee, A., *et al*, 1983, Contributions, Workshop on Nuclear Structure at High Spin, NBI

Lee, K., and T. C. Haertle, 1968, Nucl. Phys. bf A121 543

Lee, K., and D. R. Inglis, 1957, Phys. Rev. **108** 774

Lipas, P. O., 1984, in *Collective Phenomena in Atomic nuclei*, eds. T. Engeland, J. Rekstad and J. S. Vaagen, World Scientific, Singapore, p. 33

Lipas, P. O., and J. P. Davidson, 1961, Nucl. Phys. **26** 80

Mallmann, C. A., 1959, Phys. Rev. Lett. **2** 507

Mariscotti, M. A. J., 1970, Phys. Rev. Lett. **24** 1242

Mariscotti, M. A. J., G. Scharff-Goldhaber, and B. Buck, 1969, Phys. Rev. **178** 1864

Marshalek, E. R., 1971, Phys. Rev. C **4** 1710

Mayer, M. G., 1949, Phys. Rev. **75** 1969

Mayer, M. G., 1950, Phys. Rev. **78** 16, 22

Neergård, K., and P. Vogel, 1969, Phys. Lett. **30B** 75

Neergård, K., and P. Vogel, 1970a, Nucl. Phys. **A145** 33

Neergård, K., and P. Vogel, 1970b Nucl. Phys. **A149** 209

Nilsson, S. G., 1955, Dan. Mat. Fys. Medd. **29**, no. 16

Otsuka, T., A. Arima, F. Iachello and I. Talmi, 1978, Phys. Lett. **76B** 139

Rowe, D. G., 1967, Phenomenological Collective Models in *Fundamentals in Nuclear Theory*, International Atomic Agency, Vienna, p.93

Saethre, Ø, S. A. Hjorth, A. Johnson, S. Jägare, H. Ryde and Z. Szymanski, 1973, Nucl. Phys. **A207** 486

Scharff-Goldhaber, G., 1980, Nucl. Phys. **A347** 31

Scharff-Goldhaber, G., 1984, in *Interacting Boson-Boson and Boson-Fermi Systems*, ed. O. Scholten, World Scientific, Singapore, p. 364

Scharff-Goldhaber, G., and M. Dresden, 1980, Trans. New York Acad. of Sci., Ser. II **40** 166

Scharff-Goldhaber, G., C. B. Dover and A. L. Goodman, 1976, Ann. Rev. Nucl. Sci. **26** 239

Scharff-Goldhaber, G., and A. S. Goldhaber, 1970, Phys. Rev. Lett. **24** 1349

Scholten, O., 1975, *Computer Program* PHINT- *Univ. Groningen*, The Netherlands

Scholten, O., 1984, *Interacting Boson-Boson and Boson-Fermi Systems*, World Scientific, Singapore

Singh, K. and H. S. Sahota, 1985, Indian J. Phys. **59A** 157

Sood, P. C., 1967, Phys. Rev. **161** 1063

Sood, P. C., and A. K. Jain, 1975, Phys. Rev. C **12** 1064

Stachel, J., *et al*, 1982, Nucl. Phys. **A383** 429

Stephens, F. S., N. Lark and R. M. Diamond, 1965, Nucl. Phys. **63** 82

Stephens, F. S., and R. S. Simon, 1972, Nucl. Phys. **A183** 257

Strutinsky, W. M., 1957, J. Nucl. Energ. **4** 523

Sujkowski, Z., D. Chmielewska, M. J. A. de Voigt, J. F. W. Jansen and O. Scholten, 1977, Nucl. Phys. **A291** 365

Talmi, I., 1982, in *Contemporary Research topics in Nuclear Physics*, eds. D. H. Feng, M.

Vallieres, M. Guidry and L.L. Riedinger, Plenum, New York

Thieberger, P., 1970, Phys. Rev. Lett. **25** 1664

Thompson, J. V., M. W. Johns and J. C. Waddington, 1975, Can. J. Phys. **53** 1229

Van Isacker, P., K. Heyde, M. Waroquier and G. Wenes, 1982, Nucl. Phys. **A380** 383

Varshni, Y. P., 1968, Prog. Theor. Phys. **40** 1181

Varshni, Y. P., 1974, J. Phys. Soc. Japan **36** 317

Varshni, Y. P., and S. Bose, 1972, Phys. Rev. C. **6** 1770

Vogel, P., 1968, Nucl. Phys. **A112** 583

Warner, D., 1984, in Bosons in Nuclei, eds. D. H. Feng, S. Pittel and M. Vallieres, World Scientific, Singapore, p. 133

Wood, J. L., 1983, Nucl. Phys. **A396** 245c

Yoshida, N., A. Arima and T. Otsuka, 1982, Phys. Lett. **114B** 86

Chapter II Analysis of Negative–Parity Bands

1. Introduction

The first observation of a negative–parity level was done in 1953 at the Berkeley Radiation Laboratory. Asaro, Stephens and Perlman (1953) observed a 1^- state in the α–decay spectrum of ^{228}Th. The parity of this state was inferred on the evidence that the associated γ–transition had E1 multipolarity. A year later, the same authors were able to report the observation of negative–parity levels in the level scheme of two more heavy nuclei: ^{226}Th and ^{222}Ra (Stephens, Asaro and Perlman, 1954). And in 1956, the study of radiation emitted by irradiated europium isotopes had led to the observation of negative–parity levels in the level scheme of the rare–earth nuclei ^{152}Sm and ^{152}Gd (Nathan and Waggoner, 1956; Kendall and Godzins, 1956). In the last decade, the development of new experimental techniques, and in particular, of the Ge(Li) detector, has allowed the observation of many energy levels with intermediate (10 $\hbar$ to 20 $\hbar$) and high ($\geq 30\hbar$) angular momenta. Many experimental investigations using these techniques were carried out; the purpose of which was often the study of the positive–parity yrast sequence (Dors *et al*, 1979). We will briefly discuss about the experimental techniques and methods used to study the data. Particular emphasis will be given to the determination of oscillating negative–parity bands.

As a result of the experimental investigations, much information about negative–parity bands extending to high–spin values was accumulated for different nuclei. We are particularly interested in the data obtained for the negative–parity bands of the isotopes of the following rare–earth elements: dysprosium, erbium, ytterbium, hafnium and tungsten. We have compiled, to the best of our knowledge, the data available for the negative–parity bands of these five elements. Due to the large number of bands and the appearance of regularities, we have subdivided the bands into three general groups: i) regular bands, ii) oscillating bands and iii) bands showing band crossings. Each of these groups is charac-

terized by a particular band structure on a ΔE vs I plot (here, ΔE denotes the energy difference between two adjacent levels in the band and I is the spin (or angular momentum) associated with the higher level). For regular bands, the typical $\overline{\Delta E}$ vs I plot consists of a smoothly increasing curve, either slightly concave upward or downward. The second class, denoted by oscillating, is characterized by oscillations of the energy difference with increasing spin. We prefer to use this title for the group rather than the title "bands with alternating energy–shift terms" (signature terms) which has been used by Peker *et al* (1983). Such a name is rooted in the conventional Bohr–Mottelson Model and should not, in our opinion, be associated with experimental observations. Bands showing band crossings are characterized by dips in the ΔE vs I plot. Sometimes, however, this structure is obscured by a large interaction between the bands and we have found it useful to investigate the properties of these bands on the conventional $2\Im/\hbar^2$ vs $(\hbar\omega)^2$ backbending plot (Sec. 4.6 of this chapter.). This particular type of graph enhances the structural properties of the bands since the energy difference between levels rather than the level energies are used to define the points on the plot. We have therefore also used it for an analysis of regular bands. The subdivision we propose is important from a physical standpoint since it dictates which theoretical models might be applicable in the different cases.

Systematic applications of theoretical models to the study of negative–parity bands are few (Sec. 2.4 of Chap. I): only selected applications are found, usually associated with experimental investigations and restricted to a single nucleus. We note the work of Peker *et al* (1981) and of Sheline (1980), but these are concerned with transuranic elements. We do not know of any previous general phenomenological investigation of the properties of negative–parity bands for rare–earth nuclei.

The regular negative–parity bands we have considered all have 6 or more levels while the oscillating bands have ten or more levels before their separation into even and odd sequences. Furthermore, the nuclei to which we have limited our theoretical study all fall in the class of well–deformed nuclei, i.e. the ratio of E_4 to E_2 is between 3 and

10/3. Exceptions are noted for for ^{156}Dy, ^{162}Yb and ^{166}Hf which have $E_4/E_2 \sim 2.9$ (this corresponds to the transitional region between the rotational and vibrational limits). The fact that the nuclei show rotational characteristics indicates that reasonable results should be obtained within the framework of the Bohr–Mottelson Model. To analyze the experimental data, we used the equation

$$E_I = E_2 + A\{I(I+1) - K^2\} + B\{I(I+1) - K^2\}^2 + C\{I(I+1) - K^2\}^3 \qquad (1.1)$$

This equation is a truncated form of eq. (2.9) of chapter I. The oscillating term $\sum_i (-1)^{I+K}(I+K)!/(I-K)!\{I(I+1) - K^2\}^i$ has been omitted because the experimental data for the bands we will study indicate that no oscillations are present. Indeed, such an equation, without the cubic term, is often used (Dors *et al*, 1979) in the analysis of negative–parity bands. We will find that the inclusion of the cubic term is necessary to obtain good agreement with experiment.

The rotational properties of the nuclei under consideration also suggest the application of the Variable Moment of Inertia Model, which is known to provide accurate results for the energy levels of the ground state band of well–deformed nuclei (Sec. 3 of Chap. I). It is therefore of much interest to explore the merits of this model for the negative–parity bands of these nuclei.

Recent emphasis in nuclear physics has been directed towards the study of boson models such as the Interacting Boson Model (Sec. 4. of Chap. I). These models have analytical solutions such as the Ejiri equation and the Varshni formula. Although these equations are derived for the ground state band, it seems appropriate to empirically test their performance for excited negative–parity bands. We have primarily considered the Varshni formula (our investigation of the superband in Chapter III showed that the Varshni formula was to be preferred over the Ejiri equation. Since both the superbands and the regular negative–parity bands show similar phenomenology, we have opted for the Varshni formula). From our study of regular negative–parity bands in terms of the results of boson

models will arise an interesting question: are these excited bands mainly of vibrational or rotational character?

2. Experimental Assignment of Spin and Parity

The experimental data are gathered by carrying out γ–γ coincidence measurements, usually with Ge(Li) detectors (recently, Ge detectors have superseded Ge(Li) detectors (Bengtsson and Garrett, 1984)). These detectors have resolutions varying between 1 % and 2 % for energy levels in the 0.1 MeV to 1 MeV range (Dors *et al*, 1979). The assignment of the spin and parity of the energy levels is done by considering the γ-ray angular distribution and electron conversion measurements (Walker *et al*, 1979). The γ–ray distribution is obtained by fitting the experimental data with an expression in terms of Legendre polynomials (Dors *et al*, 1979):

$$W(\theta) = \sum_{k=0,2,4} A_k P_k(\cos(\theta))$$

The type of transition, whether it is of dipole or quadrupole type, can be extracted from the parameters A_k. Electron conversion measurements use the fact that nuclei in high angular momentum states can deexcite by knocking out inner shell atomic electrons (Segré, 1977). These electrons, named conversion electrons, carry information about the γ–ray transition energy and the transition's multipolarity. When the electron conversion coefficient, defined as the ratio of the number of knocked out electrons to the number of γ–rays coming from a specific transition, is small, the negative parity of the levels can be assigned (Walker *et al*, 1979).

The grouping of energy levels into collective bands, and of particular interest to us, the assignment of levels to negative–parity bands, is done on the basis of such information as in–band transitions, decay of levels to other bands, theoretical model predictions, and the empirical rule that the transition intensity between energy levels decreases as the angular momentum increases (Pavlichenkov, 1981). The strongest evidence for the grouping of a

series of levels into a collective band is the observation of strong E2 (quadrupole) transitions linking levels with angular momentum differences of $2\hbar$ (i.e. an even–spin sequence or an odd–spin sequence). The less reliable method of classification might be the use of theoretical models.

For negative–parity bands, the first three criteria mentioned have been used extensively (see references associated with the oscillating bands presented in Table 2.1). For an example of the use of the fourth criterion, one can refer to the work on ^{164}Er by Kistner, Sunyar and der Mateosian (1978) or to the work on ^{162}Dy by Walker *et al* (1981). The latter authors have also used the uncertain criterion that sufficient reason for positioning levels in a band was the absence of any other suitable level candidates.

3. Oscillating Bands

Oscillating bands have been found experimentally for many rare–earth nuclei. In particular, this type of band structure is observed for γ–bands and some negative–parity bands. We will tabulate the experimental evidence concerning the oscillating negative–parity bands of the rare–earth elements dysprosium, erbium, hafnium, ytterbium and tungsten. From this, we will investigate the experimental results suggesting the possibility of separating these oscillating bands into an even–spin band and an odd–spin band.

We have compiled the experimental data concerning 14 oscillating bands for the rare–earth elements considered. This compilation regroups all the oscillating bands with a sufficient number of energy levels to allow for theoretical study. It is interesting to note that the different bands can be classified according to the type of oscillation involved. A simple subdivision picture allows three groups: i) type 1, which show distinct oscillations over the whole band, ii) type 2, which show oscillations beginning after a few non–oscillating levels and iii) type 3, which show oscillatory behavior restricted to a part of the band. Figures 2.1, 2.2 and 2.3 show plots of the first difference of the energy ΔE as a function of the angular momentum I. These plots exhibit well the different characteristics emphasized

in the subdivision. To complete the classification, we identify the oscillatory type of each the bands in the Table 2.1. We have also prepared a detailed table (Table 2.2), which includes the oscillating negative–parity bands for the five elements considered, to facilitate the retrieval of information about the γ–transitions involved. This table gives the K^π values of the bands (this label should be viewed as a convenient way of identifying the bands (Fields *et al*, 1984). The multipolarities of the in–band transitions are separated into four columns, depending on whether the transitions are from even–parity level to even–parity level ($\Delta I = 2\hbar$), odd–parity level to odd–parity level ($\Delta I = 2\hbar$), even–parity level to an adjacent odd–parity level and odd–parity level to an adjacent even–parity level. Information about the interband transitions has been included in the last column of the table.

We have adopted to include in Table 2.2, whenever possible, the most precise information. Characterizations such as mixed indicate that only partial information was available, i.e. no multipolarity is given. In the four columns reserved to in–band γ–transitions, a " yes " indicates that the transitions are observed without a multipolarity assignment.

We see from the Table 2.2 that the even–spin levels are usually linked together by quadrupole transitions which indicate the collectivity of the sequence. In most cases, transitions are observed over all even–spin energy levels in the bands. We note, however, that for some bands, the observed even–spin level to adjacent even–spin level transitions are few. This is the case for the $K^\pi = 6^-$ band of ^{162}Dy where a single transition, from $14^- \rightarrow 12^-$ is observed (Fields *et al*, 1982) and the $K^\pi = 2^-$ band of ^{164}Er where only the $10^- \rightarrow 8^-$ and the $8^- \rightarrow 6^-$ transitions are seen (Fields *et al*, 1984). In the case of the $K^\pi = 1^-$ band of ^{174}Hf which extends from $I^\pi = 2^-$ to $I^\pi = 17^-$, no transition is observed (Walker, 1983) between the 6^- and 4^- levels and the 4^- and 2^- levels. A similar observation is made for the $K^\pi = 2^-$ band of ^{162}Dy for which the $4^- \rightarrow 2^-$ transition is missing. We note that the $K^\pi = 0^-$ band of ^{166}Yb consists uniquely of odd–spin energy levels (Fields *et al*, 1984; Walus, 1981), this band being a particular case of an oscillating

band for which no even–spin level is present.

The situation is somewhat different in the case of the odd–spin sequences. There are only three reported cases of oscillating bands for which the odd–spin level sequence is linked by quadrupole transitions. These are the $K^\pi = 5^-$ band of ^{164}Er, for which this type of transition is observed (Yates *et al*, 1980) down to the $I^\pi = 11^-$ level, the $K^\pi = 0^-$ band of ^{166}Yb, for which this type of transition is observed (Walker, 1983) down to the $I^\pi = 5^-$ level, and the $K^\pi = 2^-$ band (Dors *et al*, 1979) of ^{178}W. Transitions of unidentified multipolarities are observed between the upper odd–spin members of the $K^\pi = 1^-$ band (Walker, 1983) of ^{174}Hf, for the $13^- \rightarrow 11^-$ and $11^- \rightarrow 9^-$ transitions in the $K^\pi = 1^-$ band (Walker *et al*, 1980) of ^{172}Yb and between the odd–spin levels of ^{180}W ($K^\pi = 2^-$) (Mann *et al*, 1979), of ^{176}Hf ($K^\pi = 2^-$) (Khoo *et al*, 1973) and of ^{170}Yb ($K^\pi = 3^-, 4^-$) (Walker *et al*, 1981).

The link between odd–spin and even–spin or even–spin and odd–spin levels is less clear. Only in the case of the $K^\pi = 3^-$ band (Walker *et al*, 1981) of ^{170}Yb are all the levels linked together. Partial information concerning $\Delta I = 1$ transitions is available for two bands. Both the lower spin portions of the $K^\pi = 2^-$ band (Mann *et al*, 1979) of ^{180}W and the $K^\pi = 4^-$ band (Walker *et al*, 1981) of ^{170}Yb are linked by γ–transitions. In three additional cases, even–spin to odd–spin γ–transitions are observed: all possibilities for the $K^\pi = 5^-$ band (Fields *et al*, 1982) of ^{162}Dy, the $10^- \rightarrow 9^-$, $8^- \rightarrow 7^-$ and $6^- \rightarrow 5^-$ transitions for the $K^\pi = 5^-$ band (Yates *et al*, 1980) of ^{164}Er and the $6^- \rightarrow 5^-$ and $4^- \rightarrow 3^-$ transitions for the $K^\pi = 2^-$ band (Walker, 1979) of ^{174}Hf.

The negative–parity oscillating bands are characterized by many interband transitions. In particular, the odd–spin band members usually decay to the ground state band by γ–transitions of E1 multipolarity. These γ–transitions may be stronger than the in–band transitions, which might explain why odd–spin to odd–spin transitions are not as common as their even–spin counterparts (Walker *et al*, 1981). Interband transitions are not as important a mode of decay for the even–spin members of the oscillating bands. As observed,

these levels often decay to the bandhead level via E2 transitions although some branching to the γ–band (Fields *et al*, 1982) ($K^\pi = 2^-$ of ^{162}Dy) and to the ground state band (Fields *et al*, 1982; Khoo *et al*, 1973) ($K^\pi = 6^-$ of ^{162}Dy and $K^\pi = 2^-$ of ^{176}Hf) is seen.

On the basis of the actual status of the experimental evidence, we see that the joint assignment of even and odd angular momentum energy levels to oscillating negative–parity bands is not indisputable. Although it was not mentioned as an explicit splitting, Fields *et al* (1984) studied the $K^\pi = 2^-$ band of ^{164}Er by considering the even–spin and odd–spin parts separately. This type of separation is also implicit in the work of Mann *et al* (1979). They present a $2\Im/\hbar^2$ vs $(\hbar\omega)^2$ plot of the $K^\pi = 2^-$ band of ^{180}W which shows the odd– and even– spin members separately.

The main evidence in favor of oscillating bands would be the observation of γ–transitions linking levels separated by angular momenta of $\hbar$. For most oscillating bands, this information is lacking. Furthermore, when these transitions are seen, they usually involve regions of the bands where the oscillation is small. This implies that the purely oscillating bands such as the $K^\pi = 1^-$ bands of ^{174}Hf and ^{172}Yb and the $K^\pi = 2^-$ band of ^{178}W cannot be justified on these grounds.

Experimentalists therefore consider another criterion to assign levels to oscillating bands. The $\Delta I = \hbar$ sequence of levels is established from the observation of several γ–transitions to other bands (Kistner, Sunyar and der Mateosian, 1978) (particularly the ground state band). Branching ratios to these bands must then be in good agreement with those predicted by theoretical models (Bäcklin *et al*, 1967) for the assignment to be valid. This method is therefore dependent upon the model which is assumed.

In view of the fact that the principal model (Bohr, 1952; Bohr and Mottelson, 1953) concerning nuclear collective effects was proposed by Bohr and Mottelson long before oscillating negative–parity bands were observed experimentally, it is questionable whether the assignment of all oscillating bands is unbiased. If the oscillating negative–parity bands of the first two types are separated into even–spin and odd–spin sequences of levels, the

collective nature of the independent bands is clearly established from the fact that the levels are linked together by quadrupole transitions. Certainly, the highly regular appearence of the even–spin band and the odd–spin band on a $2\Im/\hbar^2$ vs $(\hbar\omega)^2$ plot (these graphs are presented in Sec. 4 of this chapter), would allow excellent representation from other theoretical models.

The $K^\pi = 2^-, 5^-$ bands of ^{164}Er and the $K^\pi = 0^-$ band of ^{166}Yb create difficult theoretical interpretations because they show localized interactions (type 3 oscillating bands). Their structure cannot be obtained in terms of the Bohr–Mottelson equation (eq. (2.9) of Chap. I). But we still separate the even– and odd– spin sequences and investigate their behavior on a $2\Im/\hbar^2$ vs $(\hbar\omega)^2$ plot. We find, from Figure 2.4, that the unusual structure of the $K^\pi = 2^-$ band of ^{164}Er, and in particular, the inversion of the 3^- and 4^- levels is due to band crossing effects in the even–spin level sequence. Too few levels have been observed for a discussion of the odd–spin sequence. For the $K^\pi = 5^-$ (Figure 2.5) band of the same nucleus, the structure of the even part is what we defined as regular while there is a large displacement of a single level in the odd part of the band, but the overall structure is also regular. Finally, the band for ^{166}Yb cannot be explained within our framework because only odd–spin energy levels are present. These results show that even the more complicated structures of the oscillating bands are simply explained if the bands are separated into two sequences of levels.

Furthermore, the in–band transitions between even–spin and odd–spin (or odd–spin and even–spin) members of the oscillating bands might be interpreted as interband transitions between two negative–parity bands. This situation is observed by Dracoulis *et al* (1977) in the cases of the negative–parity bands of ^{172}Hf and ^{174}W. For both of these nuclei, interband transitions are observed between the even–spin band and the odd–spin band ($\Delta I = 1$). The odd–spin bands decay to the ground state bands. As a striking example, we show in Figure 2.6 the (oscillating) band obtained when we put together the two bands of ^{172}Hf.

These general observations about the negative-parity oscillating bands have led us to study the separated sequences of levels. The results are presented in Sec. 4 of this chapter. We note that the recent report (Larabee *et al*, 1983; Simpson *et al*, 1984) of many negative-parity bands composed of all even-spin or all odd-spin levels supports our separation scheme from the experimental point of view.

4. Theoretical Analysis of Regular Bands

4.1. Introduction

The present status of theoretical knowledge for negative-parity bands is that their structure arises from many interactions between themselves. Phenomenologically, they are thought to be strongly perturbed rotational bands. The mechanism giving rise to the bands is assumed to be the alignment of an $i_{\frac{13}{2}}$ quasineutron's angular momentum along the core's angular momentum, i.e. the decoupling phenomenon (Flaum and Cline, 1976; Vogel, 1976). Such a mechanism is also thought to be responsible for the backbending effect (Chapter III). Yates *et al* (1980), consider the complex situation of a four band coupling analysis with interactions due to the Coriolis effects.

We believe that in many cases, these methods of analysis overlook the fact that interactions between bands seem not to be required to explain the structure of the regular bands and the oscillating bands which we consider in this chapter (we have established in Sec. 3 of this chapter the experimental justification for their separation into regular bands). Also, an analysis in terms of the results of anharmonic vibrator models (boson Hamiltonians) overcomes many of the problems encountered within the rotational picture. To establish this fact, we proceed, in this section, to give the results of a detailed comparison of these two approaches.

4.2. Value of K

The Variable Moment of Inertia and the Bohr–Mottelson Models both require the specification of the quantum number K. We recall that K represents the projection along the nuclear symmetry axis of the total angular momentum (see Sec. 2.2 of Chap. I). In our work, we considered K as a constant rather than an independent parameter. We chose, whenever it was provided, the value assigned for K in experimental investigations. This was the case for 14 regular bands out of the 18 we studied. The assigned values of K and the references from which we obtained this information are given in Table 2.3.

When K is not assigned experimentally, the simplest assumption is to specify it as being equal to the lowest spin value for the energy levels of the band, i.e. the bandhead spin value. A total of 4 K assignments were made according to this criterion. Certainly, this choice is justified if the bandhead level is isomeric (long–lived) since the band cannot have an unobserved lower spin extension. When this level is not isomeric, we can speculate about the possible existence of unobserved low–lying band members, and therefore, a different assignment for K. Such a question, however, must be provided with an experimental rather than a theoretical answer.

For the separated oscillating bands, the assignments of K were all done in a similar fashion: experimental papers reported the value of K for the oscillating band and we associated this value if it was even, to the even sequence of levels and if it was odd, to odd sequence of levels. For the other part of the band, we assigned for K the spin value of its lowest level.

Recent experimental investigations (Fields *et al*, 1984) suggest that little physical significance is to be given to the values of K because of interactions between the excited bands; rather, they should be viewed as a convenient way to label the bands. We agree with this fact but for other reasons. As mentioned, we think that interactions do not play an important role in the structure of regular bands. The insignificance of K is then to be attributed to the following factors: our analysis showed that the energy level predictions of the Variable Moment of Inertia are usually insensitive to variations of K (in the case of the

Bohr–Mottelson equation, the introduction of K is superfluous because a renormalisation of the parameters includes its effect). More importantly, the fact that K is associated with rotational models strongly limits its justification (as we will see, the vibrational model is to be preferred).

4.3. Calculations and Results

A least–squares fit was performed, using the Variable Moment of Inertia Model (eq. (3.18) of Chap. II), the Varshni formula (eq. (4.19) of Chap. II) with the inclusion of a bandhead parameter and the Bohr Mottelson Series expansion (truncated at the $I^3(I+1)^3$ term; eq. (1.1)), to obtain the parameters for 18 regular bands and 12 separated (oscillating) bands of the five rare–earth elements dysprosium, erbium, ytterbium, hafnium and tungsten. All the energy values were weighted with the square of their inverse. This allows us to take into account the experimental uncertainties which are usually smaller for the low–spin levels. Only for ^{174}Hf are the low–lying levels uncertain while higher spin levels are not. Also, the fact that the weighting factor does not vary a lot (relative to the variations observed for the ground state band) represents well the situation with experimental uncertainties for negative–parity bands.

The determination of the parameters in the Varshni formula and the Bohr–Mottelson expansion is direct because of the simple analytical form of the equations. For the Variable Moment of Inertia equation, the determination of the parameters is somewhat more involved (see eq. (3.6) of Chap. II). In all three cases, we did not encounter convergence problems. This is certainly due to the small number of parameters involved in the three models.

The parameters for the three models are presented in Tables 2.4, 2.5 and tables 2.6, 2.7. We give divided tables for the regular bands and separated oscillating bands to allow easy comparison between the two sets of parameters. The results of the three models are given in table 2.8. The many rows for each band of the table have the following meaning: a) the 1^{st}

row gives the spin and parity assignments of the band, with uncertain assignments shown between parentheses. We did take into consideration the uncertain levels in our analysis. b) The 2^{nd} row presents the experimental energy values, with uncertain values shown between parentheses. c) The 3^{rd} and 4^{th} rows give respectively the the Variable Moment of Inertia Model predictions and the difference between theory and experiment. The four extra levels to which do not correpond experimental levels are the model's predictions. These predictions have also been included for the other models. d) The 5^{th} and 6^{th} row provide results and relative differences obtained with the Varshni formula. e) The 7^{th} and 8^{th} row give similar information for the Bohr–Mottelson equation. Further rows are a continuation of the ones described. The omission of some rows in the second group should not cause any confusion: it indicates that no experimental data is available for these values of the spin. The order of presentation of the models remains the same. At the end of each row indicating the models' theoretical predictions, we have written the rms % deviation. These values will allow us to make a quantitative comparison of the models.

As a complement to the result tables, we have also plotted the experimental and theoretical values of the energy on $2\Im/\hbar^2$ vs $(\hbar\omega)^2$ plots (Fig. 2.7 to 2.36). These will allow us to note characteristics of the bands and qualitatively discuss certain points in Sec. 4.6.

4.4. Parameter Systematics

We have studied the possibility that there may be simple relations for the different model parameters as a function of the neutron number. We did not find any and attribute this to two reasons. For many of the nuclei we studied, more than one negative–parity band have been taken into account. This leads to more than one point for a given neutron number (coincidences are also noted because we have in some cases isotones). This obscures any possible trend (we also did not find any simple relations in plots of the parameters as a function of the number of valence nucleons). The second factor is that all the nuclei we

considered are well–deformed and are therefore in the middle of valence shells. Closed–shell effects, which give rise to striking changes in the parameter behavior (Mariscotti *et al*, 1969), do not affect the present situation. Search for sub–shell closures was also inconclusive.

We noted, however, the interesting presence of correlations between a given model's parameters. In the case of the Varshni formula, the bandhead parameter and the parameter p (associated with the angular momentum I) are correlated (see Fig. 2.37). This is a surprising results which is difficult to explain. The best correlation for the parameters of the Varshni formula if found between a and q (respectively associated with $I(I+1)$ and $I^2(I+1)$; Fig. 2.38). The highest order term seems to be dependent in some way on the preceeding one. We can speculate that this indicates the possibility of summing higher order terms in the angular momentum expansion by some type of potential energy term (certainly, the Variable Moment of Inertia formula is not the correct one). For the Bohr–Mottelson equation, only a weak correlation between the two higher terms is observed (Fig. 2.40). Other parameters of this model are not correlated (an example of this is given in Fig 2.39).

We also briefly considered the parameters obtained with the Variable Moment of Inertia Model, even though the model does not reproduce well the energy level sequence of regular bands . The moment of inertia parameter $\Im_0$ is in all cases greater than that of the ground state band (Mariscotti *et al*, 1969). In many cases, the stiffness parameter C becomes very large and essentially nullifies the potential energy term $\frac{1}{2}C(\Im - \Im_0)^2$, viz. the energy equation produces a horizontal line on the $2\Im/\hbar^2$ vs $(\hbar\omega)^2$ plot. This can be understood by considering an alternate form of the Variable Moment of Inertia equation for the energy levels:

$$E_I = \frac{I(I+1)}{2\Im}\left\{1 + \frac{I(I+1)}{4C\Im^3}\right\} \qquad (4.1)$$

obtained by substituting eq. (3.5) of Chap. I in the usual energy expression. Certainly, as $C \to \infty$, $E_I \to \frac{I(I+1)}{2\Im}$ and self–consistency of the equations imposes that $\Im = \Im_0$. The

equation we are left with is the lowest order truncation of the Bohr–Mottelson energy expansion. In such a case, $\Im_0$ is identified with the hydrodynamical moment of inertia of the nuclear band. When the parameter C takes values in the range $10^6 - 10^7$, the parameter $\Im_0$ is still related to the nuclear moment of inertia (through the Cranking Model).

In any case, the Variable Moment of Inertia parameter $\Im_0$ provides an estimate of the average moment of inertia of the negative–parity bands we have studied. For separated oscillating bands , in the situation where C is large (4 bands), the average of the individual moments of inertia is $\bar{\Im}_0 = (5.67 \pm 0.39)$ keV^{-1} and in the case were C$\sim 10^6 - 10^7$ (8 bands included), $\bar{\Im}_0 = (4.48 \pm 0.75)$ keV^{-1}. For regular bands , the average for 12 bands with large values of C is $\bar{\Im}_0 = (5.69 \pm 0.47)$ keV^{-1} and the average for 6 bands with C ranging from 10^6 to 10^7 is $\bar{\Im}_0 = (4.51 \pm 0.71)$ keV^{-1}. The uncertainties are the standard deviations in each case. Although these averages indicate similarities between the regular and oscillating bands, the large associated uncertainties render deductions difficult.

4.5. The rms % values and Relative Merits of the Models

The rms % values provide information allowing quantitative comparison of the merits of the different models we studied. We recall that the rms % value for a band is calculated by using the formula

$$\text{rms } \% = \sqrt{\frac{1}{N}\sum_{i=1}^{N}\left(\frac{E_{t_i} - E_{x_i}}{E_{x_i}}\right)^2} \times 100 \qquad (4.2)$$

where N is the number of experimentally observed levels, E_{t_i} and E_{x_i} respectively represent the theoretical and experimental energies. These rms % values are given Table 2.8.

We begin by a discussion of the model giving the less satisfactory results: the Variable Moment of Inertia Model. The overall poor performance of this model is immediately visible in the graphical analysis of the bands we have presented: the model is essentially limited to providing an average moment of inertia for the bands. The rms % values confirm this qualitative observation. In all cases, except for ^{166}Hf, for which it provides

the second best results, the model gives the worst results. It is not surprising that the Variable Moment of Inertia fits so well this nucleus since it has the suited linear increase in the moment of inertia with $(\hbar\omega)^2$. Other nuclei also show this behavior, ($^{174}Hf_d$, $^{164}Er_a$, $^{178}W_{a,b}$, $^{180}W_{b,c}$), and in these cases, the model gives reasonable results.

The situation is very poor for the more numerous type of negative–parity regular bands (the concave upward bands). In these cases, the inapplicability of the model cannot be due to the fact it has one less parameter than the other models. The potential energy term $\frac{1}{2}C(\Im - \Im_0)^2$ does not reproduce the experimental trends. It has been suggested that this term provides a summation of higher order terms in angular momentum expansions (Klein, 1980) which therefore explains its good prediction of the ground state band results. We may speculate that another potential energy term is required for summing up the higher order terms of the angular momentum expansions for negative–parity bands. Another possibility for improvement in the Variable Moment of Inertia framework is the study of 3 parameter generalizations of the model (Sec. 3 of Chap. I).

The Bohr–Mottelson series expansion and the Varshni formula provide good results for all regular bands. In 21 cases, the rms % deviation is smaller for the Varshni formula than for the Bohr–Mottelson equation while the converse is true in 9 cases. These 9 bands are: $^{162}Dy_{b,c}$, $^{170}Yb_c$, $^{172}Yb_{a,b}$, $^{174}Hf_d$, $^{178}W_d$ and $^{180}W_{a,b}$. The average of rms % deviations for all the bands is 0.089 for the Varshni formula and 0.186 for the Bohr–Mottelson equation.

This indicates that the Varshni formula is to be preferred over the rotational expansion for the isotopes of the rare–earths elements we have studied. This result is very interesting because we must remember that the nuclei considered are well–deformed ($E_4/E_2 \sim 10/3$) and that the Varshni formula is obtained in the framework of boson Hamiltonians which correspond to anharmonic vibrator models. We can speculate to which extent vibrational degrees of freedom gain importance as the nucleus acquires angular momentum (further discussion concerning this point is given below in Sec. 5.

We may try to gain further insight in the performance of these two models by con-

sidering other factors. In the 9 cases where the Bohr–Mottelson series works better, the average rms % deviation is 0.037 while the average for the Varshni formula is 0.058. The proximity of these two averages led us to consider another method to separate the models: high spin level predictions.

For all the regular bands, we determined the parameters of each model by a least–squares fit to the energy levels of the bands with the exclusion of the last one. Predictions were then calculated for the last level and the relative % deviations evaluated. The results are presented in Table 2.9.

We have found that the predictive power of the Bohr–Mottelson expansion is poor (the same problem was also observed in analyses of the ground state band (Diamond, 1964)). In 4 cases where it fitted better ($^{162}Dy_{c,b}$; $^{172}Yb_c$; $^{180}W_a$), it gives worse predictions than the Varshni formula. For $^{180}W_b$, the predictions of the two models are equal. The marginal preference of the Bohr–Mottelson equation over the Varshni formula is therefore restricted to only 4 bands out of the 30 we analyzed: $^{170}Yb_c$, $^{172}Yb_a$, $^{174}Hf_d$ and $^{178}W_b$ (in these cases, the Varshni formula also works very well). These bands, except for $^{178}W_b$, have near perfect rotational characteristics, with respective maximum relative variations in the moment of inertia $2\Im/\hbar^2$ of 5%, 4%, 7% and 20 %.

We are therefore led to conclude that the reasonable Bohr–Mottelson results are due to the number of parameters involved in the analysis rather than due to a correct physical description of the negative–parity bands we studied. This is not the case, however, for the Varshni formula. The overall results are very good and the predictive power of the equation is reasonable. It would therefore be of interest to extend our investigation to other regions of the periodic table to see to what extent boson Hamiltonian results can be applied to excited bands. Certainly, our results support the interesting possibility of vibrational bands in well–deformed nuclei.

4.6. Graphical Analysis of Regular Bands

We have also chosen to analyze our results by considering the typical backbending plots which represent the moment of inertia, $2\Im/\hbar^2$, as a function of the angular frequency $(\hbar\omega)^2$. Different formulas have been proposed to obtain these values from the experimental data (Sorensen, 1973); we chose the simplest expressions:

$$\begin{aligned} (2\Im/\hbar^2)_{\Delta I=2} &\sim \frac{4I-2}{E(I+2)-E(I)} \\ (2\Im/\hbar^2)_{\Delta I=1} &\sim \frac{2I}{E(I+1)-E(I)} \end{aligned} \tag{4.3}$$

$$\begin{aligned} \left(\hbar\omega\right)^2_{\Delta I=2} &\sim \frac{E(I+2)-E(I)}{2} \\ (\hbar\omega)^2_{\Delta I=1} &\sim E(I+1)-E(I) \end{aligned} \tag{4.4}$$

where the subscripts identify the formula to use for the two spin increment possibilities. The principal reason for our choice of graph was that this type enhances the structural properties of the bands since the energy differences between levels rather than the level energies are used to define the points. We also note that on such plots, rotational motion, i.e. $E(I) = E_K + I(I+1)$, appears as horizontal lines.

From the plots (Fig. 2.7 to Fig. 2.36), a simple classification into two groups becomes evident: bands showing essentially a linear behavior on the plot and bands showing an upward concave curve. For separated oscillating bands, 4 curves fall in the linear category ($^{178}W_{a,b}$; $^{180}W_{a,b}$) while three regular bands are found to exhibit a similar behavior ($^{164}Er_a$; ^{166}Hf; $^{174}Hf_d$). The more common type of structure is however the concave upward one. Fourteen regular bands are of this type, with striking examples those observed for ^{166}Yb and $^{172}Hf_a$. There are six separated oscillating bands which fall in this category ($^{174}Hf_{a,b}$; $^{172}Yb_{c,d}$; $^{170}Yb_{c,d}$). We observe that the separated oscillating bands for ^{162}Dy present anomalous characteristics. They are concave downward rather than concave upward. This is the only case where we observe this structure. Furthermore, the bands show irregular variations in the moment of inertia $(2\Im/\hbar^2)$. In view of their peculiarity, and the fact that they are unique to ^{162}Dy, we cannot deduce much information about their relation to other bands.

5. Bands Showing Band Crossings

Recent experimental studies have permitted the observation of many band crossings in the negative–parity bands of rare–earth nuclei. We have gathered much information about these bands during our compilation of regular negative–parity bands and present these interacting bands by using the backbending plot described in Sec. 4.6 of this chapter (Fig. 2.41 to Fig. 2.53). The bands, and the sources of experimental data, are given in Table 2.10.

The accepted mechanism explaining these effects is the rotation–alignment of quasiparticles (Stephens and Simon, 1972; Flaum and Cline, 1976) i.e. the alignment of the angular momentum of quasineutrons (or quasiprotons) along the axis perpendicular to the nuclear symmetry axis. In view of the number of alignments necessary to explain the experimental data for negative–parity bands, the prolate axial symmetry assumed for the low–energy states of well–deformed nuclei might be destroyed. For high spins, the added angular momenta of the quasiparticles may produce oblate nuclear shapes (the possibility of observing such effects in the yrast band of rare–earth nuclei has generated many experimental investigations (Simpson *et al*, 1984; Fewell *et al*, 1985). The fingerprint of prolate to oblate shape transitions is the loss of collectivity in the level sequence and the appearance of single–particle properties for the states.

Assuming that the band crossing model is the correct theoretical interpretation of the negative–parity bands we present in this section, we observe that many band intersections are necessary to explain the structures appearing in the graphs. Often, two intersections, each characterized by a rapid increase in the moment of inertia, are seen for each band. In the particular case of the odd sequence of ^{158}Er, three crossings are observed (Larabee *et al*, 1983). This indicates that a systematic theoretical description of the bands would involve a large number of parameters. This fact, in turn, would obscure the meaning of the

results obtained. We have, for such reasons, not attempted any band-crossing calculation.

A systematic study of the plots reveals interesting properties: the most noticeable is the appearence, at definite values of the moment of inertia, of "plateaux". These plateaux correspond to near perfect rotational motion and would indicate that for small intervals of the spins, the nuclei assume rigid rotator characteristics. These structures are particularly well-defined for the highest spins of the bands. We believe that the near equality of the moments of inertia for the rotational regions of some of the bands is due to their similar number of valence nucleons. This is clear when we consider Fig. 2.41 for the N = 88 isotones or compare Fig. 2.42 to Fig 2.44. Similar frequency values are also noted for the transitions from one plateau to another.

A natural question which arises from the plots of this section is to what extent the initial part of the bands can be identified with the regular bands we considered in Sec 4. of this chapter. Certainly, the backbending bands appear to have the suited initial variation of $2\Im/\hbar^2$ as a function of $(\hbar\omega)^2$, i.e. a concave upward structure. It may therefore be that the regular bands are simply the initial portions of backbending bands. To determine this, we have plotted, in Fig 2.54 the highest spin as a function of the neutron number for all the bands for which we presented plots. The backbending bands and regular bands are respectively symbolized by dark symbols and open symbols.

Fig. 2.54 is very interesting for two reasons: it clearly shows that the observation of high spin bands is favored for the nuclei with fewer neutrons. This effect cannot be attributed to magic numbers since the middle of the shell corresponds to N = 104. The decrease in highest spin observed in approximatively linear with increasing neutron number. The second point of interest lies in the perfect dichotomy between bands showing 2 band crossings and regular bands. For bands showing a single band crossing, the situation is not as clear cut. The evidence observed seems to indicate that at least some of the regular bands will show backbending as higher spin values are observed.

Table 2.1. Type of oscillating negative–parity bands

Nucleus	Ref.	Band, K^π	Type 1	Type 2	Type 3
^{162}Dy	a	2^-		•	
		5^-		•	
		6^-	•		
^{164}Er	b	2^-			•
	c	5^-			•
^{168}Er	d	1^-	•		
^{166}Yb	e,f	0^-			•
^{170}Yb	g	3^-	•		
		4^-		•	
^{172}Yb	h	1^-	•		
^{174}Hf	i	1^-	•		
^{176}Hf	j	2^-		•	
^{178}W	k	2^-		•	
^{180}W	l	2^-		•	

References:

a) Fields *et al* (1982)
b) Fields *et al* (1984)
c) Yates *et al* (1980)
d) Burke *et al* (1985)
e) Walus *et al* (1981)
f) Fields, Hicks and Peterson (1984)
g) Walker *et al* (1981)
h) Walker *et al* (1980)
i) Walker (1983)
j) Khoo *et al* (1973)
k) Dors *et al* (1979)
l) Mann *et al* (1979)

Table 2.2. Experimental γ–transitions for Oscillating Bands.

Nucleus	Band K^π	In–band γ–transition multipolarities				Interband γ–transitions
		even–even	odd–odd	odd–even	even–odd	
^{162}Dy	2^-	E2				Even → γ–band, E1; Odd → GSB, E1
	5^-	E2			E2–M1	Even → $K^\pi = 2^-$, E2–M1; Odd → GSB, E1
	6^-	yes				Even and Odd → $K^\pi = 5^-$
^{164}Er	2^-	yes				Many transitions to other bands
	5^-	E2	E2		mixed	Odd → GSB
^{168}Er	1^-					No transition in level scheme
^{166}Yb	0^-	no even	E2	not applicable		Few transitions to GSB
^{170}Yb	3^-	E2	yes	yes	yes	Odd → GSB, E1
	4^-	E2	yes	yes	E2–M1	Odd → GSB, E1
^{172}Yb	1^-	E2	yes			Even and Odd → GSB
^{174}Hf	1^-	yes	yes			Odd → GSB
^{176}Hf	2^-	E2	yes		yes	Even and Odd → GSB, E1
^{178}W	2^-	E2	E2			Odd → GSB, E1
^{180}W	2^-	yes	yes	yes	yes	Odd → GSB, E1–M2–E3

Table 2.3. Values of K assigned for regular negative-parity bands. The identification of a band is made by the specification of the initial spin value, the final spin value and the spin increment between levels (see Tables 2.4 – 2.7).

Nucleus	Ref.	Band			K
^{162}Dy	a	1	11	2	0
^{164}Er	b	7	13	1	7
^{164}Er	b	1	11	2	0
^{166}Yb	c	6	22	2	5
^{166}Yb	c	2	12	2	2
^{170}Yb	d	7	12	1	7
^{170}Yb	d	1	15	2	1
^{172}Yb	e	6	14	1	6
^{172}Yb	e	4	12	1	4
^{172}Hf	f	4	24	2	0
^{172}Hf	f	5	25	2	1
^{174}Hf	g	6	15	1	6
^{174}Hf	g	8	13	1	8
^{178}W	h	7	16	1	7

References:

a) Helmer (1985)
b) Shurshikov (1986)
c) Fields *et al* (1984)
d) Walker *et al* (1981)
e) Walker *et al* (1980)
f) Paul *et al* (1985)
g) Walker (1983)
h) Dors *et al* (1979)

Table 2.4. Parameters for the VMI Model and the Varshni formula fits of regular negative-parity bands. The references are given in Table 2.5.

Nucleus	Sources of exptl. data	I_i, I_f, ΔI	VMI MODEL E_o (keV)	$\Im_0$ (10^{-3}keV^{-1})	C (keV^3)	VARSHNI FORMULA E_1 (keV)	p (keV)	a (keV)	q (keV)
^{156}Dy	a	3 13 2	1321.50	4.71626	$\sim 10^{18}$	1397.70	-92.5376	21.9608	-.439323
^{162}Dy *c*	b	1 11 2	1246.01	5.30613	$\sim 10^{20}$	1266.32	-9.41504	9.76181	.039278
^{162}Er	b	1 13 2	1278.22	6.12855	$\sim 10^{15}$	1395.06	-73.9442	15.8740	-.213217
^{164}Er *a*	c	7 13 1	1905.42	4.41162	8.308×10^6	1433.71	-35.2542	15.6432	-.198799
^{164}Er *b*	c	1 11 2	1346.84	6.16106	$\sim 10^{18}$	1338.72	-15.6435	7.15275	.207714
^{162}Yb	b	8 22 2	2193.92	5.86904	1.825×10^7	2601.81	-240.245	25.3924	-.390793
^{166}Yb *a*	d	6 22 2	1714.17	6.37913	$\sim 10^{19}$	1816.50	-84.4151	14.1000	-.146327
^{166}Yb *b*	e	2 12 2	1473.59	5.09024	5.360×10^6	1510.32	-57.0224	18.5633	-.444753
^{170}Yb *a*	f	7 12 1	2113.04	4.91584	$\sim 10^{20}$	2412.84	-279.419	37.0858	-.877349
^{170}Yb *b*	f, g	1 15 2	1299.71	5.94088	$\sim 10^{15}$	1385.37	-41.4576	11.1364	-.009140
^{172}Yb *a*	h	6 14 1	1494.07	5.66139	$\sim 10^{20}$	1255.65	-24.3268	10.8066	-.050934
^{172}Yb *b*	h	4 12 1	1583.56	5.68069	$\sim 10^{18}$	1639.57	-74.0560	15.5414	-.180487
^{166}Hf	i	7 21 2	1649.56	4.54423	2.285×10^6	1016.77	24.8261	10.3284	-.108502
^{172}Hf *a*	j	4 24 2	1228.84	5.65096	8.292×10^7	1340.87	-39.1035	12.1018	-.084090
^{172}Hf *b*	j	5 25 2	1245.50	5.88337	$\sim 10^{18}$	1409.65	-51.0206	12.2485	-.083935
^{174}Hf *c*	k	6 15 1	1652.15	5.70778	$\sim 10^{20}$	1474.39	-39.3394	11.7152	-.068686
^{174}Hf *d*	k	8 13 1	1693.52	3.84038	9.355×10^6	1002.11	-58.0155	19.9030	-.301022
^{178}W *c*	l	7 16 1	1632.28	5.74324	$\sim 10^{20}$	2381.34	-323.672	33.1478	-.599593

Table 2.5. Parameters for the VMI Model and Varshni formula fits of oscillating negative–parity bands.

Nucleus	Sources of exptl. data	I_i, I_f, ΔI	VMI MODEL E_o (keV)	$\Im_0$ (10^{-2}keV^{-1})	C (keV^3)	VARSHNI FORMULA E_1 (keV)	p (keV)	a (keV)	q (keV)
^{162}Dy *a*	b	2 12 2	1128.01	4.73088	4.110×10^7	1076.47	6.63444	9.64449	.032946
^{162}Dy *b*	b	3 13 2	1185.95	4.96653	2.736×10^6	1010.23	47.9762	4.31651	.152647
^{170}Yb *c*	f	4 16 2	1217.80	5.55755	$\sim 10^{17}$	1101.06	-7.31446	9.34463	.001678
^{170}Yb *d*	f	5 17 2	1300.40	5.65824	3.798×10^7	1105.73	-10.2715	9.89671	-.038850
^{172}Yb *c*	h	2 14 2	1178.12	5.20468	3.455×10^7	1148.66	-6.24323	10.5096	-.045219
^{172}Yb *d*	h	1 13 2	1130.38	6.15229	$\sim 10^{16}$	1147.41	-7.74726	78.1623	.071041
^{174}Hf *a*	k	3 17 2	1266.46	5.75658	$\sim 10^{20}$	1315.76	-46.8015	12.4206	-.083294
^{174}Hf *b*	k	2 14 2	1278.98	5.20784	$\sim 10^{17}$	1288.06	-27.6595	12.9158	-.120395
^{178}W *a*	l	2 12 2	1017.74	3.79107	9.416×10^6	975.775	-9.71135	15.1009	-.166482
^{178}W *b*	l	3 13 2	1081.16	3.83937	2.768×10^6	966.966	-3.34536	14.3053	-.224905
^{180}W *a*	m	2 10 2	980.405	3.87096	7.929×10^6	933.714	-5.49597	14.2434	-.146791
^{180}W *b*	m	3 11 2	1044.21	3.92521	5.473×10^6	932.448	-3.91237	13.9467	-.157918

References:

a) de Boer *et al* (1977)
b) Helmer (1985)
c) Shurshikov (1986)
d) Walus *et al* (1981)
e) Fields *et al* (1984)
f) Walker *et al* (1981)
g) Camp and Bernthal (1972)
h) Walker *et al* (1980)
i) Agarwal *et al* (1983)
j) Paul *et al* (1985)
k) Walker (1983)
l) Dora *et al* (1979)
m) Mann *et al* (1979)

Table 2.6. Parameters for the Bohr–Mottelson fits of regular negative–parity bands. The letters following the nuclei allow the identification of the $2\Im/\hbar^2$ vs $(\hbar\omega)^2$ plots for each band. The references have been given in Table 2.5.

Nucleus	Sources of exptl. data	I_i,	I_f,	ΔI	BOHR–MOTTELSON MODEL E_2 (keV)	A (keV)	B (10^{-3}keV)	C (10^{-5}keV)
^{156}Dy	a	3	13	2	1337.50	8.92724	26.1622	-9.92956
^{162}Dy *c*	b	1	11	2	1260.73	7.82570	25.3002	-9.95840
^{162}Er	b	1	13	2	1332.86	3.30683	60.9238	-18.8377
^{164}Er *a*	c	7	13	1	1906.50	11.2221	-1.68504	-.730485
^{164}Er *b*	c	1	11	2	1373.65	4.96290	40.0192	-11.5040
^{162}Yb	b	8	22	2	2218.33	7.40267	7.18204	-1.26068
^{166}Yb *a*	d	6	22	2	1738.94	7.04760	4.56759	-.654336
^{166}Yb *b*	e	2	12	2	1481.36	8.68508	19.4199	-10.3040
^{170}Yb *a*	f	7	12	1	2125.41	9.00004	23.0431	-12.2134
^{170}Yb *b*	f, g	1	15	2	1348.75	5.02626	31.1829	-6.88381
^{172}Yb *a*	h	6	14	1	1499.36	8.50913	3.65200	-1.06871
^{172}Yb *b*	h	4	12	1	1609.10	6.94112	24.4785	-8.15206
^{166}Hf	i	7	21	2	1652.81	10.6868	-6.87552	.520331
^{172}Hf *a*	j	4	24	2	1247.16	8.28806	2.84004	-.375332
^{172}Hf *b*	j	5	25	2	1275.57	7.77883	3.26648	-.362787
^{174}Hf *c*	k	6	15	1	1662.80	8.20968	5.13379	-1.21328
^{174}Hf *d*	k	8	13	1	1694.86	12.8692	-2.70107	-1.08840
^{178}W *c*	l	7	16	1	1689.49	5.90093	25.8175	-6.16270

Table 2.7. Parameters for the Bohr–Mottelson fits of separated oscillating negative–parity bands. The letters following each nucleus have the same meaning as in Table 2.6. The references are given in Table 2.5.

Nucleus	Sources of exptl. data	I_i,	I_f,	ΔI	BOHR–MOTTELSON MODEL E_2 (keV)	A (keV)	B (10^{-3}keV)	C (10^{-5}keV)
^{162}Dy *a*	b	2	12	2	1126.06	10.8658	-6.62811	2.83438
^{162}Dy *b*	b	3	13	2	1182.23	10.5701	-16.2385	4.92396
^{170}Yb *c*	f	4	16	2	1223.94	8.65595	2.63278	-.478239
^{170}Yb *d*	f	5	17	2	1301.43	8.75734	.555320	-.221556
^{172}Yb *c*	h	2	14	2	1179.38	9.46181	1.73128	-.774783
^{172}Yb *d*	h	1	13	2	1147.21	6.73450	14.7616	-3.62181
^{174}Hf *a*	k	3	17	2	1239.03	6.90022	12.9838	-2.36579
^{174}Hf *b*	k	2	14	2	1288.04	8.78683	10.3566	-3.20299
^{178}W *a*	l	2	12	2	1018.69	13.0234	-2.65539	-.970387
^{178}W *b*	l	3	13	2	1082.18	12.8108	-13.2878	1.82902
^{180}W *a*	m	2	10	2	980.718	12.8435	-4.70747	-.440956
^{180}W *b*	m	3	11	2	1044.34	12.7070	-8.38401	1.10903

Table 2.8. Theoretical results of the Variable Moment of Inertia Model, the Varshni formula and the Bohr–Mottelson Model for regular negative–parity bands. The many rows for each band of the table have the following meaning: a) the 1^{st} row gives the spin and parity assignments of the band, with uncertain assignments shown between parentheses. We did take into consideration the uncertain levels in our analysis. b) The 2^{nd} row presents the experimental energy values, with uncertain values shown between parentheses. c) The 3^{rd} and 4^{th} rows give respectively the the Variable Moment of Inertia Model predictions and the difference between theory and experiment. The four extra levels to which do not correpond experimental levels are the model's predictions. These predictions have also been included for the other models. d) The 5^{th} and 6^{th} row provide results and relative differences obtained with the Varshni formula. e) The 7^{th} and 8^{th} row give similar information for the Bohr–Mottelson equation. Further rows are a continuation of the ones described. The omission of some rows in the second group should not cause any confusion: it indicates that no experimental data is available for these values of the spin. The order of presentation of the models remains the same. At the end of each row indicating the models' theoretical predictions, we have written the rms % deviation.

^{156}Dy	3^-	5^-	7^-	9^-	11^-	(13^-)	15^-	17^-	19^-	21^-	rms % deviation
	1368.31	1525.94	1809.97	2186.58	2636.55	(3154.29)					
	1353.30	1544.13	1819.78	2180.23	2625.50	3155.58	3770.47	4470.18	5254.70	6124.03	0.728
	15.01	-18.19	-9.81	6.35	11.05	-1.29					
	1367.80	1527.94	1807.53	2185.48	2640.72	3152.14	3698.67	4259.21	4812.68	5337.99	0.107
	0.51	-2.00	2.44	1.10	-4.17	2.15					
	1364.51	1535.59	1804.56	2179.49	2646.58	3150.80	3571.78	3695.28	3179.99	1519.77	0.372
	3.80	-9.65	5.41	7.09	-10.03	3.49					

^{162}Dy	1^-	3^-	5^-	(7^-)	(9^-)	(11^-)	13^-	15^-	17^-	19^-	rms % deviation
	1275.97	1357.95	1518.94	1755.5	2101.0	2504.6					
	1264.85	1359.08	1528.70	1773.70	2094.08	2489.85	2961.00	3507.54	4129.46	4826.77	0.672
	11.12	-1.13	-9.76	-18.20	6.92	14.75					
	1276.51	1356.63	1517.99	1762.47	2091.96	2508.35	3013.51	3609.33	4297.70	5080.51	0.252
	-0.54	1.32	0.95	-6.97	9.04	-3.75					
	1276.48	1358.11	1515.58	1760.82	2097.38	2505.51	2922.70	3219.54	3171.06	2423.47	0.170
	-0.51	-0.16	3.36	-5.32	3.62	-0.91					

^{162}Dy	2^-	4^-	6^-	8^-	10^-	(12^-)	14^-	16^-	18^-	20^-	rms % deviation
	1148.38	1297.16	1530.53	1845.91	2234.63	2724.8					
	1149.15	1296.96	1528.76	1843.93	2241.65	2720.92	3280.57	3919.32	4635.76	5428.41	0.157
	-0.77	0.20	1.77	1.98	-7.02	3.88					
	1148.00	1298.53	1529.65	1842.93	2239.95	2722.30	3291.56	3949.30	4697.12	5536.59	0.133
	0.38	-1.37	0.88	2.98	-5.32	2.50					
	1147.77	1298.33	1530.94	1843.20	2237.12	2724.06	3330.92	4107.62	5135.96	6539.71	0.088
	0.61	-1.17	-0.41	2.71	-2.49	0.74					

^{162}Dy	3^-	5^-	7^-	9^-	(11^-)	(13^-)	15^-	17^-	19^-	21^-	rms % deviation
	1210.24	1408.46	1637.73	1959.48	2331.9	2778.21					
	1216.09	1394.24	1644.47	1961.02	2338.31	2771.19	3255.16	3786.24	4361.04	4976.56	0.511
	-5.85	14.22	-6.74	-1.54	-6.41	7.02					
	1211.45	1402.50	1647.63	1954.15	2329.39	2780.69	3315.36	3940.75	4664.16	5492.94	0.329
	-1.21	5.96	-9.90	5.33	2.51	-2.48					
	1213.80	1397.50	1648.27	1958.04	2328.31	2779.80	3364.37	4179.15	5383.06	7215.50	0.436
	-3.56	10.96	-10.54	1.44	3.59	-1.59					

^{162}Er	1^-	3^-	5^-	7^-	9^-	11^-	13^-	15^-	17^-	19^-	rms % deviation
	1352.17	1356.77	1469.11	1682.22	1985.98	2368.18	2817.75				
	1286.38	1367.96	1514.82	1726.94	2004.33	2346.99	2754.92	3228.11	3766.57	4370.31	
	65.79	-11.19	-45.71	-44.72	-18.35	21.19	62.83				
	1352.44	1356.04	1469.58	1682.81	1985.52	2367.45	2818.38	3328.08	3886.30	4482.81	
	-0.27	0.73	-0.47	-0.59	0.46	0.73	-0.63				
	1336.23	1376.36	1475.40	1667.69	1976.95	2388.08	2810.29	3031.51	2664.13	1082.07	
	15.94	-19.59	-6.29	14.53	9.03	-19.90	7.46				
	21^-										
	5039.31										2.611
	5107.39										0.033
	-2650.81										0.877
^{164}Er	7^-	(8^-)	(9^-)	(10^-)	(11^-)	(12^-)	(13^-)	14^-	15^-	16^-	rms % deviation
	1985.02	2163.5	2363.25	2583.3	2822.1	3078.9	3352.1				
	1984.57	2164.06	2363.78	2583.12	2821.49	3078.27	3352.88	3644.75	3953.33	4278.09	
	0.45	-0.56	-0.53	0.18	0.61	0.63	-0.78				
	1985.02	2163.48	2363.28	2583.24	2822.16	3078.85	3352.11	3640.75	3943.59	4259.42	
	0.00	0.02	-0.03	0.06	-0.06	0.05	-0.01				
	1984.96	2163.62	2363.26	2583.11	2822.14	3079.01	3352.04	3639.09	3937.54	4244.22	
	0.06	-0.12	-0.01	0.19	-0.04	-0.11	0.06				
	17^-										
	4618.52										0.021
	4587.06										0.002
	4555.29										0.004

^{164}Er	1^-	(3^-)	$(5)^-$	(7^-)	(9^-)	(11^-)	13^-	15^-	17^-	19^-	rms % deviation
	1387	1434	1554	1764	2055	2463					
	1354.96	1436.11	1582.19	1793.19	2069.12	2409.97	2815.74	3286.44	3822.06	4422.61	1.658
	32.04	-2.11	-28.19	-29.19	-14.12	53.03					
	1386.85	1434.15	1555.29	1760.24	2058.97	2461.46	2977.66	3617.55	4391.10	5308.28	0.125
	0.15	-0.15	-1.29	3.76	-3.97	1.54					
	1383.73	1438.77	1555.45	1756.87	2060.60	2461.46	2908.97	3279.54	3343.34	2725.85	0.263
	3.27	-4.77	-1.45	7.13	-5.60	1.54					

^{162}Yb	8^-	10^-	12^-	14^-	16^-	18^-	20^-	22^-	24^-	26^-	rms % deviation
	2280.4	2572.7	2938.5	3417.0	3972.5	4562.4	5169.8	5816.6			
	2262.04	2584.60	2972.93	3425.89	3942.26	4520.69	5159.81	5858.18	6614.34	7426.82	
	18.36	-11.90	-34.43	-8.89	30.24	41.71	9.99	-41.58			
	2283.01	2562.65	2948.52	3421.85	3963.89	4555.88	5179.06	5814.67	6443.95	7048.15	
	-2.61	10.05	-10.02	-4.85	8.61	6.52	-9.26	1.93			
	2278.00	2572.82	2950.35	3412.98	3955.36	4560.47	5195.11	5804.81	6308.20	6590.73	
	2.40	-0.12	-11.85	4.02	17.14	1.93	-25.31	11.79			
	28^-	30^-									
	8294.19	9215.00									0.730
	7608.51	8106.27									0.224
	6497.85	5827.62									0.286

^{166}Yb	6^-	8^-	10^-	12^-	14^-	16^-	18^-	20^-	22^-	24^-	rms % deviation
	1865.2	2072.8	2361.4	2728.9	3166	3666	4218	4818	5467		
	1847.42	2082.56	2380.41	2740.96	3164.21	3650.17	4198.84	4810.20	5484.28	6221.06	
	17.78	-9.76	-19.01	-12.06	1.79	15.83	19.16	7.80	-17.28		
	1865.35	2072.11	2362.41	2729.22	3165.52	3664.28	4218.48	4821.09	5465.10	6143.48	
	-0.15	0.69	-1.01	-0.32	0.48	1.72	-0.48	-3.09	1.90		
	1860.04	2079.59	2366.97	2725.85	3157.65	3659.77	4223.59	4832.15	5457.45	6057.55	
	5.16	-6.79	-5.57	3.05	8.35	6.23	-5.59	-14.15	9.55		
	26^-	28^-	30^-								
	7020.54	7882.72	8807.62								0.527
	6849.20	7575.24	8314.58								0.035
	6573.34	6924.97	7008.02								0.232

^{166}Yb	(2^-)	(4^-)	(6^-)	(8^-)	(10^-)	(12^-)	14^-	16^-	18^-	20^-	rms % deviation
	1502.5	1617.4	1835.7	2136.5	2490.2	2890.4					
	1493.22	1629.88	1842.09	2126.83	2480.58	2899.61	3380.18	3918.72	4511.85	5156.49	0.509
	9.28	-12.48	-6.39	9.67	9.62	-9.21					
	1502.32	1617.92	1835.77	2134.52	2492.83	2889.35	3302.73	3711.61	4094.67	4430.53	0.061
	0.18	-0.52	-0.07	1.98	-2.63	1.05					
	1498.81	1624.87	1833.78	2129.34	2497.46	2888.31	3193.83	3220.38	2656.69	1037.10	0.285
	3.69	-7.47	1.92	7.16	-7.26	2.09					

^{170}Yb	7^-	8^-	9^-	10^-	11^-	(12^-)	13^-	14^-	15^-	16^-	rms % deviation
	2189.9	2341.9	2525.6	2733.1	296.20	3203.0					
	2184.24	2346.98	2530.06	2733.48	2957.25	3201.36	3465.81	3750.60	4055.74	4381.22	0.162
	5.66	-5.08	-4.46	-0.38	2.95	1.64					
	2189.79	2342.31	2525.14	2733.00	2960.65	3202.80	3454.20	3709.59	3963.69	4211.25	0.013
	0.11	-0.41	0.46	0.10	-0.45	0.20					
	2189.50	2343.11	2524.73	2732.43	2961.32	3202.62	3442.69	3662.02	3834.04	3923.92	0.033
	0.40	-1.21	0.87	0.67	-1.12	0.38					

^{170}Yb	1^-	3^-	(5)	(7)	$9^{(-)}$	$11^{(-)}$	(13^-)	(15^-)	17^-	19^-	rms % deviation
	1365	1397	1510.4	1712.6	2006.10	2388.4	2856.0	3399.1			
	1308.13	1392.29	1543.78	1762.60	2048.76	2402.24	2823.05	3311.20	3866.67	4489.47	
	56.87	4.71	-33.38	-50.00	-42.66	-13.84	32.95	87.90			
	1366.17	1394.30	1510.80	1715.22	2007.12	2386.07	2851.62	3403.34	4040.78	4763.52	
	-1.17	2.70	-0.40	-2.62	-1.02	2.33	4.38	-4.24			
	1353.81	1407.72	1519.06	1708.07	1994.56	2387.57	2871.89	3391.45	3829.43	3985.30	
	11.19	-10.72	-8.66	4.53	11.54	0.83	-15.89	7.65			
	21^-	23^-									
	5179.61	5937.07									2.339
	5571.10	6463.10									0.122
	3548.66	2069.86									0.542

^{170}Yb	4^-	6^-	8^-	10^-	12^-	14^-	(16^-)	18^-	20^-	22^-	rms % deviation
	1258.7	1450.5	1716.1	2057.1	2474.3	2967.1	3532.3				
	1253.79	1451.72	1721.62	2063.50	2477.35	2963.17	3520.97	4150.75	4852.50	5626.22	
	4.91	-1.22	-5.52	-6.40	-3.05	3.93	11.33				
	1258.83	1450.07	1716.32	2057.67	2474.19	2965.96	3533.07	4175.59	4893.61	5687.20	
	-0.13	0.43	-0.22	-0.57	0.11	1.14	-0.77				
	1258.61	1450.69	1716.09	2056.89	2474.25	2967.36	3532.17	4159.89	4835.31	5534.84	
	0.09	-0.19	0.01	0.21	0.05	-0.26	0.13				
	24^-										
	6471.91										0.266
	6556.45										0.024
	6224.40										0.008
^{170}Yb	5^-	7^-	9^-	11^-	13^-	(15^-)	(17^-)	19^-	21^-	23^-	rms % deviation
	1345.4	1573.0	1872.4	2242.4	2681.9	3187.0	3757.3				
	1344.58	1574.03	1873.44	2242.30	2680.02	3185.89	3759.13	4398.89	5104.27	5874.29	
	0.82	-1.03	-1.04	0.10	1.88	1.11	-1.83				
	1345.45	1572.82	1872.52	2242.70	2681.48	3187.01	3757.41	4390.82	5085.39	5839.23	
	-0.05	0.18	-0.12	-0.30	0.42	-0.01	-0.11				
	1345.23	1573.38	1872.39	2242.11	2681.45	3187.91	3756.93	4381.15	5049.54	5746.50	
	0.17	-0.38	0.01	0.29	0.45	-0.91	0.37				
	25^-										
	6707.95										0.053
	6650.49										0.009
	6450.78										0.017

^{172}Yb	6^-	7^-	8^-	9^-	10^-	11^-	12^-	13^-	14^-	15^-	rms % deviation
	1550.6	1670.8	1809.9	1967.9	2144.8	2340.5	2554.1	2786.7	3034.1		
	1547.06	1670.71	1812.01	1970.98	2147.62	2341.92	2553.88	2783.51	3030.80	3295.75	
	3.54	0.09	-2.11	-3.08	-2.82	-1.42	0.22	3.19	3.30		
	1550.73	1670.57	1809.77	1968.05	2145.08	2340.57	2554.21	2785.69	3034.71	3300.97	
	-0.13	0.23	0.13	-0.15	-0.28	-0.07	-0.11	1.01	-0.61		
	1550.54	1670.92	1809.92	1967.82	2144.70	2340.44	2554.58	2786.28	3034.22	3296.47	
	0.06	-0.12	-0.02	0.08	0.10	0.06	-0.48	0.42	-0.12		
	16^-	17^-	18^-								
	3578.36	3878.64	4196.59								0.123
	3584.15	3883.96	4200.08								0.016
	3570.44	3852.70	4138.90								0.009

^{172}Yb	4^-	5^-	6^-	7^-	8^-	9^-	10^-	11^-	(12^-)	13^-	rms % deviation
	1640.8	1706.4	1802.3	1921.6	2063.9	2225.1	2411.3	2609.0	2840.7		
	1618.77	1706.78	1812.41	1935.63	2076.46	2234.89	2410.92	2604.56	2815.80	3044.65	
	22.03	-0.38	-10.11	-14.03	-12.56	-9.79	0.38	4.44	24.90		
	1639.74	1708.46	1802.49	1920.75	2062.14	2225.60	2410.03	2614.35	2837.48	3078.34	
	1.06	-2.06	-0.19	0.85	1.76	-0.50	1.27	-5.35	3.22		
	1637.25	1710.85	1804.68	1920.69	2060.25	2223.75	2410.15	2616.41	2836.94	3062.96	
	3.55	-4.45	-2.38	0.91	3.65	1.35	1.15	-7.41	3.76		
	14^-	15^-	16^-								
	3291.10	3555.15	3836.81								0.668
	3335.85	3608.91	3896.46								0.098
	3281.74	3475.90	3622.56								0.173

^{172}Yb	2$^-$	4$^-$	6$^-$	8$^-$	10$^-$	12$^-$	(14$^-$)	16$^-$	18$^-$	20$^-$	rms % deviation
	1198.5	1330.9	1540.8	1828.7	2192.9	2629.7	3134.5				
	1197.33	1331.70	1542.47	1829.13	2191.01	2627.29	3137.02	3719.11	4372.41	5095.67	
	1.17	-0.80	-1.67	-0.43	1.89	2.41	-2.52				
	1198.69	1330.26	1541.21	1829.38	2192.54	2628.59	3135.33	3710.59	4352.20	5057.99	
	-0.19	0.64	-0.41	-0.66	0.36	1.11	-0.83				
	1198.31	1331.18	1541.00	1828.35	2192.56	2630.37	3134.25	3690.36	4276.08	4857.33	
	0.19	-0.28	-0.20	0.35	0.34	-0.67	0.25				
	22$^-$										
	5887.58										0.083
	5825.79										0.032
	5385.35										0.018

^{172}Yb	1$^-$	3$^-$	5$^-$	7$^-$	9$^-$	11$^-$	13$^-$	15$^-$	17$^-$	19$^-$	rms % deviation
	1155.0	1221.8	1353.2	1557.3	1839.4	2199.1	2635.8				
	1138.51	1219.78	1366.06	1577.37	1853.69	2195.02	2601.38	3072.75	3609.13	4210.53	
	16.49	2.02	-12.86	-20.07	-14.29	4.08	34.42				
	1155.44	1220.52	1353.82	1558.74	1838.69	2197.08	2637.33	3162.84	3777.03	4483.30	
	-0.44	1.28	-0.62	-1.44	0.71	2.02	-1.53				
	1153.96	1223.03	1354.04	1556.24	1837.97	2201.33	2635.00	3105.51	3546.83	3848.25	
	1.04	-1.23	-0.84	1.06	1.43	-2.23	0.80				
	21$^-$										
	4876.95										0.998
	5285.06										0.072
	3840.60										0.079

^{166}Hf	$7^{(-)}$	$9^{(-)}$	$11^{(-)}$	$13^{(-)}$	$15^{(-)}$	$17^{(-)}$	(19^-)	(21^-)	23^-	25^-	rms % deviation
	1727.0	2079.5	2498.0	2963.8	3478.0	4033.8	4629.7	5258.1			
	1725.97	2082.35	2496.73	2962.99	3476.23	4032.44	4628.32	5261.06	5928.27	6627.88	
	1.03	-2.85	1.27	0.81	-0.23	1.36	1.38	-2.96			
	1726.41	2081.87	2495.66	2962.56	3477.37	4034.88	4629.87	5257.15	5911.51	6587.72	
	0.59	-2.37	2.34	1.24	-1.37	-1.08	-0.17	0.95			
	1727.28	2079.77	2495.42	2961.77	3479.42	4033.52	4625.54	5260.24	5950.88	6721.66	
	-0.28	-0.27	2.58	[illegible]	-3.42	0.28	4.16	-2.14			
	27^-	29^-									
	7358.09	8117.29									0.062
	7280.60	7984.93									0.058
	7610.45	8671.72									0.063

^{172}Hf	4^-	(6^-)	(8^-)	(10^-)	(12^-)	(14^-)	(16^-)	(18^-)	(20^-)	(22^-)	rms % deviation
	1418	1597	1852	2186	2598	3085	3643	4264	4941	5669	
	1405.74	1600.20	1865.14	2200.35	2605.57	3080.50	3624.77	4237.97	4919.65	5669.33	
	12.26	-3.20	-13.14	-14.35	-7.57	4.50	18.23	26.03	21.35	-0.33	
	1419.76	1593.33	1850.94	2188.53	2602.09	3087.57	3640.94	4258.16	4935.20	5668.01	
	-1.76	3.67	1.06	-2.53	-4.09	-2.57	2.06	5.84	5.80	0.99	
	1414.03	1599.99	1857.22	2188.22	2594.96	3078.14	3636.10	4263.72	4951.05	5681.81	
	3.97	-2.99	-5.22	-2.22	3.04	6.86	6.90	0.28	-10.05	-12.81	
	(24^-)	26^-	28^-	30^-	32^-						
	(6444)										
	6486.48	7370.53	8320.90	9336.98	10418.11						0.528
	-42.48										
	6452.57	7284.83	8160.76	9076.33	10027.49						0.124
	-8.57										
	6431.69	7166.51	7840.15	8392.40	8746.53						0.198
	12.31										

^{172}Hf	$(5)^-$	$(7)^-$	$(9)^-$	$(11)^-$	$(13)^-$	$(15)^-$	$(17)^-$	$(19)^-$	$(21)^-$	$(23)^-$	rms % deviation
	1503	1727	1968.7	2337.4	2778.0	3286.1	3858.4	4492.2	5183.9	5931.0	
	1491.96	1712.92	2001.87	2358.81	2783.74	3276.65	3837.56	4466.45	5163.33	5928.20	
	11.04	14.08	-33.17	-21.41	-5.74	9.45	20.84	25.75	20.57	2.80	
	1509.41	1705.52	1984.84	2343.35	2777.02	3281.81	3853.71	4488.68	5182.69	5931.71	
	-6.41	21.48	-16.14	-5.95	0.98	4.29	4.69	3.52	1.21	-0.71	
	1503.81	1712.68	1991.20	2342.50	2769.04	3271.77	3849.05	4495.45	5200.38	5946.53	
	-0.81	14.32	-22.50	-5.10	8.96	14.33	9.35	-3.25	-16.48	-15.53	
	$(25)^-$	27^-	29^-	31^-	33^-						
	6725.4										
	6761.05	7661.90	8630.73	9667.55	10772.36						0.743
	-35.65										
	6731.72	7578.68	8468.57	9397.35	10361.01						0.478
	-6.32										
	6708.16	7449.24	8121.36	8661.54	8989.87						0.490
	17.24										

^{174}Hf	(3^-)	(5^-)	7^-	9^-	11^-	13^-	15^-	(17^-)	19^-	21^-	rms % deviation
	1321	1443	1650.6	1943.9	2319.2	2772.0	3296.3	3885.9			
	1292.52	1448.86	1674.69	1970.00	2334.80	2769.09	3272.86	3846.12	4488.86	5201.09	
	28.48	-5.86	-24.09	-26.10	-15.60	2.91	23.44	39.78			
	1321.40	1441.88	1651.05	1944.93	2319.52	2770.82	3294.82	3887.54	4544.98	5263.13	
	-0.40	1.12	-0.45	-1.03	-0.32	1.18	1.48	-1.64			
	1316.47	1449.48	1653.88	1939.32	2312.59	2773.05	3306.85	3880.18	4431.28	4861.55	
	4.53	-6.48	-3.28	4.58	6.61	-1.05	-10.55	5.72			
	23^-	25^-									
	5982.80	6834.00									1.160
	6038.00	6865.58									0.045
	5025.35	4718.95									0.279

^{174}Hf	(2^-)	(4^-)	6^-	8^-	10^-	12^-	14^-	16^-	18^-	20^-	rms % deviation
	1309	1425.5	1634.4	1928.4	2299.4	2744.2	3260.2				
	1298.18	1432.59	1643.81	1931.84	2296.68	2738.32	3256.77	3852.02	4524.09	5272.96	
	10.82	-7.09	-9.41	-3.44	2.72	5.88	3.43				
	1308.79	1426.11	1634.23	1927.37	2299.77	2745.63	3259.18	3834.65	4466.24	5148.19	
	0.21	-0.61	0.17	1.03	-0.37	-1.43	1.02				
	1305.65	1431.15	1635.14	1923.36	2297.66	2750.43	3257.62	3770.22	4204.35	4429.76	
	3.35	-5.65	-0.74	5.04	1.74	-6.23	2.58				
	22^-										
	6098.64										0.442
	5874.71										0.036
	4256.96										0.226

^{174}Hf	6^-	7^-	8^-	9^-	10^-	11^-	12^-	13^-	14^-	15^-	rms % deviation
	1713.5	1827.4	1963.4	2119.0	2295.7	2488.0	2700.8	2932.7	3180.70	3449.70	
	1704.71	1827.35	1967.51	2125.19	2300.39	2493.11	2703.35	2931.11	3176.39	3439.18	
	8.79	0.05	-4.11	-6.19	-4.69	-5.11	-2.55	1.59	4.31	10.52	
	1713.08	1828.14	1963.61	2119.07	2294.11	2488.33	2701.31	2932.63	3181.89	3448.68	
	0.42	-0.74	-0.21	-0.07	1.59	-0.33	-0.51	0.07	-1.19	1.02	
	1712.24	1828.95	1964.44	2119.18	2293.51	2487.51	2700.92	2933.09	3182.80	3448.22	
	1.26	-1.55	-1.04	-0.18	2.19	0.49	-0.12	-0.39	-2.10	1.48	
	16^-	17^-	18^-	19^-							
	3719.50	4017.34	4332.70	4665.58							0.245
	3732.57	4033.17	4350.05	4682.80							0.032
	3726.74	4014.86	4308.03	4600.55							0.056

^{174}Hf	8^-	9^-	10^-	11^-	(12^-)	(13^-)	14^-	15^-	16^-	17^-	rms % deviation
	1797.5	2028.0	2279.2	2554.6	2847.4	3157.9					
	1797.29	2028.07	2280.42	2553.52	2846.55	3158.77	3489.45	3837.93	4203.56	4585.76	0.033
	0.21	-0.07	-1.22	1.08	0.85	-0.87					
	1797.61	2027.41	2280.16	2554.05	2847.28	3158.04	3484.52	3824.92	4177.43	4540.25	0.023
	-0.11	0.59	-0.96	0.55	0.12	-0.14					
	1797.64	2027.44	2280.07	2554.05	2847.49	3157.93	3482.31	3816.83	4156.85	4496.77	0.021
	-0.14	0.56	-0.87	0.55	-0.09	-0.03					

^{178}W	2^-	4^-	6^-	8^-	10^-	12^-	14^-	16^-	18^-	20^-	rms % deviation
	1044.9	1225.9	1509.4	1889.4	2357.2	2903.0					
	1044.09	1227.17	1510.26	1888.17	2355.08	2905.08	3532.50	4232.13	4999.21	5829.49	0.079
	0.81	-1.27	-0.86	1.23	2.12	-2.08					
	1044.96	1225.63	1509.79	1889.46	2356.63	2903.32	3521.55	4203.31	4940.62	5725.48	0.018
	-0.06	0.27	-0.39	-0.06	0.57	-0.32					
	1044.73	1226.34	1509.21	1888.95	2357.78	2902.82	3504.00	4131.45	4742.53	5278.30	0.022
	0.17	-0.44	0.19	0.45	-0.58	0.18					

^{178}W	3^-	5^-	7^-	9^-	11^-	13^-	15^-	17^-	19^-	21^-	rms % deviation
	1120.6	1345.2	1657.0	2042.7	2490.5	2995.6					
	1120.05	1346.51	1657.04	2041.15	2490.12	2996.83	3555.12	4160.59	4809.25	5497.84	0.055
	0.55	-1.31	-0.04	1.55	0.38	-1.23					
	1120.50	1345.66	1656.48	2042.16	2491.90	2994.92	3540.40	4117.56	4715.60	5323.73	0.033
	0.10	-0.46	0.52	0.54	-1.40	0.68					
	1120.49	1345.52	1656.83	2042.39	2490.91	2995.46	3557.88	4194.05	4940.03	5858.95	0.015
	0.11	-0.32	0.17	0.31	-0.41	0.14					

^{178}W	7^-	8^-	9^-	10^-	11^-	12^-	13^-	14^-	15^-	16^-	rms % deviation
	1739.5	1828.1	1965.4	2134.1	2328.8	2547.3	2785.8	3045.6	3318.8	3614.4	
	1693.22	1832.52	1989.22	2163.34	2354.87	2563.81	2790.16	3033.93	3295.10	3573.69	
	46.28	-4.42	-23.82	-29.24	-26.07	-16.51	-4.36	11.67	23.70	40.71	
	1736.87	1833.24	1965.92	2131.33	2325.85	2545.89	2787.87	3048.17	3323.20	3609.36	
	2.63	-5.14	-0.52	2.77	2.95	1.41	-2.07	-2.57	-4.40	5.04	
	1732.04	1838.12	1970.58	2131.53	2321.89	2540.98	2786.01	3051.57	3329.01	3605.86	
	7.46	-10.02	-5.18	2.57	6.91	6.32	-0.21	-5.97	-10.21	8.54	
	17^-	18^-	19^-	20^-							
	3869.69	4183.10	4513.93	4862.16							1.188
	3903.06	4200.70	4498.67	4793.39							0.137
	3865.16	4084.72	4236.40	4285.31							0.301

^{180}W	2^-	4^-	6^-	8^-	10^-	12^-	14^-	16^-	18^-	20^-	rms % deviation
	1006.41	1184.91	1461.84	1830.85	2284.0						
	1006.21	1185.33	1461.85	1830.23	2284.39	2818.26	3426.11	4102.72	4843.40		0.025
	0.20	-0.42	-0.01	0.62	-0.39						
	1006.42	1184.85	1461.97	1830.72	2284.06	2814.94	3416.32	4081.15	4802.38		0.006
	-0.01	0.06	-0.13	0.13	-0.06						
	1006.39	1184.99	1461.73	1830.92	2283.98	2808.68	3388.17	3999.79	4613.75		0.005
	0.02	-0.08	0.11	-0.07	0.02						

^{180}W	3^-	5^-	7^-	9^-	11^-	13^-	15^-	17^-	19^-	21^-	rms % deviation
	1082.39	1307.58	1624.22	2024.48	2501.1						
	1082.34	1307.71	1624.16	2024.37	2501.19	3048.09	3659.29	4329.76	5055.16		0.006
	0.05	-0.13	0.06	0.11	-0.09						
	1082.39	1307.60	1624.17	2024.53	2501.08	3046.25	3652.47	4312.14	5017.69		0.002
	0.00	-0.02	0.05	-0.05	0.02						
	1082.39	1307.59	1624.20	2024.49	2501.10	3049.15	3668.98	4369.32	5170.98		0.001
	0.00	-0.01	0.02	-0.01	0.00						

Table 2.9. Theoretical predictions by the Varshni formula and the Bohr–Mottelson Model of the last level of negative–parity bands.

Nucleus	Last Exptl. Level (keV)	Varshni Formula		Bohr–Mottelson Model	
		Predictions (keV)	% Deviations	Predictions (keV)	% Deviations
^{156}Dy	3154.29	3126.69	0.87	2980.86	5.50
^{162}Dy *a*	2724.8	2693.86	1.14	2678.66	1.69
^{162}Dy *b*	2778.21	2810.98	1.18	2863.73	3.08
^{162}Dy *c*	2504.6	2555.97	2.01	2691.33	3.46
^{162}Er	2817.75	2822.55	0.17	2525.46	10.34
^{164}Er *a*	3352.1	3352.44	0.01	3351.05	0.03
^{164}Er *b*	2463	2441.33	0.88	2306.85	6.34
^{162}Yb	5816.6	5805.28	0.19	5671.40	2.50
^{166}Yb *a*	5467	5458.68	0.15	5378.88	1.61
^{166}Yb *b*	2890.4	2875.22	0.53	2732.99	5.45
^{170}Yb *a*	3203	3200.39	0.08	3190.12	0.40
^{170}Yb *b*	3399.1	3421.08	0.65	3240.26	4.67
^{170}Yb *c*	3532.3	3537.88	0.16	3529.64	0.08
^{170}Yb *d*	3757.3	3758.15	0.02	3749.99	0.19
^{172}Yb *a*	3034.1	3037.26	0.10	3035.11	0.03
^{172}Yb *b*	2840.7	2823.87	0.59	2801.64	1.38
^{172}Yb *c*	3134.5	3140.6	0.19	3127.12	0.24
^{172}Yb *d*	2635.8	2647.28	0.44	2605.50	1.15
^{160}Hf	5258.1	5252.99	0.10	5283.50	0.48
^{172}Hf *a*	6444	6468.23	0.38	6369.99	1.15
^{172}Hf *b*	6725.4	6743.54	0.27	6625.67	1.48
^{174}Hf *a*	3885.9	3894.22	0.21	3799.73	2.22
^{174}Hf *b*	3260.2	3252.65	0.23	3182.87	2.37
^{174}Hf *c*	3449.70	3445.57	0.12	3439.37	0.30
^{174}Hf *d*	3157.9	3160.28	0.08	3158.68	0.02
^{178}W *a*	2903	2906.78	0.13	2892.50	0.36
^{178}W *b*	2995.6	2987.14	0.28	2988.92	0.22
^{178}W *c*	3614.4	3593.70	0.57	3759.05	4.00
^{180}W *a*	2284	2285.59	0.07	2280.39	0.16
^{180}W *b*	2501.1	2500.53	0.02	2500.56	0.02

Table 2.10. Backbending Negative-parity Bands

Nucleus	Ref.	Spin: $I_i^\pi \rightarrow I_f^\pi$	N – Z
$^{154}_{66}Dy_{88}$	a	$3^- \rightarrow 25^-$	22
$^{156}_{68}Er_{88}$	b	$7^- \rightarrow 23^-$	20
$^{158}_{68}Er_{90}$	c	$8^- \rightarrow 34^-$; $9^- \rightarrow 45^-$	22
$^{160}_{68}Er_{92}$	c	$10^- \rightarrow 38^-$; $11^- \rightarrow 37^-$	24
$^{158}_{70}Yb_{88}$	d	$7^- \rightarrow 31^-$	18
$^{160}_{70}Yb_{90}$	e	$6^- \rightarrow 42^-$; $9^- \rightarrow 39^-$	20
$^{162}_{70}Yb_{92}$	f	$7^- \rightarrow 23^-$	22
$^{168}_{70}Yb_{98}$	g	$6^- \rightarrow 30^-$; $13^- \rightarrow 39^-$	28
$^{168}_{72}Hf_{96}$	h	$8^- \rightarrow 30^-$; $9^- \rightarrow 33^-$	24
$^{170}_{72}Hf_{98}$	i	$11^- \rightarrow 25^-$	26
$^{178}_{72}Hf_{104}$	j	$8^- \rightarrow 13^-$	32
$^{166}_{74}W_{92}$	k	$5^- \rightarrow 19^-$	18
$^{168}_{74}W_{94}$	l	$5^- \rightarrow 29^-$	20
$^{170}_{74}W_{96}$	m	$10^- \rightarrow 26^-$; $5^- \rightarrow 29^-$	22
$^{174}_{74}W_{100}$	n	$4^- \rightarrow 18^-$; $5^- \rightarrow 21^-$	26

References:

a) Pakkanen *et al* (1982)
b) Sunyar *et al* (1976)
c) Larabee *et al* (1983)
d) Baktash *et al* (1985)
e) Simpson (1985)
f) Helmer (1985)
g) Bacelar *et al* (1985)
h) Chapman *et al* (1983)
i) Lisle *et al* (1981)
j) Horen and Harmats (1976)
k) Gerl *et al* (1985)
l) Dracoulis *et al* (1983)
m) Recht *et al* (1985)
n) Dracoulis *et al* (1977)

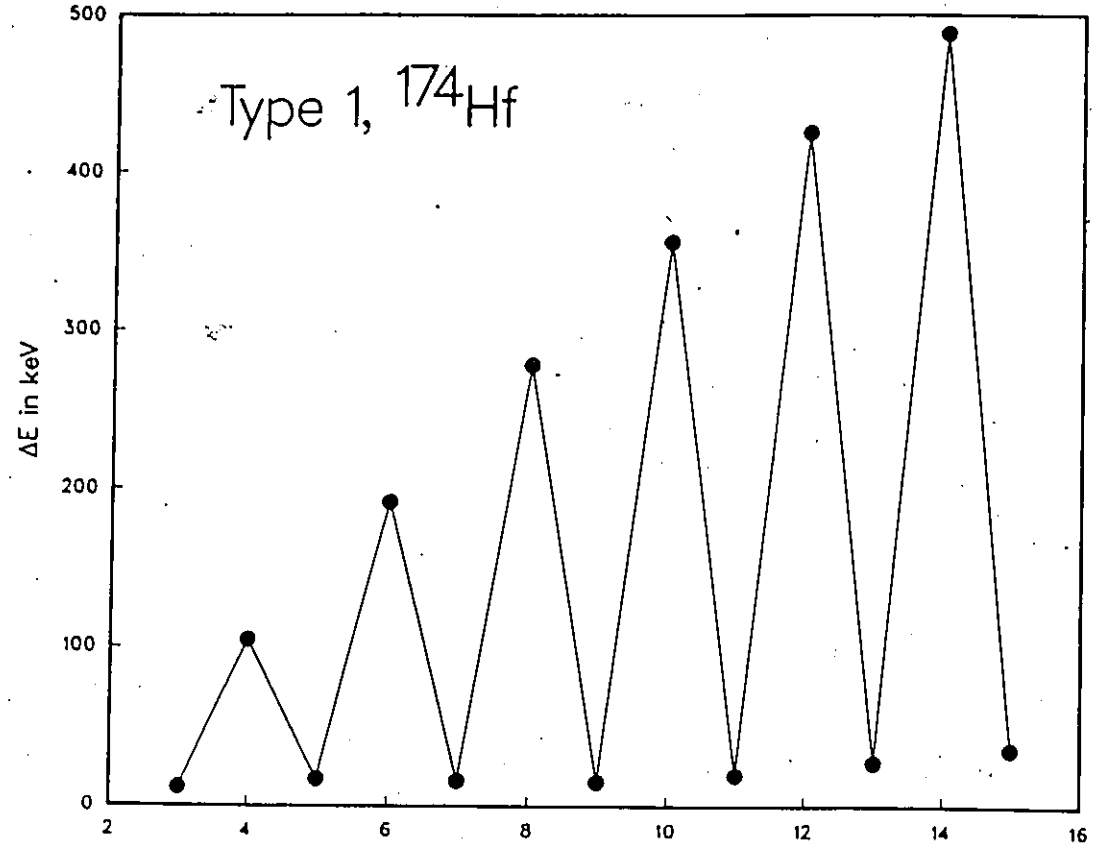
Type 1, ^{174}Hf
ΔE in keV
Spin in units of ħ
0
100
200
300
400
500
2
4
6
8
10
12
14
16

Fig. 2.1

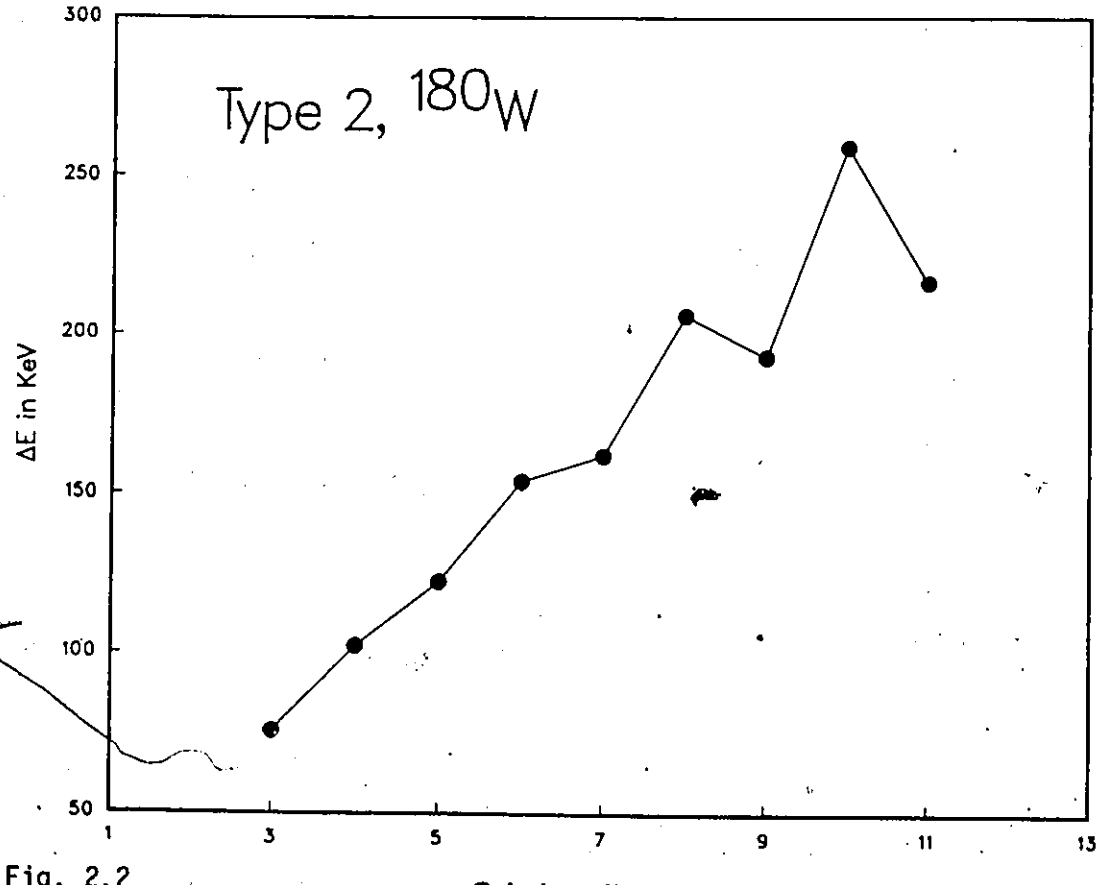
Type 2, ^{180}W
ΔE in KeV
Spin in units of ħ
50
100
150
200
250
300
1
3
5
7
9
11
13

Fig. 2.2

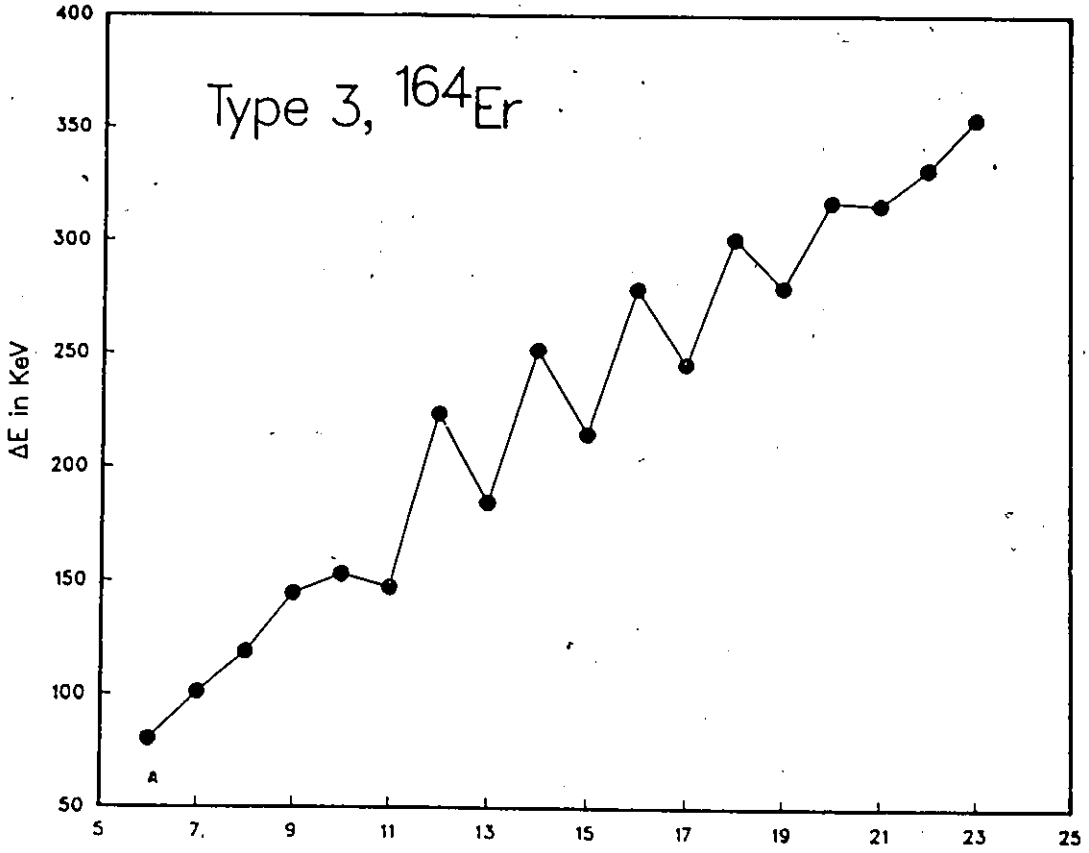
Type 3, 164Er
ΔE in KeV
Spin in units of ħ
A
400
350
300
250
200
150
100
50
5
7
9
11
13
15
17
19
21
23
25

Fig. 2.3

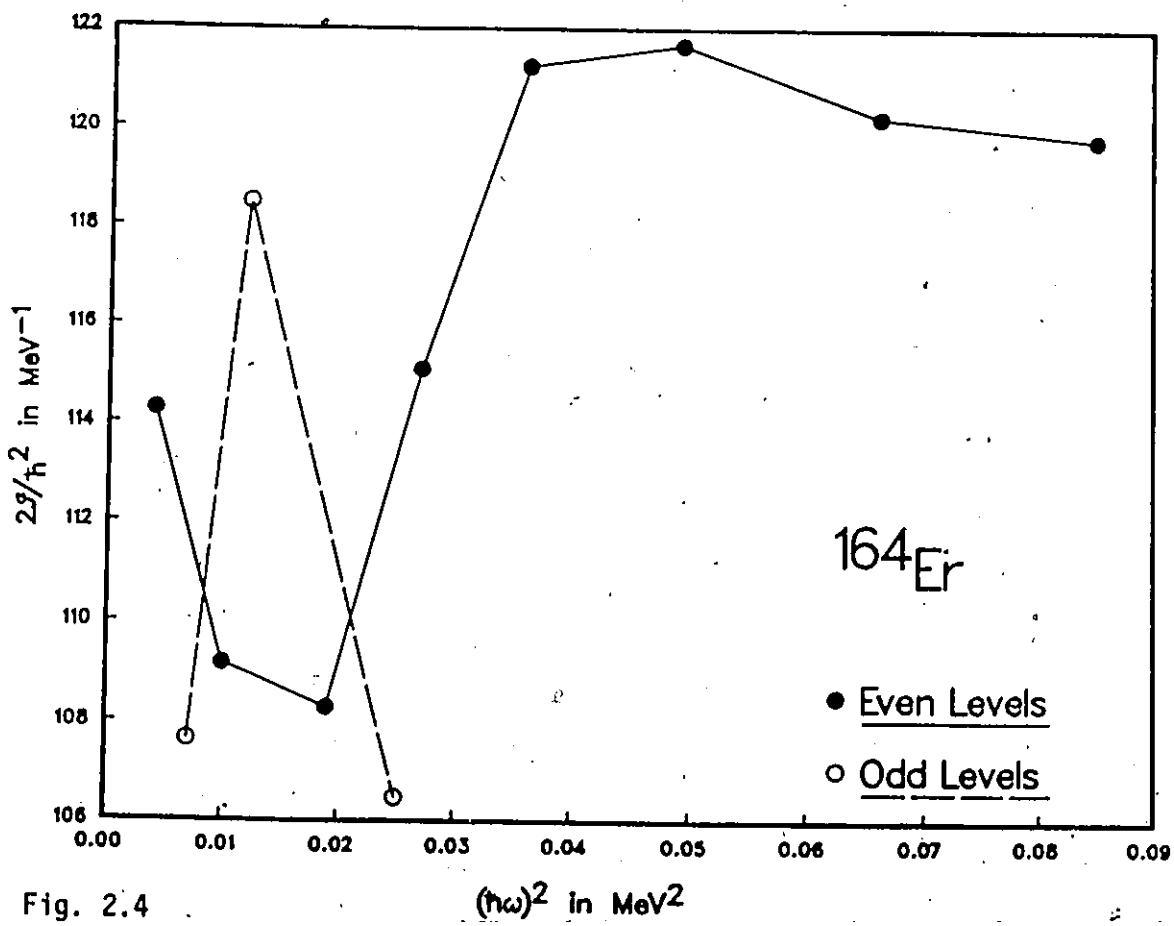
2ϑ/ħ2 in MeV−1
(ħω)2 in MeV2
164Er
Even Levels
Odd Levels
122
120
118
116
114
112
110
108
106
0.00
0.01
0.02
0.03
0.04
0.05
0.06
0.07
0.08
0.09

Fig. 2.4

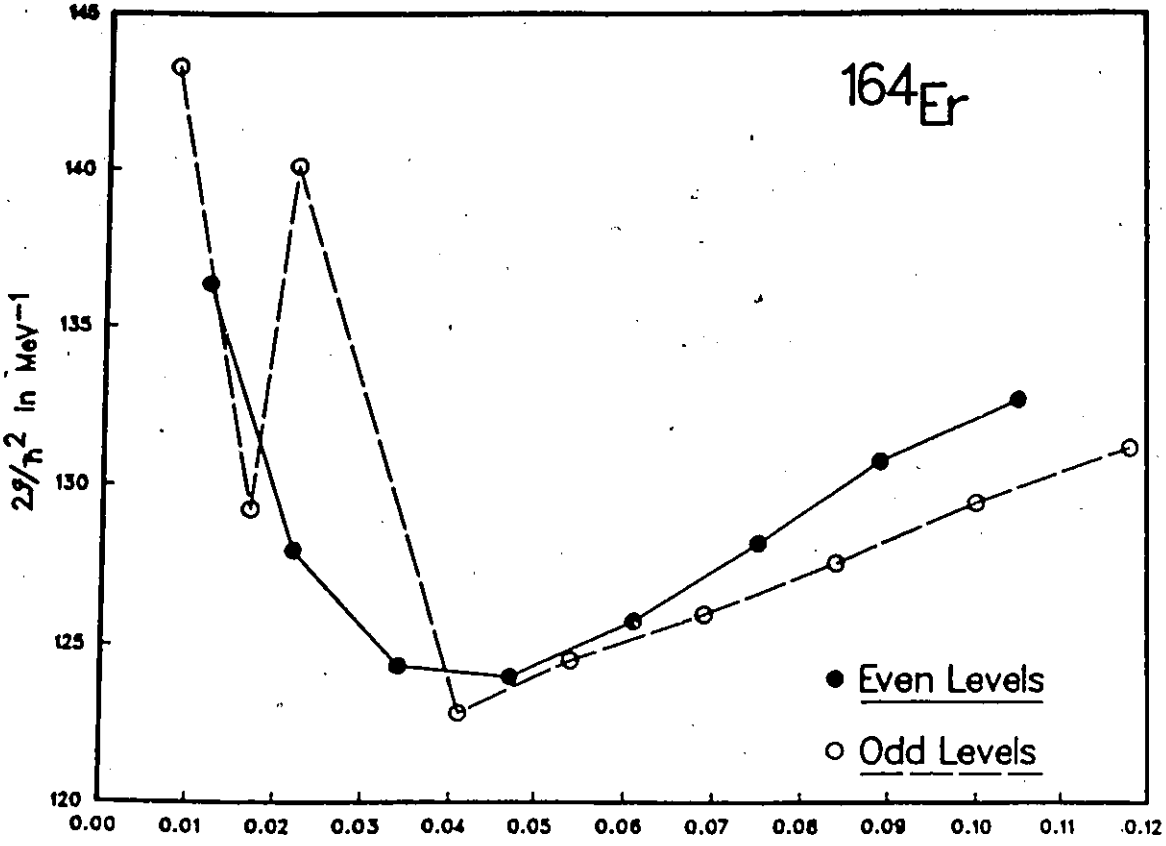
164Er
Even Levels
Odd Levels
2ℐ/ħ² in MeV⁻¹
(ħω)² in MeV²
145
140
135
130
125
120
0.00
0.01
0.02
0.03
0.04
0.05
0.06
0.07
0.08
0.09
0.10
0.11
0.12

Fig. 2.5

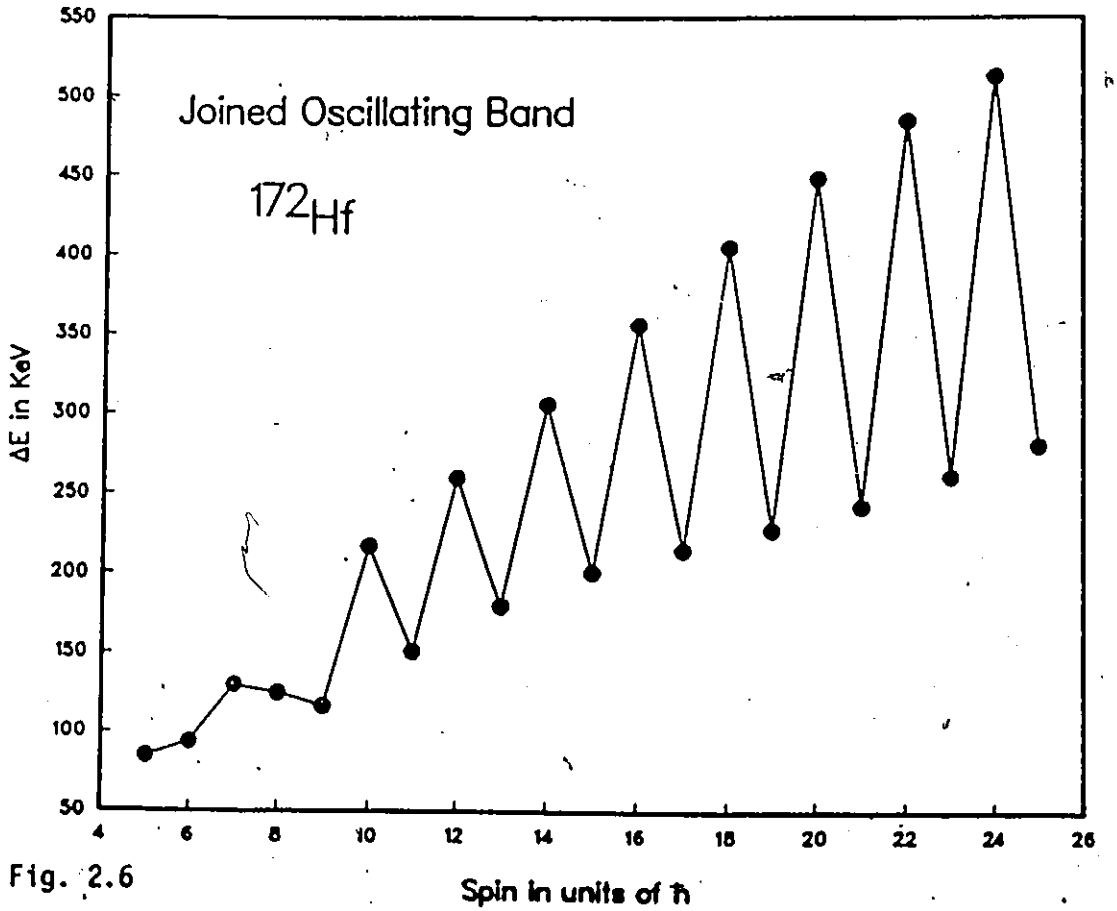
Joined Oscillating Band
172Hf
ΔE in KeV
Spin in units of ħ
550
500
450
400
350
300
250
200
150
100
50
4
6
8
10
12
14
16
18
20
22
24
26

Fig. 2.6

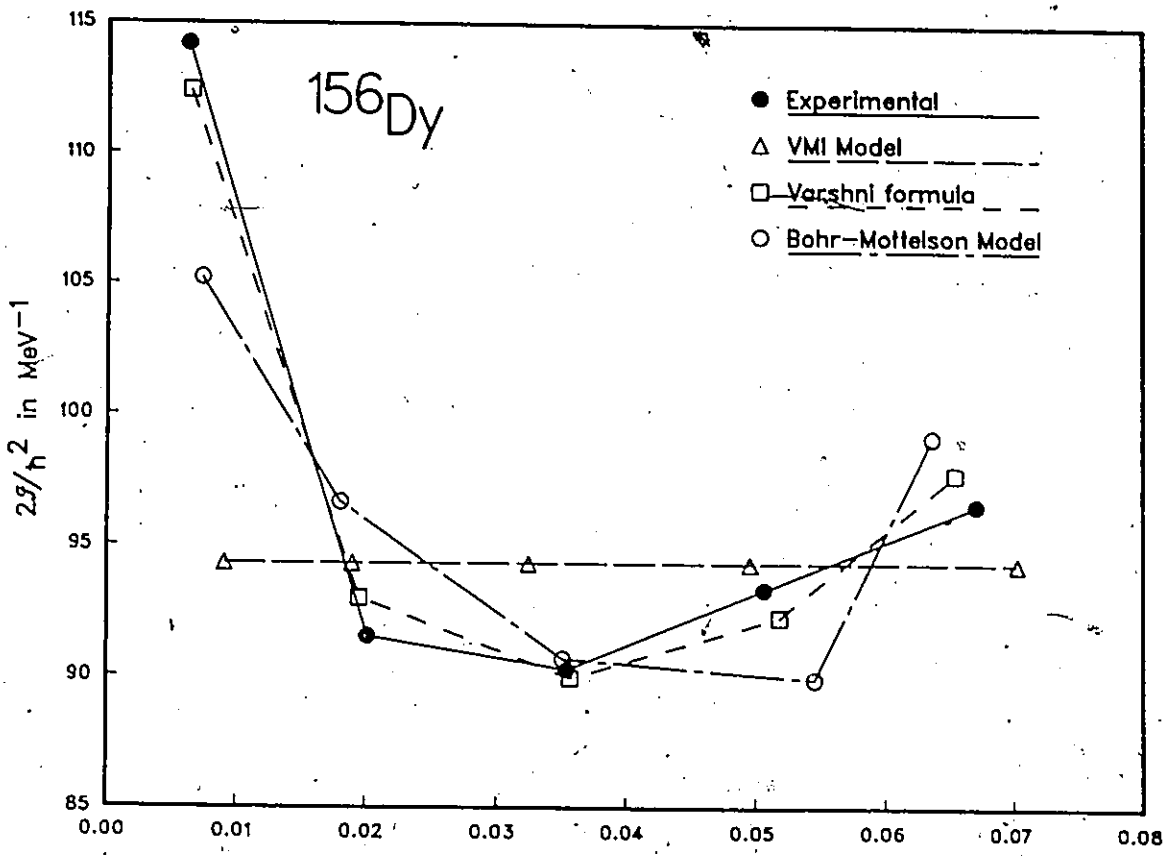
156Dy
Experimental
VMI Model
Varshni formula
Bohr-Mottelson Model
2ℑ/ħ² in MeV⁻¹
(ħω)² in MeV²
115
110
105
100
95
90
85
0.00
0.01
0.02
0.03
0.04
0.05
0.06
0.07
0.08

Fig. 2.7

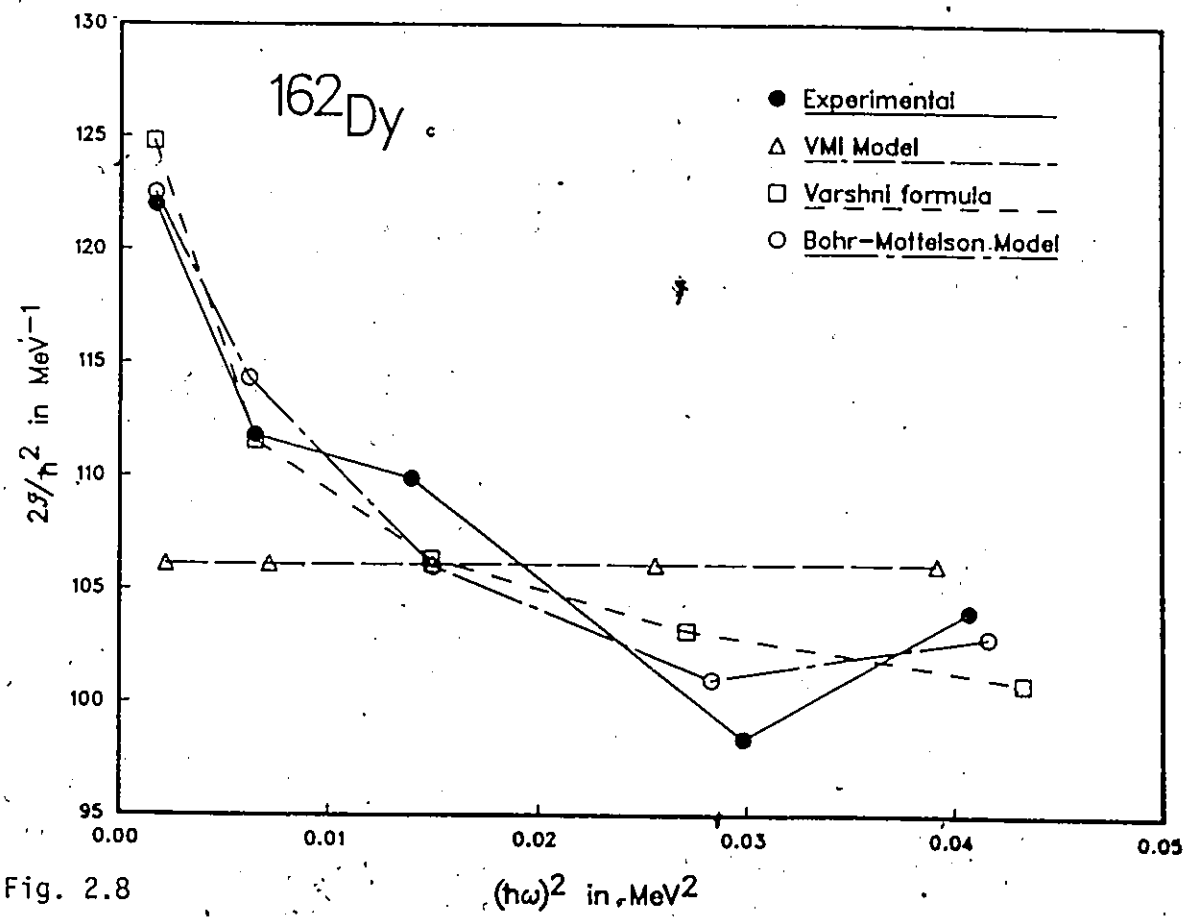
162Dy
Experimental
VMI Model
Varshni formula
Bohr-Mottelson Model
2ℑ/ħ² in MeV⁻¹
(ħω)² in MeV²
130
125
120
115
110
105
100
95
0.00
0.01
0.02
0.03
0.04
0.05

Fig. 2.8

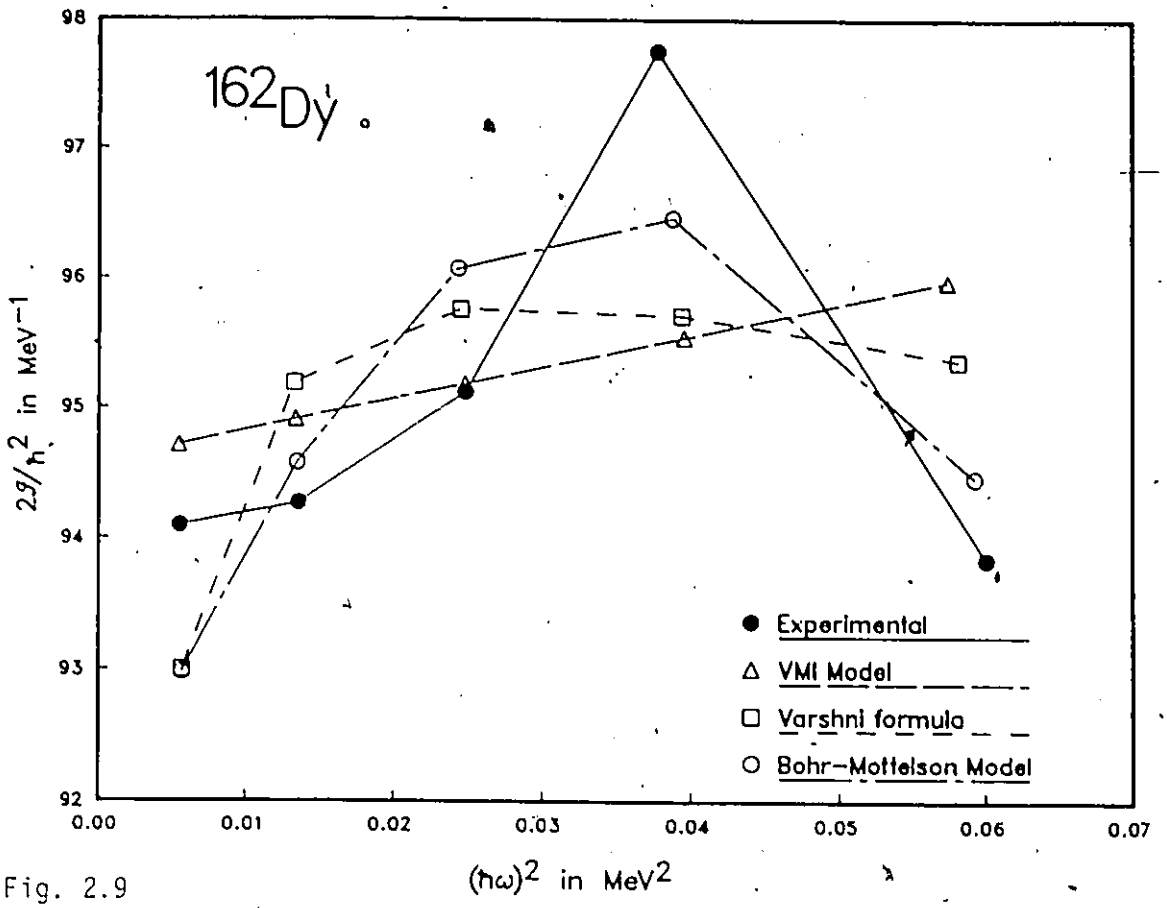

Fig. 2.9

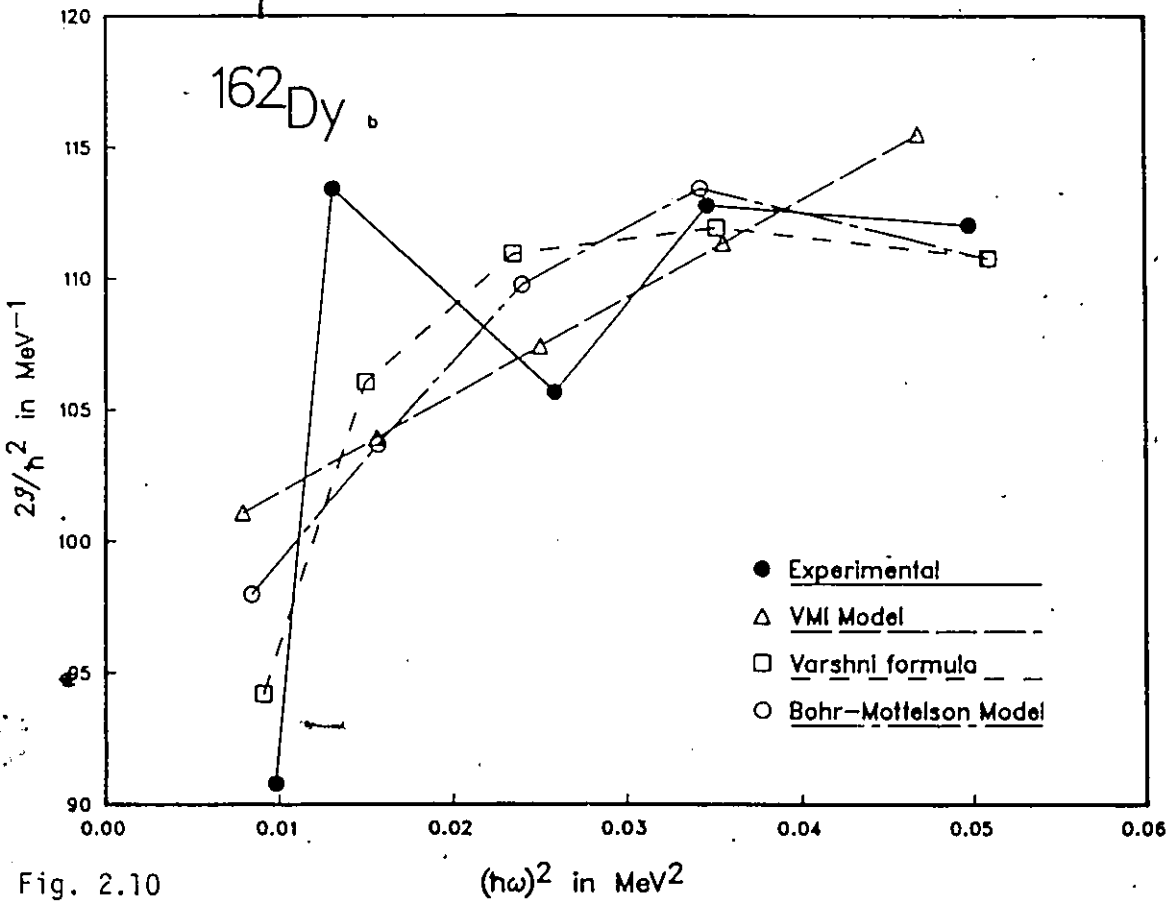

Fig. 2.10

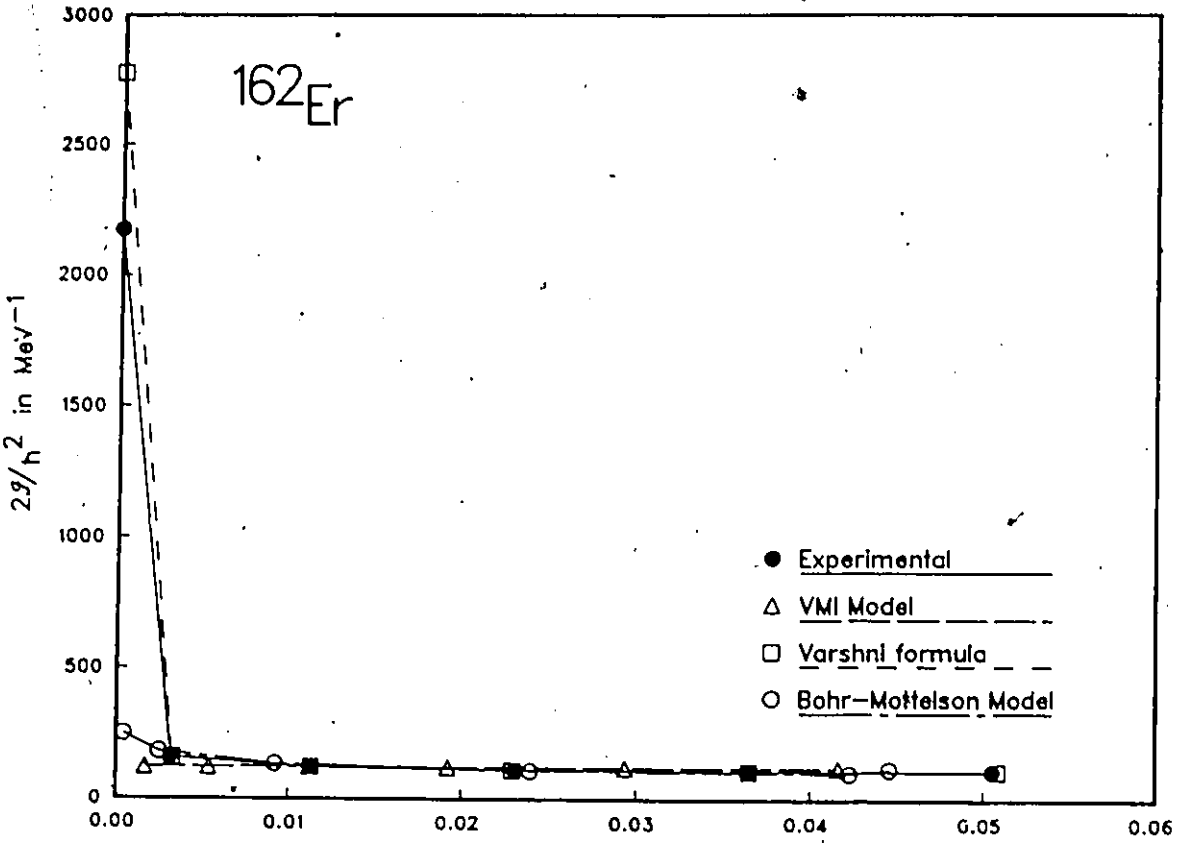

Fig. 2.11

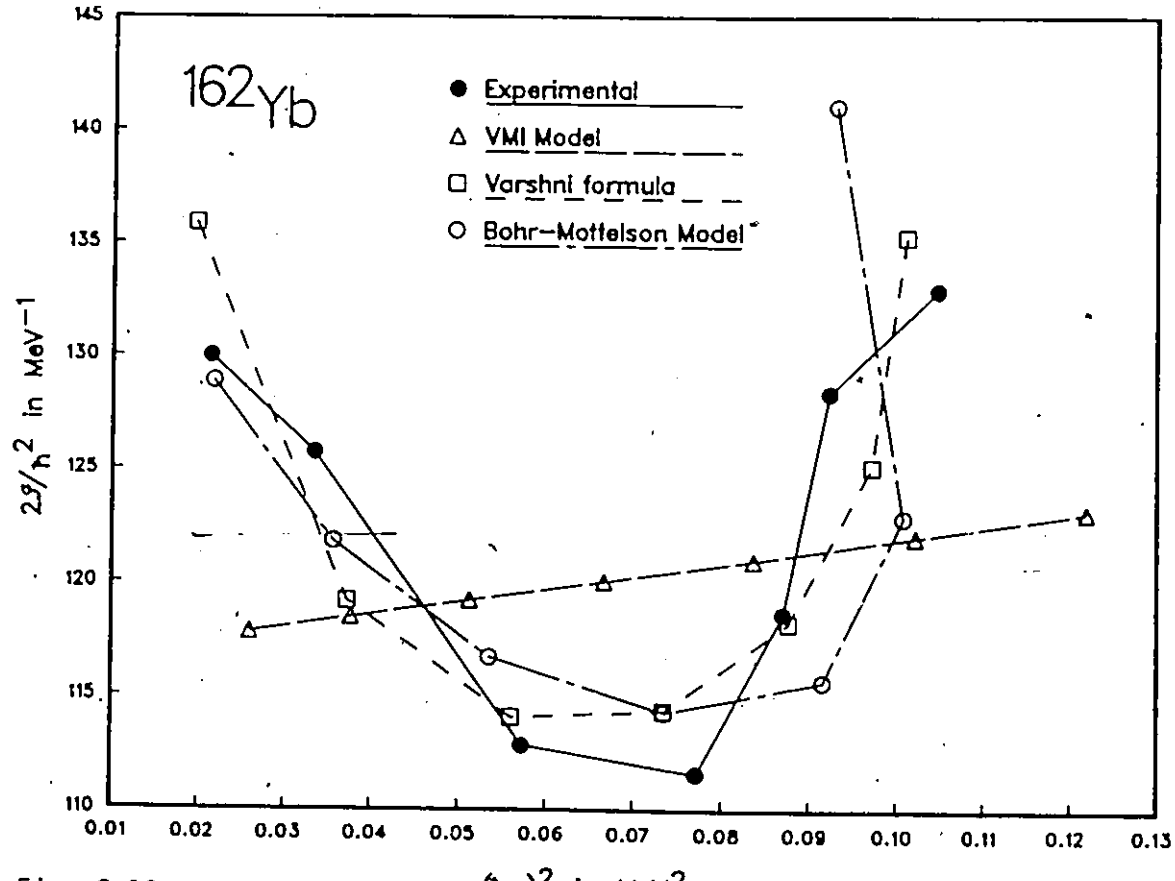

Fig. 2.12

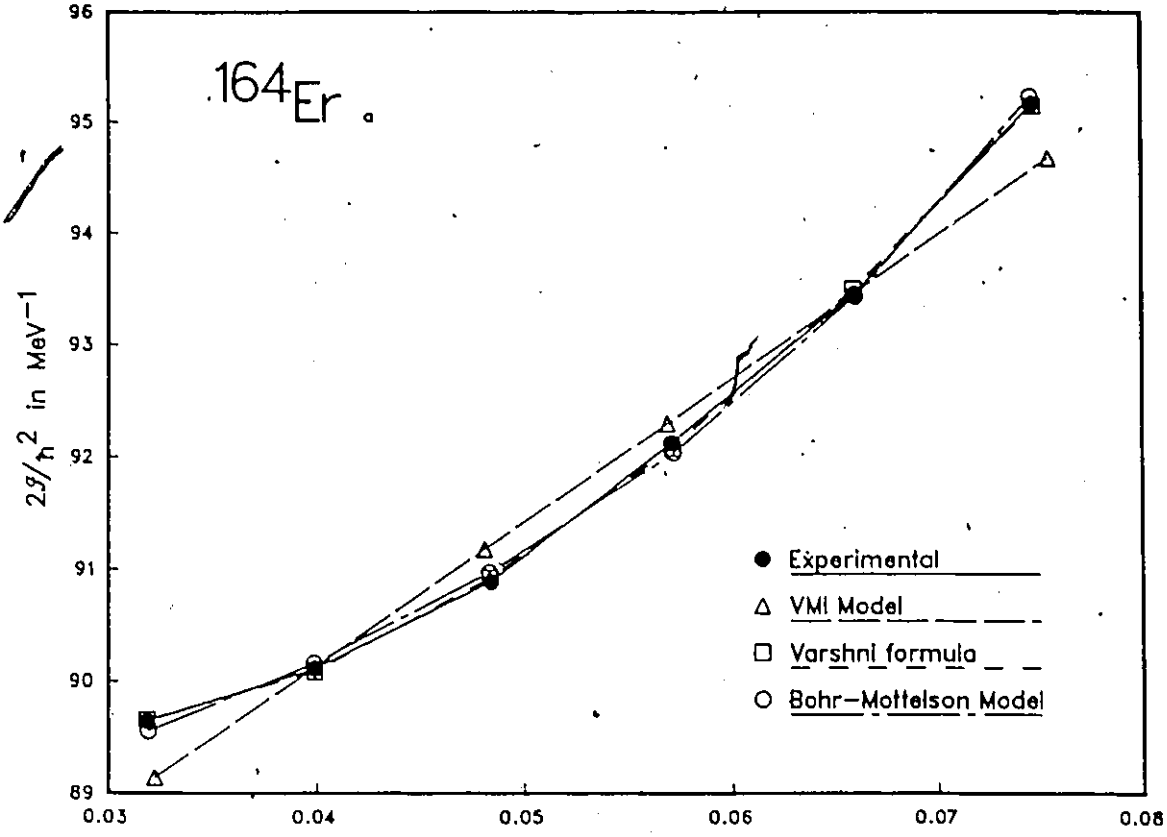

Fig. 2.13

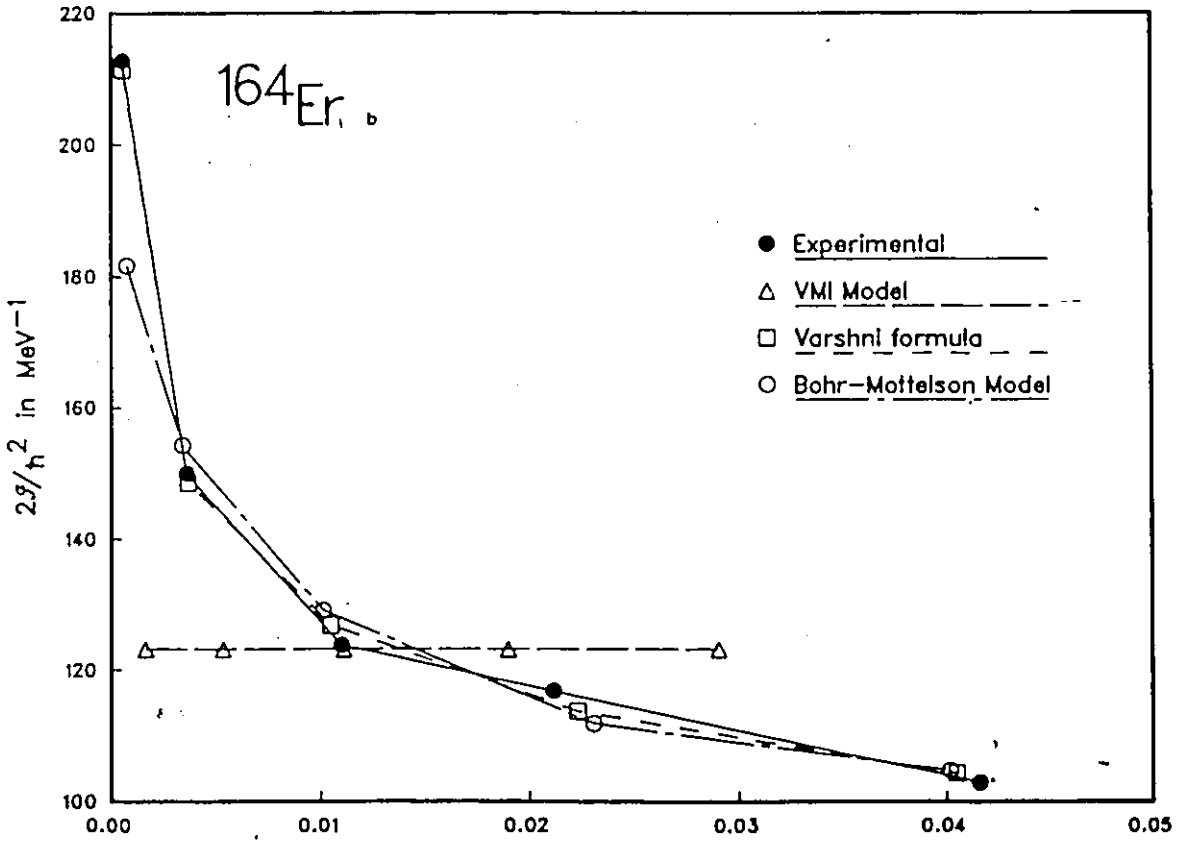

Fig 2.14

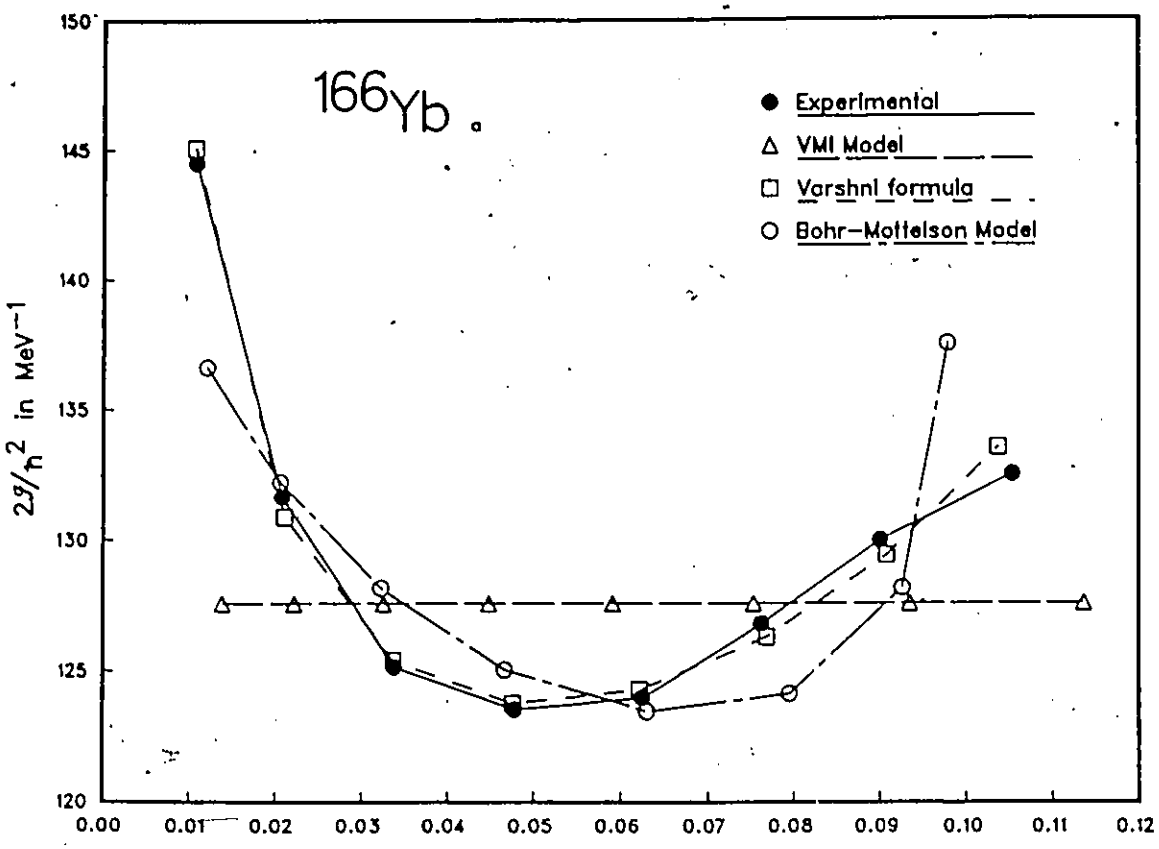

Fig. 2.15

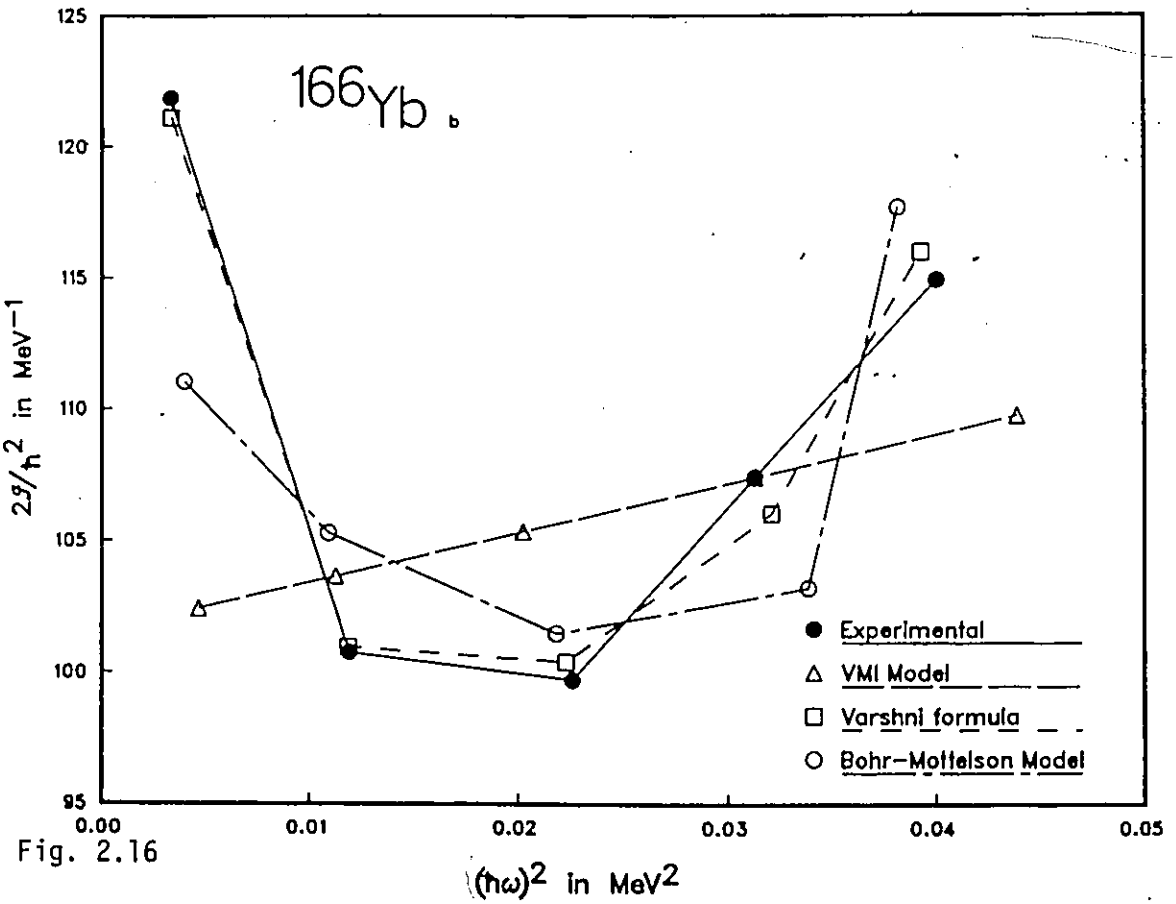

Fig. 2.16

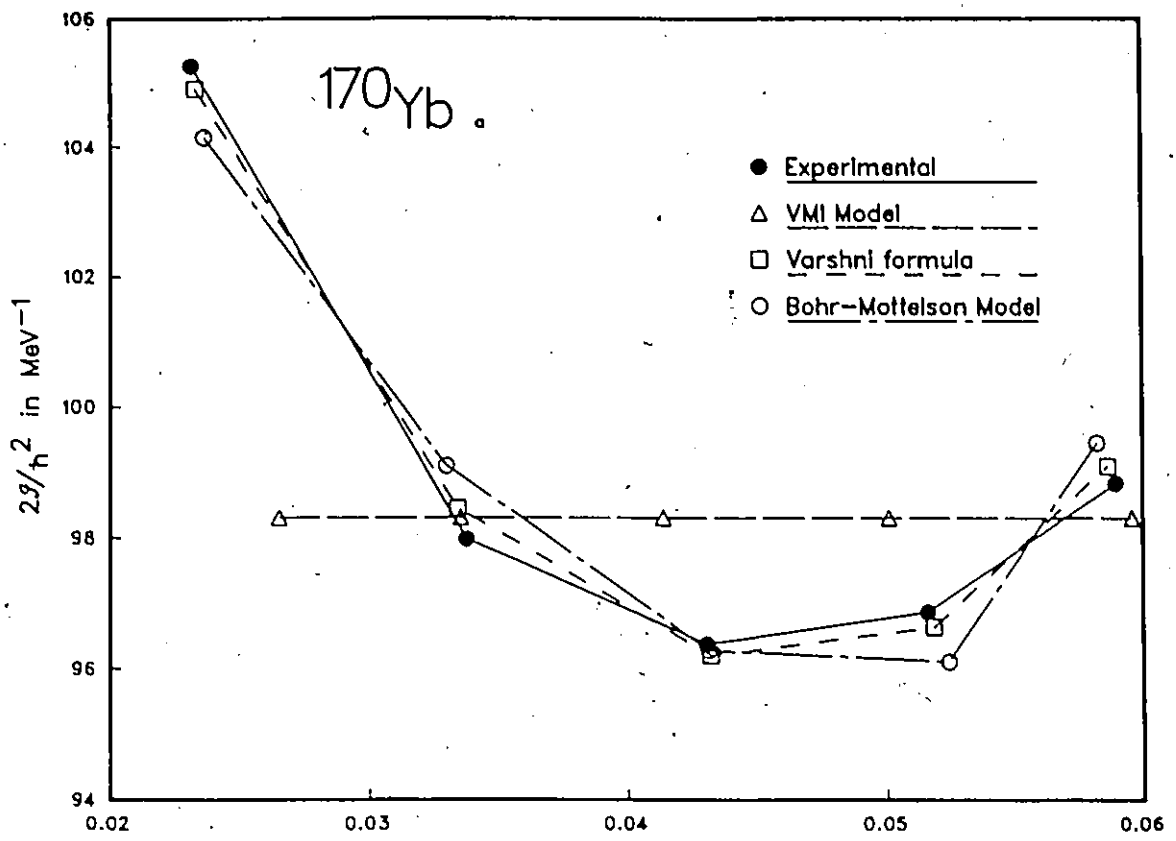

Fig. 2.17

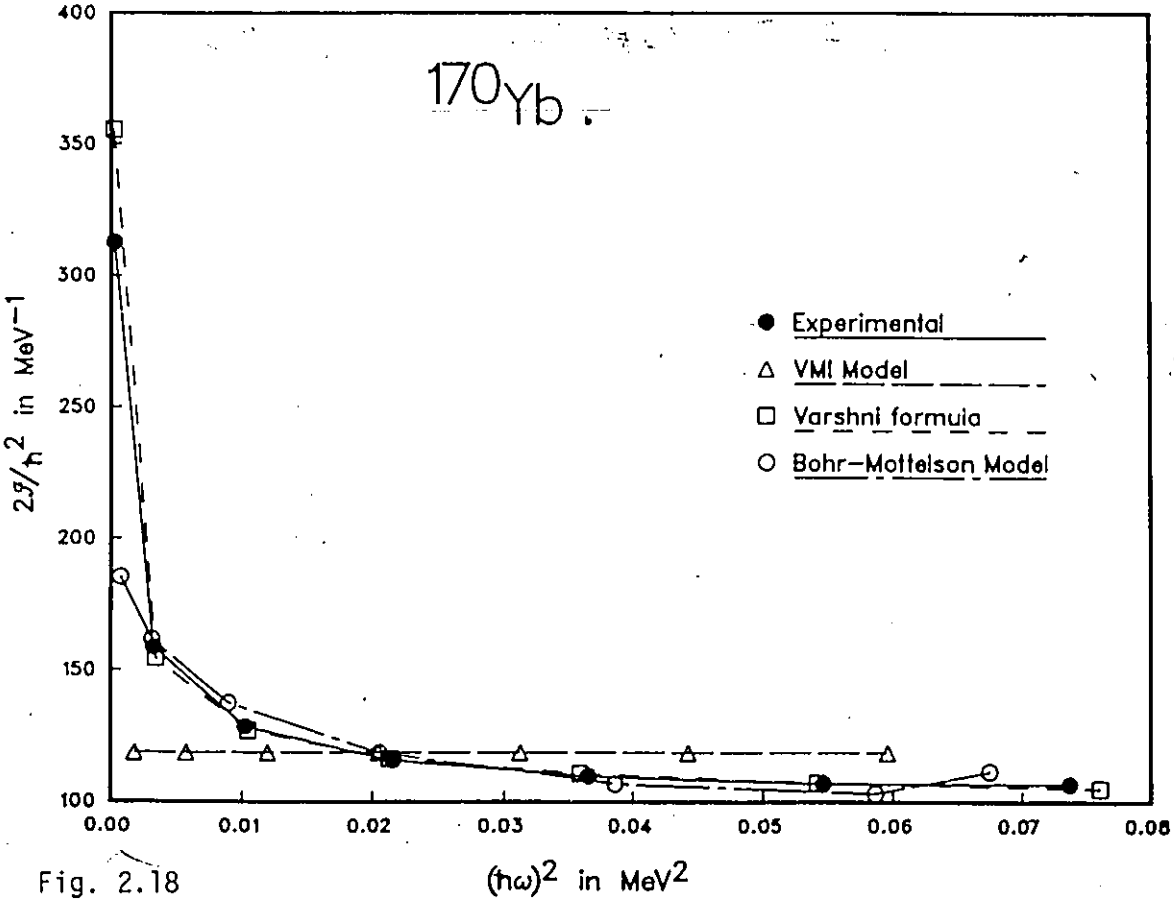

Fig. 2.18

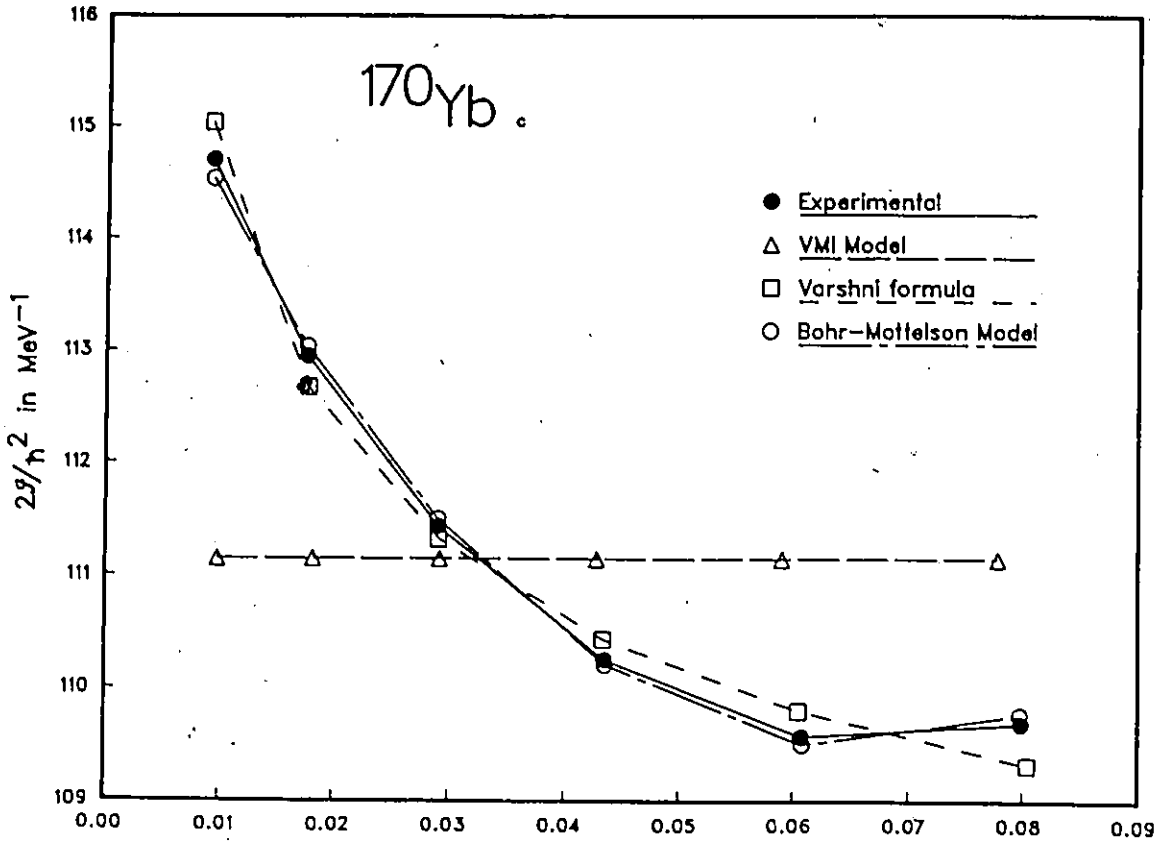

Fig. 2.19

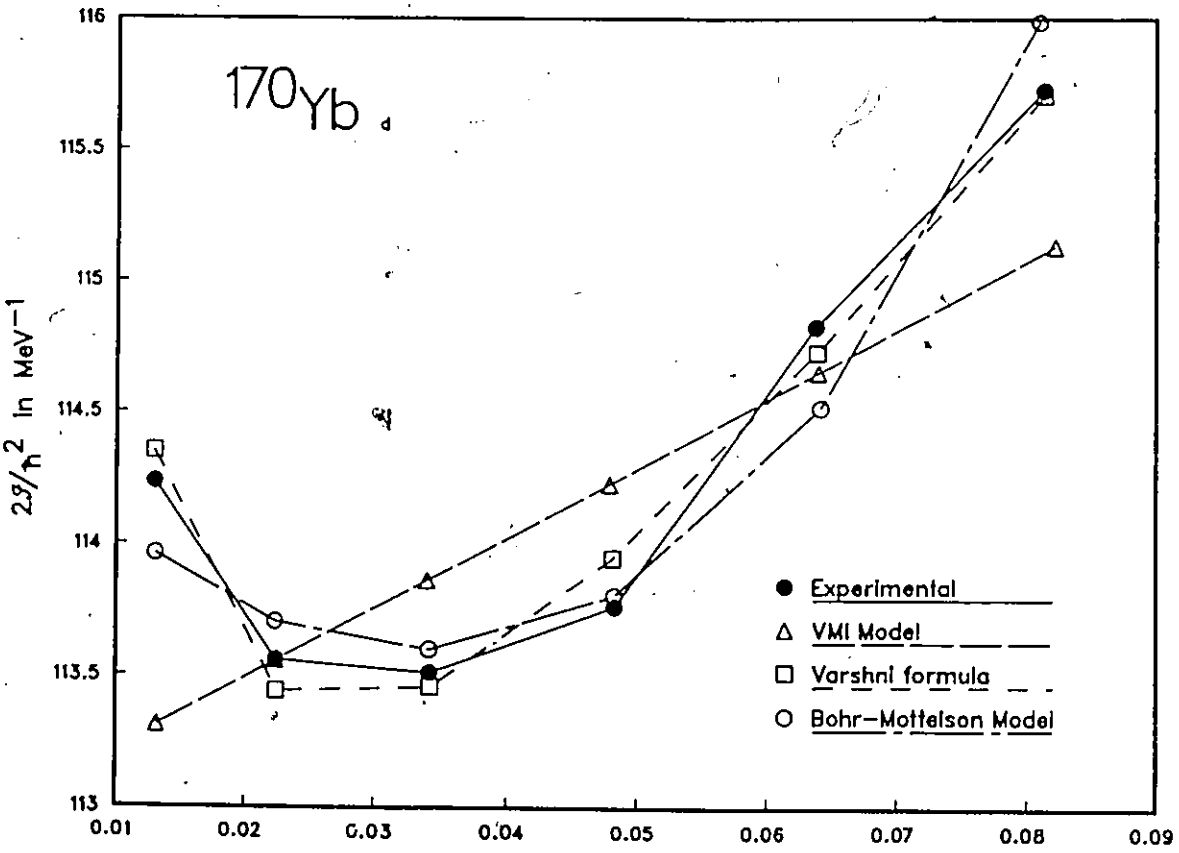

Fig. 2.20

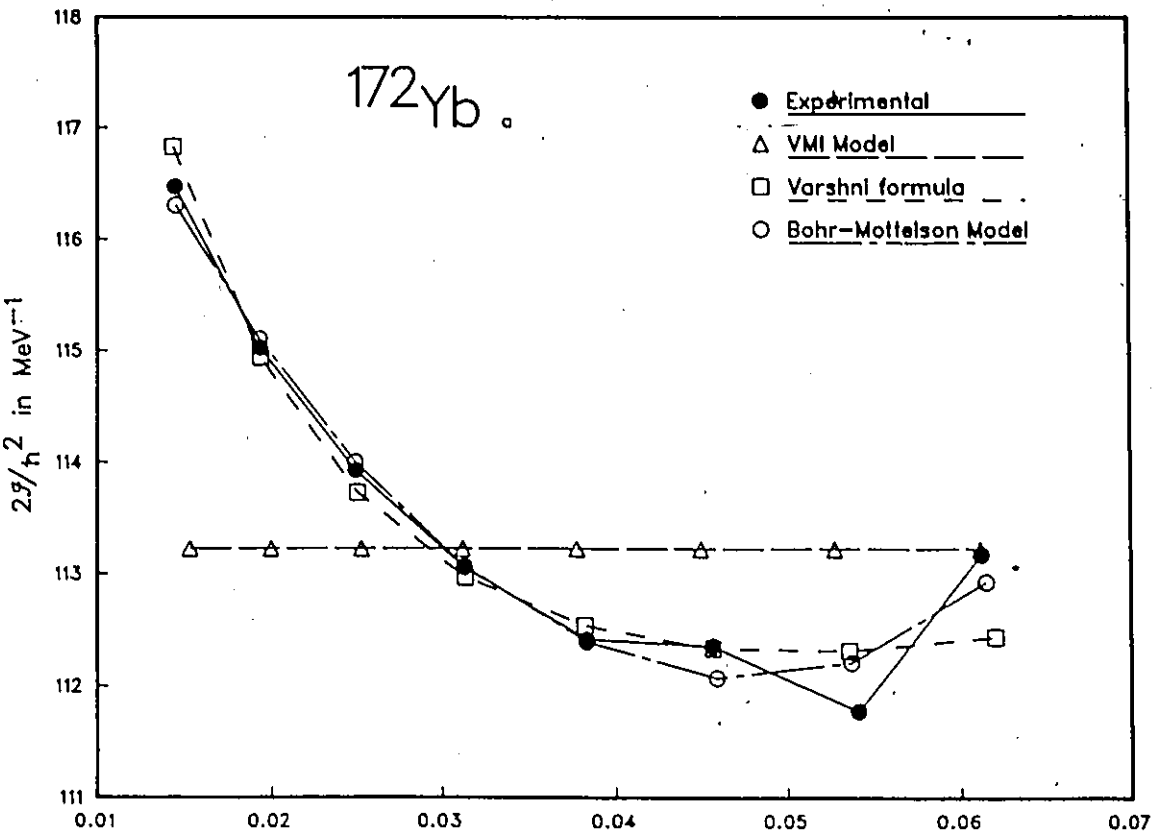

Fig. 2.21

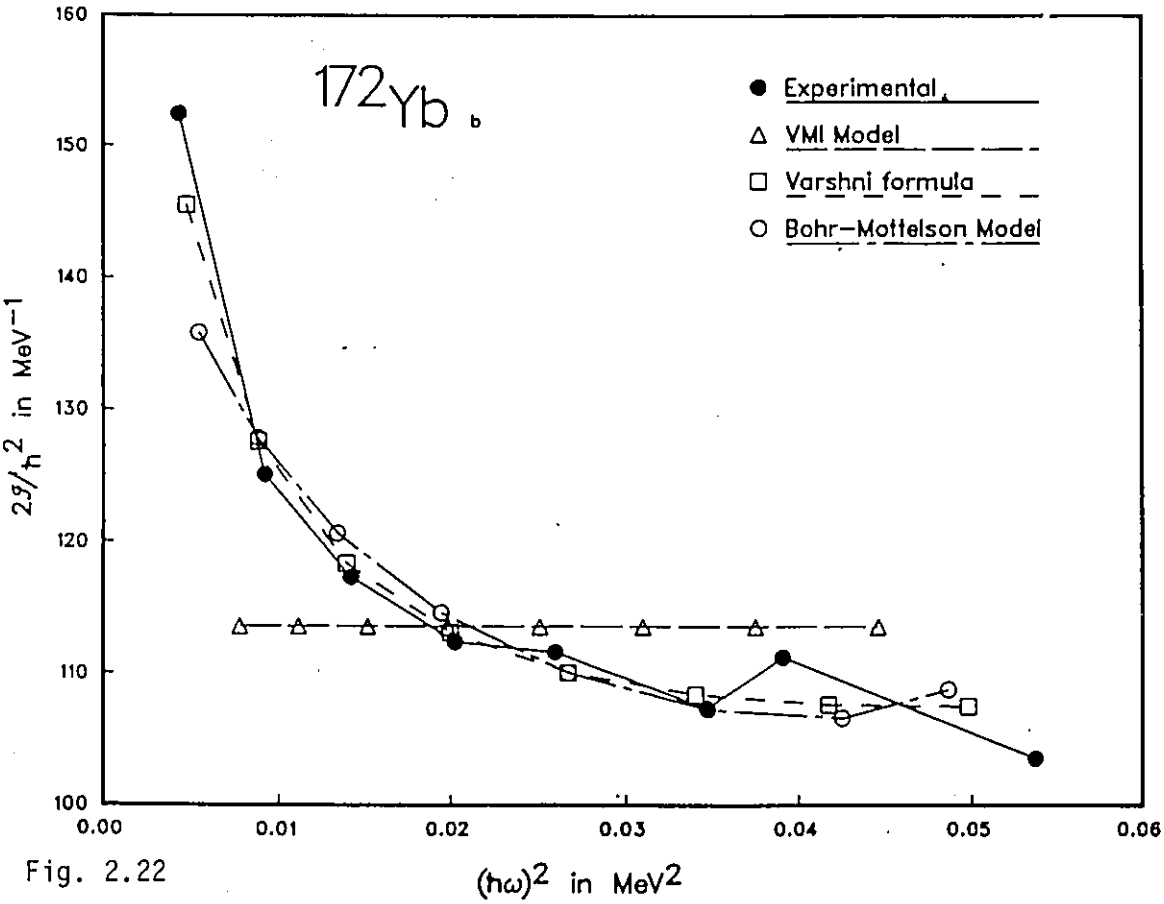

Fig. 2.22

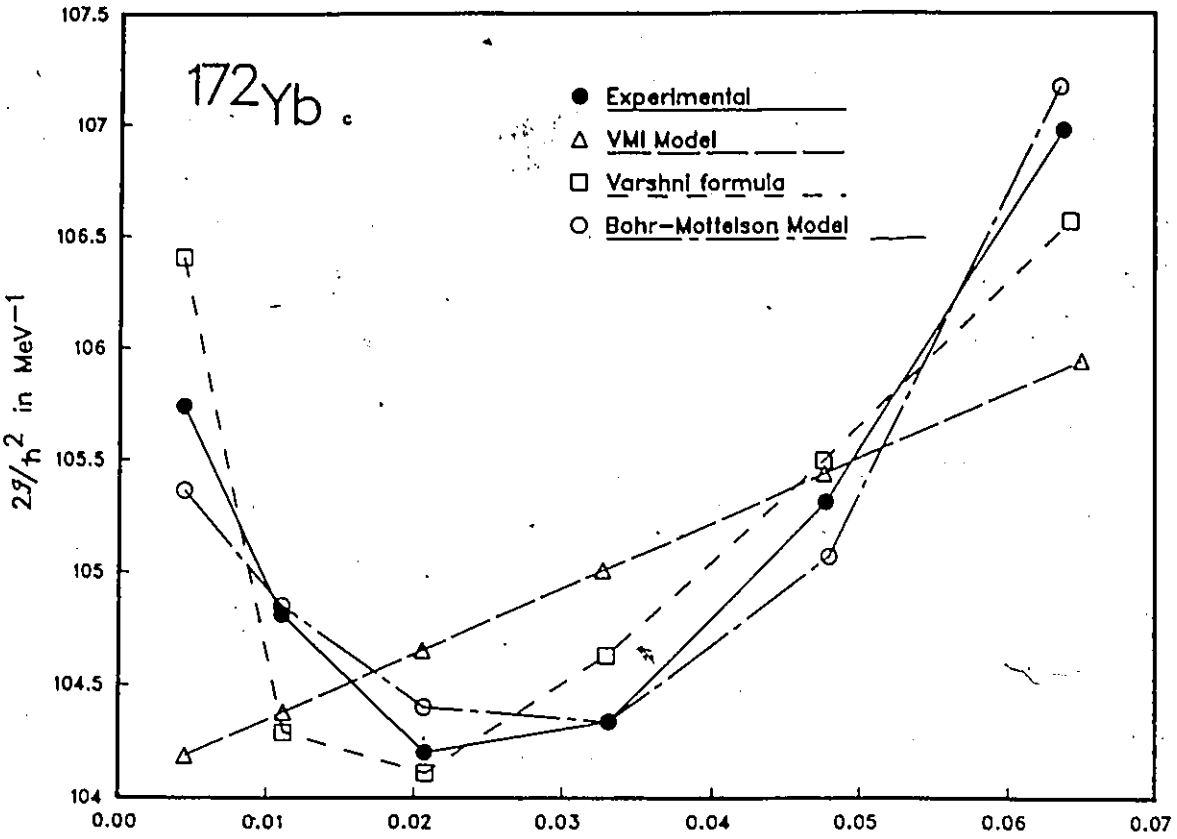

Fig. 2.23

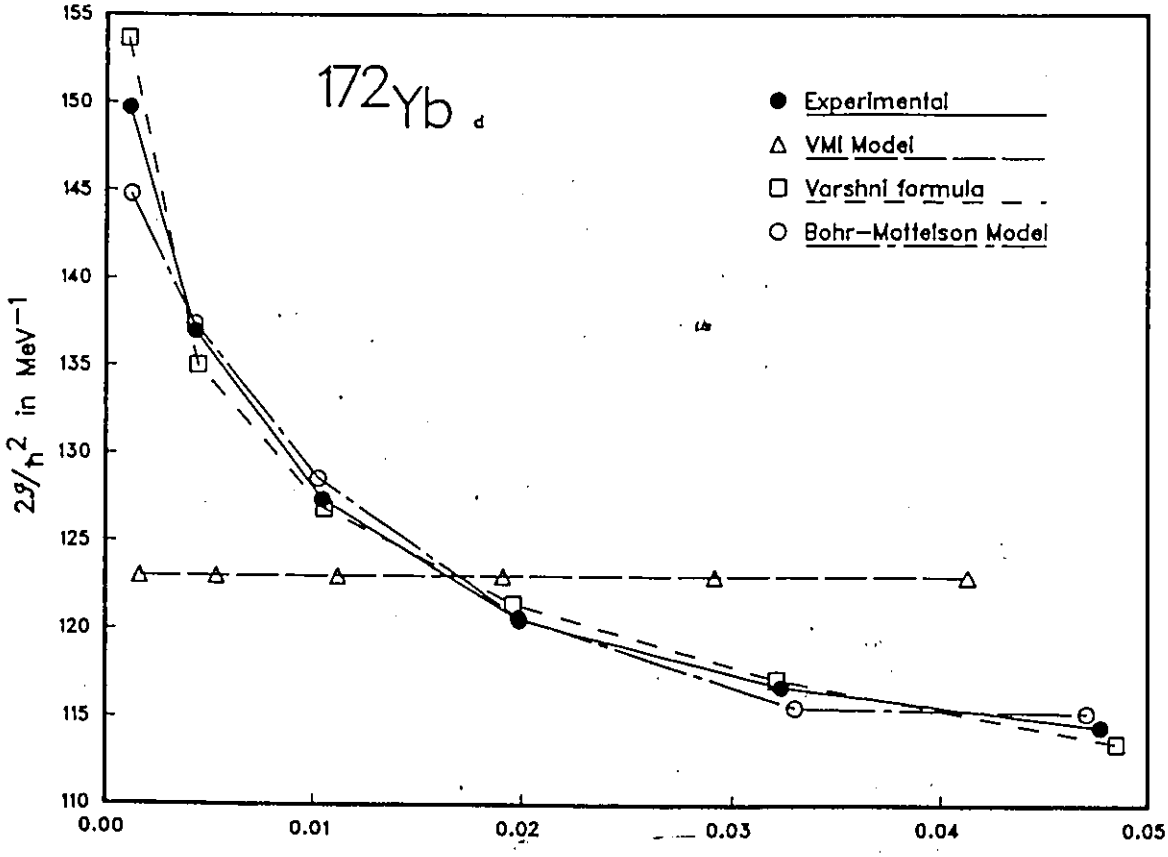

Fig. 2.24

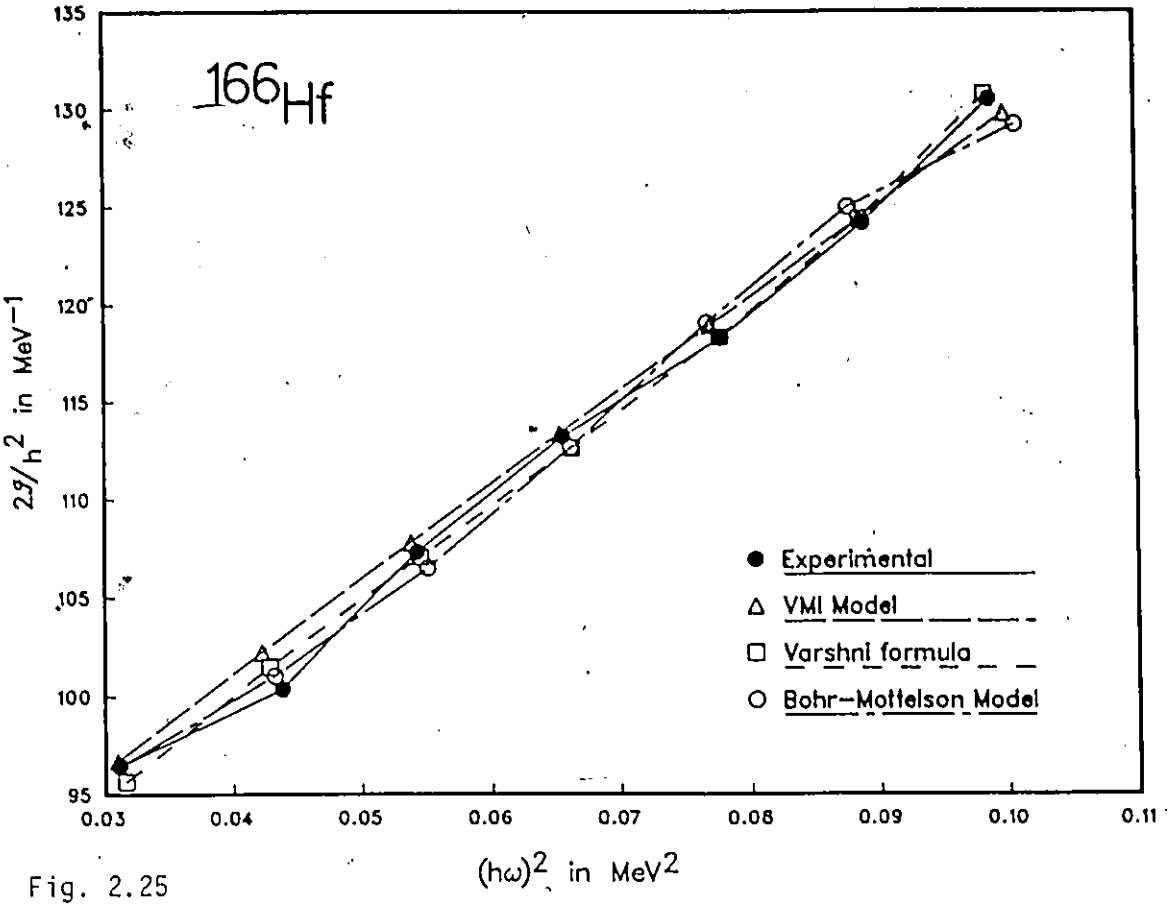

Fig. 2.25

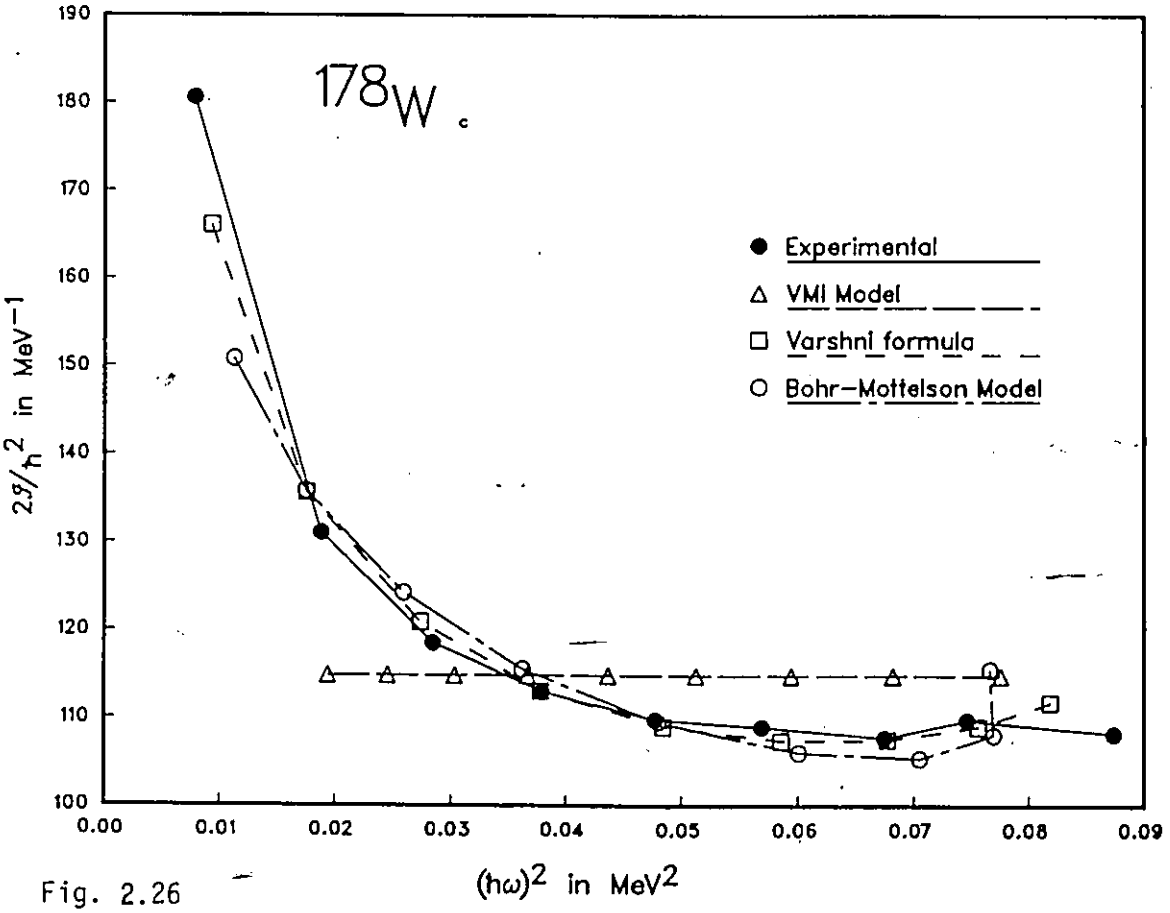

Fig. 2.26

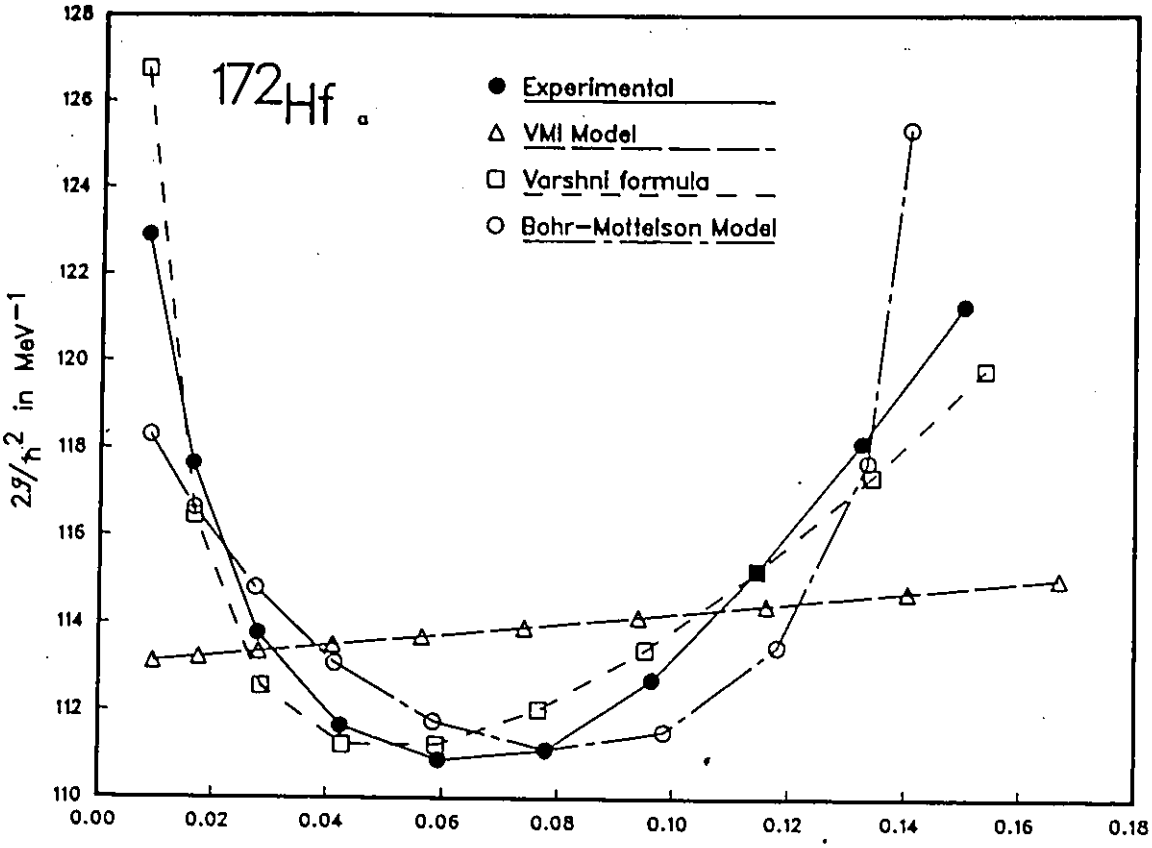

Fig. 2.27

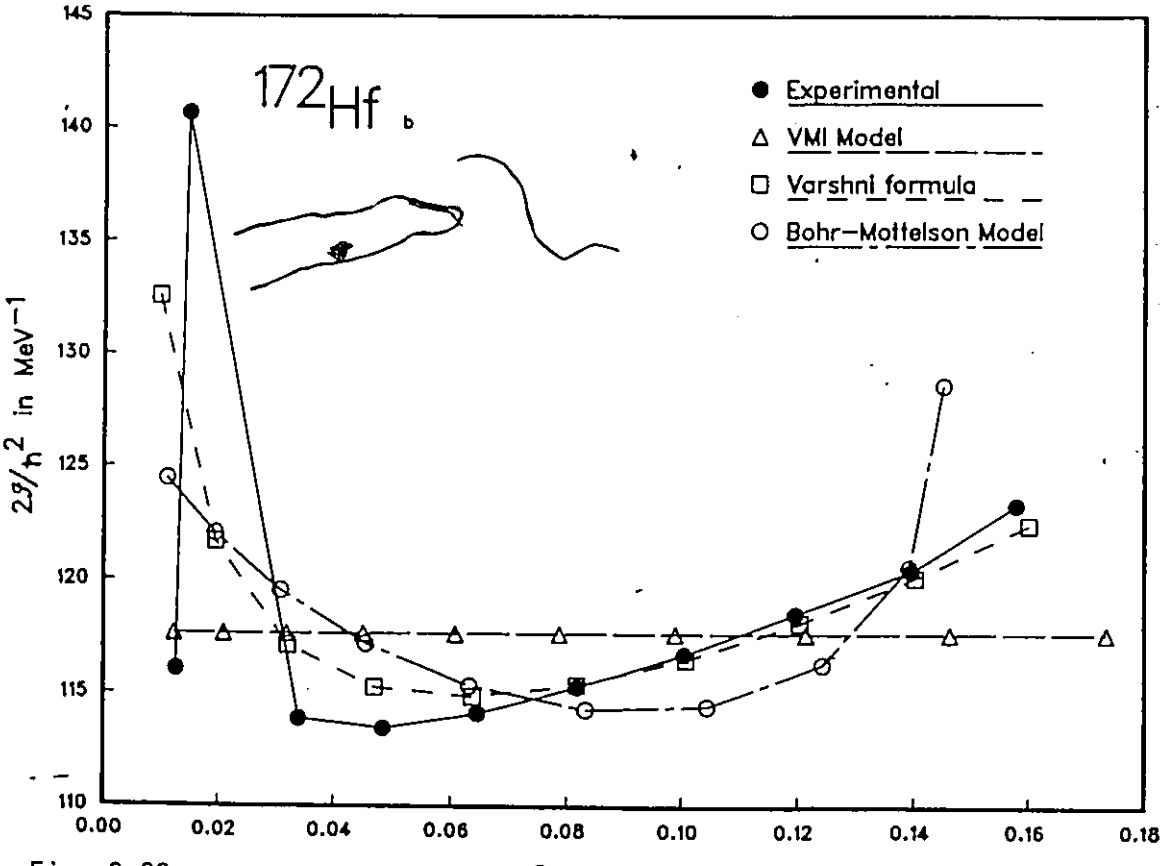

Fig. 2.28

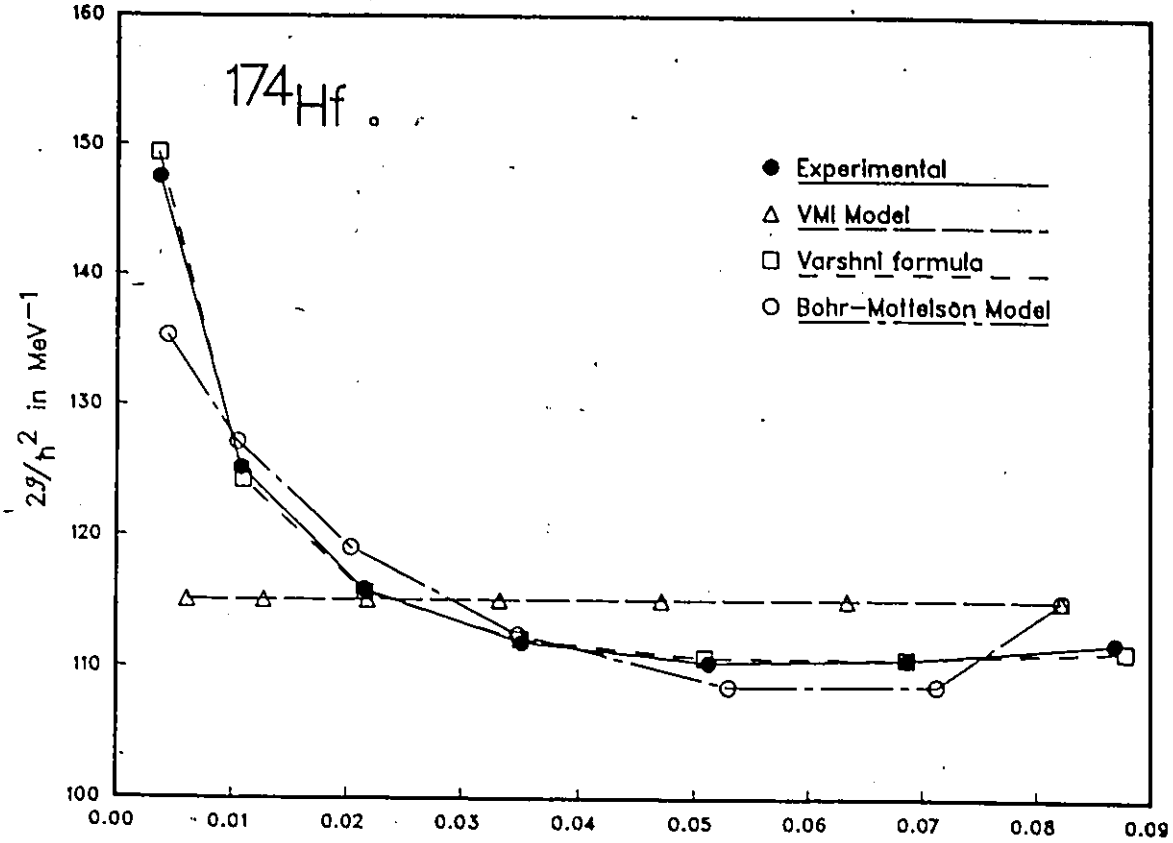

Fig. 2.29

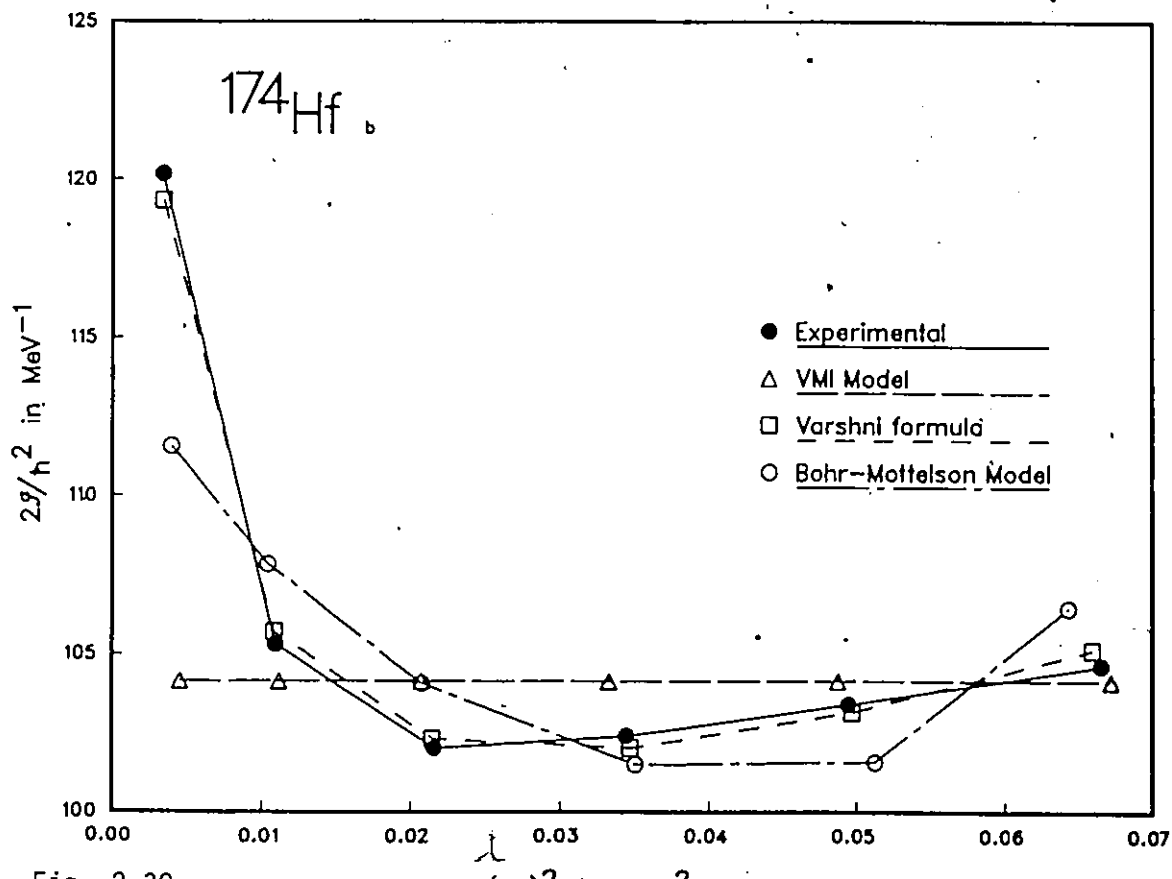

Fig. 2.30

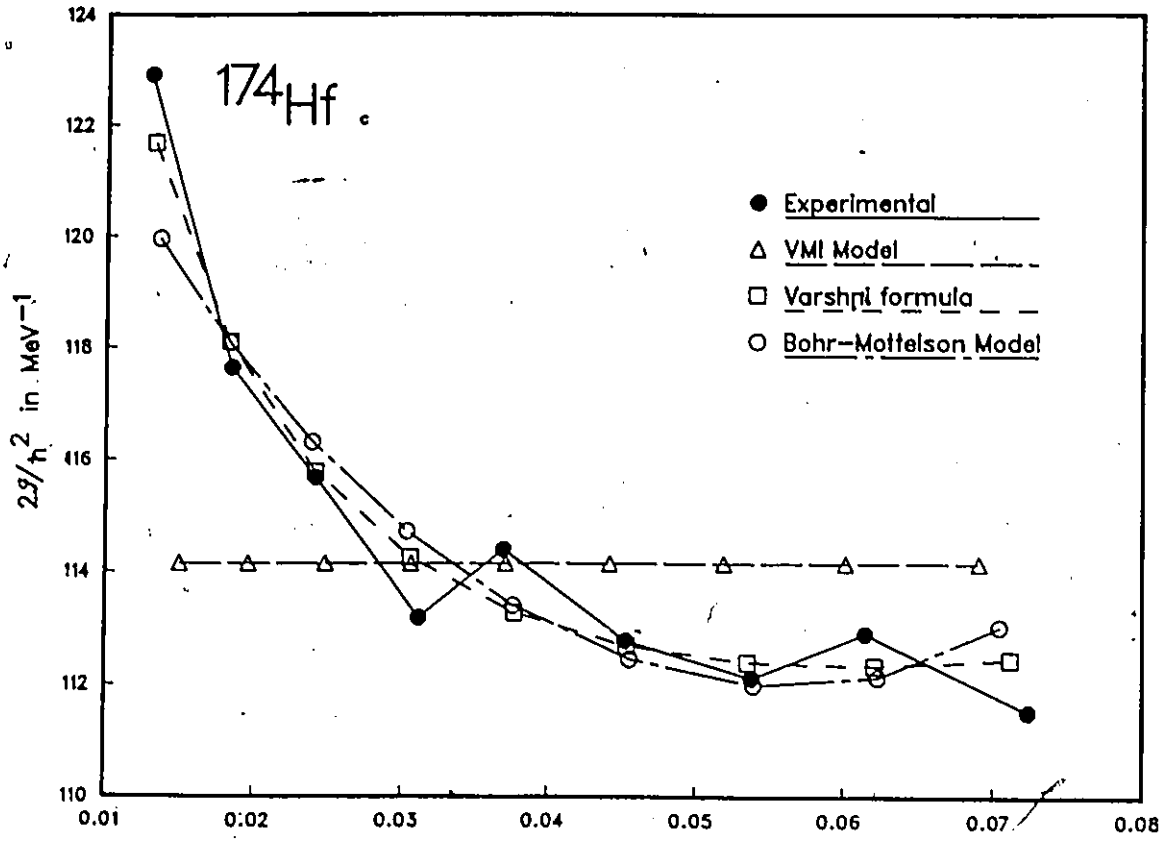

Fig. 2.31

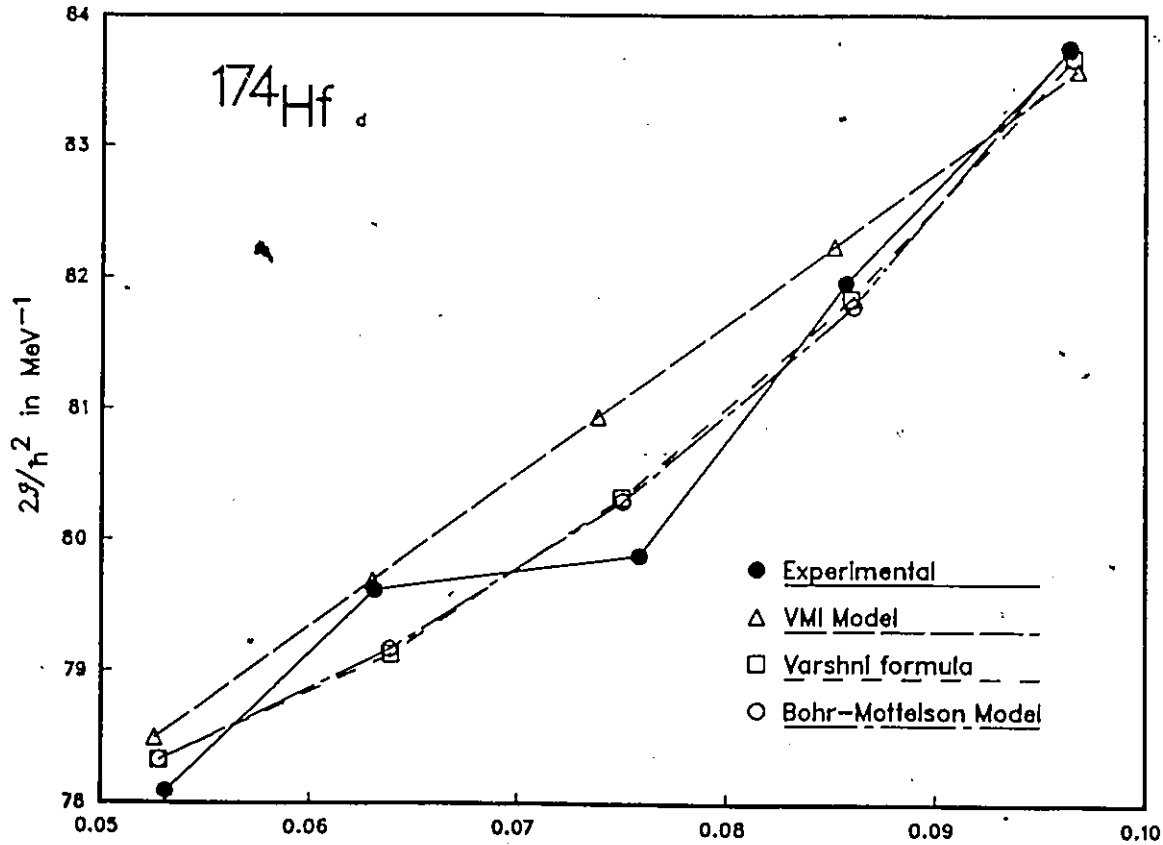

Fig. 2.32

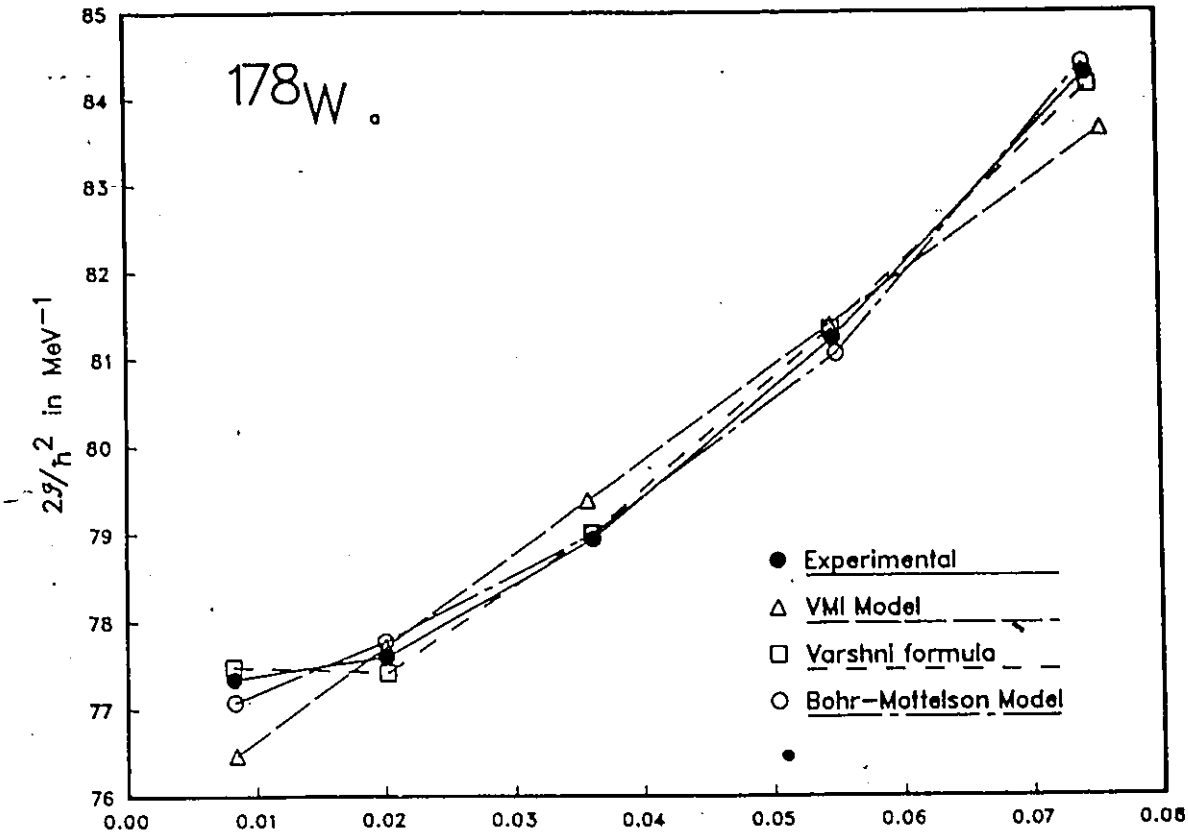

Fig. 2.33

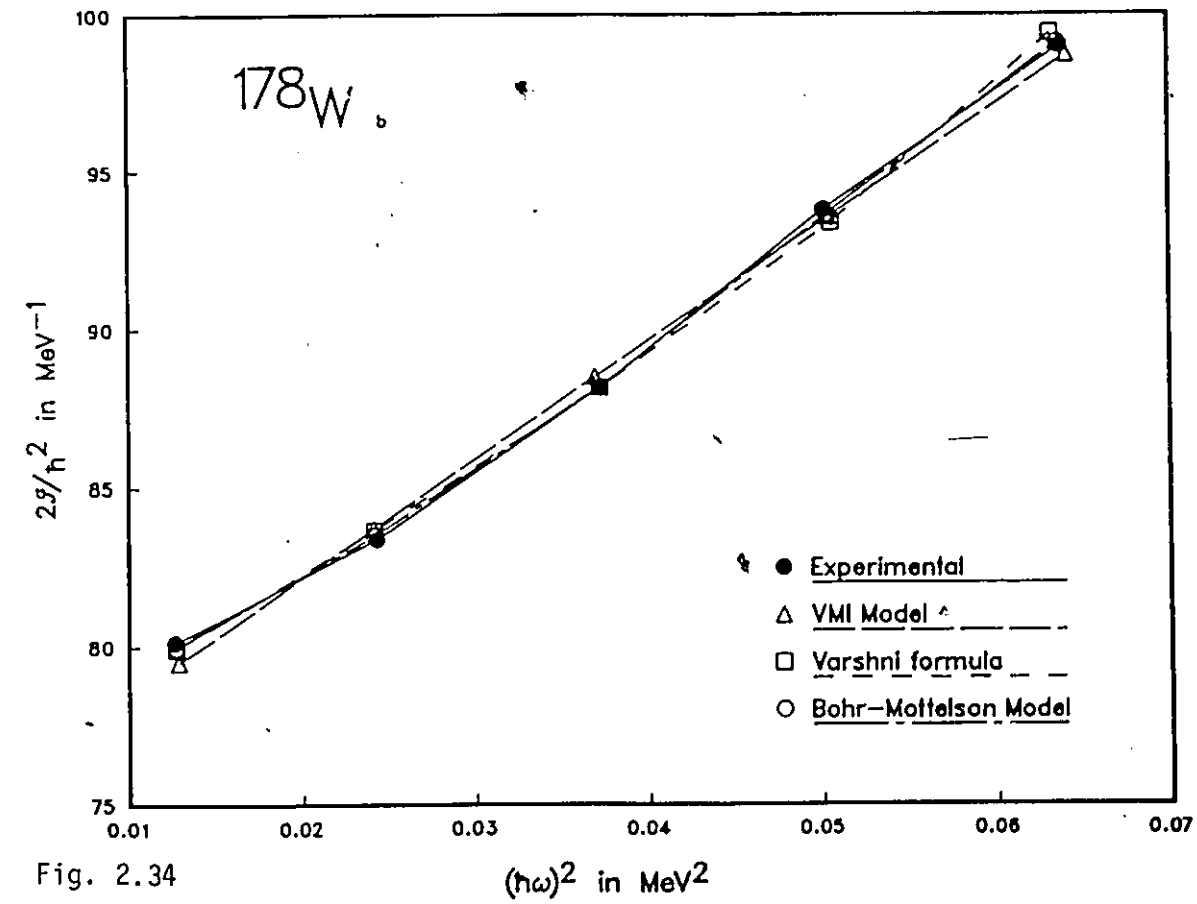

Fig. 2.34

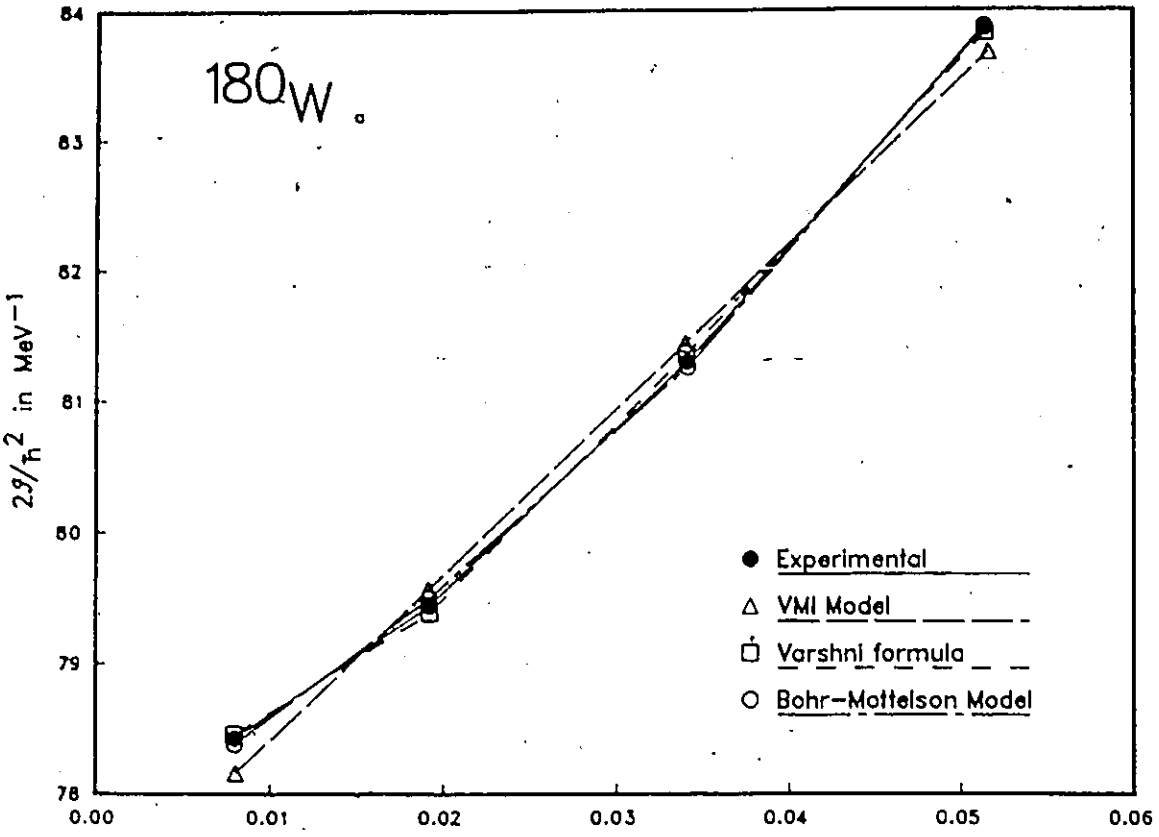

Fig. 2.35

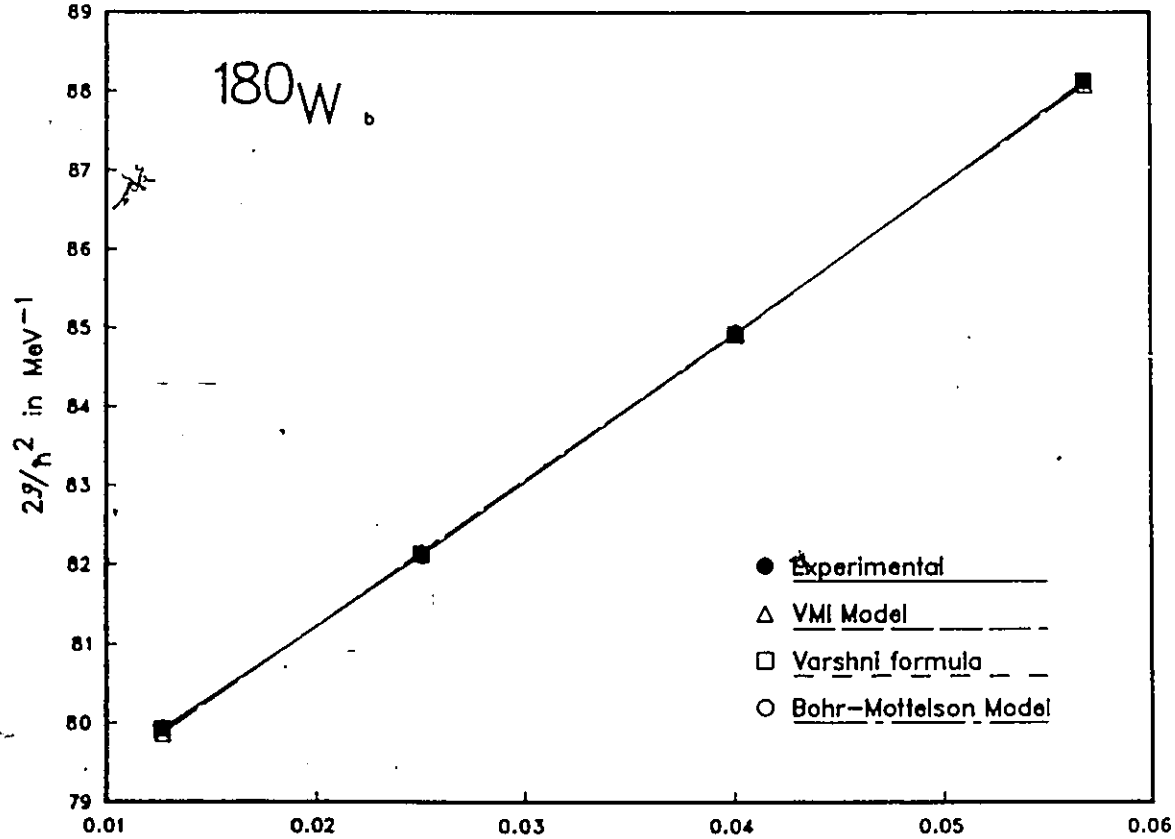

Fig. 2.36

Correlation E_1–p, Varshni formula

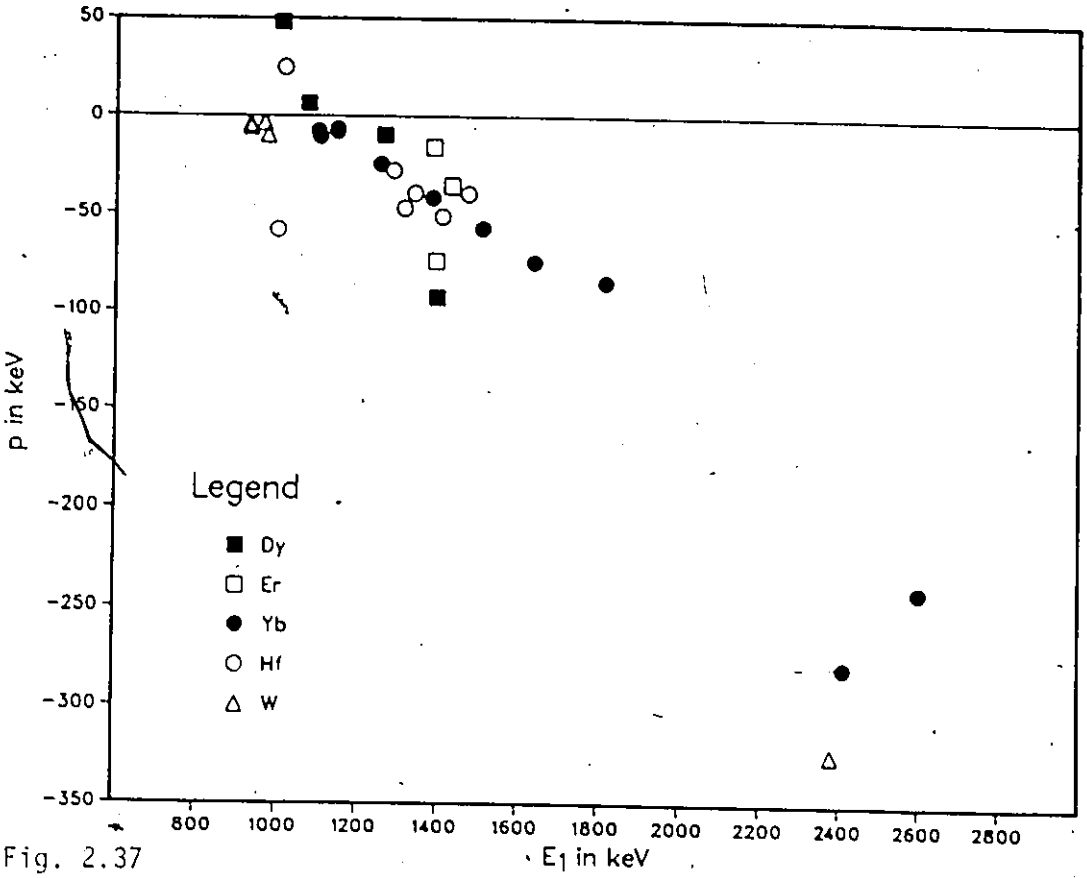

Fig. 2.37

Correlation a–q, Varshni formula

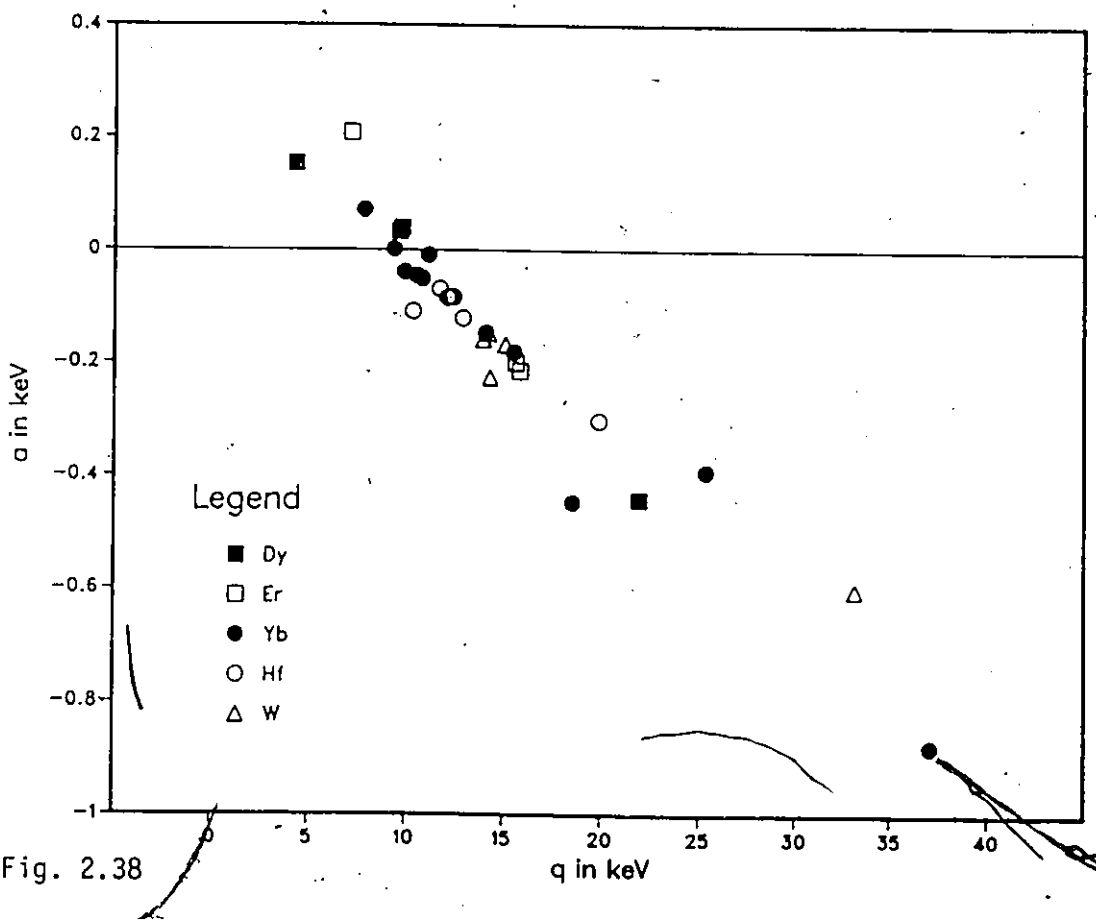

Fig. 2.38

Correlation A–C, Bohr–Mottelson Model

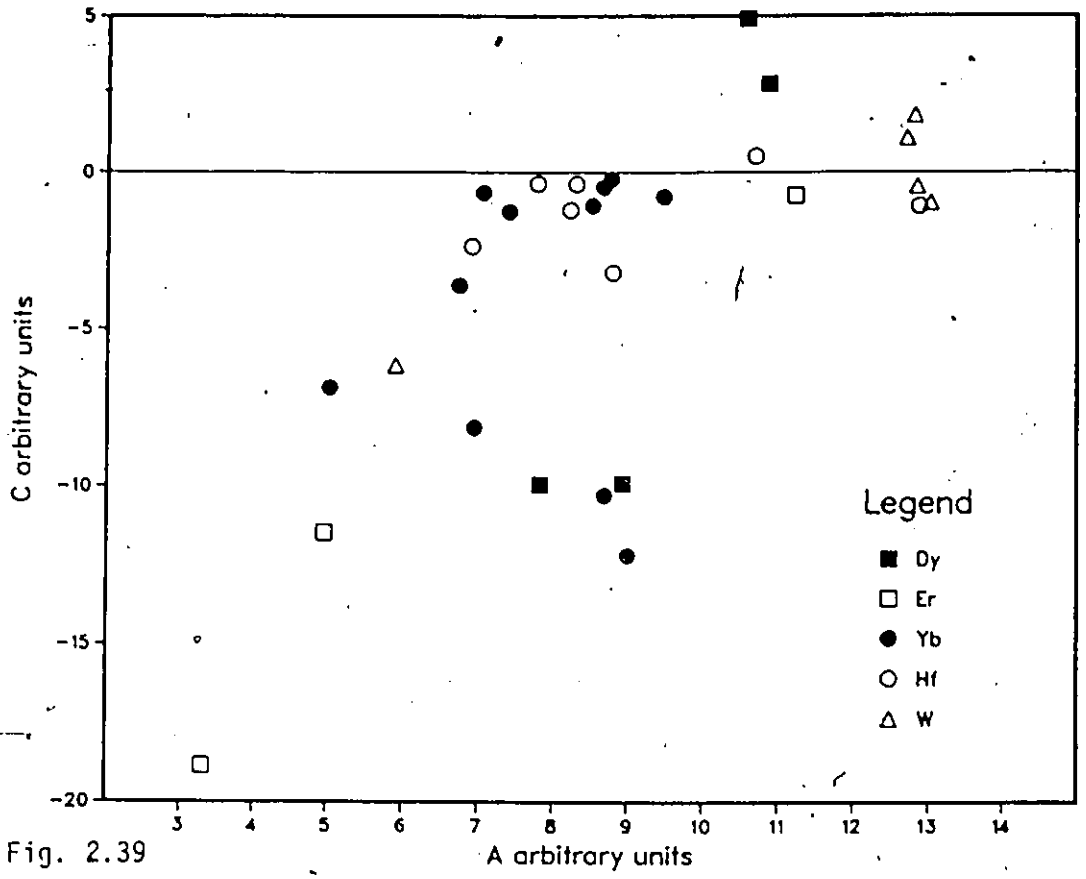

Fig. 2.39

Correlation B–C, Bohr–Mottelson Model

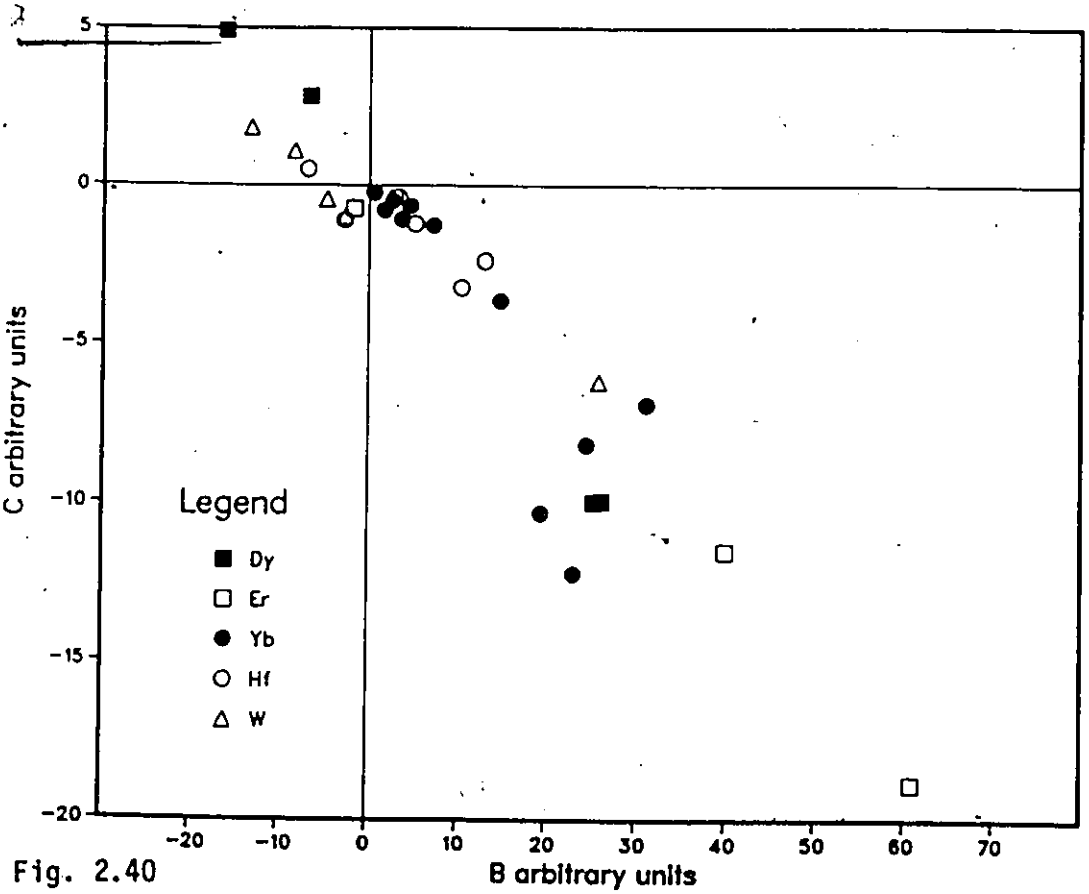

Fig. 2.40

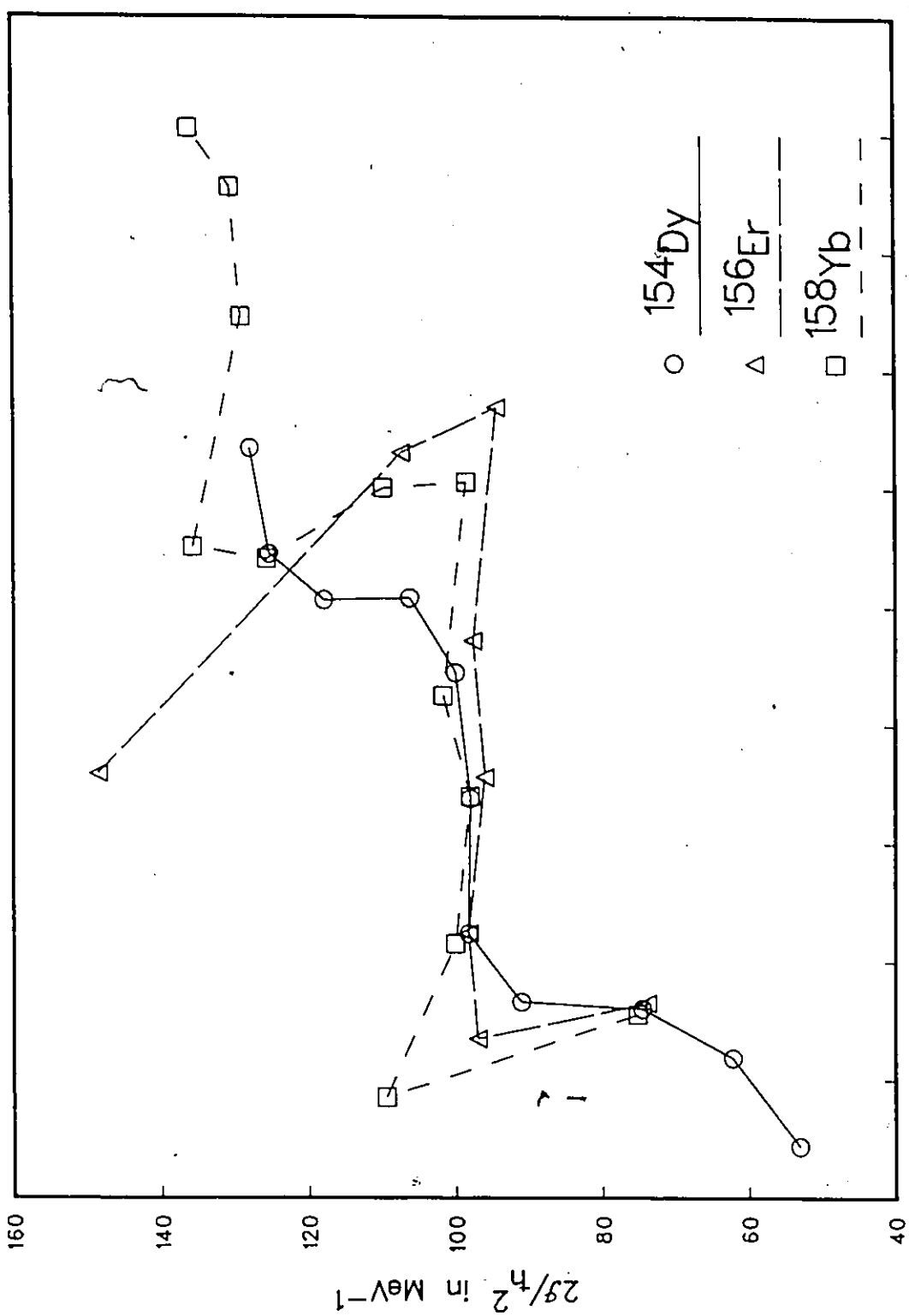
N = 88 Isotones
154_{Dy}
156_{Er}
158_{Yb}
$2\mathcal{I}/\hbar^2$ in MeV^{-1}
$(\hbar\omega)^2$ in MeV^2
160
140
120
100
80
60
40
0.02
0.04
0.06
0.08
0.10
0.12
0.14
0.16
0.18
0.20
0.22

Fig. 2.41

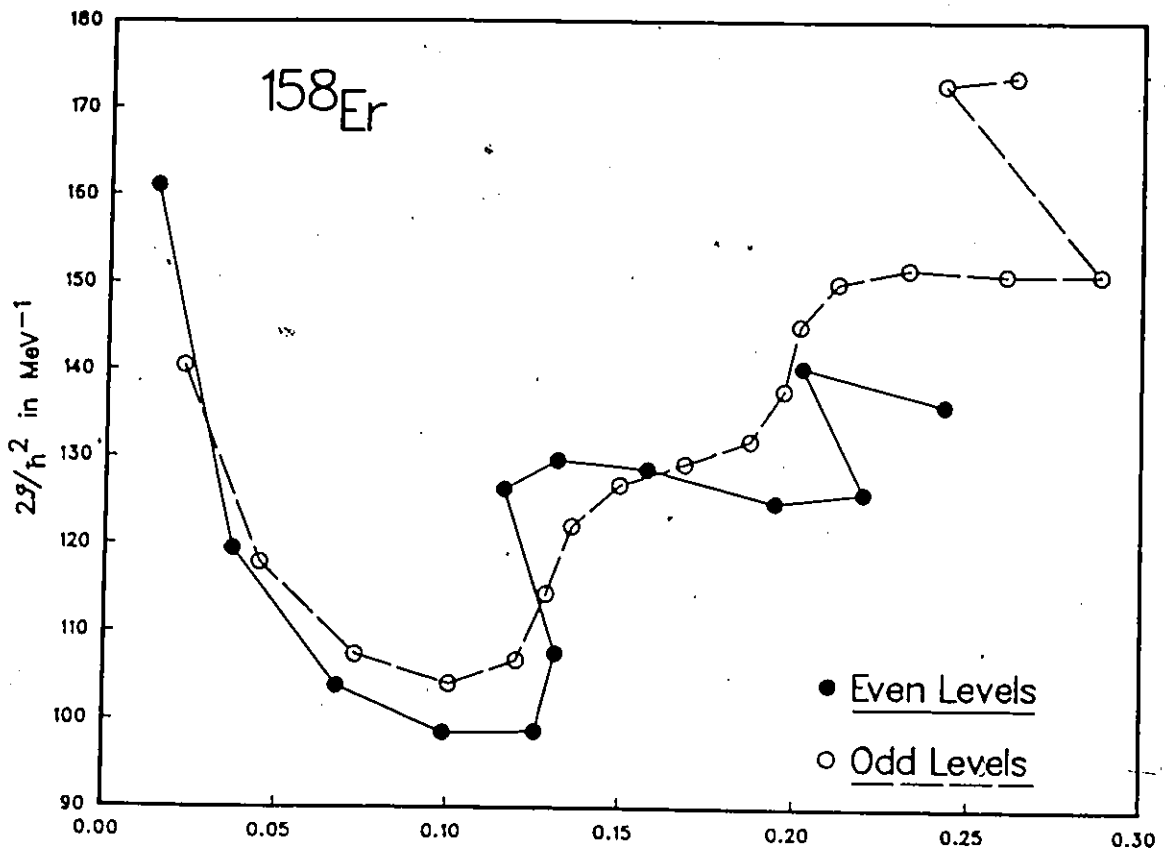

Fig. 2.42

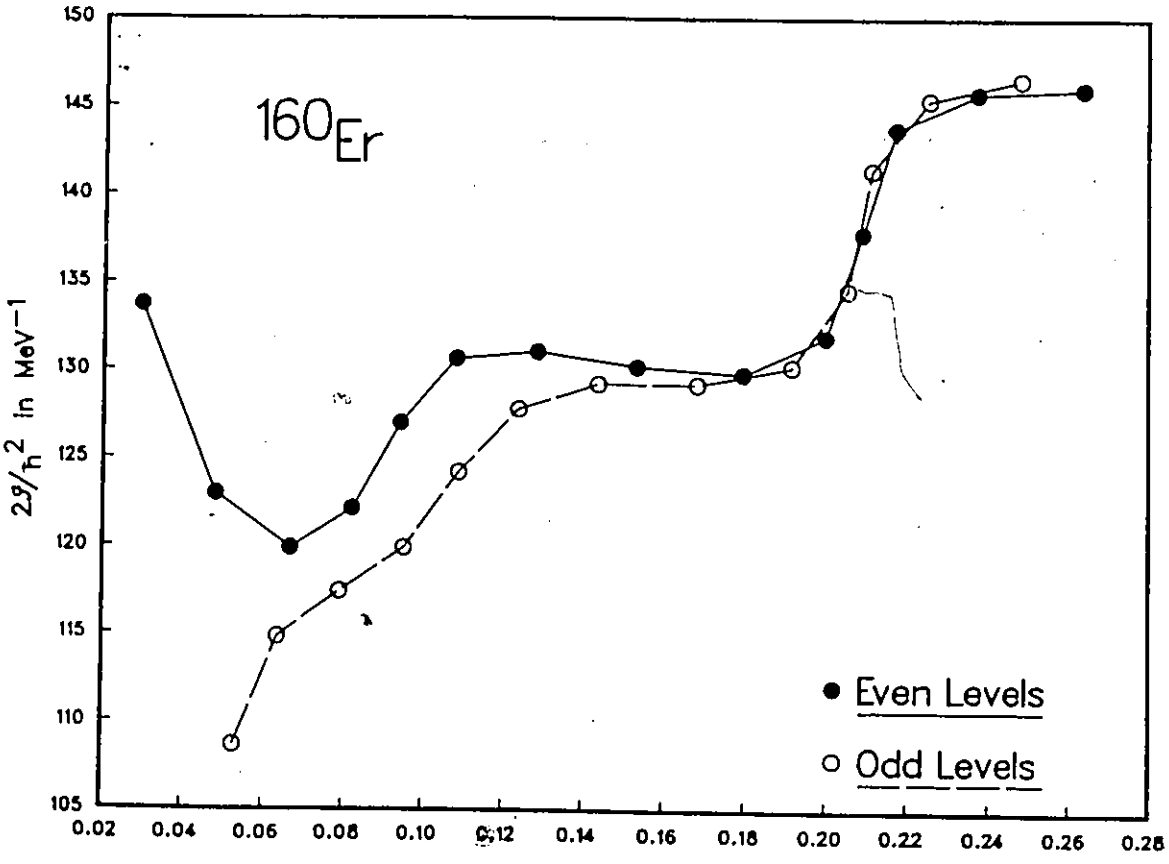

Fig. 2.43

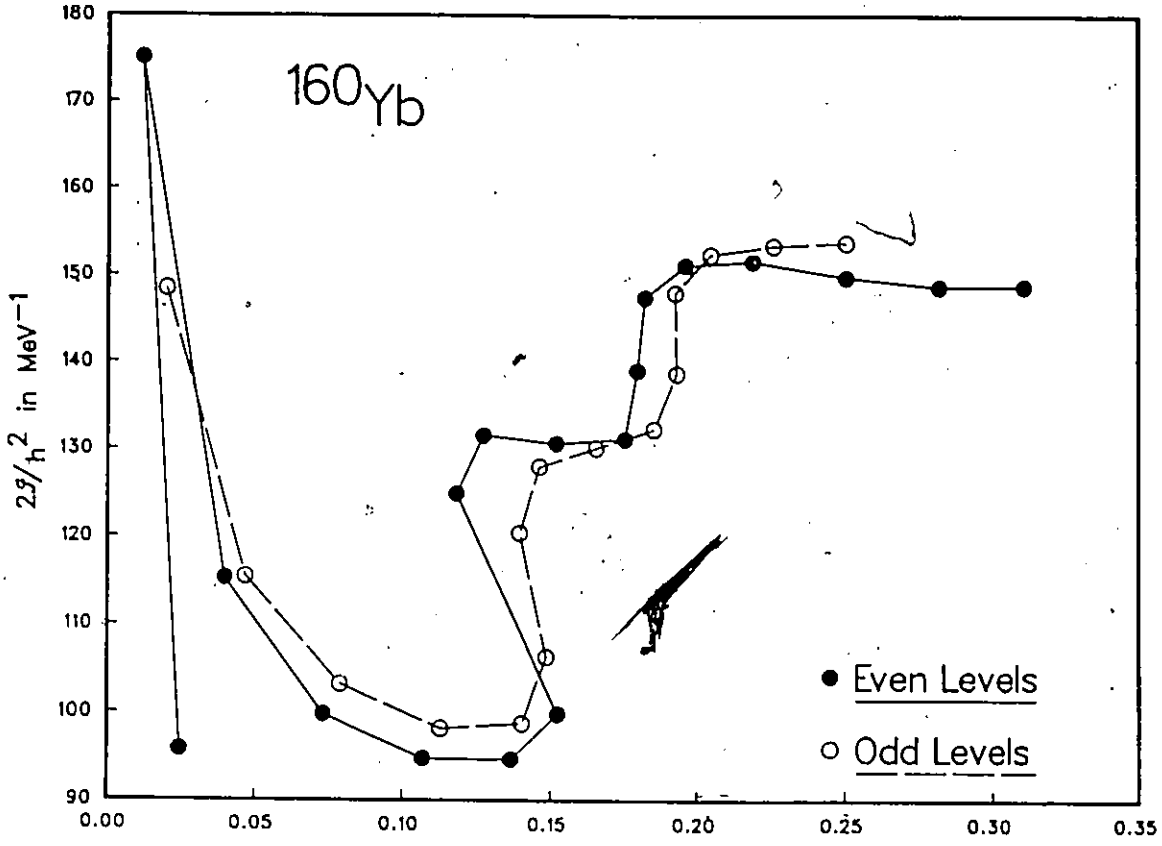

Fig. 2.44

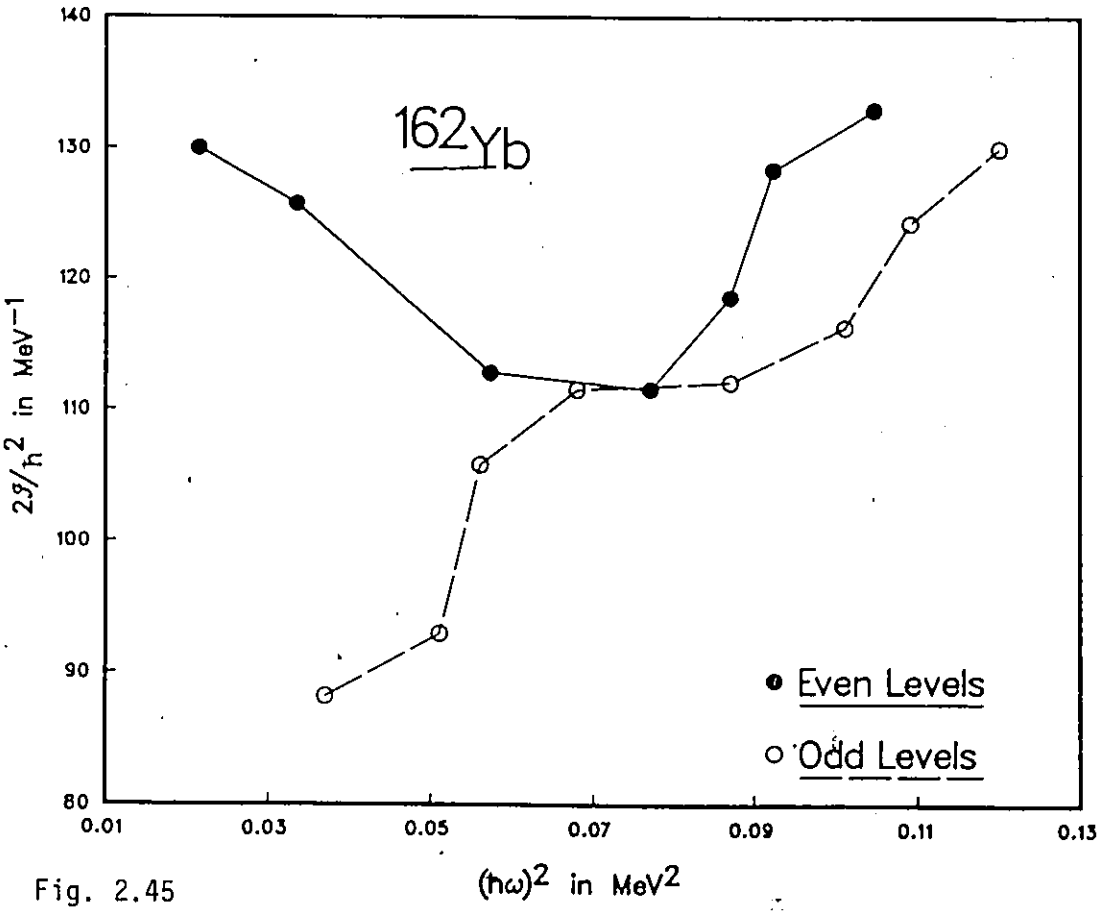

Fig. 2.45

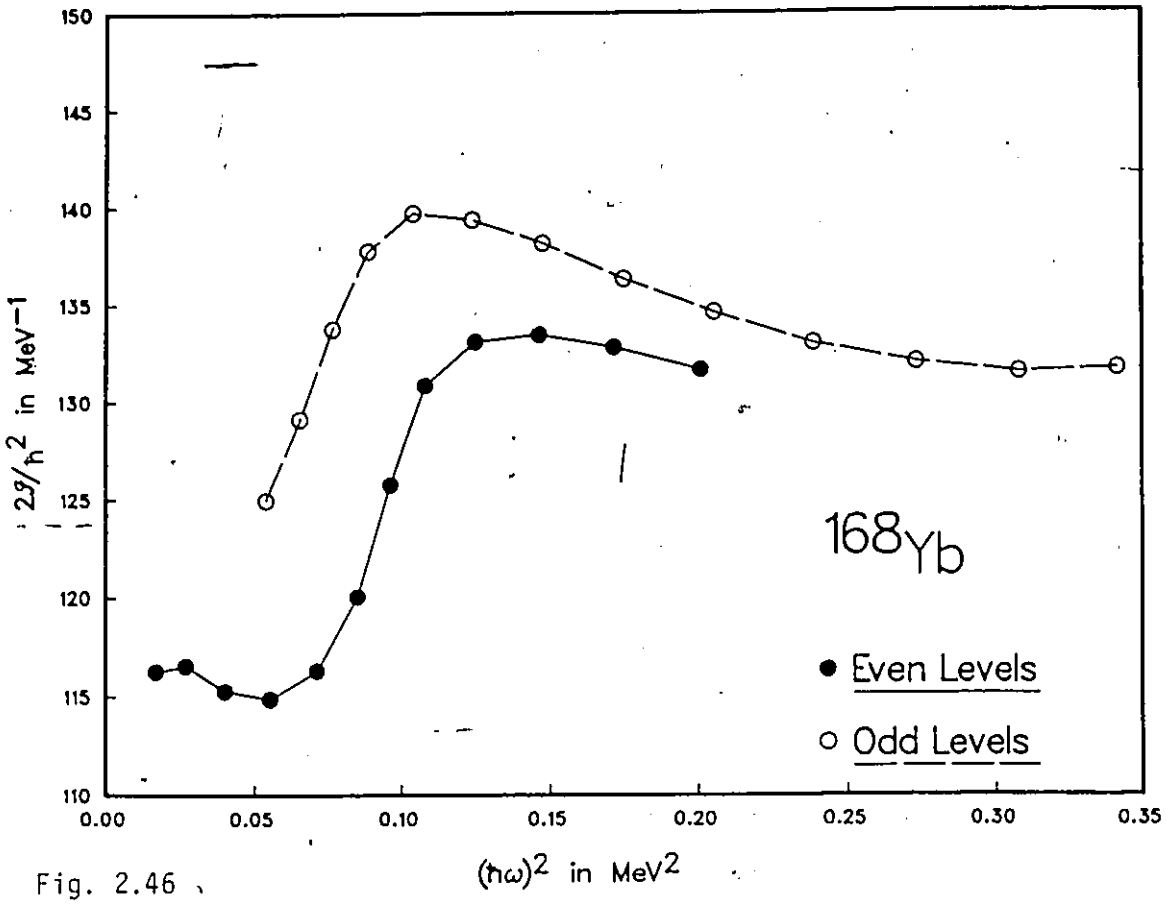

Fig. 2.46

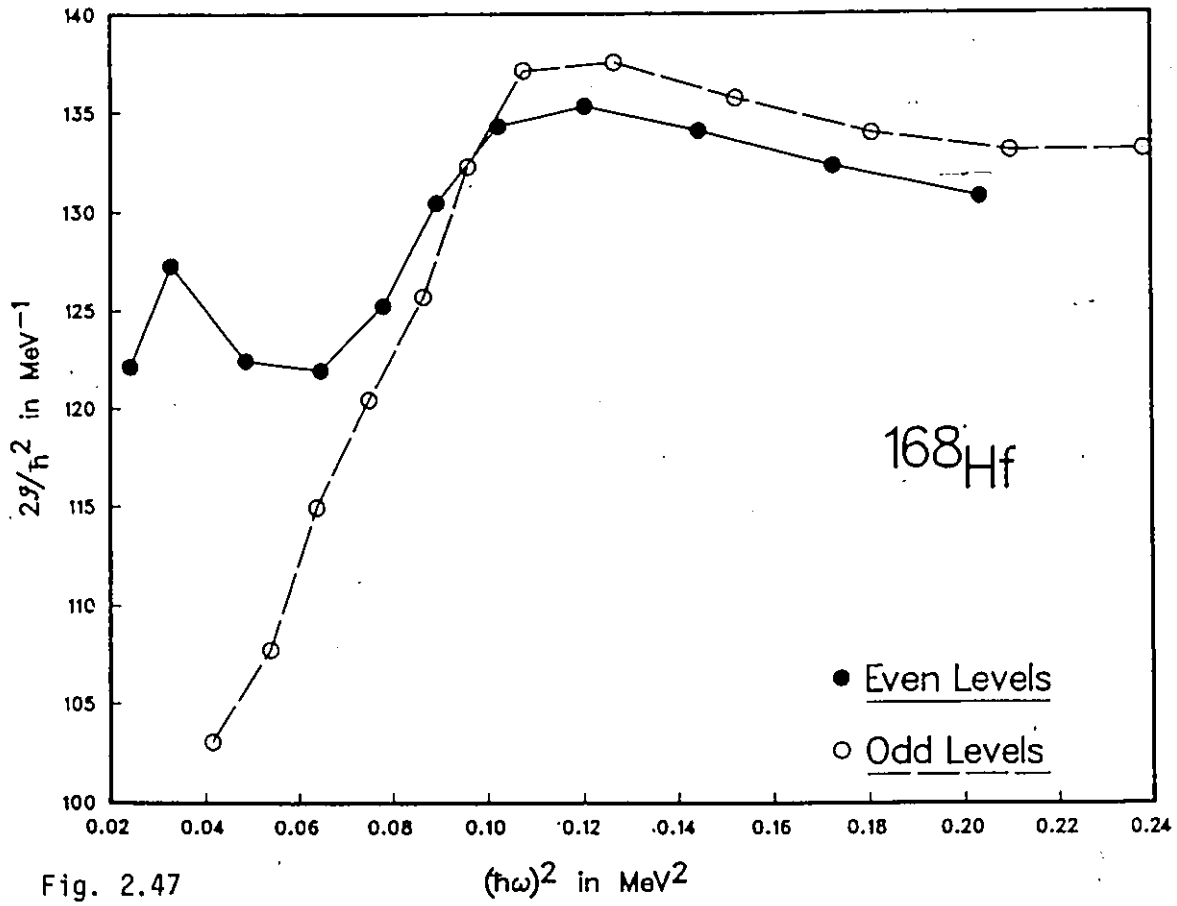

Fig. 2.47

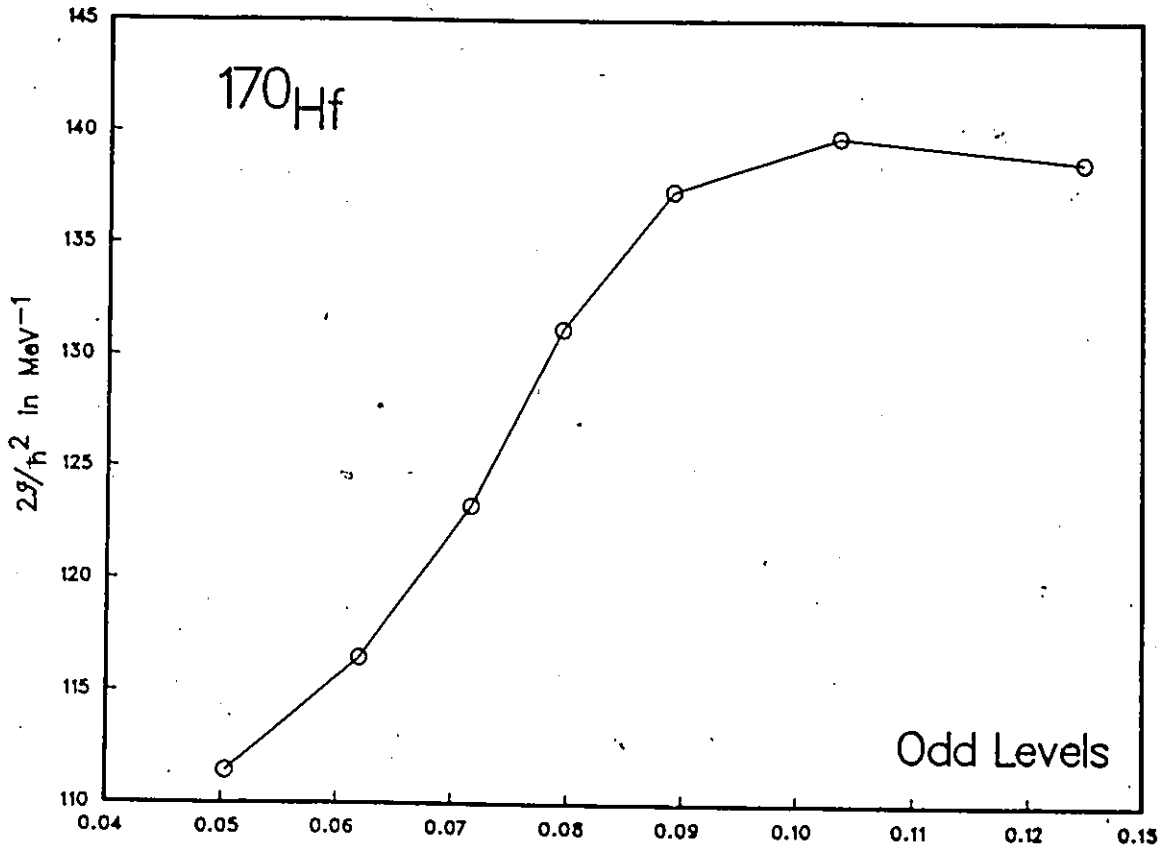

Fig. 2.48

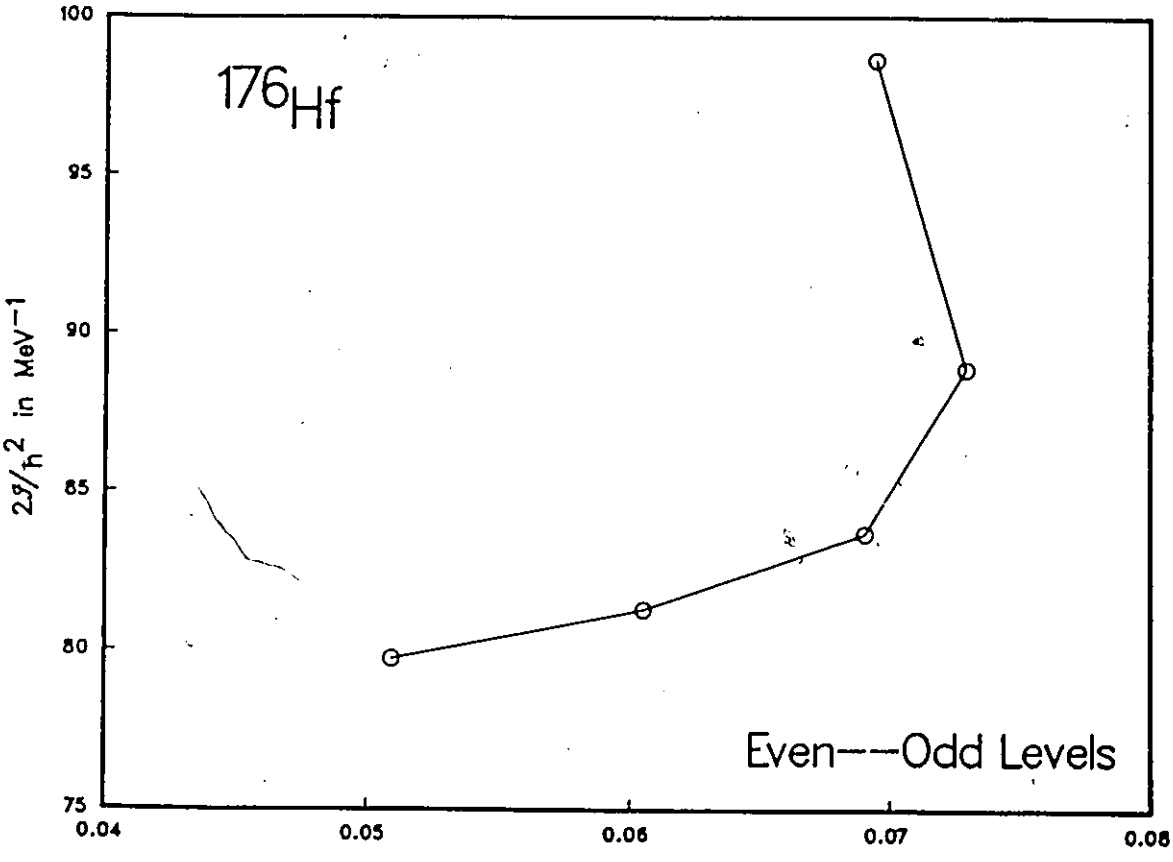

Fig. 2.49

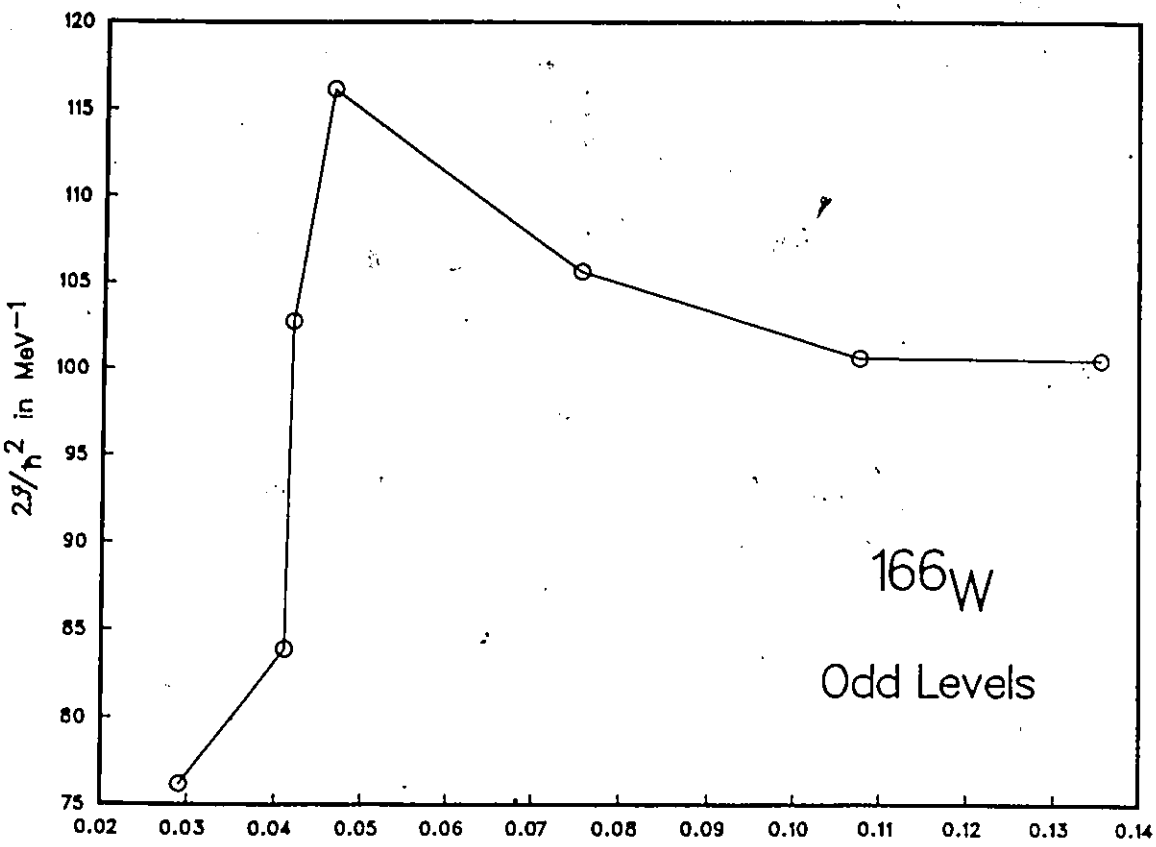

Fig. 2.50

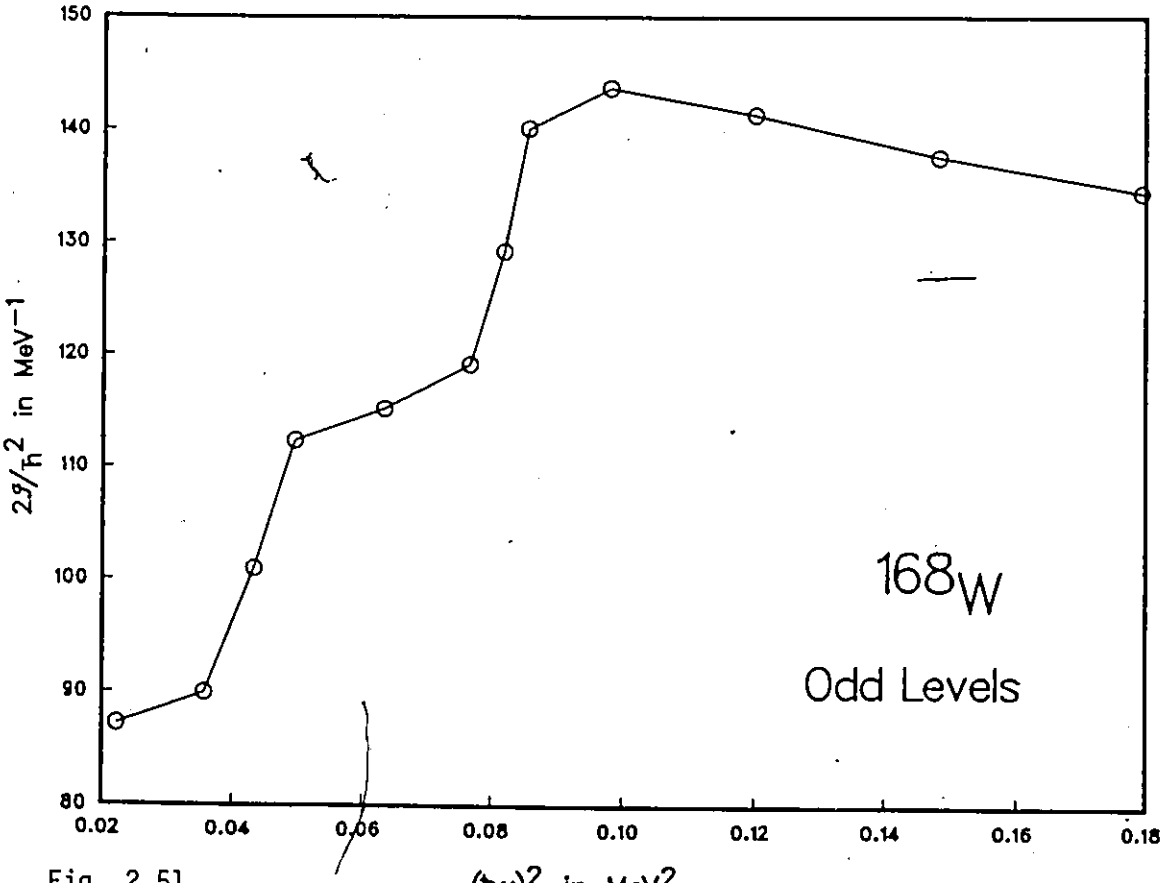

Fig. 2.51

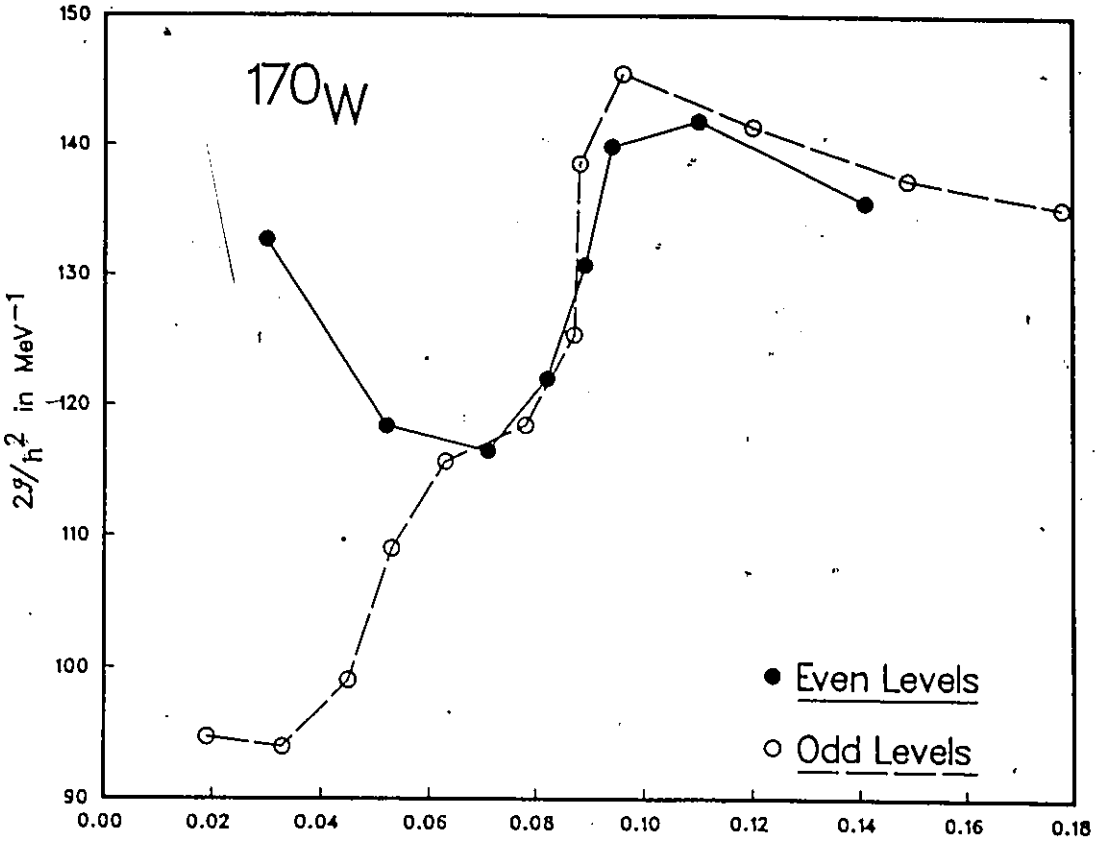

Fig. 2.52

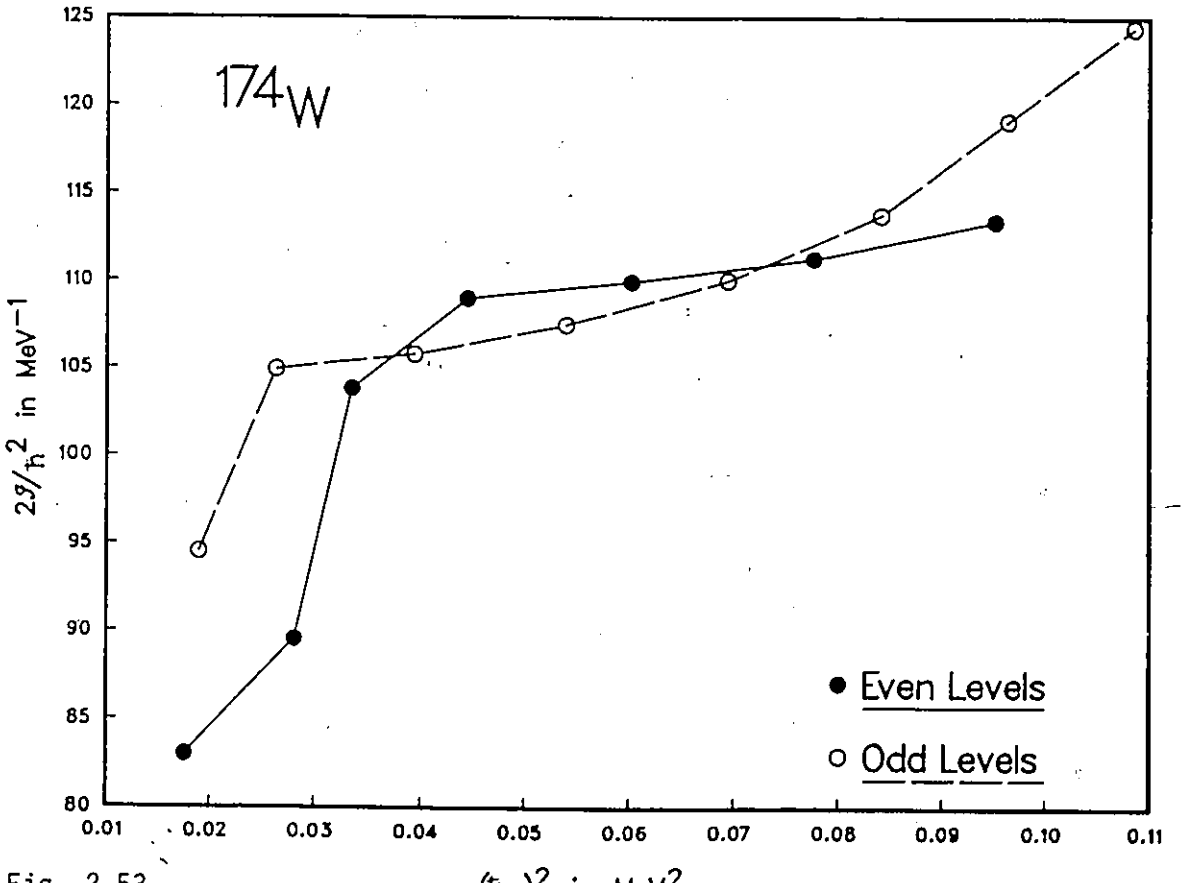

Fig. 2.53

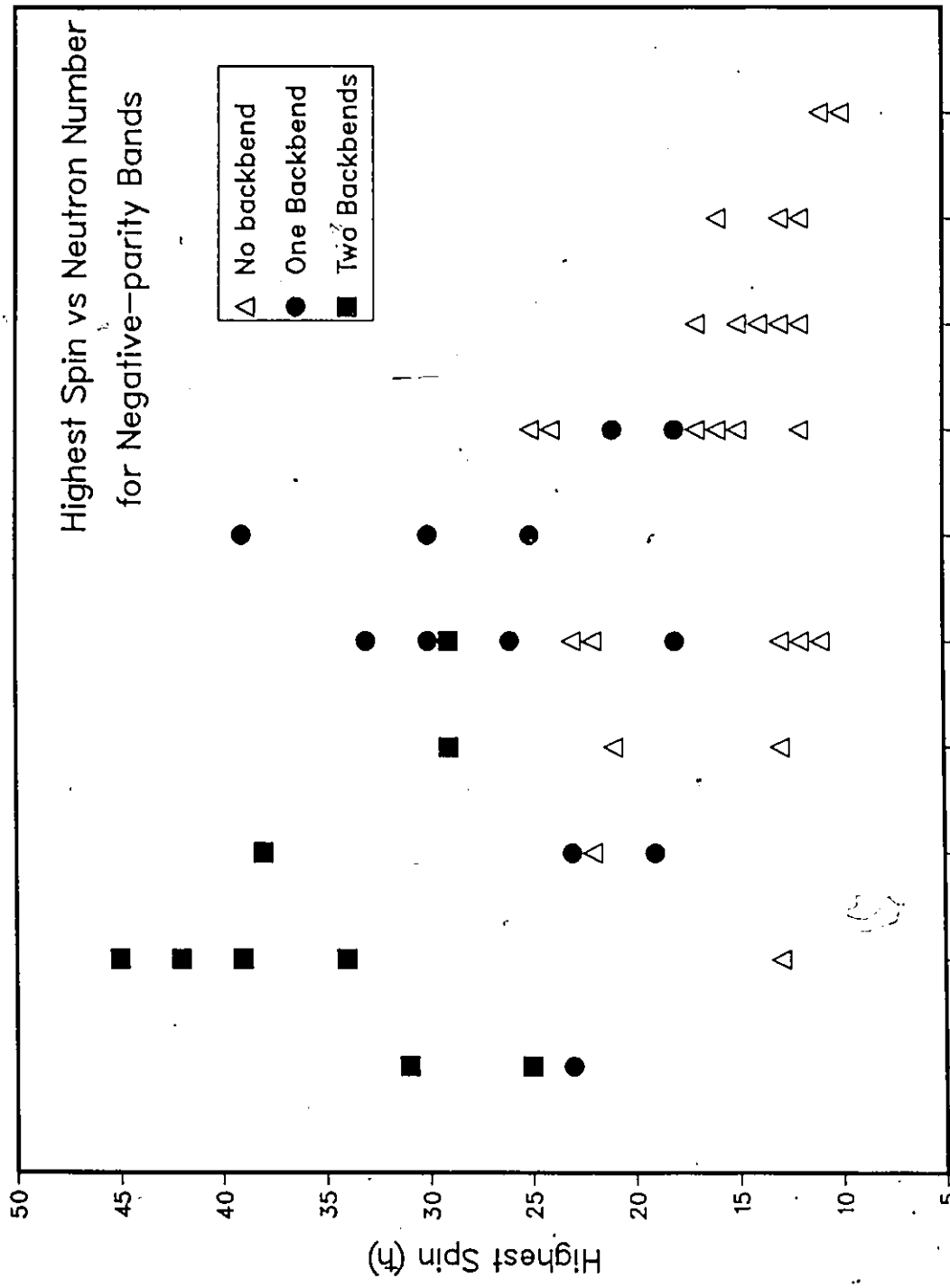
Highest Spin vs Neutron Number
for Negative-parity Bands
No backbend
One Backbend
Two Backbends
Highest Spin (ħ)
Neutron Number
50
45
40
35
30
25
20
15
10
5
88
90
92
94
96
98
100
102
104
106

Fig. 2.54

References

Agarwal, Y. K., *et al*, 1983, Nucl. Phys. **A399** 199

Asaro, F., F. Stephens Jr. and I. Perlman, 1953, Phys. Rev. **92** 1495

Bacelar, J. C., *et al*, 1985, Nucl. Phys. **A442** 509

Bäcklin, A., *et al*, 1967, Phys. Rev. **160** 1011

Baktash, C., *et al*, 1985, Phys. Rev. Lett. **54** 978

Bengtsson, R., and J. D. Garrett, 1984, in *Collective Phenomena in Atomic Nuclei*, eds. T. Engeland, J. Rekstad and J. S. Vaagen, World Scientific, Singapore, p. 194

Bohr, A., 1952, Dan. Mat. Fys. Medd. **26**, no. 14

Bohr, A., and B. R. Mottelson, 1953, Dan. Mat. Fys. Medd. **27**, no. 16

Burke, D. G., B. L. W. Maddock and W. F. Davidson, 1985, Nucl. Phys. **A442** 424

Camp, D. C., and F. M. Bernthal, 1972, Phys. Rev. C **6** 1040

Chapman, R., *et al*, 1983, Phys. Rev. Lett. **51** 2265

de Boer, F. W. N., *et al*, 1977, Nucl. Phys. **A290** 173

Diamond, R. M., F. S. Stephens and W. J. Swiatecki, 1964, Phys. Rev. Lett. **11** 315

Dors, C. L., F. M. Bernthal, T.L. Khoo, C. H. King, J. Borgreen and G. Sletten, 1979, Nucl. Phys. **A314** 61

Dracoulis, G. D., H. Hübel, A. P. Byrne and R. F. Davie, 1983, Nucl. Phys. **A405** 363

Dracoulis, G. D., P. M. Walker and A. Johnston, 1977, J. Phys. G.: Nucl. Phys. **3** L249

Fewell, M. P., *et al*, 1985, Phys. Rev. C **31** 1057

Fields, C. A., K. H. Hicks and R. J. Peterson, 1984, Nucl. Phys. **A431** 473

Fields, C. A., *et al*, 1982, Nucl. Phys. **A389** 218

Fields, C. A., *et al*, 1984, Nucl. Phys. **A422** 215

Flaum, C., and D. Cline, 1976, Phys. Rev. C. **14** 1224

Gerl, J., G. D. Dracoulis, A. P. Byrne, A. R. Poletti, S.J. Poletti and A. E. Stuchbery, 1985, Nucl. Phys. **A443** 348

Helmer, R. G., 1985, Nucl. Data **44** 659

Horen, D. J., and B. Harmatz, 1976, Nucl. Data **19** 383

Kendall, H., and L. Grodzins, 1956, Bull. Am. Phys. Soc. **1** 164

Khoo, T. L., J. C. Waddington, Z. Preibisz and M. W. Johns, 1973, Nucl. Phys. **A202** 289

Kistner, O. C., A. W. Sunyar and E. der Mateosian, 1978, Phys. Rev. C **17** 1417

Klein, A., 1980, Phys. Lett. **93B** 1

Larabee, A., *et al*, 1983, Contributions, Workshop on Nuclear Structure at High Spin, NBI

Lisle, J. C., J. D. Garrett, G. B. Hagemann, B. Herskind and S. Ogaza, 1981, Nucl. Phys. **A366** 281

Lipas, P. O., 1984, in *Collective Phenomena in Atomic nuclei*, eds. T. Engeland, J. Rekstad and J. S. Vaagen, World Scientific, Singapore, p. 33

Mann, L. G., *et al*, 1979, Phys. Rev. C **19** 1191

Mariscotti, M. A. J., G. Scharff-Goldhaber, and B. Buck, 1969, Phys. Rev. **178** 1864

Nathan, O., and M. A. Waggoner, (1956/57) Nucl. Phys. **2** 548

Pakkanen, A., *et al*, 1982, Phys. Rev. Lett. **48** 1530

Paul, E. S., *et al*, 1985, J. Phys. G: Nucl. Phys. **11** L53

Pavlichenkov, I. M., 1981, Sov. Phys. Usp. **24**(2) 79

Peker, L. K., J. H. Hamilton and J. O. Rasmussen, 1981, Phys. Rev. C **24** 1336

Recht, J., *et al*, 1985, Nucl. Phys. **A440** 366

Segrè, E., 1977, *Nuclei and Particles*, 2nd ed., Benjamin/Cummings, Reading, Mass.

Sheline, R. K., 1980, Phys. Rev. C **21** 1660

Shurshikov, E. N., 1986, Nucl. Data **47** 433

Simpson, J., 1985, Contributions, XIII International Winter Meeting on Nuclear Physics, Bormio, It.

Simpson, J., *et al*, 1984, Phys. Rev. Lett. **53** 648

Sorensen, R. A., 1973, Rev. Mod. Phys. **45** 353

Stephens, F. Jr., F. Asaro and I. Perlman, 1954, Phys. Rev. **96** 1568

Stephens, F. S., and R. S. Simon, 1972, Nucl. Phys. **A183** 257

Sunyar, A. W., E. der Mateosian, O. C. Kistner, A. Johnson, A. H. Lumpkin and P. Thieberger, 1976, Phys. Lett. **62B** 283

Vogel, P., 1976, Phys. Lett. **60B** 431

Walker, P. M., 1983, Phys. Scr. T5 **29**

Walker, P. M., S. R. Faber, W. H. Bentley, R. M. Ronningen and R. B. Firestone, 1980, Nucl. Phys. **A343** 45

Walker, P. M., S. R. Faber, W. H. Bentley, R. M. Ronningen, R. B. Firestone and F. M. Bernthal, 1979, Phys. Lett. **86B** 9

Walker, P. M., *et al*, 1981, Nucl. Phys. **A365** 61

Walus, W., *et al*, 1981, Phys. Scr. **24** 324

Yates, S. M., *et al*, 1980, Phys. Rev. C **21** 2366

Chapter III The Backbending effect in the Yrast Band of Even–even Nuclei

1. Introduction

The experimental observation of abrupt changes in the moment of inertia of the ground state band of even–even rare–earths (Johnson *et al*, 1971, 1972) was amongst the more important discoveries of the last decade in low–energy nuclear physics. This phenomenon was named the backbending effect (this comes from the s–shape appearance of the curves obtained by presenting the experimental data on $2\Im/\hbar^2$ vs $(\hbar\omega)^2$ plots (see Fig. 3.1 to 3.22 and Sec. 4.6 of Chap. II)).

Many experimental investigations were carried out to study the systematics of the effect and to see for which nuclei it occurred. The present experimental status for even–even rare–earths is that backbending is the usual structure of the yrast band (i.e. the band composed of levels, which for a given spin, lie lowest in energy: the initial levels of the ground state band are part of the yrast band) when sufficiently high spin levels are observed (Lieder and Ryde, 1978; de Voigt *et al*, 1983). The sharp change in the moment of inertia takes place between the critical spins $I_c \sim 12\hbar$ and $I_c \sim 18\hbar$. For other even–even nuclei, backbending has not been as frequently observed. It is noted, however, in palladium isotopes and the first part of the backbending curve, corresponding to the upbending of the ground state band, has recently been discovered for the actinide nucleus plutonium (Spreng *et al*, 1983).

The initial theoretical interpretation of the backbending effect was founded on the following idea put forth by Mottelson and Valatin (1960): the large angular velocities acquired by the nucleus, and therefore, the introduction of significant Coriolis forces, as higher spin values are reached would cause the destruction of the pairing correlations between nucleons, i.e. a phase transition would occur between a state with pairing correlations to one without. We recall that the pairing correlation is the tendency of identical nucleons to couple two by two. The Mottelson–Valatin effect is similar to the Meissner effect in

superconductivity, in which case, the imposition of a strong magnetic field destroys the superconducting state.

In the nuclear case, a first (second) backbend would be due to the loss of pairing correlations between the neutron (proton) Cooper pairs and would happen at approximatively $(\hbar\omega)^2 = 0.05$ (0.10) MeV^2. A detailed discussion of this theory is given by Sorensen (1973). It is now believed, however that the Mottelson–Valatin effect is not the cause of backbending. The theory predicted critical spin values which are, in some cases, larger than the experimentally observed values by a factor of 2 and it is believed that the overall loss of pairing correlations is much more gradual. Recently, a third backbend in the yrast line of ^{158}Er has been observed by Burde *et al* (1982).

The nowadays accepted mechanism producing the backbends of the yrast band is the decoupling from the core, by loss of pairing correlation in a single nucleon pair, of (usually) an $i_{\frac{13}{2}}$ quasineutron. It is once more the Coriolis force which is responsible for this process. The decoupled particle aligns its angular momentum along the core's angular momentum (Stephens and Simon, 1972; Stephens, 1975). As a result, high spin spectra are due to quasiparticles and it is thought that rotational bands are built on these quasiparticle states. It is the crossing of the ground state band with one of these rotational bands (called the superband or Stockholm band for the city where the effect was discovered) which then gives rise to the backbending effect.

The phenomenological picture for the interpretation of the backbending effect therefore involves two bands which interact and perturb each other's structures. In the simplest situation, only one level of each band is significantly affected – those closest to the crossing spin (see Sec. 2) — and degenerate perturbation theory can be applied to obtain an analytical expression for the energy level sequence of the yrast band. We note that according to this model, the yrast band is to be viewed as being composed of the ground state band for lower spins, a strongly perturbed level at the critical or crossing spin, and the superband at higher spins (when 2^{nd} ar 3^{rd} backbends occur, other superbands must be introduced).

In this chapter, we consider this type of band crossing model with the aim of reproducing the experimental energy level sequence of the yrast band of selected even–even nuclei (see Sec. 3.1). We may mention that when we began this work, such an analysis had not yet been carried out. Bonatsos (1985), however, has recently published in Physical Review C a paper similar in spirit to our work. He used the Variable Moment of Inertia Model (Mariscotti *et al*, 1969; Scharff–Goldhaber *et al*, 1976) to represent the ground state band (eqs. (3.18) and (3.4) of Chap. I) and the Bohr–Mottelson rotational expression (eq. (2.6) of Chap. I) to parametrize the superband.

Before his publication, we had studied a band crossing model for which both the ground state band and the superband were represented by the Ejiri equation (1966), an energy equation derived within the framework of the Interacting Boson Model (Arima and Iachello, 1976, 1978, 1979) but obtained unsatisfactory results. To improve the agreement with experiment, we used another boson Hamiltonian result, the Varshni formula (1968), to represent the superband. Reasonable results were, however, limited to vibrational nuclei, i.e. $E_4/E_2 \sim 2$, nuclei (Pari and Varshni, 1985). This was due to the use of the Ejiri equation for the ground state band.

At the time of Bonatsos' work, we were considering the possibility of mixing a Variable Moment of Inertia ground state band with a superband represented by the Varshni formula. This model is studied in detail in Sec. 3 of this chapter. Since Bonatsos (1985) did not provide numerical results or parameter tables, we found it interesting to compare the two model's agreement with experiment. Due to the fact that Bonatsos (1985) covers previous phenomenological attempts at understanding the backbending effect, we will only refer to works which are directly related to our discussion of the results we present.

2. Two–Band Crossing Models for the Yrast Band of Even–even Nuclei

We assume that the backbending effect is due to the crossing, in the Energy vs Spin plane, of two bands (Stephens and Simon, 1972; Bengtsson and Frauendorf, 1979; Bonatsos,

1985): the ground state band and an excited positive parity band (the superband, for which we do not attempt to specify the origin and therefore treat phenomenologically). These two bands will interact if for a given value of spin, a level of each band occurs at approximatively the same energy (Landau and Lifshitz, 1980). Owing to the small relative energy difference between these levels, the effect of their mixing must be evaluated by degenerate perturbation theory.

The problem is then to calculate the new energies of the interacting levels. This is done by diagonalizing the following 2×2 matrix:

$$\begin{pmatrix} \langle\phi|H|\phi\rangle & \langle\phi|H|\phi'\rangle \\ \langle\phi'|H|\phi\rangle & \langle\phi'|H|\phi'\rangle \end{pmatrix}$$

$$= \begin{pmatrix} E + \Delta E & V \\ V^* & E' + \Delta E' \end{pmatrix} \qquad (2.1)$$

where $H = H_0 + W$, i.e. the unperturbed Hamiltonian plus the interaction W, $|\phi\rangle$ and $|\phi'\rangle$ are the eigenstates of H_0 corresponding to the unperturbed eigenvalues E and E', ΔE and $\Delta E'$ are the diagonal contributions of the W, and V, V^* are the non-zero interband matrix elements. The result of the diagonalization gives the unperturbed energy values $E_\pm$:

$$E_\pm = \frac{1}{2}(E + \Delta E + E' + \Delta E') \pm \frac{1}{2}((E + \Delta E - E' - \Delta E')^2 + 4|V|^2)^{\frac{1}{2}} \qquad (2.2)$$

where the E_+ solution corresponds to the new energy of the level belonging to the superband and E_-, to the energy of the perturbed ground state band level. We note that the effect of the interaction is a repulsion between the levels.

We extend these results to the whole band by making the following assumptions: i) the quantities ΔE and $\Delta E'$ are neglected (we have searched the literature for the justification of this assumption but have not found anything. The fact that little is known about the actual form of the interaction W lets us believe that ΔE and $\Delta E'$ are neglected for the sake of simplicity in the analytical expression). ii) The effect of W leads to noticeable changes only in the the two levels where the crossing occurs and $|V|^2$ can then be treated as a constant for the whole band (Bonatsos (1985) has suggested that an interaction term

proportional to $\sqrt{I(I+1)}$ but the validity of such an expression is arguable since eq. (2.2) holds only for a 2×2 diagonalization). We can then write the energy expression for the yrast band:

$$E_I = \frac{1}{2}(E_{gsb}(I) + E_s(I)) - \frac{1}{2}((E_{gsb}(I) - E_s(I))^2 + 4|V|^2)^{\frac{1}{2}} \tag{2.3}$$

where we have explicitly indicated the dependence on the spin I of the ground state band, E_{gsb}, and of the superband, E_s. The interaction $|V|^2$ is treated as an independent parameter. We remark that the other solution, i.e. with the positive rather than the negative sign corresponds to what is known as the yrare band. The band crossing models should therefore predict the position of these levels.

We have mentioned, in Sec. 1, various possible parametrizations for the ground state band and the superband. From our initial study of the backbending effect, we concluded that the Varshni formula (eq. (4.19) of Chap. I, with the inclusion of a bandhead parameter) was a reasonable choice for the representation of the superband. For the ground state band, the natural choice was the Variable Moment of Inertia Model equation (see Sec. 3 of Chap. I). In further discussion we will refer to this model as the Variable Moment of Inertia and Varshni formula band crossing model, or in abbreviated form, the VMI–V Model.

Another possibility is to use the Bohr–Mottelson Model to parametrize the superband (eq. (2.6) of Chap. I). This, with the Variable Moment of Inertia equation for the ground state band, corresponds to the Variable Moment of Inertia and Bohr–Mottelson band crossing model, or VMI–BM Model, of Bonatsos (1985). We mention that this model will only be considered for I–independent interactions. A detailed study and comparison of these two models is presented in Sec. 3 of this chapter.

Before proceeding to the analysis of the results, we note that both the VMI–V and VMI–BM Models are subject to the variational condition

$$\frac{\partial E_I}{\partial \Im} = 0 \tag{2.4}$$

where E_I refers to the eq. (2.3) and $\Im$ is the variable moment of inertia. Carrying out the derivative provides two possibilities to satisfy this equation:

$$\frac{\partial E_{gsb}}{\partial \Im} = 0 \tag{2.5}$$

or,

$$V = 0 \tag{2.6}$$

we have used the variational condition (2.5) in our analysis and further discussion of eq. (2.6) is left to Sec. 3.3.

3. Analysis of the Yrast Band of Selected Even–even Nuclei

3.1 Selection of Even–even Nuclei

Physically reasonable results will be obtained within the framework of band crossing models if both the ground state band and the superband portions of the yrast band are well–defined. It is therefore clear that limitations for the applicability of the models depend upon the number of levels observed for the superband.

At least two levels of the superband must be observed experimentally to allow a determination of the Bohr–Mottelson parameters in the VMI–BM Model. The number of superband levels is increased to four in the case of the VMI–V Model. It is this second criterion which we used to select the even–even nuclei we study in this chapter: we considered all even–even nuclei which have a superband consisting of four or more experimentally determined levels. A list of these nuclei can be found in Table 3.1. We note that for nuclei which show a second backbend (for example: ^{158}Er, ^{160}Er), we did not consider the levels which belong to the second superband. A study of these energy levels would involve the introduction of another superband.

Although arbitrary, we believe that our selection criterion is reasonable. Indeed, very little can be deduced about the superband if only three or two levels are observed for the

band. Futhermore, the present status of the experimental data allows us to consider the yrast band of 22 even–even nuclei. This set of nuclei spans the vibrational to rotational regions, with examples of vibrational spectra being found for ^{104}Pd and ^{156}Yb with respective values of E_4/E_2 being equal to 2.38 and 2.31. Rotational characteristics are noted, for example, in ^{166}Yb and ^{172}Hf with E_4/E_2 respectively equal to 3.23 and 3.25. The applicability of a given model will therefore have to be good for different type of nuclear spectra.

3.2 Calculations and Results

A least–squares fit analysis was performed, using the VMI–BM and the VMI–V Models to obtain the parameters for the yrast band of 22 even–even nuclei. All the energy levels were weighted by the square of their inverse. This allows us to take into account in a reasonable way the experimental uncertainties which are much smaller for the low–spin levels.

The determination of the parameters was straightforward in the case of the VMI–BM Model. This is due to the relatively small number of parameters (5) involved in the analysis and to the fact that there are, in all cases, many levels to fix the superband parameters. The situation was different in the case of the VMI–V Model. Although, in general, the convergence process did not create any problem, we encountered difficulties for the following nuclei: ^{158}Dy, ^{170}Hf and ^{172}Hf.

The first three nuclei all show a much more gradual backbend than what is observed for the neighbouring isotopes. The superband in the VMI–V Model then has the tendency to be concave downward rather than concave upward as is usually observed. This gives a completely different set of parameters, as can be seen in Table 3.2, for ^{170}Hf. In the case of ^{158}Dy, we were able to obtain fits of similar accuracy with both a set of parameters corresponding to the upward concave case and the downward concave case. We present the parameters for the upward concave case since they seem easier to justify physically

(the bandhead energy is greater than zero). For ^{172}Hf, the upward concave possibility gives the better results. We note that in all three cases, the fact that only four levels are observed for the superband may also contribute to the difficulties we encountered because the superband parameters may tend to improve the fit in the interacting region.

We present the parameters obtained from our analysis with the VMI–BM Model in Table 3.1 and those obtained with the VMI–V Model in Table 3.2. The comparative results of the two models are given in Table 3.3. As a complement to the tables, we have also plotted the experimental and theoretical values of the energy on $2\Im/\hbar^2$ vs $(\hbar\omega)^2$ plots (Fig. 3.1 to Fig 3.22).

3.3 Parameter Systematics

There are many points of interest concerning the parameter values we obtained for the VMI–V and VMI–BM Models. We therefore divide our discussion in subsections.

The Interaction parameters H_0 and H_1

For both the VMI–BM and VMI–V Models, the interpretation of the results obtained from the least–squares fitting procedure for the interaction parameters has caused us difficulty. Physically, the parameters are to be associated with the square root of the interaction strength |V| of eq. (2.3). Furthermore, this parameter is restricted to positive values by the hermiticity of the perturbing potential:

$$\langle\phi|\mathrm{W}|\phi'\rangle = \langle\phi'|\mathrm{W}|\phi\rangle^* \tag{3.1}$$

which implies

$$\langle\phi|\mathrm{W}|\phi'\rangle\langle\phi'|\mathrm{W}|\phi\rangle = \langle\phi|\mathrm{W}|\phi'\rangle\langle\phi|\mathrm{W}|\phi'\rangle^* = \mathrm{V}\mathrm{V}^* \geq 0 \tag{3.2}$$

where we have used the same symbols as in Sec. 2.

In many cases, however, the least–squares fitting procedure did not converge for positive values of the interaction parameters and we allowed for the possibility of negative

values of the interaction strength. We obtained convergence to negative values of this parameter for all the nuclei showing a zero interaction strength. We chose this value since there is some ambiguity in explaining negative values (see below). This choice, however, is different from eq. (2.6) which is a physical criterion.

Although unexpected, this result can be explained if we carefully consider the assumptions leading to eq. (2.3). The solution resides in a renormalization of the parameters obtained by including the diagonal contributions of the interaction potential W. We recall that such terms are usually neglected in the band crossing equation, although we have not been able to find the justification for this. By including ΔE and $\Delta E'$ we get new expressions for both the bandhead parameter of the superband, say E_0, and the general interaction parameter, say V':

$$\begin{aligned} E_0' &= E_0 + \Delta E + \Delta E' \\ V' &= 4|V|^2 - 4\Delta E^2 - 2\Delta E(E_{gsb} - E_s) \end{aligned} \tag{3.3}$$

and V' can take negative values depending on the values of the three quantities to the right.

We did not attempt to use ΔE and $\Delta E'$ as independent parameters since the analysis would have involved too many variables. Furthermore, we realized that large variations in V' led to little differences in the energies of the levels. As an example, we considered, within the framework of the VMI–V Model, $V' = 100$ keV and $V' = -1000$ keV for the nucleus ^{162}Hf. The observed variation of the energy levels in the backbending region was only ~ 2 keV ($\sim 0.1\%$) when we considered these two interaction strengths. We therefore use these two points to justify our choice of zero for the interaction parameters H_0 and H_1 of Tables 3.1 and 3.2.

In view of our preceding discussion, the following two results should not come as a surprise. Sharp backbends theoretically correspond to small interactions between the bands. This is not, however, what we observe: the largest interaction strength for both the VMI–BM and the VMI–V Models occurs for ^{104}Pd, a sharp backbending nucleus. The

largest interaction parameters should be observed for nuclei such as ^{158}Dy or $^{170,\ 172}$Hf. Although these nuclei show sizeable values of the interaction parameter, there are many sharply backbending nuclei showing similar values.

Another point is the prediction, by Bengtsson *et al* (1978) that the interaction strength between the ground state band and the superband should be an oscillating function of the neutron number. Bonatsos (1985) has claimed that his model results for the interaction parameter reproduce the expected behavior. We have plotted this parameter as a function of the neutron number for the two models we considered but our results do not confirm the theoretical predictions.

The bandhead parameter in the VMI–V model

A close investigation of the bandhead parameters for the VMI–V model reveals that they usually lie higher in energy than some of the levels of the yrare band. We recall that the yrare band corresponds to the second solution of eq. (2.2) (with the plus sign). This implies that there will be a minimum in the sequence of levels of the superband below the critical spin (the following clarification may be useful: the yrare band is the band formed by the superband at lower spins, a strongly perturbed level at the crossing point, and the ground state band at higher spin). This particularity of our results can be explained if one assumes that the superband is built on a state with a value of spin greater than that at which occurs the minimum, but smaller than the critical spin, i.e. a non–zero K value. The part of the band occurring before the minimum would therefore have no physical significance. It would, however, be tempting to assume that this is not the case: the Varshni formula is able to predict the upbending of the yrast band and this fact was only pointed out after the discovery of backbending (Varshni, 1974; Sood and Jain, 1975). Furthermore, a similar structure for the yrare band has been reported in a previous investigation of the backbending effect (Rasmussen et al, 1979). Even though the origin of the superband was quite different (it resulted from the interaction of two

rotational bands) in this work, the coincidence is worth mentioning.

Variation of the Parmeters with Neutron Number and Correlations Between Parameters

We have searched for regularities as a function of the neutron number for the parameters of the VMI–V and VMI–BM Models. For this, we considered the nuclei with $88 \leq N \leq 100$ (with the exclusion of ^{172}Hf, which has a very different set of parameters) and concentrated our attention on the parameters associated with the superband. Our results were inconclusive for the VMI–V Model. For the VMI–BM Model, we noted that the bandhead parameter E_0 usually decreased as the neutron number increased (for nuclei in the specified neutron number range).

Correlations between the parameters of the VMI–V Model for the superband were found to be quite interesting. The simple relations involved, see Fig. 3.23 and Fig. 3.24 for two particularly good correlations, between the parameters made us try to find a reformulation involving less parameters for the superband. We obtained from this investigation results intermediate between the VMI–V and VMI–BM Models' results. Correlations were also noted between the parameters of the Varshni formula in our study of negative parity bands (Sec. 4.4 of Chap. 2). We suggested there that this may point towards the possibility of an energy term which would sum up the angular momentum expansion. Such a possibility may also be the case for the superbands studied but we have not obtained any results in this direction.

4. Comparison of the VMI–BM and VMI–V Models

From Table 3.3, we see that both the VMI–BM and VMI–V models give essentially the same results for the low–spin portions of the yrast bands. This is to be expected since the models have the same ground state band parametrization. The results of interest, which will quantitatively separate the models, are therefore to be found in the interaction and high spin regions of the yrast band. From the graphs we present, Fig. 3.1 to Fig. 3.22, it

is clear that for sharply backbending nuclei, the parametrization of the superband in the VMI–V framework gives much better agreement with experiment. The curvature of the superband is well-accounted for and in cases such as the tungsten isotopes or ^{164}Hf, very good reproduction of the sharp backbending curve is obtained. Also, the Varshni formula reproduces the initial decrease of the moment of inertia of the superband.

On the other hand, the VMI–BM Model's parametrization gives an average moment of inertia for the superband. For this model, good results are obtained for "flat" superbands such as those observed for the dysprosium isotopes.

To quantitatively evaluate the merits of both models, we present in Table 3.3 the rms % deviations (eq. (4.2) of Chap. 2). In all cases, this value is smaller for the VMI–V Model, indicating the better agreement of this model with experiment. This result is even more interesting when we realize that % deviations are involved, therefore rendering the rms % value less sensitive to errors in high energy values (the high-spin levels which differentiate both models). Overall, the rms % average for the 22 yrast bands we considered is 0.613 for the VMI–BM Model and 0.313 for the VMI–V Model.

It is somewhat unjustified, however, to consider both models on the same footing since the VMI–V Model involves two extra parameters. It can certainly be argued that this is the reason why we obtain a better fit to the experimental data. To determine whether the inclusion of the extra parameters in the VMI–V Model is physically reasonable, we used a more demanding criterion depending on the number of parameters:

$$\Omega = \frac{1}{n-m} \sum_{i}^{n} \left(\frac{\mathrm{E}_{t_i} - \mathrm{E}_{x_i}}{\mathrm{E}_{x_i}} \right)^2 = \text{minimum} \qquad (4.1)$$

(the Gauss criterion (Worthing and Geffner, 1960)), where n is the number of experimental levels and m is the number of independent parameters. The values of omega are presented in Table 3.4.

We observe that these values indicate a good performance of the VMI–BM Model for the following nuclei: $^{154,\,156}$Dy, ^{156}Er and ^{182}Os, all of which have a relatively flat

superband. The VMI–V Model provides marginally worse ($\Delta\Omega \sim 10$) results in these three cases. Slightly better results ($\Delta\Omega \sim 10$) are obtained for the VMI–V Model in the following cases: $^{154,\ 158}$Dy, $^{164,\ 166}$Yb and $^{170,\ 172}$Hf.

We note that in this last group (^{158}Dy and $^{170,\ 172}$Hf), there are the three nuclei which have strongly interacting yrast sequences. Although the VMI–V Model still gives better agreement under the Gauss criterion constraint, we believe that the higher-spin levels are better reproduced by the VMI–BM Model (the predicted trend by the VMI–V Model for the high-spin levels is poor). From this argument, we conclude that the VMI–BM Model is better in these three cases.

For the other nuclei, the performance of the VMI–V Model is much superior to that of the VMI–BM Model. Striking examples are noted for ^{130}Ce, ^{158}Yb, $^{164,\ 168}$Hf and $^{168,\ 170}$W, in which cases the VMI–V Model's Ω values are at least five times smaller that the VMI–BM Model ones.

The VMI–V Model is therefore superior to the VMI–BM Model in 68% of the cases studied. The better results are obtained for the VMI–V Model when the superband shows a concave upward structure while the VMI–BM gives better results for the case of flat superbands and provides more reasonable results for strongly interacting ground state bands and superbands.

Another criterion to investigate the performance of the two models is the prediction of levels of the yrare band (eq. (2.2), the solution with the minus sign). The parameters obtained for the ground state band should predict the position of these levels.

We have searched experimental works for these levels. In many cases, the extension of the ground state band beyond the backbending point is known for a few levels. In both the VMI–V and VMI–BM Models, these levels essentially correspond to the variable Moment of inertia part of the equation and little differences between the predictions is to be expected. This is what we observe, even though the VMI–BM Model gives slightly better results in the cases we considered. As an example of the prediction of the yrare

levels for spins higher than the critical crossing spin, we consider the nucleus ^{168}Hf in Table 3.5. As seen, just beyond backbend the VMI–BM gives better results. For higher spin levels, the two Models converge to approximatively the same results.

Experimental observation of levels of the yrare band below the backbending critical spin are much less common. We present in Table 3.6 the two cases where we found such data reported. For ^{166}Hf (Agarwal *et al*, 1983), only a single level is reported, while 4 are observed for ^{166}Yb (Fields *et al*, 1984). As seen, the prediction of the lower levels of the superband is better for the VMI–V Model, with good agreement noted for the first two levels below backbending for ^{166}Yb.

5. General Comments on Two–band Crossing Models

We have discussed, in Sec. 4, the better agreement with experiment for the VMI–V Model and justified the introduction of two extra parameters for the representation of the superband. The VMI–V Model is then particular ly successful in describing upward concave superbands while the VMI–BM works well for flat superbands. In view of some of the difficulties pointed out during the discussion of our results, and particularly concerning the interaction strength parameter (Sec. 3.3), the agreement with experiment should be considered with caution. After all, five and seven parameters are used in the fits to the experimental data.

From our study, we therefore arrive at the conclusion that the two-band crossing formalism which is usually used in nuclear physics to explain the backbending effect might be too a simple picture to account for the experimental results. For example, the strongly interacting nuclei are not well explained by the VMI–V Model (although the observation of more superband levels might change this situation) while the weakly interacting ones are well reproduced, a surprising result if one assumes that the strength of the backbending effect can be explained by a single interaction parameter. Furthermore, this parameter does not influence much the quality of the results when it should, in the backbending region,

be of much importance. Also, from the experimental backbending curves, it is seen that in many cases the interaction is not restricted to a single level and that a larger number of levels should be introduced in the diagonalization process. From these points, we see that other detailed analysis must be carried to deduce the correct cause of the backbending effect.

Table 3.1. Parameters obtained for the Variable Moment of Inertia and Bohr–Mottelson band crossing model. The parameters are given with more significant figures than warranted by experiment to insure the exact reproducibility of our results.

Nucleus	Sources of exptl. data	$\Im_0$ (10^{-2} keV^{-1})	C (10^6 keV^3)	E_0 (keV)	A (keV)	H_0 (keV)
^{104}Pd	a	0.19293	10.3840	2412.38	14.5409	98.8018
^{128}Ce	b	1.33534	5.48285	1255.93	11.6096	0
^{130}Ce	a	1.02767	5.85483	1461.32	11.7240	0
^{154}Dy	a	2.9×10^{-4}	1.22944	1918.83	7.97629	59.5585
^{156}Dy	a	2.04291	1.80937	1349.64	7.85647	0
^{158}Dy	a	2.93029	2.58063	1069.68	7.92922	39.7392
^{156}Er	a	0.25300	2.07446	1954.38	8.94481	10.4091
^{158}Er	a	1.31479	2.05060	1424.69	8.30278	0
^{160}Er	a	2.28476	2.70781	1247.79	8.16081	33.4607
^{158}Yb	c	0.25361	2.39692	2306.23	8.34749	21.9583
^{160}Yb	a	0.92037	2.50988	1642.84	8.24601	0
^{164}Yb	a	2.33762	2.81822	1197.56	8.05539	0
^{166}Yb	a	2.87775	3.72996	1193.02	7.60710	19.8770
^{162}Hf	a	0.71979	3.08532	1856.92	8.23911	0
^{164}Hf	a	1.21061	2.99070	1495.48	8.31289	0
^{166}Hf	a	1.74603	2.63300	1310.65	8.00239	0
^{168}Hf	a	2.32700	2.62933	1197.54	7.78531	0
^{170}Hf	a	2.72669	1.92952	972.570	8.32605	70.1457
^{172}Hf	d	3.04129	3.16425	1180.35	8.08630	46.8901
^{168}W	a	1.29147	2.73714	1377.12	7.96428	15.1070
^{170}W	a	1.74304	2.21979	1265.57	7.73586	0
^{182}Os	a	2.22001	3.23618	1145.02	8.01206	61.1064

References:

a) Sakai (1984)

b) Carvalho *et al* (1985)

c) Baktash *et al* (1985)

d) Paul *et al* (1985)

Table 3.2. Parameters obtained for the Variable Moment of Inertia and Varshni formula band crossing model. The sources of experimental data can be found in Table 3.1. Our use of the same symbols for the Variable Moment of Inertia parameters in Table 3.1 and Table 3.2 should not cause any confusion.

Nucleus	$\Im_0$ (10^{-2} keV^{-1})	C (10^6 keV^3)	E_1 (keV)	p (keV)	a (keV)	q (keV)	H_1 (keV)
^{104}Pd	0.18922	10.6281	6820.80	-883.005	68.9208	-1.11347	228.546
^{128}Ce	1.33064	5.38066	2797.41	-222.779	19.9799	-0.07029	16.1180
^{130}Ce	1.02151	5.78670	3942.43	-408.109	30.7200	-0.27855	44.5405
^{154}Dy	2.9×10^{-4}	1.23706	4674.80	-381.105	24.1523	-0.22879	109.324
^{160}Dy	2.04293	1.80943	3004.15	-235.934	18.0005	-0.14402	0
^{158}Dy	2.94230	2.64503	1064.92	-40.1149	11.5506	-0.08352	33.1698
^{160}Er	0.25239	2.07208	3374.67	-245.890	21.6696	-0.21936	9.83246
^{158}Er	1.31479	2.05060	4160.98	-433.297	28.7176	-0.31653	0
^{160}Er	2.27934	2.70216	3249.76	-300.044	21.5894	-0.19571	57.5253
^{158}Yb	0.25385	2.39381	5694.28	-625.054	42.2989	-0.60708	0
^{160}Yb	0.92037	2.50988	3088.88	-238.361	19.6499	-0.17633	0
^{164}Yb	2.32809	2.80161	1684.05	-50.5554	9.06595	0.01042	29.7070
^{166}Yb	2.86149	3.64223	3061.44	-260.181	18.4699	-0.14731	50.8579
^{162}Hf	0.71979	3.08532	3464.46	-266.343	21.0710	-0.20033	0
^{164}Hf	1.21061	2.99071	4077.39	-400.066	25.9928	-0.24439	0
^{166}Hf	1.72355	2.59907	5685.36	-700.591	41.3428	-0.51854	86.2331
^{168}Hf	2.31284	2.61572	2823.65	-229.483	17.3700	-0.12933	45.5059
^{170}Hf	2.77398	1.91787	-177.437	125.941	4.30847	0.03246	0.0697
^{172}Hf	3.05620	3.28141	1019.92	-24.9740	11.0116	-0.06805	37.2084
^{168}W	1.28152	2.73733	6132.36	-777.554	45.0615	-0.57348	80.2057
^{170}W	1.72407	2.20409	3165.21	-281.865	20.1149	-0.17692	61.5114
^{182}Os	2.17990	3.06911	2230.00	-149.453	14.0370	-0.07516	102.724

Table 3.3. Experimental and calculated energies of the yrast band, and energy differences between the experimental and calculated values, of selected even–even nuclei. The five first rows associated with each nucleus respectively represent: i) the experimental energy values for levels of the yrast band, ii) the theoretical predictions obtained from the Variable Moment of Inertia and Bohr–Mottelson band crossing model, iii) the differences between the experimental values and the precedent model's results, iv) the theoretical predictions obtained from the Variable Moment of Inertia and Varshni formula band crossing model and v) the differences between the experimental values and the precedent model's result. The significance of the subsequent five rows for each nucleus is the same as before, with the values of the spin beginning at 22^+. All the experimental energy levels presented in the table have been taken into account in our analysis.

	2^+ 22^+	4^+ 24^+	6^+ 26^+	8^+ 28^+	10^+ 30^+	12^+ 32^+	14^+ 34^+	16^+ 36^+	18^+ 38^+	20^+ 40^+	*rms %* *deviation*
^{104}Pd	555.79	1323.59	2249.8	3220.7	4023.1	4635.0	5432.1	6358.3	7422.4		
	555.69	1326.62	2237.80	3234.07	3987.97	4670.20	5459.02	6362.18	7380.94		0.517
	0.10	-3.03	12.00	-13.37	35.13	-35.20	-26.92	-3.88	41.46		
	555.23	1328.98	2239.62	3225.99	4020.88	4639.86	5423.62	6365.84	7419.84		0.226
	0.56	-5.39	10.18	-5.29	2.22	-4.86	8.48	-7.54	2.56		
^{128}Ce	207.3	606.9	1157.5	1820.5	2532.1	3108.1	3668.6	4359.2	5187.1	6145.3	
	206.14	613.10	1158.65	1809.94	2532.99	3067.03	3693.95	4413.74	5226.41	6131.96	
	1.16	-6.20	-1.15	10.56	-0.89	41.07	-25.35	-54.54	-39.31	13.34	
	206.35	612.86	1157.03	1806.05	2539.64	3108.26	3667.15	4361.23	5187.51	6142.66	
	0.95	-5.96	0.47	14.45	-7.54	-0.16	1.45	-2.03	-0.41	2.64	
	7222.00										
	7130.39										0.838
	91.61										
	7223.33										0.416
	-1.33										
^{130}Ce	253.9	710.5	1324.4	2053	2809	3312	3860	4553	5384	6341	
	252.29	719.43	1325.89	2037.37	2750.96	3290.26	3923.36	4650.25	5470.93	6385.40	
	1.61	-8.93	-1.49	15.63	58.04	21.74	-63.36	-97.25	-86.93	-44.40	
	252.40	719.43	1324.83	2033.81	2815.51	3310.90	3858.59	4554.40	5386.38	6341.40	
	1.50	-8.93	-0.43	19.19	-6.51	1.10	1.41	-1.40	-2.38	-0.40	
	7408	8570	9812	11123							
	7393.66	8495.72	9691.57	10981.21							1.241
	14.34	74.28	120.43	141.79							
	7406.16	8567.32	9811.53	11125.42							0.462
	1.84	2.68	0.47	-2.42							

	2^+ 22^+	4^+ 24^+	6^+ 26^+	8^+ 28^+	10^+ 30^+	12^+ 32^+	14^+ 34^+	16^+ 36^+	18^+ 38^+	20^+ 40^+	*rms* % *deviation*
^{154}Dy	334.6	746.7	1223.7	1747.3	2304.3	2893.0	3509.2	4091.0	4637.6	5249.9	
	332.03	743.14	1219.61	1747.11	2316.48	2918.86	3524.87	4068.75	4635.46	5260.36	
	2.57	3.56	4.09	0.19	-12.18	-25.86	-15.67	22.25	2.14	-10.46	
	331.68	743.17	1219.94	1747.44	2316.12	2916.64	3527.17	4082.76	4630.40	5247.77	
	2.92	3.53	3.76	-0.14	-11.82	-23.64	-17.97	8.24	7.20	2.13	
	5935.1	6691.0	7514.0	8401.3							
	5947.45	6697.56	7510.87	8387.20							0.433
	-12.35	-6.56	3.13	14.10							
	5940.82	6701.90	7520.87	8386.82							0.415
	-5.72	-10.90	-6.87	14.48							
^{156}Dy	137.83	404.12	770.33	1215.69	1725.02	2285.88	2887.82	3498.91	4026.07	4635.56	
	136.19	408.84	777.34	1219.32	1721.36	2274.60	2872.72	3486.60	4036.55	4649.36	
	1.64	-4.72	-7.01	-3.63	3.66	11.28	15.10	12.31	-10.48	-13.80	
	136.19	408.83	777.34	1219.32	1721.37	2274.61	2872.73	3498.55	4026.90	4635.88	
	1.64	-4.71	-7.01	-3.63	3.65	11.27	15.09	0.36	-0.83	-0.32	
	5320.26	6068.7	6876.6	7738	8650						
	5325.01	6063.52	6864.88	7729.09	8656.16						0.554
	-4.75	5.18	11.72	8.91	-6.16						
	5318.58	6068.09	6877.49	7739.87	8648.33						0.533
	1.68	0.61	-0.89	-1.87	1.67						
^{158}Dy	98.94	317.26	637.87	1044.1	1519.9	2049.2	2612.6	3190.7	3781.7	4407.5	
	98.66	318.91	638.97	1041.53	1513.55	2044.78	2623.58	3203.56	3772.62	4394.21	
	0.28	-1.65	-1.10	2.57	6.35	4.42	-10.98	-12.86	9.08	13.29	
	98.72	318.58	638.65	1041.75	1514.84	2047.36	2623.99	3189.23	3773.15	4408.28	
	0.22	-1.32	-0.78	2.35	5.06	1.84	-11.39	1.47	8.55	-0.78	
	5085.6	5820.3	6612.9								
	5077.32	5823.17	6632.09								0.312
	8.28	-2.87	-19.19								
	5094.07	5827.11	6603.61								0.234
	-8.47	-6.81	9.29								

	2^+ 22^+	4^+ 24^+	6^+ 26^+	8^+ 28^+	10^+ 30^+	12^+ 32^+	14^+ 34^+	16^+ 36^+	18^+ 38^+	20^+ 40^+	*rms %* *deviation*
^{156}Er	344.5	796.9	1340.3	1958.7	2632.9	3314.6	3837.3	4381.3	5006.4	5716.6	
	342.83	803.57	1346.87	1954.08	2614.29	3317.59	3832.33	4387.14	5013.34	5711.07	
	1.67	-6.67	-6.57	4.62	18.61	-2.99	4.97	-5.84	-6.94	5.53	
	342.87	803.52	1346.69	1953.74	2613.82	3318.85	3837.48	4379.70	5009.12	5715.35	
	1.63	-6.62	-6.39	4.96	19.08	-4.25	-0.18	1.60	-2.72	1.25	
	6488.7	7315.6									
	6480.34	7321.16									0.390
	8.36	-5.56									
	6487.87	7316.17									0.382
	0.83	-0.57									
^{158}Er	192.18	527.21	970.6	1494.3	2074.1	2682.9	3193.3	3666.6	4233.5	4892.9	
	190.73	534.08	974.49	1487.97	2061.02	2684.92	3168.27	3683.05	4264.24	4911.86	
	1.45	-6.87	-3.89	6.33	13.08	-2.02	25.03	-16.45	-30.74	-18.96	
	190.73	534.08	974.49	1487.97	2061.02	2684.92	3194.92	3661.88	4234.49	4897.58	
	1.45	-6.87	-3.89	6.33	13.08	-2.02	-1.62	4.72	-0.99	-4.68	
	5632.9	6439.1	7285.1	8144.3							
	5625.90	6406.36	7253.24	8166.55							0.600
	7.00	32.74	31.86	-22.25							
	5635.94	6434.38	7277.71	8150.73							0.468
	-3.04	4.72	7.39	-6.43							
^{160}Er	125.61	389.53	764.7	1228.4	1760.1	2339.3	2931.5	3465.4	4020.8	4661	
	125.15	391.79	766.04	1225.28	1754.44	2341.56	2939.80	3462.43	4035.84	4673.16	
	0.46	-2.26	-1.34	3.12	5.66	-2.26	-8.30	2.97	-15.04	-12.16	
	125.11	391.94	766.25	1225.32	1753.79	2338.90	2942.33	3455.20	4019.47	4666.20	
	0.50	-2.41	-1.55	3.08	6.31	0.40	-10.83	10.20	1.33	-5.20	
	5383	6177	7029	7931	8867	9829	10811				
	5375.36	6142.68	6975.17	7872.88	8835.79	9863.90	10957.12				0.515
	7.64	34.32	53.83	58.12	31.21	-34.90	-146.12				
	5389.03	6179.21	7027.59	7924.85	8861.67	9828.71	10816.64				0.247
	-6.03	-2.21	1.41	6.15	5.33	0.29	-5.64				

	2^+ 22^+	4^+ 24^+	6^+ 26^+	8^+ 28^+	10^+ 30^+	12^+ 32^+	14^+ 34^+	16^+ 36^+	18^+ 38^+	20^+ 40^+	*rms %* *deviation*
^{158}Yb	358	834	1403	2046	2743	3476	4043	4551	5178	5861	
	356.81	838.66	1407.36	2043.20	2734.62	3472.19	4056.81	4575.79	5160.45	5811.70	
	1.19	-4.66	-4.36	2.80	8.38	3.81	-13.81	-24.79	17.55	49.30	
	356.87	838.55	1407.08	2042.80	2734.33	3474.13	4041.48	4556.71	5172.36	5859.28	
	1.13	-4.55	-4.08	3.20	8.67	1.87	1.52	-5.71	5.64	1.72	
	6586.00	7327.00	8059.00								
	6529.66	7314.38	8165.85								0.582
	56.34	12.62	-106.85								
	6588.34	7330.40	8056.32								0.222
	-2.34	-3.40	2.68								
^{160}Yb	243.3	638.9	1148.0	1737.7	2374.9	2961.9	3365.9	3850.0	4428.0	5092.5	
	241.99	645.84	1149.70	1728.95	2369.87	2929.22	3374.50	3885.75	4462.98	5106.16	
	1.31	-6.94	-1.70	8.75	5.03	32.68	-8.60	-35.75	-34.98	-13.66	
	241.99	645.84	1149.70	1728.95	2369.87	2963.84	3359.89	3852.48	4433.15	5093.44	
	1.31	-6.94	-1.70	8.75	5.03	-1.94	6.01	-2.48	-5.15	-0.94	
	5829.30	6625.20	7461.50								
	5815.32	6590.45	7431.54								0.628
	13.98	34.75	29.96								
	5824.87	6618.99	7467.33								0.379
	4.43	6.21	-5.83								

	2^+ 22^+	4^+ 24^+	6^+ 26^+	8^+ 28^+	10^+ 30^+	12^+ 32^+	14^+ 34^+	16^+ 36^+	18^+ 38^+	20^+ 40^+	*rms %* *deviation*
^{164}Yb	123.8	385.9	760.2	1222	1752	2329	2899	3389	3932	4565	
	123.71	387.26	759.30	1217.71	1747.71	2339.06	2889.19	3388.63	3952.50	4580.82	
	0.09	-1.36	0.90	4.29	4.29	-10.06	9.81	0.37	-20.50	-15.82	
	123.56	387.62	760.00	1218.42	1747.82	2336.17	2900.48	3383.47	3936.92	4566.77	
	0.24	-1.72	0.20	3.58	4.18	-7.17	-1.48	5.53	-4.92	-1.77	
	5278.00	6058.00									
	5273.59	6030.79									0.320
	4.41	27.21									
	5274.00	6059.24									0.210
	4.00	-1.24									
^{166}Yb	102.3	330.4	667.9	1098.1	1605.8	2175.6	2779.2	3273.6	3783	4371	
	102.25	330.89	667.87	1096.61	1603.87	2179.02	2780.09	3260.57	3793.78	4387.40	
	0.05	-0.49	0.03	1.49	1.93	-3.42	-0.89	13.03	-10.78	-16.40	
	102.10	331.33	668.59	1096.96	1602.85	2174.65	2784.73	3270.34	3782.48	4373.85	
	0.20	-0.93	-0.69	1.14	2.95	0.95	-5.53	3.26	0.52	-2.85	
	5039.00	5777.00									
	5011.73	5756.88									0.221
	-2.73	20.12									
	5040.23	5775.07									0.139
	-1.23	1.93									

	2^+ 22^+	4^+ 24^+	6^+ 26^+	8^+ 28^+	10^+ 30^+	12^+ 32^+	14^+ 34^+	16^+ 36^+	18^+ 38^+	20^+ 40^+	*rms* % *deviation*
^{162}Hf	284	728	1291	1938	2633	3183	3564	4065	4650	5307	
	282.70	735.10	1292.18	1928.42	2629.60	3142.22	3587.13	4097.96	4674.70	5317.35	
	1.30	-7.10	-1.18	9.58	3.40	40.78	-23.13	-32.96	-24.70	-10.35	
	282.70	735.10	1292.18	1928.42	2629.60	3180.40	3571.60	4062.45	4643.34	5304.65	
	1.30	-7.10	-1.18	9.58	3.40	2.60	-7.60	2.55	6.66	2.35	
	6031	6821	7683								
	6025.91	6800.39	7640.78								0.612
	5.09	20.61	42.22								
	6036.77	6830.08	7674.96								0.345
	-5.77	-9.08	8.04								
^{164}Hf	211	588	1087	1671	2307	2875	3214	3682	4266	4942	
	210.17	593.00	1086.47	1663.26	2307.96	2792.29	3241.19	3756.59	4338.49	4986.89	
	0.83	-5.00	0.53	7.74	-0.96	82.71	-27.19	-74.59	-72.49	-44.89	
	210.17	593.00	1086.47	1663.26	2307.97	2873.98	3216.45	3682.80	4261.29	4940.19	
	0.83	-5.00	0.53	7.74	-0.97	1.02	-2.45	-0.80	4.71	1.81	
	5703	6549	7466								
	5701.80	6483.21	7331.13								1.306
	1.20	65.79	134.87								
	5707.77	6552.30	7462.05								0.295
	-4.77	-3.30	3.95								
^{166}Hf	158.7	470.7	897.4	1407.0	1972.8	2567.2	3010.8	3450.9	4011.3	4673.7	
	158.39	472.97	896.14	1402.31	1976.28	2559.02	2991.15	3487.30	4047.47	4671.65	
	0.31	-2.27	1.26	4.69	-3.48	8.18	19.65	-36.40	-36.17	2.05	
	158.21	473.80	897.03	1401.74	1970.54	2572.62	3008.60	3451.44	4012.29	4673.75	
	0.49	-3.10	0.37	5.26	2.26	-5.42	2.20	-0.54	-0.99	-0.05	
	5412.8										
	5359.86										0.591
	52.94										
	5412.21										0.258
	0.59										

	2^+ 22^+	4^+ 24^+	6^+ 26^+	8^+ 28^+	10^+ 30^+	12^+ 32^+	14^+ 34^+	16^+ 36^+	18^+ 38^+	20^+ 40^+	*rms %* *deviation*
^{168}Hf	123.9	385.6	757.0	1213.6	1735.6	2305.5	2856.9	3309.7	3831.7	4439.1	
	123.92	386.54	755.68	1209.22	1732.57	2315.70	2832.46	3315.14	3860.12	4467.37	
	-0.02	-0.94	1.32	4.38	3.03	-10.20	24.44	-5.44	-28.42	-28.27	
	123.70	387.07	756.77	1210.40	1732.88	2311.01	2857.38	3307.47	3833.44	4440.02	
	0.20	-1.47	0.23	3.20	2.72	-5.51	-0.48	2.23	-1.74	-0.92	
	5123.2	5874.1	6686.4	7560.9							
	5136.91	5868.73	6662.83	7519.21							0.437
	-13.71	5.37	23.57	41.69							
	5121.99	5873.39	6688.12	7559.99							0.154
	1.21	0.71	-1.72	0.91							
^{170}Hf	100.8	332.0	642.8	1043.2	1505.4	2016.3	2567.0	3151.4	3766.6	4421.1	
	101.00	327.97	649.52	1046.36	1504.99	2014.96	2566.30	3148.96	3763.30	4423.59	
	-0.20	4.03	-6.72	-3.16	0.41	1.34	0.70	2.44	3.30	-2.49	
	100.68	329.40	648.74	1043.97	1502.35	2014.91	2575.10	3150.79	3762.83	4423.61	
	0.12	2.60	-5.94	-0.77	3.05	1.39	-8.10	0.61	3.77	-2.51	
	5130.40	5902.70	6739.30								
	5138.89	5907.52	6714.04								0.472
	-8.49	-4.82	25.26								
	5134.71	5897.67	6714.05								0.372
	-4.31	5.03	25.25								
^{172}Hf	95.4	309.6	628.8	1038.0	1521.8	2065.0	2654.2	3277.0	3919.9	4574.9	
	95.14	311.35	629.98	1035.32	1514.77	2058.34	2657.06	3295.58	3923.80	4565.75	
	0.26	-1.75	-1.18	2.68	7.03	6.66	-2.86	-18.58	-3.90	9.15	
	95.21	310.92	629.51	1035.54	1516.43	2062.03	2662.06	3287.92	3906.92	4567.46	
	0.19	-1.32	-0.71	2.46	5.37	2.97	-7.86	-10.92	12.98	7.44	
	5273.20	6032.20	6848.90	7724.60							
	5264.42	6025.85	6851.19	7740.70							0.302
	8.78	6.35	-2.29	-16.10							
	5280.25	6043.85	6855.46	7711.97							0.248
	-7.05	-11.65	-6.56	12.63							

	2^+ 22^+	4^+ 24^+	6^+ 26^+	8^+ 28^+	10^+ 30^+	12^+ 32^+	14^+ 34^+	16^+ 36^+	18^+ 38^+	20^+ 40^+	*rms %* *deviation*
^{168}W	199.3	562.7	1042.7	1601.1	2202.7	2722.9	3010.9	3447.6	4012.7	4683.8	
	199.04	565.39	1039.52	1594.71	2211.59	2618.72	3049.22	3543.14	4100.70	4721.95	
	0.26	-2.69	3.18	6.39	-8.89	104.18	-38.32	-95.54	-88.00	-38.15	
	198.91	565.93	1040.24	1594.48	2208.81	2721.92	3013.05	3445.70	4011.71	4685.19	
	0.39	-3.23	2.46	6.62	-6.11	0.98	-2.15	1.90	0.99	-1.39	
	5437.90	6246.50	7078.50								
	5406.90	6155.55	6967.92								1.640
	31.00	90.95	110.58								
	5439.02	6245.83	7078.20								0.229
	-1.12	0.67	0.30								
^{170}W	156.7	462.7	875.9	1363.8	1901.9	2484.7	2911.3	3344.2	3874.4	4490.9	
	156.78	463.50	872.64	1359.70	1910.34	2472.36	2890.10	3369.72	3911.23	4514.63	
	-0.08	-0.80	3.26	4.10	-8.44	12.34	21.20	-25.52	-36.83	-23.73	
	156.57	464.25	873.71	1360.06	1907.20	2484.59	2908.77	3349.37	3876.59	4485.76	
	0.13	-1.55	2.19	3.74	-5.30	0.11	2.53	-5.17	-2.19	5.14	
	5176.90	5918.90	6714.70	7569.80	8488.70						
	5179.92	5907.09	6696.14	7547.09	8459.92						0.471
	-3.02	11.81	18.56	22.71	28.78						
	5169.07	5918.25	6724.91	7580.61	8476.87						0.177
	7.83	0.65	-10.21	-10.81	11.83						
^{182}Os	127.0	400.5	794.4	1278.3	1812.4	2346.5	2841.0	3320.4	3857.4	4480.5	
	126.69	403.12	792.64	1271.02	1817.60	2357.10	2815.77	3317.42	3880.18	4506.12	
	0.31	-2.62	1.76	7.28	-5.20	-10.60	25.23	2.98	-22.78	-25.62	
	126.50	404.24	793.34	1268.87	1809.86	2365.79	2828.92	3310.08	3863.76	4493.78	
	0.50	-3.74	1.06	9.43	2.54	-19.29	12.08	10.32	-6.36	-13.28	
	5192.20	5987.40									
	5195.75	5949.25									0.503
	-3.55	38.15									
	5198.24	5974.09									0.478
	-6.04	13.31									

Table 3.4. The Gauss criterion sum, Ω, for the Variable Moment of Inertia and Bohr–Mottelson band crossing model and the Variable Moment of Inertia and Varshni formula band crossing model.

Nucleus	Ω VMI–BM Model	Ω VMI–V Model
^{104}Pd	60.25	23.08
^{128}Ce	128.68	47.57
^{130}Ce	239.44	40.93
^{154}Dy	29.18	34.45
^{156}Dy	46.04	53.30
^{158}Dy	15.81	11.89
^{156}Er	26.08	35.06
^{158}Er	56.03	43.77
^{160}Er	37.54	10.35
^{158}Yb	54.98	10.72
^{160}Yb	64.06	31.08
^{164}Yb	17.55	10.55
^{166}Yb	8.40	4.62
^{162}Hf	60.88	25.77
^{164}Hf	277.22	18.83
^{166}Hf	64.05	18.31
^{168}Hf	29.67	4.75
^{170}Hf	36.20	30.00
^{172}Hf	14.21	12.32
^{168}W	436.94	11.38
^{170}W	33.26	5.84
^{182}Os	43.32	54.80

Table 3.5. Prediction of Yrare Levels Above the Critical Spin for ^{168}Hf.

Spin	Exptl. Level (keV)	VMI–V Predictions (keV)	% Deviations	VMI–BM Predictions (keV)	% Deviations
14^+	2938.3	2977	1.3	2951	0.4
16^+	3622.8	3645	0.6	3633	0.3
18^+	4321.8	4367	1.0	4359	0.9
20^+	5048.8	5131	1.6	5123	1.5
22^+	5814	5931	2.0	5929	2.0

Table 3.6. Prediction of Yrare Levels Below the Critical Spin. The single 12^+ level refers to ^{166}Hf while the other levels are for ^{166}Yb.

Spin	Exptl. Level (keV)	VMI–V Predictions (keV)	% Deviations	VMI–BM Predictions (keV)	% Deviations
8^+	2030	2227	9.7	1741	14.1
10^+	2214.2	2333	5.4	2031	8.3
12^+	2530.0	2552	0.9	2381	5.9
14^+	2897.0	2897	0.0	2828	2.4
12^+	2736	2797	2.2	2608	4.7

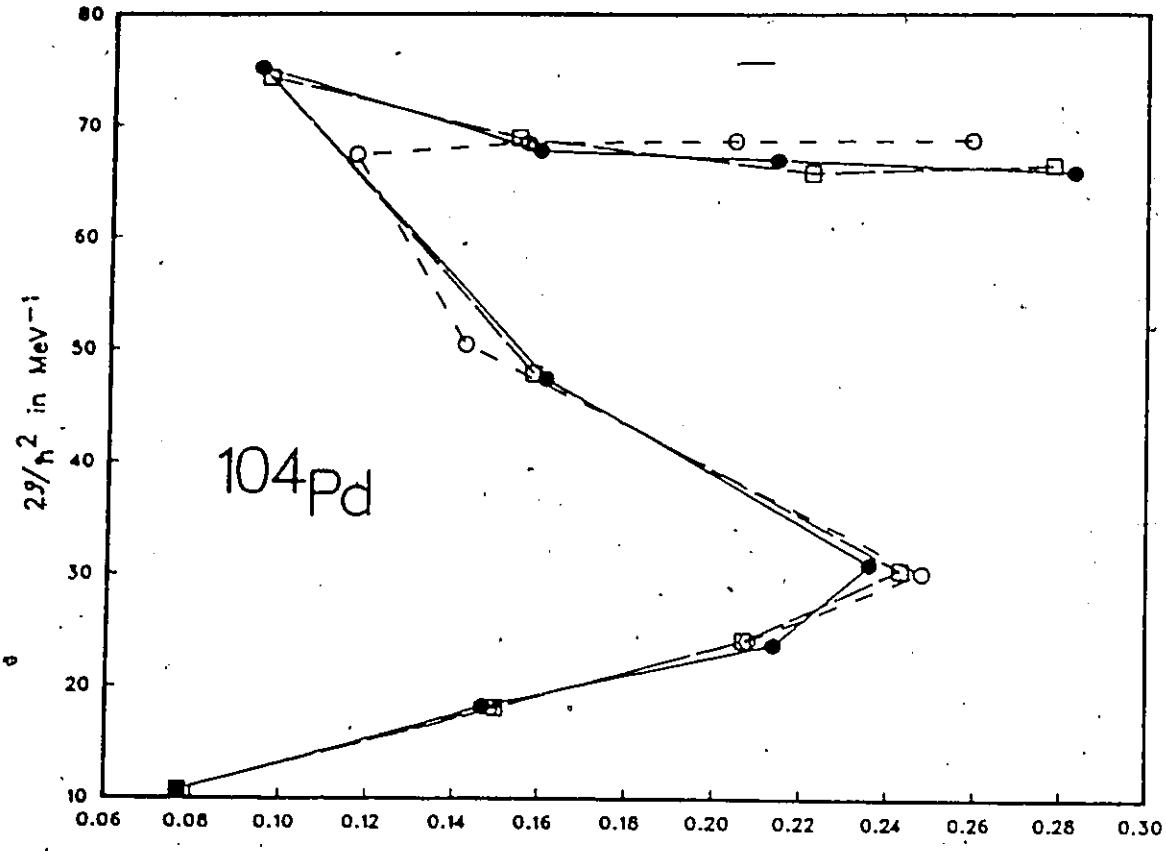
104Pd
$2\mathcal{I}/\hbar^2$ in MeV^{-1}
$(\hbar\omega)^2$ in MeV^2

Fig. 3.1

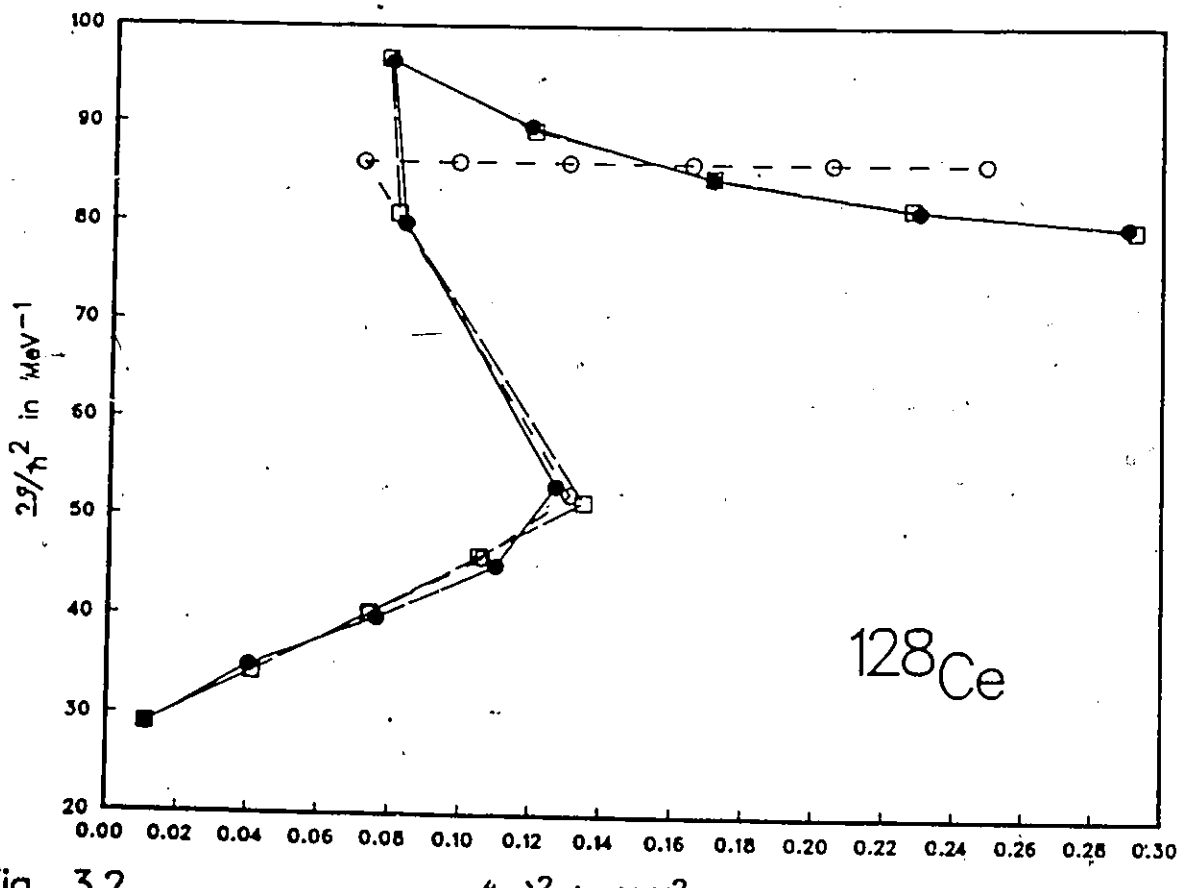
128Ce
$2\mathcal{I}/\hbar^2$ in MeV^{-1}
$(\hbar\omega)^2$ in MeV^2

Fig. 3.2

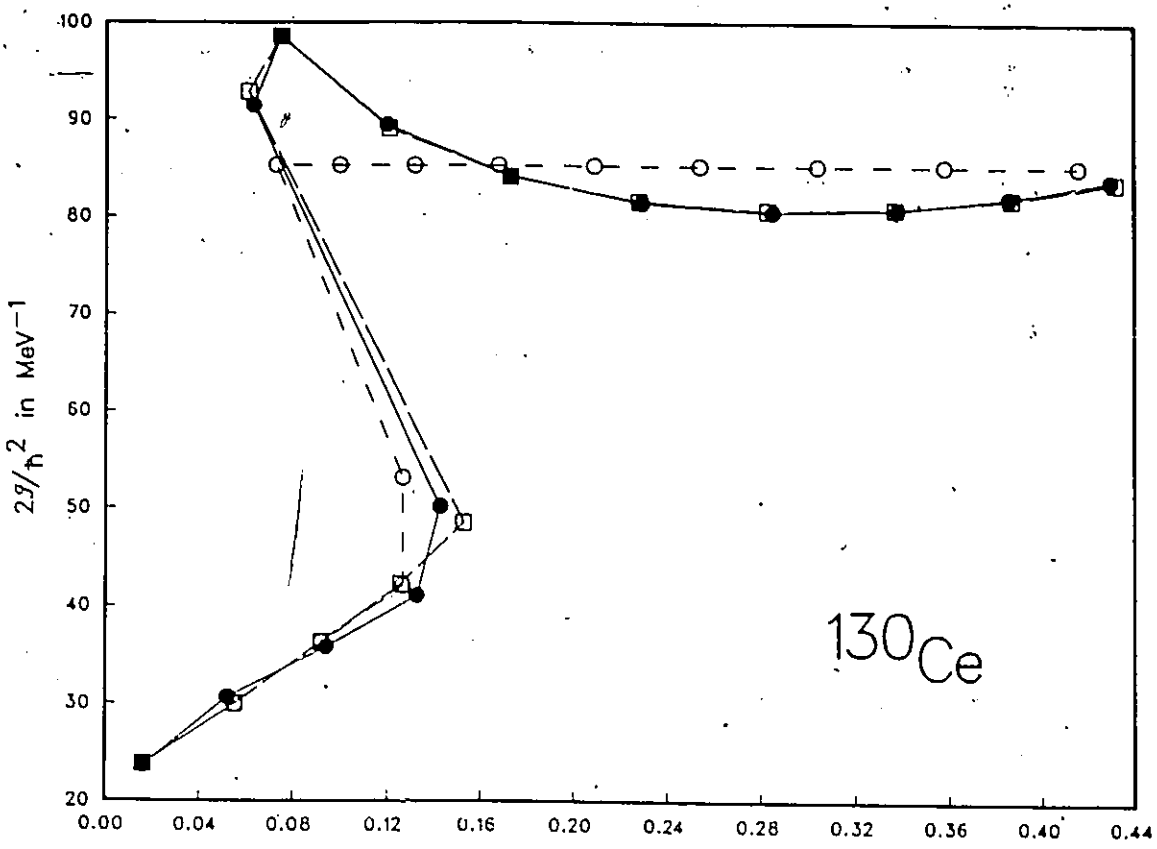
100
90
80
70
60
50
40
30
20
$2\mathcal{I}/\hbar^2$ in MeV^{-1}
0.00
0.04
0.08
0.12
0.16
0.20
0.24
0.28
0.32
0.36
0.40
0.44
$(\hbar\omega)^2$ in MeV^2
^{130}Ce

Fig. 3.3

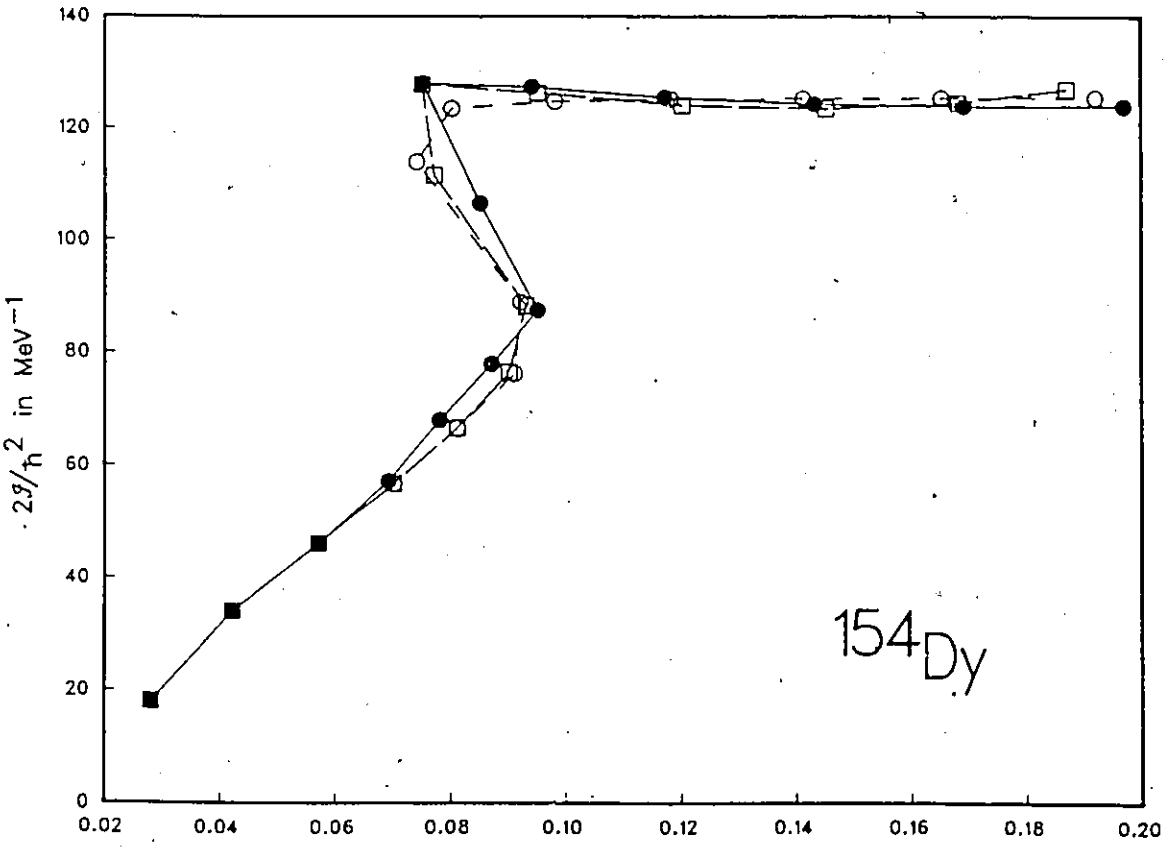
140
120
100
80
60
40
20
0
$2\mathcal{I}/\hbar^2$ in MeV^{-1}
0.02
0.04
0.06
0.08
0.10
0.12
0.14
0.16
0.18
0.20
$(\hbar\omega)^2$ in MeV^2
^{154}Dy

Fig. 3.4

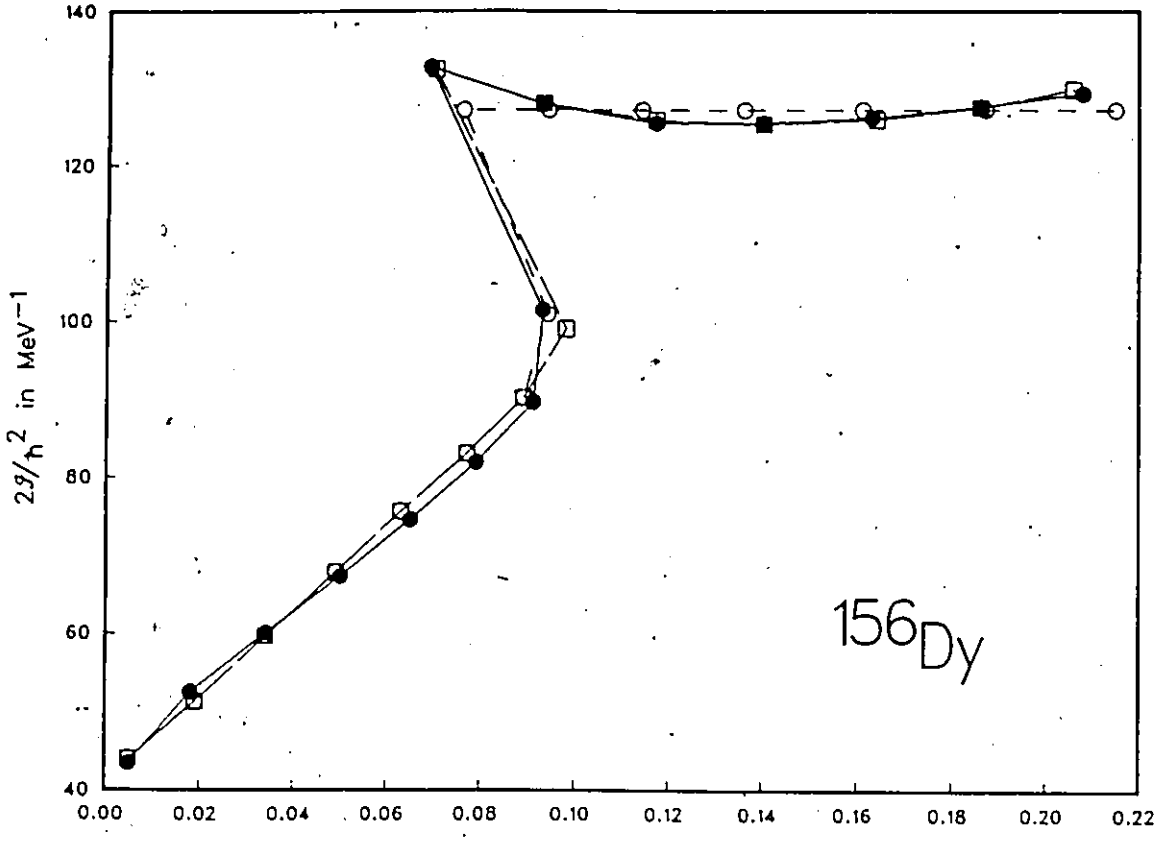
140
120
100
80
60
40
$2\mathcal{I}/\hbar^2$ in MeV^{-1}
0.00
0.02
0.04
0.06
0.08
0.10
0.12
0.14
0.16
0.18
0.20
0.22
$(\hbar\omega)^2$ in MeV^2
^{156}Dy

Fig. 3.5

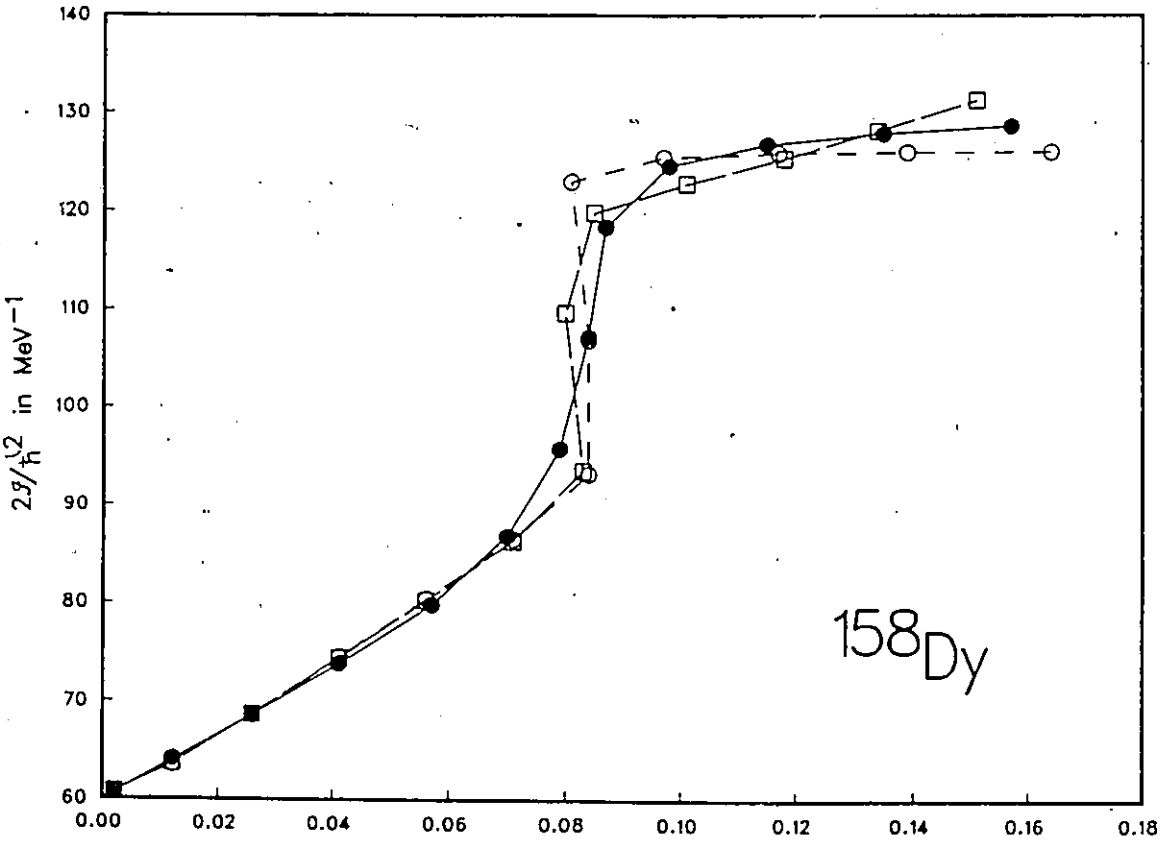
140
130
120
110
100
90
80
70
60
$2\mathcal{I}/\hbar^2$ in MeV^{-1}
0.00
0.02
0.04
0.06
0.08
0.10
0.12
0.14
0.16
0.18
$(\hbar\omega)^2$ in MeV^2
^{158}Dy

Fig. 3.6

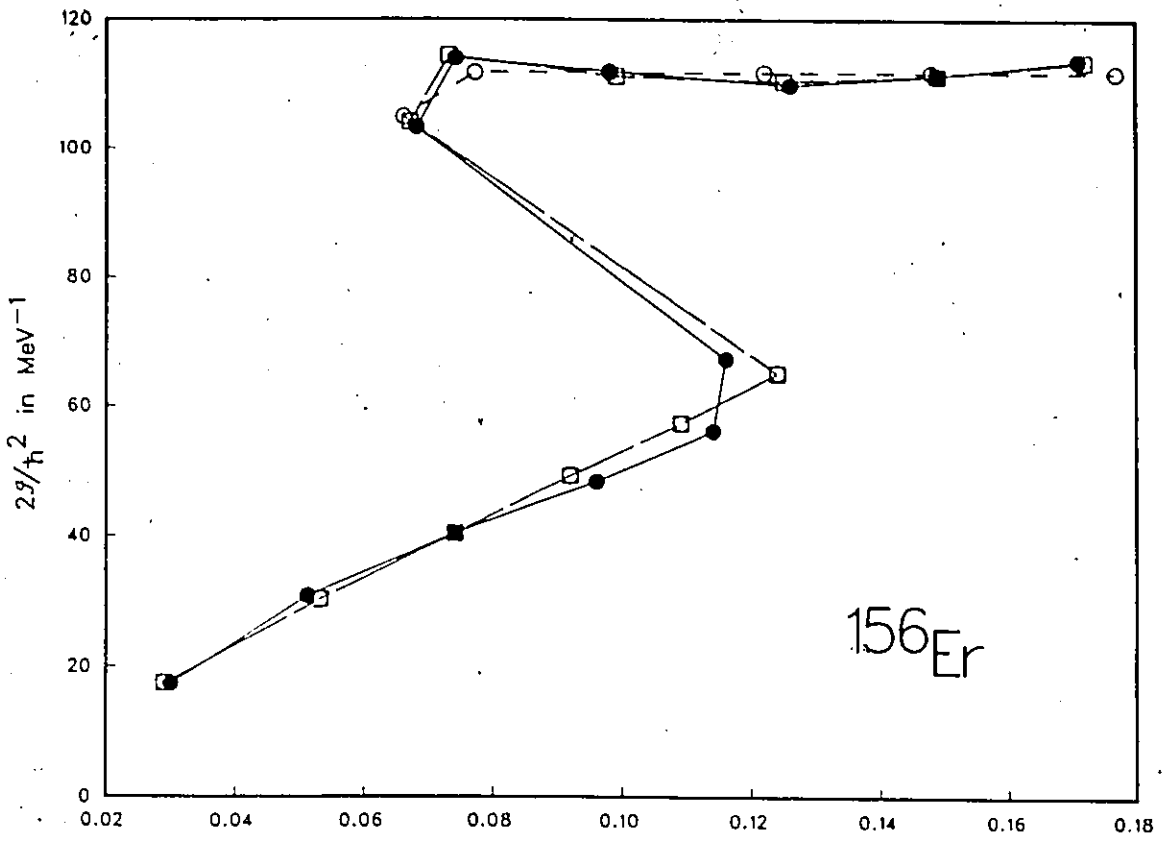
120
100
80
60
40
20
0
$2\vartheta/\hbar^2$ in MeV^{-1}
0.02
0.04
0.06
0.08
0.10
0.12
0.14
0.16
0.18
$(\hbar\omega)^2$ in MeV^2
^{156}Er

Fig. 3.7

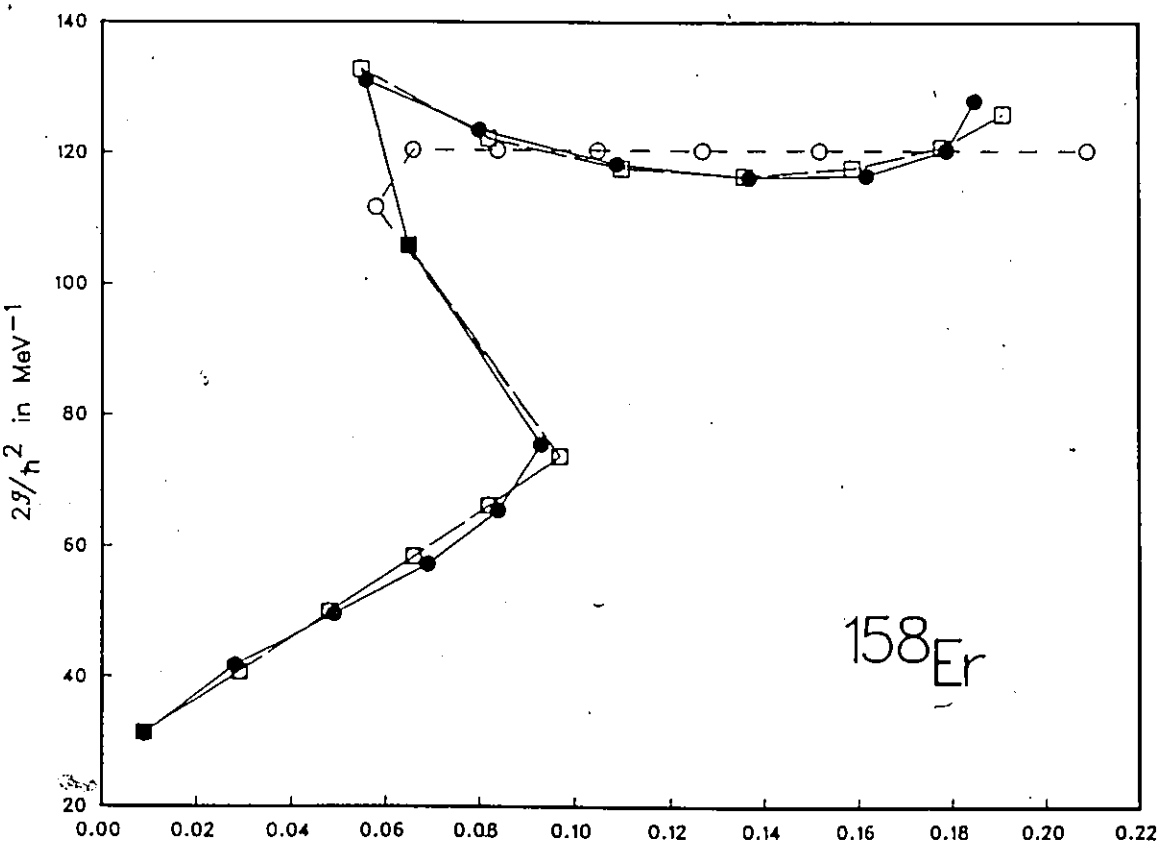
140
120
100
80
60
40
20
$2\vartheta/\hbar^2$ in MeV^{-1}
0.00
0.02
0.04
0.06
0.08
0.10
0.12
0.14
0.16
0.18
0.20
0.22
$(\hbar\omega)^2$ in MeV^2
^{158}Er

Fig. 3.8

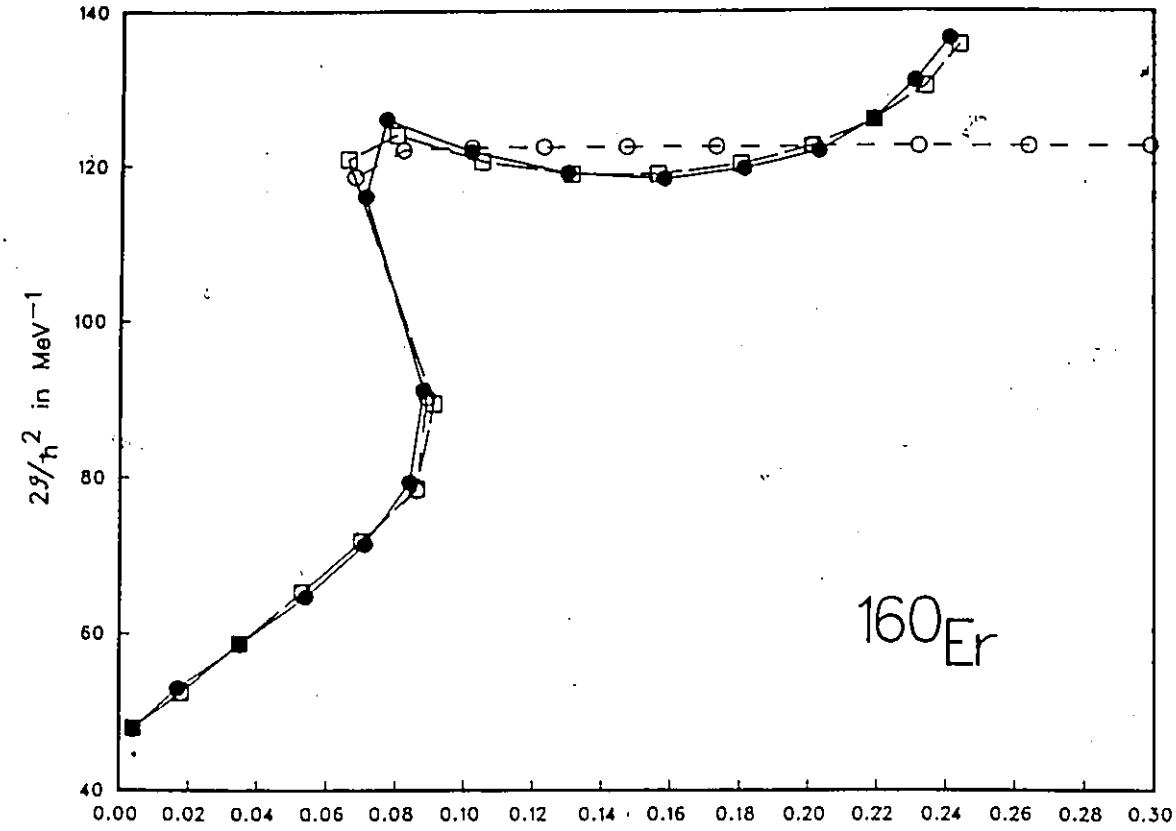

Fig. 3.9

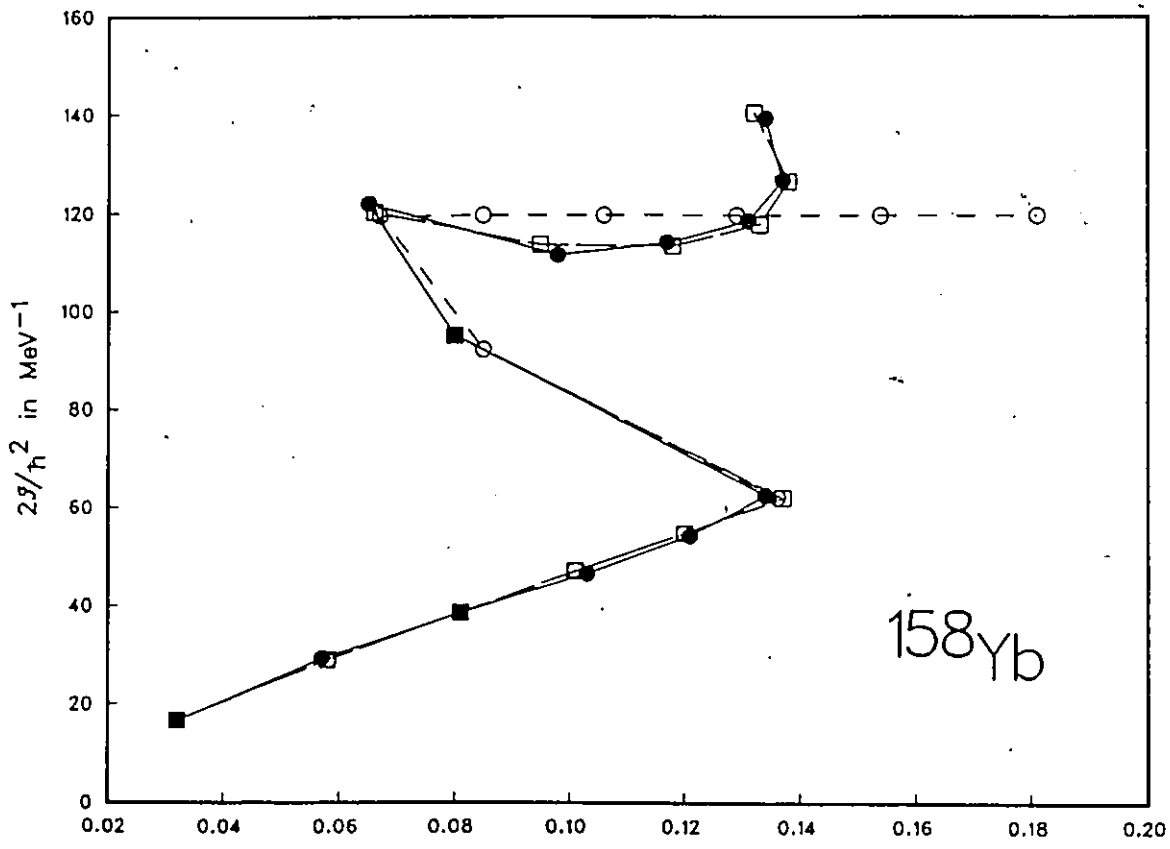

Fig. 3.10

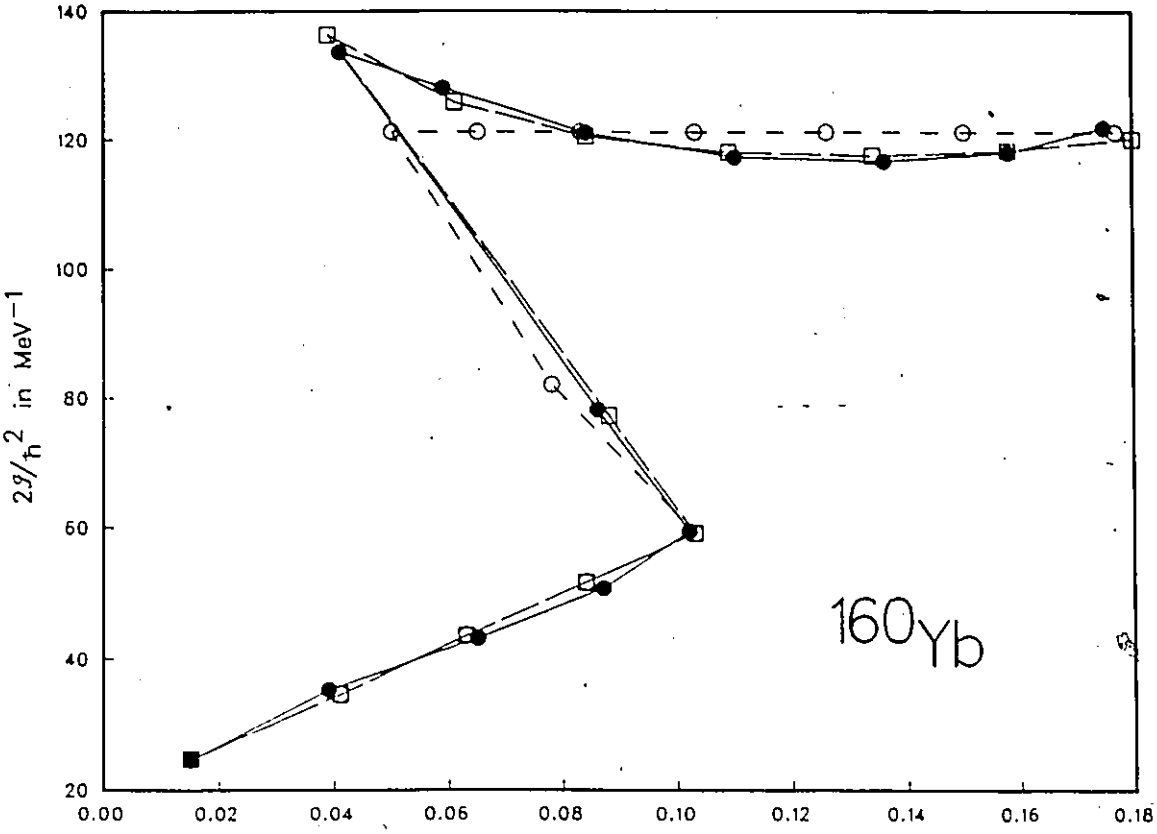

Fig. 3.11

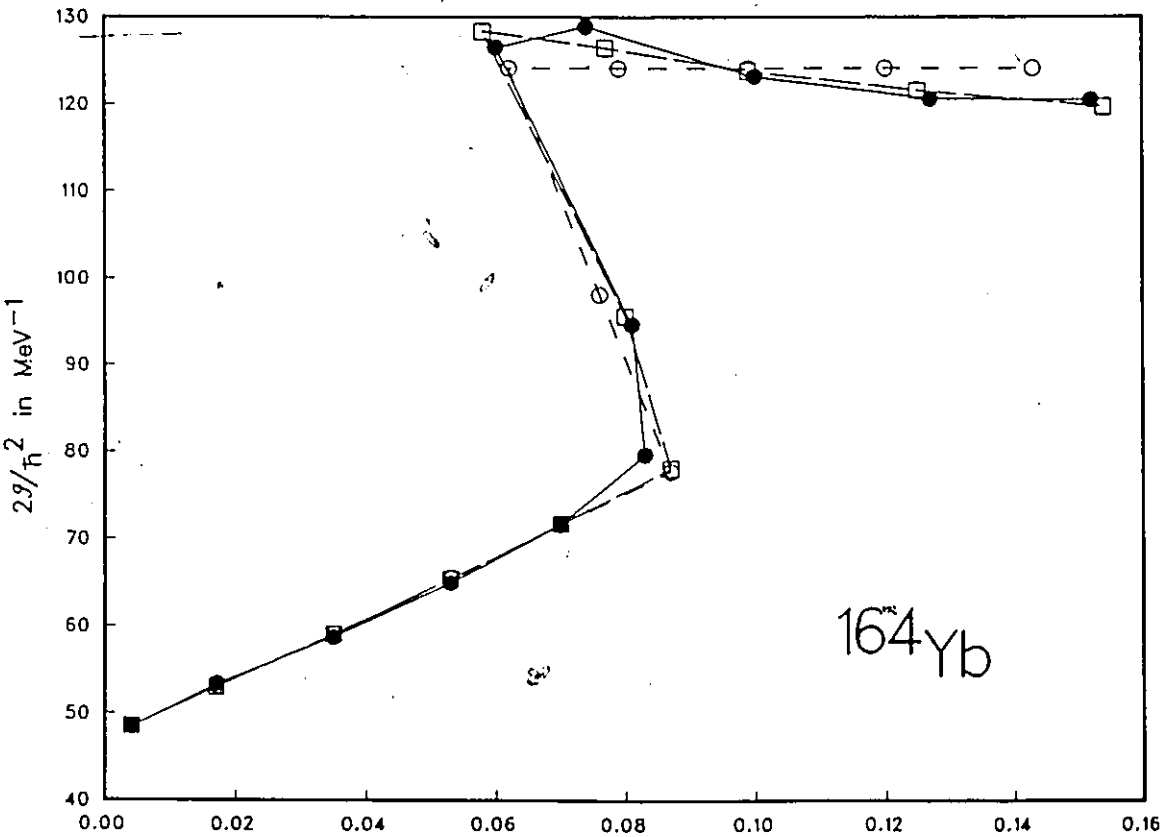

Fig. 3.12

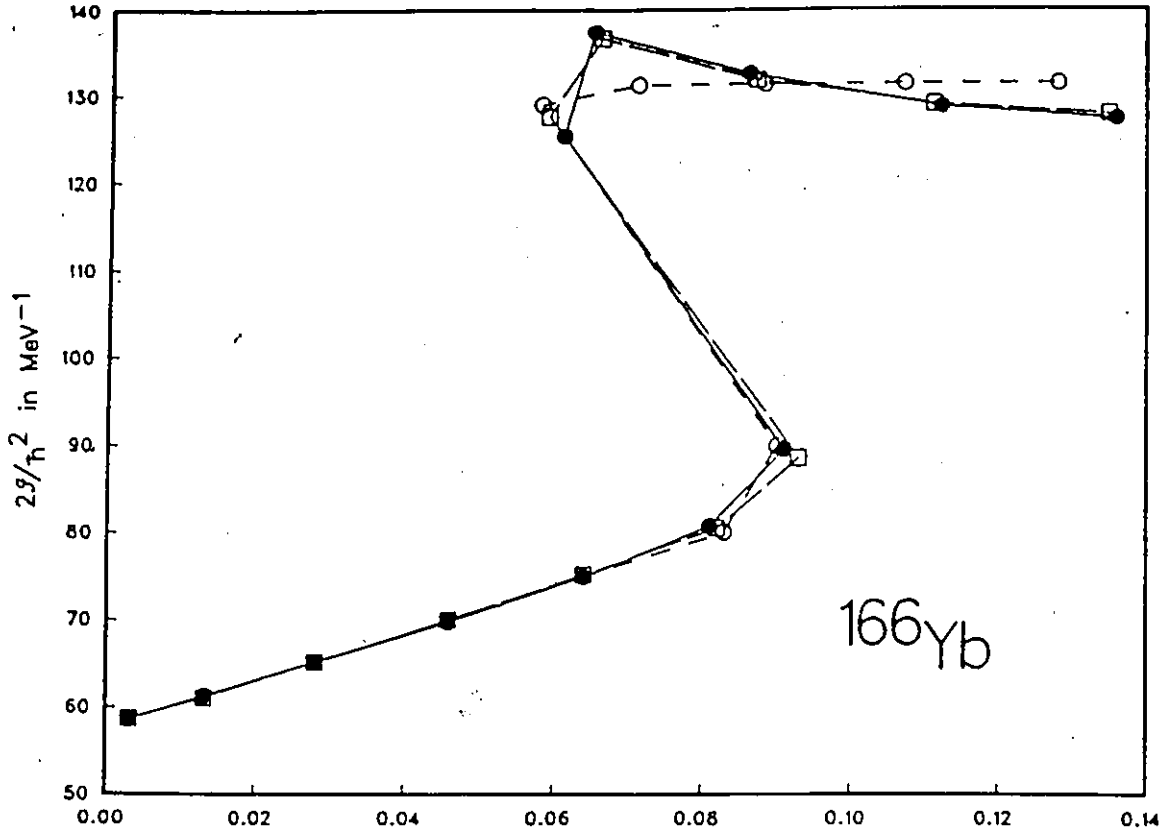

Fig. 3.13

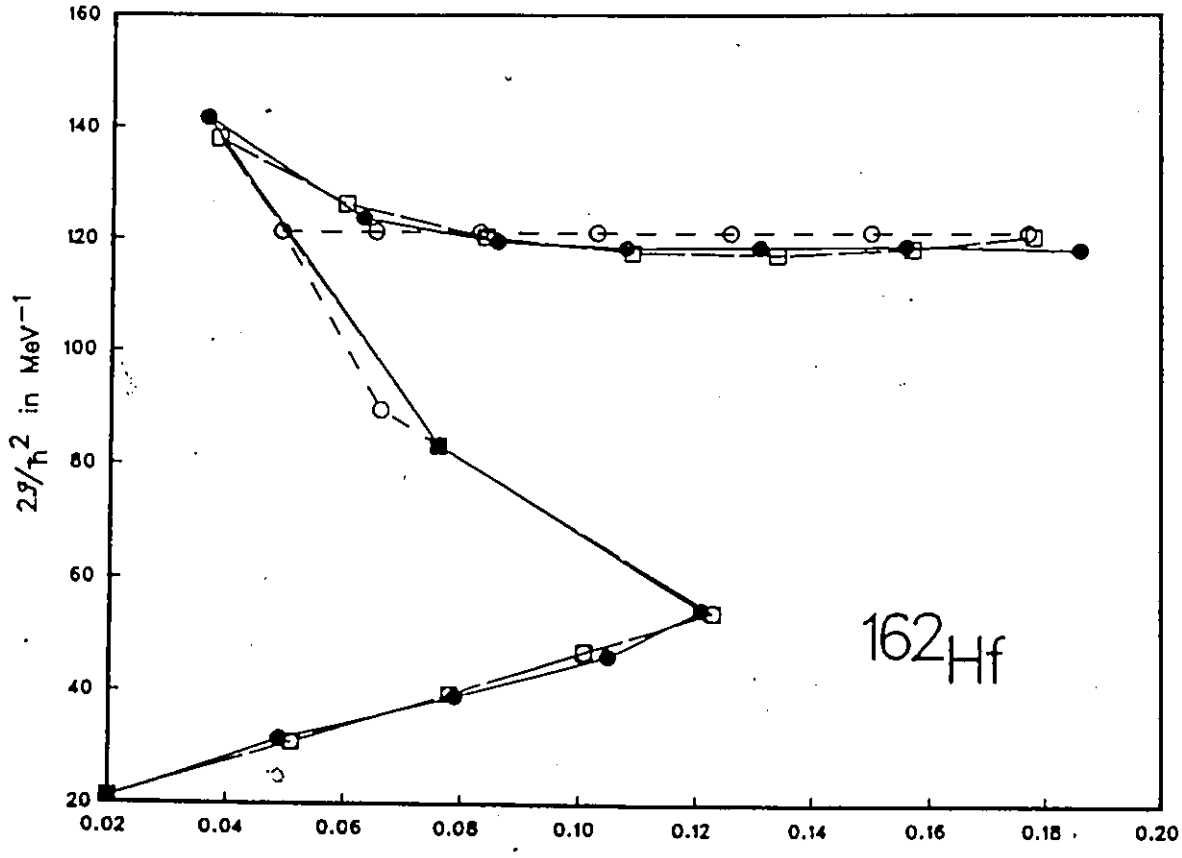

Fig. 3.14

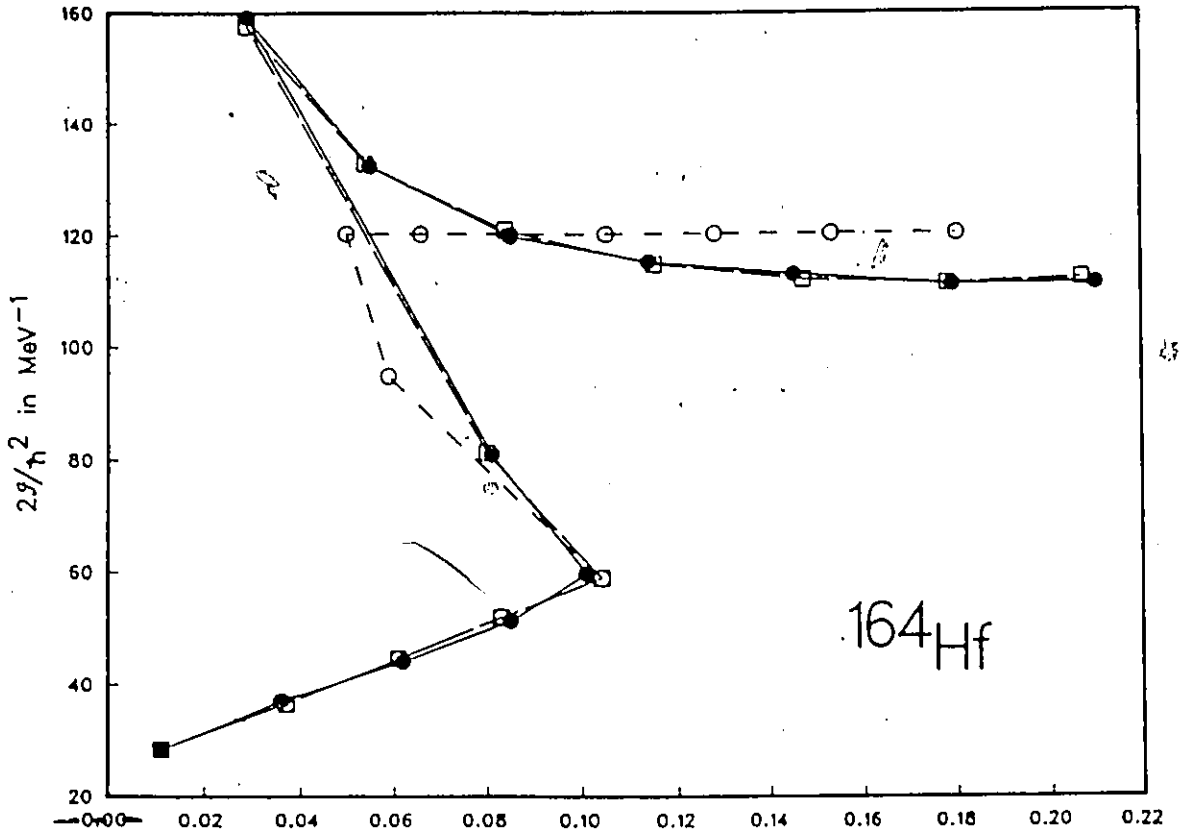

Fig. 3.15

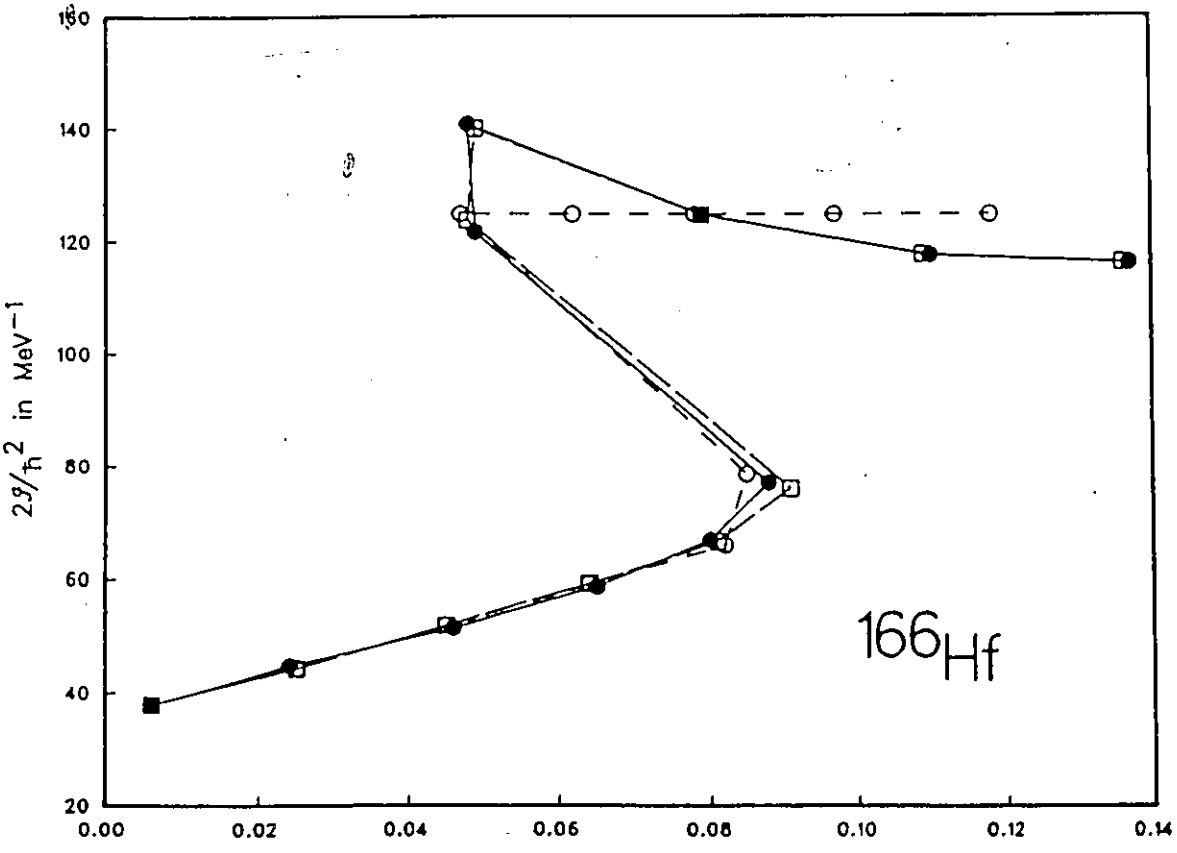

Fig. 3.16

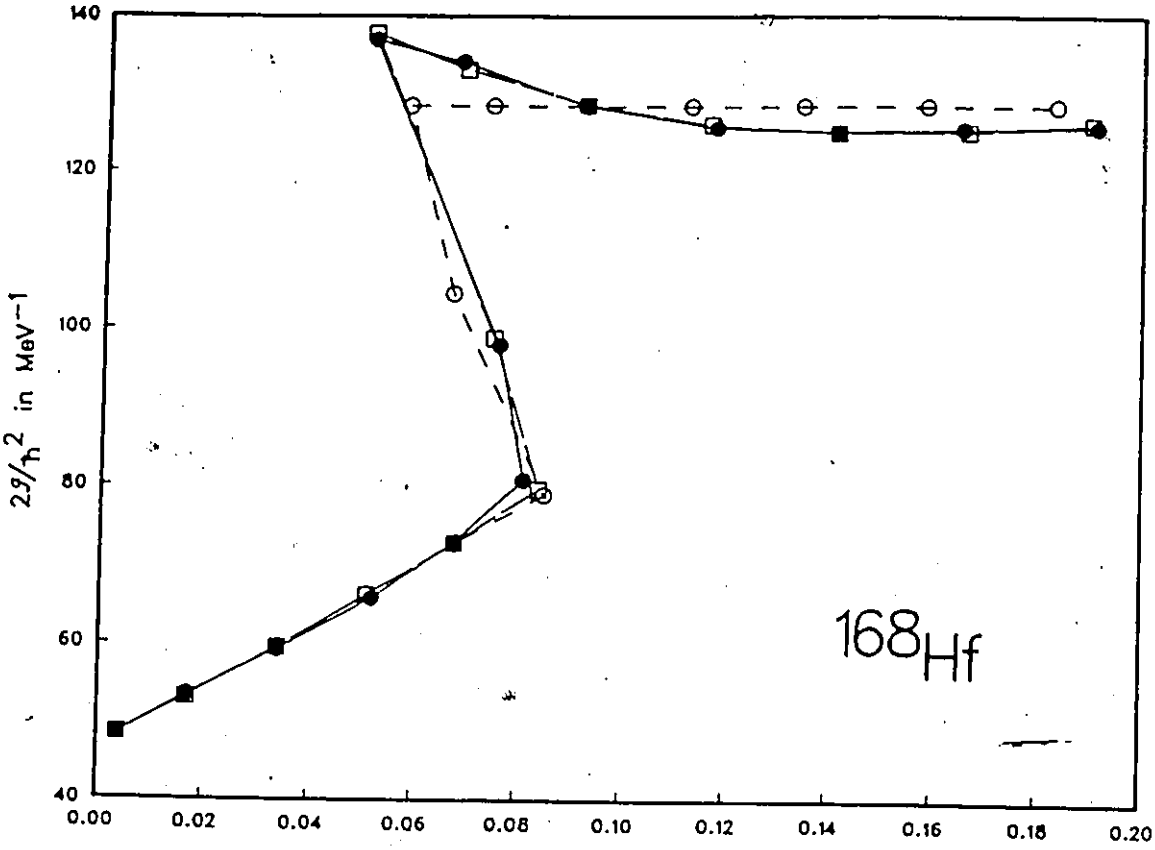

Fig. 3.17

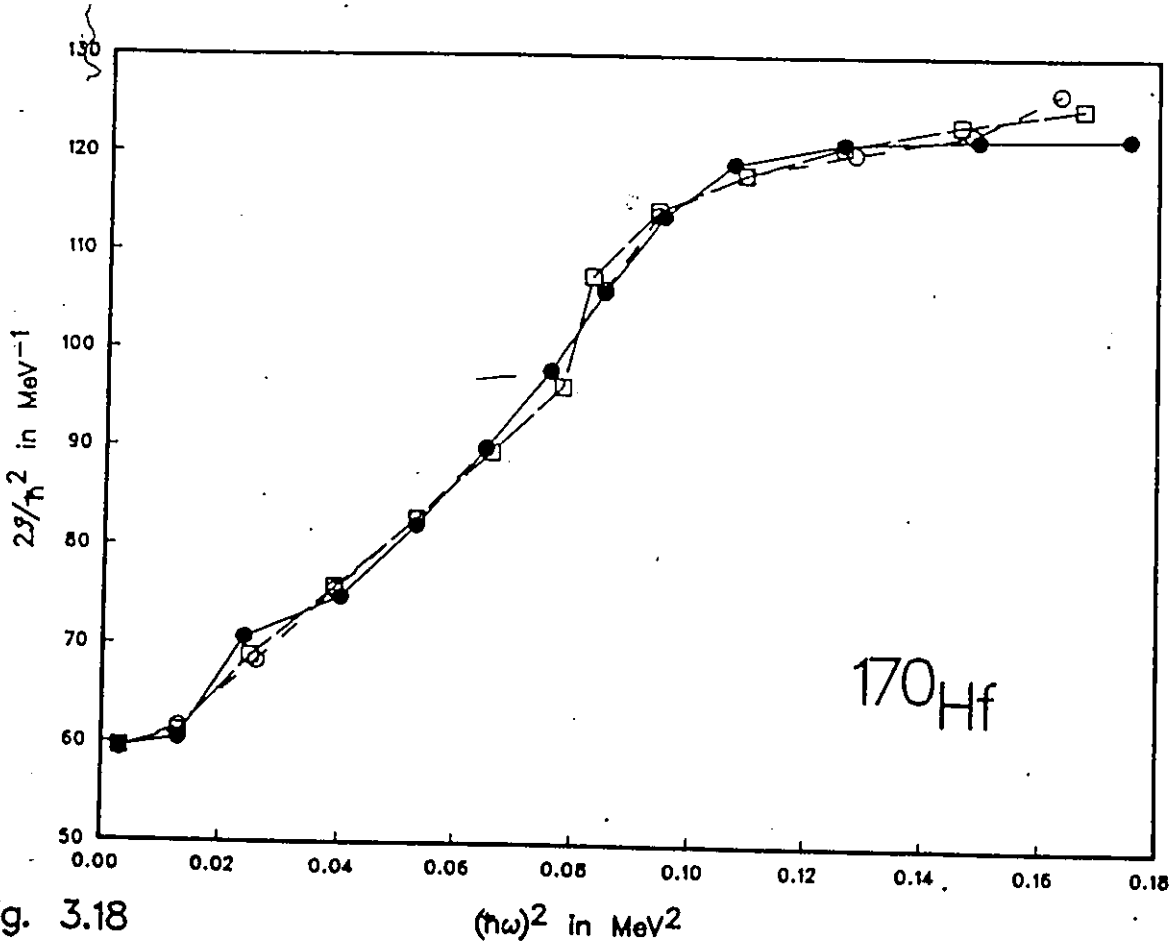

Fig. 3.18

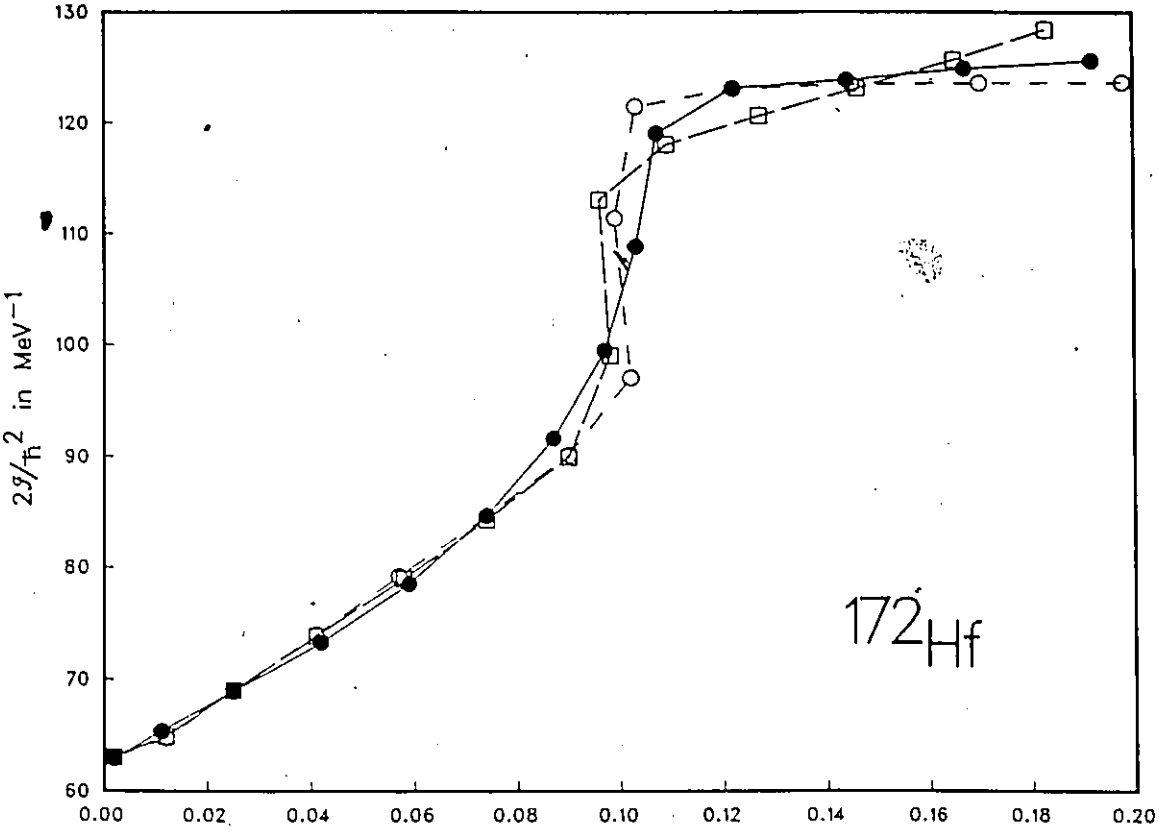

Fig. 3.19

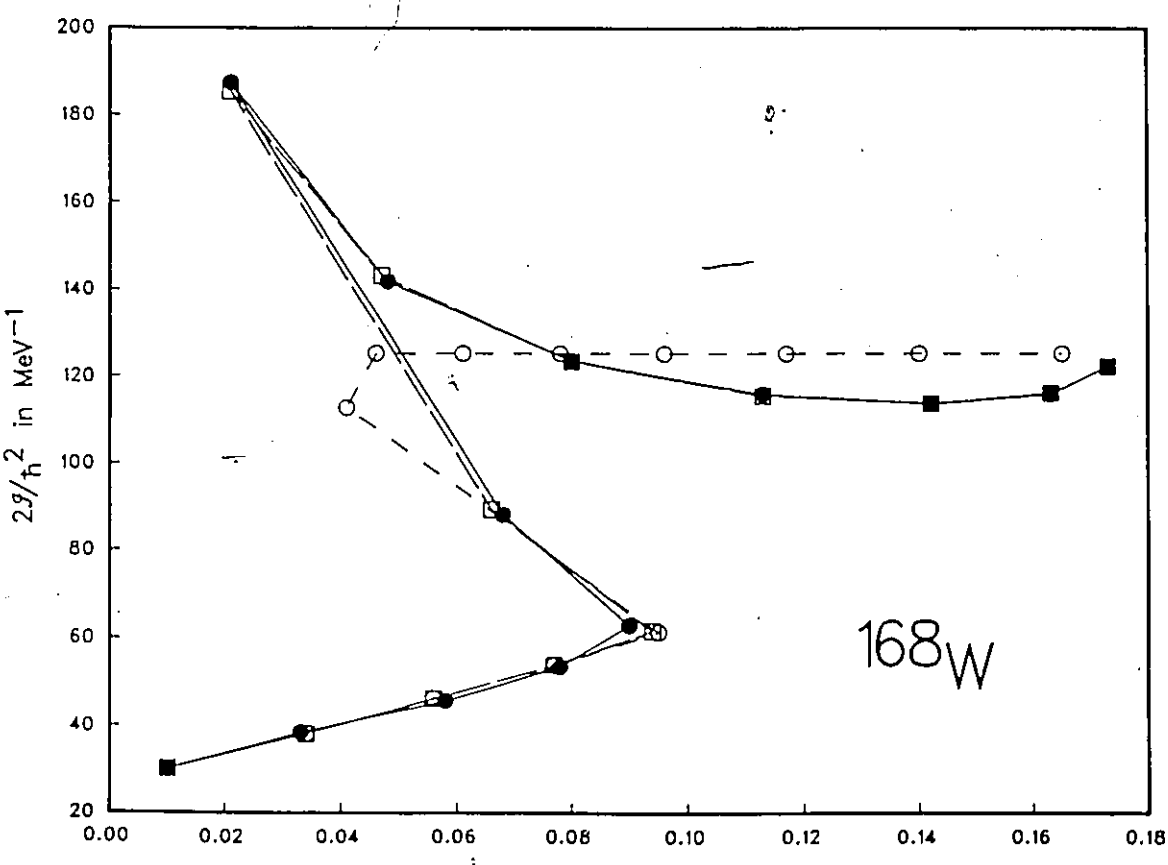

Fig. 3.20

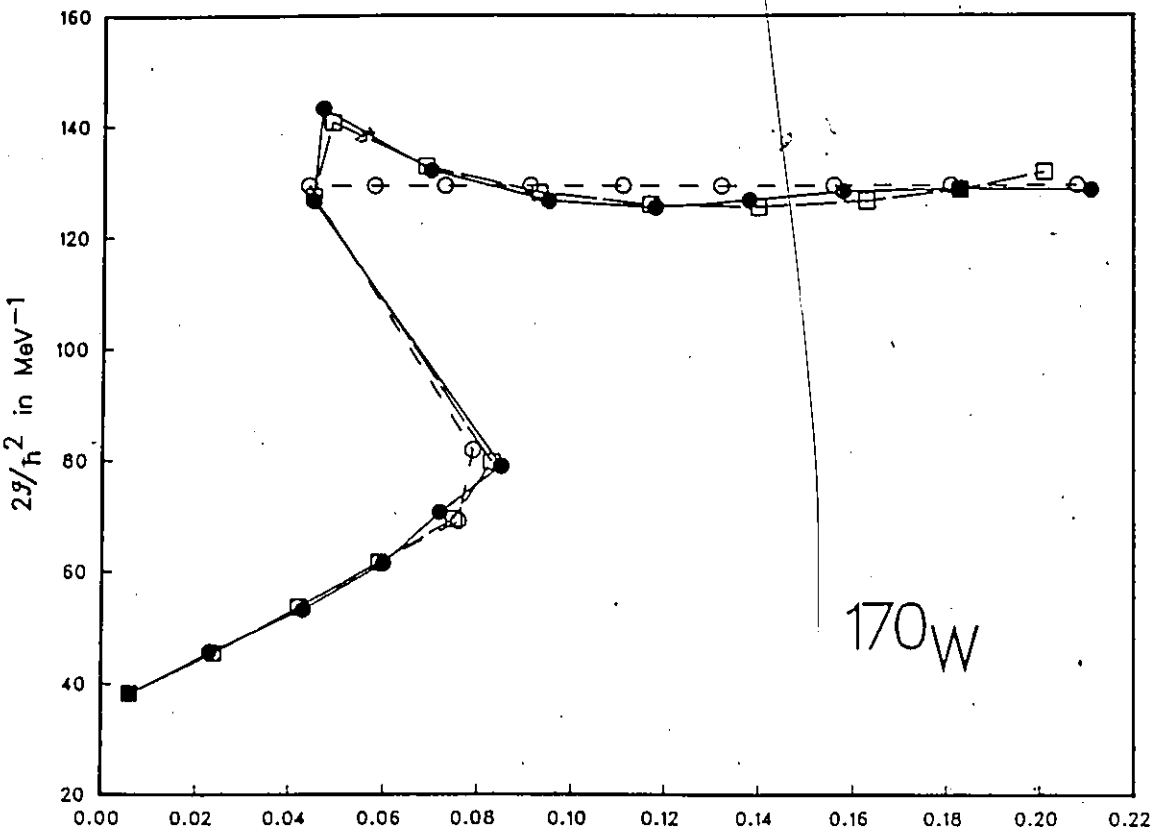

Fig. 3.21

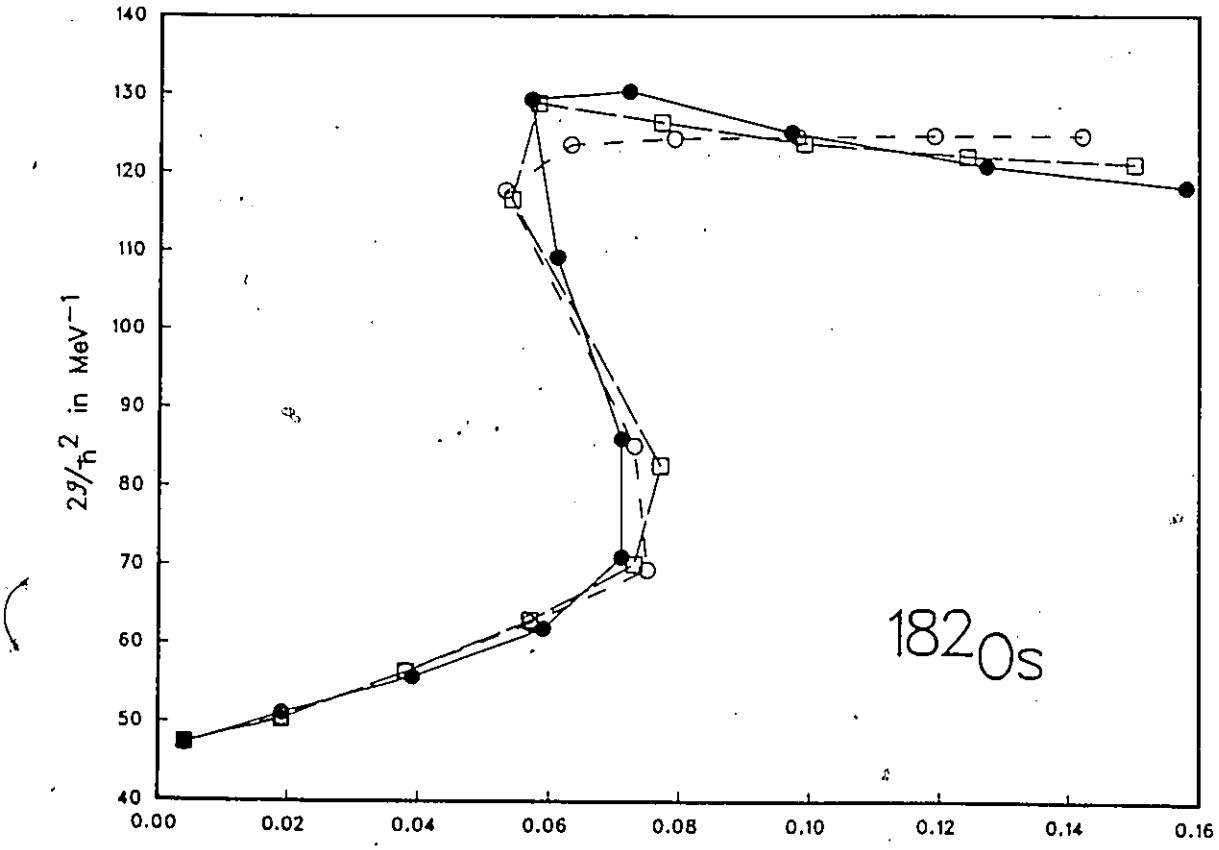

Fig. 3.22

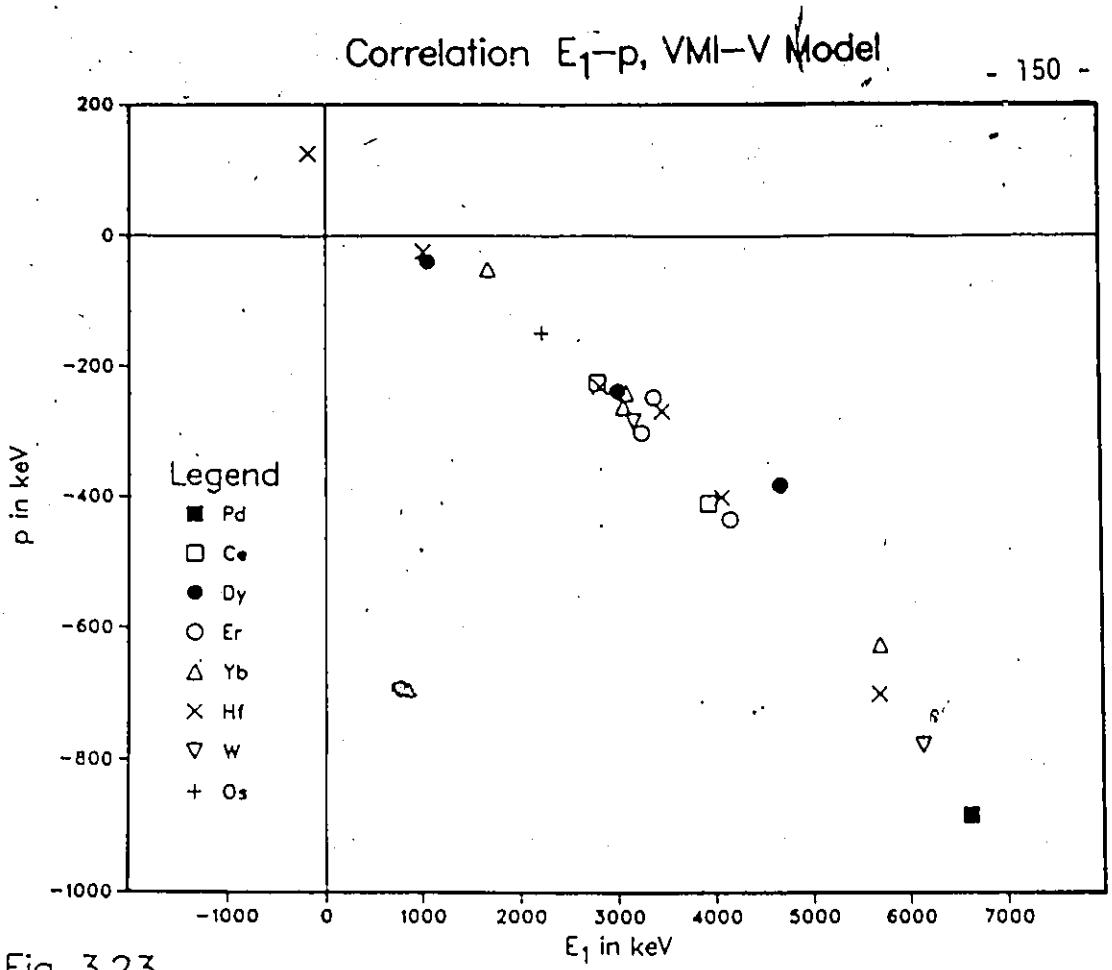

Fig. 3.23

Fig. 3.24

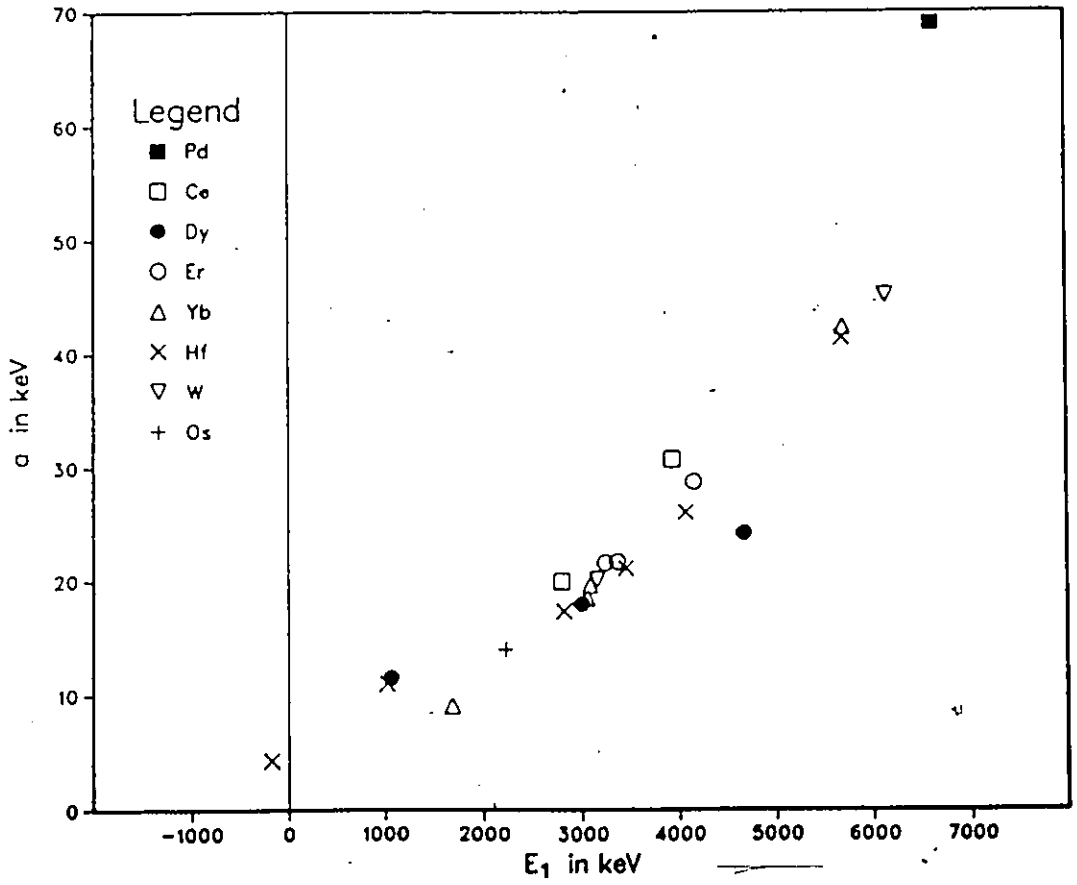

References

Agarwal, Y. K., *et al*, 1983, Nucl. Phys. **A399** 199

Arima, A., and F. Iachello, 1976, Ann. Phys. **99** 253

Arima, A., and F. Iachello, 1978, Ann. Phys. **111** 201

Arima, A., and F. Iachello, 1979, Ann. Phys. **123** 468

Baktash, C., *et al*, 1985, Phys. Rev. Lett. **54** 978

Bonatsos, D., 1985, Phys. Rev. C **31** 2256

Bonatsos, D., and A. Klein, 1984, Phys. Rev. C **29** 1879

Bengtsson, R., and S. Frauendorf, 1979a, Nucl. Phys. **A314** 27

Bengtsson, R., and S. Frauendorf, 1979b, Nucl. Phys. **A327** 139

Bengtsson, R., I. Hamamoto and B. Mottelson, 1978, Phys. Lett. **73B** 259

Burde, J., *et al*, 1982, Phys. Rev. Lett., **48** 533

Carvalho, J. L. S., *et al*, 1985, Phys. Rev. C **31** 1049

de Voigt, M. J. A., J. Dudek and Z. Szymanski, 1983, Rev. Mod. Phys. **55** 949

Ejiri, H., 1966, Rep. No. INSJ 101

Fields, C. A., K. H. Hicks and R. J. Peterson, 1984, Nucl. Phys. **A431** 473

Johnson, A., H. Ryde and J. Sztarkier, 1971, Phys. Lett. **34B** 605

Johnson, A., H. Ryde and A. S. Hjorth, 1972, Nucl. Phys. **A179** 753

Lieder, R. M., and H. Ryde, 1978, in *Advances in Nuclear Physics*, Vol. 10, eds. M. Baranger and E. Vogt, Plenum, New York, p. 10

Mariscotti, M. A. J., G. Scharff-Goldhaber, and B. Buck, 1969, Phys. Rev. **178** 1864

Mottelson, B. R., and J. G. Valatin, 1960, Phys. Rev. Lett. **5** 511

Paul, E. S., *et al*, 1985, J. Phys. G: Nucl. Phys. **11** L53

Pari, G., and Y. P. Varshni, 1985, Bull. Amer. Phys. Soc. **30** 1275

Rasmussen, J. O., *et al*, 1978, Nucl. Phys. **A332** 82

Sakai, M., 1984, *Table of Members of Quasi-Bands*, INS-Rep.-493

Scharff-Goldhaber, G., C. B. Dover and A. L. Goodman, 1976, Ann. Rev. Nucl. Sci. **26** 239

Spreng, W., *et al*, 1983, Phys. Rev. Lett. **51** 1522

Sood, P. C., and A. K. Jain, 1975, Phys. Rev. C **12** 1064

Stephens, F. S., 1975, Rev. Mod. Phys. **47** 43

Stephens, F. S., and R. S. Simon, 1972, Nucl. Phys. **A183** 257

Varshni, Y. P., 1968, Prog. Theor. Phys. **40** 1181

Varshni, Y. P., 1974, J. Phys. Soc. Japan **36** 317

Walus, W., *et al*, 1981, Phys. Scr. **24** 324